



8-2002

Creating true molecular composites containing a liquid crystalline polymer by optimizing intermolecular hydrogen bonding

Sriram Viswanathan
University of Tennessee

Follow this and additional works at: https://trace.tennessee.edu/utk_graddiss

Recommended Citation

Viswanathan, Sriram, "Creating true molecular composites containing a liquid crystalline polymer by optimizing intermolecular hydrogen bonding. " PhD diss., University of Tennessee, 2002.
https://trace.tennessee.edu/utk_graddiss/6325

This Dissertation is brought to you for free and open access by the Graduate School at TRACE: Tennessee Research and Creative Exchange. It has been accepted for inclusion in Doctoral Dissertations by an authorized administrator of TRACE: Tennessee Research and Creative Exchange. For more information, please contact trace@utk.edu.

To the Graduate Council:

I am submitting herewith a dissertation written by Sriram Viswanathan entitled "Creating true molecular composites containing a liquid crystalline polymer by optimizing intermolecular hydrogen bonding." I have examined the final electronic copy of this dissertation for form and content and recommend that it be accepted in partial fulfillment of the requirements for the degree of Doctor of Philosophy, with a major in Chemistry.

Mark D. Dadmun, Major Professor

We have read this dissertation and recommend its acceptance:

Jeffery Kovac, Roberto Benson, Robert Hinde

Accepted for the Council:

Carolyn R. Hodges

Vice Provost and Dean of the Graduate School

(Original signatures are on file with official student records.)

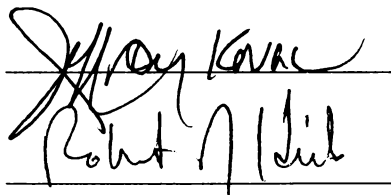
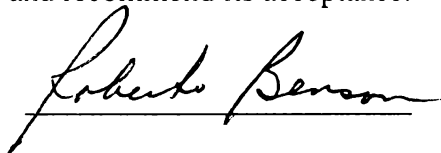
To the Graduate Council:

I am submitting herewith a dissertation written by Sriram Viswanathan entitled "Creating True Molecular Composites containing a Liquid Crystalline Polymer by Optimizing Intermolecular Hydrogen Bonding." I have examined the final **paper** copy of this dissertation for form and content and recommend that it be accepted in partial fulfillment of the requirements for the degree of Doctor of Philosophy, with a major in Chemistry.

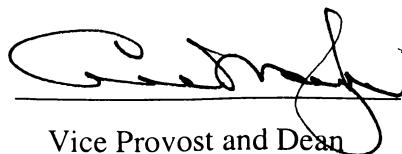


Mark D. Dadmun, Major Professor

We have read this dissertation
and recommend its acceptance:



Accepted for the Council:



Vice Provost and Dean
of Graduate Studies

**CREATING TRUE MOLECULAR COMPOSITES
CONTAINING A LIQUID CRYSTALLINE POLYMER BY
OPTIMIZING INTERMOLECULAR HYDROGEN BONDING**

A Dissertation

Presented for the

Doctor of Philosophy

Degree

The University of Tennessee, Knoxville

Sriram Viswanathan

August 2002

This dissertation is dedicated to my parents
for inspiring and encouraging me to reach
higher in order to achieve my goals.

ACKNOWLEDGMENTS

I would like to express my sincere gratitude to Professor Mark Dadmun for his guidance, encouragement and constructive criticisms during my years of candidacy. I would like to thank Professors Jeffrey Kovac, Roberto Benson and Robert Hinde for serving on my dissertation committee. I would also like to thank my fellow graduate students, Bijan Radmard and Eric Eastwood for instrumental assistance. Special thanks are due to all my colleagues in the Chemistry Department for their sincere friendship. In addition, I would like to thank my family members for their love, support and encouragement during my academic career. Financial support of the National Science Foundation, Division of Materials Research is gratefully acknowledged.

ABSTRACT

Blending a liquid crystalline polymer (LCP) with an amorphous polymer to create a molecular composite offers a method to use the desirable properties of a LCP at a more modest cost. However, very few such blends are miscible. This study seeks to correlate the extent of intermolecular hydrogen bonding between the two polymers in a blend with the phase behavior of the blend. Using Fourier Transform Infrared technique to quantify the amount of intermolecular hydrogen bonding between the two polymers and Differential Scanning Calorimetry and optical microscopy to determine the blend phase behavior, this study provides results which demonstrate that the broadest miscibility window in the blends studied corresponds to the system that optimizes the extent of intermolecular hydrogen bonding.

The first part of this study demonstrates that it is possible to create a true molecular composite by inducing miscibility in a blend containing a LCP and an amorphous polymer by slightly modifying the structure of the amorphous polymer to promote hydrogen bonding between the two polymers. The system that maximizes the extent of intermolecular hydrogen bonding is one where the hydrogen bonding moieties on one of the polymers are spaced out along the chain. The results show that by optimizing the extent of hydrogen bonding between the two blend components, the broadest miscibility window in the phase diagram can be found. To sum up, these results provide guidelines by which miscibility may be induced in polymer blends by such minor structural modification of the polymers.

As an extension to the first part, further work shows that structural modification of the LCP in addition to that of the amorphous polymer can further improve miscibility

in the blend. This is demonstrated by eliminating hydrogen bonding between the LCP chains which contributes to the improvement in intermolecular H-bonding and thereby an expansion in the miscibility window.

Finally, using an association model, theoretical miscibility windows were predicted for blends containing the LCP and the amorphous polymer and compared to the experimentally determined miscibility windows to validate the findings.

TABLE OF CONTENTS

| Chapter | Page |
|--|------|
| 1. Introduction..... | 1 |
| 1.1 Motivation and Objective..... | 1 |
| 1.2 Literature Review..... | 3 |
| Thermodynamics of Mixing in Polymer Blends..... | 3 |
| Hydrogen bonded Rod/Coil Polymer Blends..... | 7 |
| Functional Group Accessibility in Polymer Blends..... | 9 |
| 1.3 Goals and Justifications..... | 13 |
| 2. Creating Miscible Liquid Crystalline Polyurethane/Poly(Styrene-co-4-Vinyl phenol) Blends..... | 15 |
| 2.1 Introduction..... | 15 |
| 2.2 Experimental..... | 15 |
| Materials..... | 15 |
| Experimental Techniques..... | 16 |
| Polymer Synthesis and Characterization..... | 17 |
| 2.3 Results and Discussion..... | 33 |
| FT-IR Studies..... | 33 |
| Thermal and Optical Phase Behavior Studies..... | 59 |
| 2.4 Summary..... | 68 |
| 3. Creating Miscible N-methyl Liquid Crystalline Polyurethane/Poly(Styrene-co-4- | |

| | | |
|-----|--|-----|
| | Vinyl phenol) Blends..... | 70 |
| 3.1 | Introduction..... | 70 |
| 3.2 | Experimental..... | 71 |
| 3.3 | Results and Discussion..... | 78 |
| | FT-IR Studies..... | 78 |
| | Thermal and Optical Phase Behavior Studies..... | 90 |
| 3.4 | Summary..... | 105 |
| 4. | Thermal History Effects in Liquid Crystalline Polymer Blends..... | 106 |
| 5. | Correlation of Association Model to Hydrogen Bonding Liquid Crystalline Polymer Blends..... | 133 |
| 5.1 | Introduction..... | 133 |
| | Association Model..... | 133 |
| | Stoichiometric Equations Describing Hydrogen Bonding..... | 137 |
| | Free Energy of Mixing in Hydrogen Bonding Polymer Blends..... | 139 |
| 5.2 | Results and Discussion..... | 147 |
| | Determination of Self-Association Equilibrium Constants..... | 148 |
| | Determination of Inter-Association Equilibrium Constants..... | 154 |
| | Mapping Theoretical Phase Diagrams..... | 159 |
| | Effect of Functional Group Accessibility on Blend Miscibility..... | 170 |
| 6. | Conclusions and Future Work..... | 185 |
| | LIST OF REFERENCES..... | 188 |
| | APPENDIX..... | 195 |
| | VITA..... | 205 |

LIST OF TABLES

| Table | Page |
|-------|---|
| 1. | Molecular Weights and Phase Transitions of Liquid Crystalline Polyurethane (LCPU), N-methyl Liquid Crystalline Polyurethane (LCPU-M) and Poly(Styrene-co-4-Vinyl phenol) (PS-co-VPh) Copolymers.....34 |
| 2. | Results of the deconvolution of the C=O stretching band for pure LCPU and blends containing 80 wt.% PS-co-VPh copolymer for various copolymer compositions measured at 180°C.....49 |
| 3. | Deconvolution results of the C=O stretching region for multiple samples of LCPU/PS-co-VPh blends containing 80 wt.% PS-co-VPh(5) copolymer measured at 140°C and 70°C (for determining Absorption Coefficient Ratio).....53 |
| 4. | Deconvolution results of the C=O stretching region for pure LCPU-M and blends containing 80 wt.% PS-co-VPh copolymer for various copolymer compositions measured at 180°C.....83 |
| 5. | Deconvolution results of the C=O stretching region for annealed (1 hour) and “as-cast, heat-treated” LCPU-M blends containing 60 wt.% PS-co-VPh(40) copolymer.....119 |
| 6. | Molar Volume Data for Different Copolymer Compositions of LCPU-M/PS-co-VPh Blends.....151 |
| 7. | Self-association Equilibrium Constant (K_2) of Hydroxyl-Hydroxyl Dimer Hydrogen Bonding for Different Copolymer Compositions and Temperatures of LCPU-M/PS-co-VPh blends.....152 |
| 8. | Self-association Equilibrium Constant (K_B) of Hydroxyl-Hydroxyl Multimer Hydrogen Bonding for Different Copolymer Compositions and Temperatures of LCPU-M/PS-co-VPh Blends.....153 |
| 9. | Fraction of Hydrogen Bonded Carbonyl Groups (Determined Experimentally from IR Spectroscopy) of 20/80 (w/w) LCPU-M/PS-co-VPh Blends at Different Copolymer Compositions and Temperatures.....156 |
| 10. | Interassociation Equilibrium Constant (K_A) for Different Copolymer Compositions and Temperatures of Miscible 20/80 (w/w) LCPU/PS-co-VPh Blends.....158 |
| 11. | Useful Parameters for $\Phi_A f_{HB}^{C=O}$ versus Φ_A plot (Figure 77) Obtained for |

| | | |
|-----|--|-----|
| | Different Blend Compositions of LCPU-M/PS-co-VPh(5). $f_{HB}^{C=O}$ is obtained Experimentally at 150°C from IR Spectroscopy..... | 168 |
| 12. | Useful Parameters for $f_{HB}^{C=O}$ versus Φ_B plot (dashed line in Figure 70) Obtained for Different Blend Compositions of LCPU-M/PS-co-VPh(5). $f_{HB}^{C=O}$ is Obtained Experimentally at 150°C from IR Spectroscopy..... | 171 |
| 13. | Useful Parameters Obtained Using “Two-Phase Lever Rule” Method for Different Copolymer Compositions and Temperatures of LCPU-M/PS-co-VPh Blends. Φ_X and Φ_Y Denote the Composition Limits of the Two-Phase Region of the Phase Diagram..... | 172 |
| 14. | Van’t Hoff Plot Parameters for Different Copolymer Compositions and Temperatures of Miscible LCPU-M/PS-co-VPh Blends..... | 180 |
| 15. | Useful Parameters for K_A^{STD} versus R_B plot (Figure 85) for Different Copolymer Compositions of 20/80 (w/w) LCPU-M/PS-co-VPh Blends..... | 183 |
| 16. | Results of the Best-fit Method for determining the Interassociation Equilibrium Constant (K_A) of 20/80 (w/w) LCPU-M/PS-co-VPh(30) blend measured at 150°C..... | 204 |

LIST OF FIGURES

| Figure | Page |
|---|------|
| 1. Synthesis of the Liquid Crystalline Polyurethane (LCPU) used in this study..... | 18 |
| 2. Characteristic Proton NMR spectra of pure LCPU. Lower case letters refer to Proton NMR results (see also Figure 3)..... | 20 |
| 3. Structure of the Liquid Crystalline Polyurethane (LCPU) with Proton NMR results specified by lower case letters (see also Figure 2)..... | 21 |
| 4. FT-IR spectra of pure LCPU measured at 30°C upon cooling from the melt..... | 22 |
| 5. Synthesis of Poly(Styrene-co-4-Vinyl phenol) (PS-co-VPh) copolymer used in this study..... | 24 |
| 6. Characteristic ¹ H-NMR spectra of Poly(Styrene-co-4-Acetoxystyrene) containing 5 mol% 4-acetoxy styrene..... | 25 |
| 7. Characteristic ¹ H-NMR spectra of Poly(Styrene-co-4-Acetoxystyrene) containing 10 mol% 4-acetoxy styrene..... | 26 |
| 8. Characteristic ¹ H-NMR spectra of Poly(Styrene-co-4-Acetoxystyrene) containing 20 mol% 4-acetoxy styrene..... | 27 |
| 9. Characteristic ¹ H-NMR spectra of poly(Styrene-co-4-Acetoxystyrene) containing 30 mol% 4-acetoxy styrene..... | 28 |
| 10. Characteristic ¹ H-NMR spectra of poly(Styrene-co-4-Acetoxystyrene) containing 40 mol% 4-acetoxy styrene..... | 29 |
| 11. Characteristic ¹ H-NMR spectra of poly(Styrene-co-4-Acetoxystyrene) containing 50 mol% 4-acetoxy styrene..... | 30 |
| 12. Characteristic ¹ H-NMR spectra of Poly(Styrene-co-4-Vinylphenol)..... | 32 |
| 13. DSC curve of pure LCPU..... | 35 |
| 14. DSC curves of (a) PS-co-VPh (5 mol% VPh) (b) PS-co-VPh (10 mol% VPh) (c) PS-co-VPh (20 mol% VPh) (d) PS-co-VPh (30 mol% VPh) (e) PS-co-VPh (40 mol% VPh) (f) PS-co-VPh (50 mol% VPh) (g) pure PVPh..... | 36 |
| 15. Possible hydrogen bonding associations in LCPU/PS-co-VPh blends and LCPU-M/PS-co-VPh blends..... | 37 |

| | | |
|-----|---|----|
| 16. | FT-IR spectra of C=O stretching region for pure LCPU as a function of temperature..... | 39 |
| 17. | Example of result of the deconvolution procedure for the carbonyl stretching regime of FT-IR spectra of pure LCPU measured at 1) 30°C (upon cooling) 2) 180°C..... | 40 |
| 18. | Area plots corresponding to the contributing peaks of pure LCPU obtained from deconvolution of C=O stretching band of the FT-IR spectra upon cooling from 180°C to 30°C..... | 41 |
| 19. | FT-IR spectra of C=O stretching region for blends measured at 180°C. Compositions of blends are 80 wt.% PS-co-VPh and 20 wt.% LCPU. Curve (a) is the pure LCPU, while the remaining curves are for blends containing PS-co-VPh with b) 5 mole % c) 10 mole % d) 20 mole % e) 30 mole % f) 40 mole % g) 50 mole % h) 100 mole % VPh..... | 46 |
| 20. | FT-IR spectra of C=O stretching region for blends containing PS-co-VPh(20) measured at 180°C. The curves correspond to blends with a composition of (LCPU/PS-co-VPh wt/wt) a) 100/0 b) 80/20 c) 60/40 d) 50/50 e) 40/60 f) 20/80 g) 0/100..... | 48 |
| 21. | Percent of carbonyl groups participating in intermolecularly hydrogen bonding as a function of PS-co-VPh copolymer composition for different blend compositions of LCPU/PS-co-VPh measured at 180°C. Error Bar in the plot corresponds to $\pm 2\%$ | 55 |
| 22. | Percent of hydroxyl groups participating in intermolecularly hydrogen bonding as a function of PS-co-VPh copolymer composition for different blend compositions of LCPU/PS-co-VPh measured at 180°C. Error Bar in the plot corresponds to $\pm 2\%$ | 56 |
| 23. | Representative DSC curves of blends containing LCPU and PS-co-VPh(10). Compositions of the blends are (LCPU/PS-co-VPh(10) wt/wt) a) 25/75 b) 20/80 c) 15/85 d) 10/90 e) 5/95 f) 0/100..... | 60 |
| 24. | Representative DSC curves of blends containing LCPU and PS-co-VPh(20). Compositions of the blends are (LCPU/PS-co-VPh(20) wt/wt) a) 40/60 b) 35/65 c) 30/70 d) 25/75 e) 20/80 f) 15/85 g) 10/90 h) 5/95 i) 0/100..... | 61 |
| 25. | Representative DSC curves of blends containing LCPU and PS-co-VPh(30). Compositions of the blends are (LCPU/PS-co-VPh(30) wt/wt) a) 25/75 b) 20/80 c) 15/85 d) 10/90 e) 5/95 f) 0/100..... | 62 |

| | | |
|-----|--|----|
| 26. | Experimental and theoretical glass transition temperatures of blends containing PS-co-VPh(10) and LCPU..... | 63 |
| 27. | Experimental and theoretical glass transition temperatures of blends containing PS-co-VPh(20) and LCPU..... | 64 |
| 28. | Experimental and theoretical glass transition temperatures of blends containing PS-co-VPh(30) and LCPU..... | 65 |
| 29. | Phase diagram of blends containing PS-co-VPh(10), PS-co-VPh(20) and PS-co-VPh(30) as determined from phase contrast optical microscopy..... | 67 |
| 30. | Synthesis of the N-methyl Liquid Crystalline Polyurethane (LCPU-M) used in this study..... | 72 |
| 31. | Characteristic Proton NMR spectra of pure LCPU (curve a) and pure LCPU-M (curve b). Lower case letters refer to Proton NMR results (see also Figure 32)..... | 73 |
| 32. | Structure of the N-methyl Liquid Crystalline Polyurethane (LCPU-M) with Proton NMR results specified by lower case letters (see also Figure 31)..... | 74 |
| 33. | DSC curve of the N-methyl Liquid Crystalline Polyurethane (LCPU-M)..... | 76 |
| 34. | FT-IR spectra of pure LCPU (curve a) and LCPU-M (curve b) measured at 30°C upon cooling from the melt..... | 77 |
| 35. | FT-IR spectra of C=O stretching region for blends containing 80 wt.% PS-co-VPh and 20 wt.% LCPU-M measured at 180°C. Curve (a) is the pure LCPU-M, while the remaining curves are for blends containing PS-co-VPh with b) 5 mole % c) 10 mole % d) 20 mole % e) 30 mole % f) 40 mole % g) 50 mole % h) 100 mole % VPh..... | 80 |
| 36. | FT-IR spectra of C=O stretching region for blends containing PS-co-VPh(40) measured at 180°C. The curves correspond to blends with a composition of (LCPU-M/PS-co-VPh wt/wt) a) 100/0 b) 80/20 c) 60/40 d) 50/50 e) 40/60 f) 20/80 g) 0/100..... | 82 |
| 37. | Percent of carbonyl groups participating in intermolecularly hydrogen bonding as a function of PS-co-VPh copolymer composition for different blend compositions of LCPU-M and PS-co-VPh measured at 180°C. Error Bar in the plot corresponds to ± 2%..... | 85 |
| 38. | Percent of hydroxyl groups participating in intermolecularly hydrogen bonding as a function of PS-co-VPh copolymer composition for different blend compositions | |

| | | |
|-----|---|-----|
| | of LCPU-M and PS-co-VPh measured at 180°C. Error Bar in the plot corresponds to $\pm 2\%$ | 87 |
| 39. | Representative DSC curves of blends containing LCPU-M and PS-co-VPh(5). Compositions of the blends are (LCPU-M/PS-co-VPh(5) wt/wt) a) 25/75 b) 20/80 c) 15/85 d) 10/90 e) 5/95 f) 0/100..... | 91 |
| 40. | Representative DSC curves of blends containing LCPU-M and PS-co-VPh(10). Compositions of the blends are (LCPU-M/PS-co-VPh(10) wt/wt) a) 35/65 b) 30/70 c) 25/75 d) 20/80 e) 15/85 f) 10/90 g) 5/95 h) 0/100..... | 92 |
| 41. | Representative DSC curves of blends containing LCPU-M and PS-co-VPh(20). Compositions of the blends are (LCPU-M/PS-co-VPh(20) wt/wt) a) 45/55 b) 40/60 c) 35/65 d) 30/70 e) 25/75 f) 20/80 g) 15/85 h) 10/90 i) 5/95 j) 0/100..... | 93 |
| 42. | Representative DSC curves of blends containing LCPU-M and PS-co-VPh(30). Compositions of the blends are (LCPU-M/PS-co-VPh(30) wt/wt) a) 45/55 b) 40/60 c) 35/65 d) 30/70 e) 25/75 f) 20/80 g) 15/85 h) 10/90 i) 5/95 j) 0/100..... | 94 |
| 43. | Representative DSC curves of blends containing LCPU-M and PS-co-VPh(40). Compositions of the blends are (LCPU-M/PS-co-VPh(40) wt/wt) a) 50/50 b) 45/55 c) 40/60 d) 35/65 e) 30/70 f) 25/75 g) 20/80 h) 15/85 i) 10/90 j) 5/95 k) 0/100..... | 95 |
| 44. | Representative DSC curves of blends containing LCPU-M and PS-co-VPh(50). Compositions of the blends are (LCPU-M/PS-co-VPh(50) wt/wt) a) 25/75 b) 20/80 c) 15/85 d) 10/90 e) 5/95 f) 0/100..... | 96 |
| 45. | Experimental and theoretical glass transition temperatures of blends containing PS-co-VPh(5) and LCPU-M..... | 97 |
| 46. | Experimental and theoretical glass transition temperatures of blends containing PS-co-VPh(10) and LCPU-M..... | 98 |
| 47. | Experimental and theoretical glass transition temperatures of blends containing PS-co-VPh(20) and LCPU-M..... | 99 |
| 48. | Experimental and theoretical glass transition temperatures of blends containing PS-co-VPh(30) and LCPU-M..... | 100 |
| 49. | Experimental and theoretical glass transition temperatures of blends containing PS-co-VPh(40) and LCPU-M..... | 101 |
| 50. | Experimental and theoretical glass transition temperatures of blends containing PS-co-VPh(50) and LCPU-M..... | 102 |

51. Phase diagram of blends containing LCPU-M and PS-co-VPh as determined from phase contrast optical microscopy.....103
52. Phase diagram of LCPU/PS-co-VPh(20) and LCPU-M/PS-co-VPh(40) blends as determined from phase contrast optical microscopy.....108
53. FT-IR spectra of C=O stretching region of “annealed” and “as-cast, heat-treated” blends of 80/20 (w/w) LCPU/PS-co-VPh(20). Curve (a) corresponds to sample at 30°C while the remaining curves are for samples heat-treated at b) 140°C (as-cast, heat-treated) c) 140°C (annealed) d) 180°C (as-cast, heat-treated) e) 180°C (annealed).....111
54. FT-IR spectra of C=O stretching region of “annealed” and “as-cast, heat-treated” blends of 40/60 (w/w) LCPU/PS-co-VPh(20). Curve (a) corresponds to sample at 30°C while the remaining curves are for samples heat-treated at b) 140°C (as-cast, heat-treated) c) 140°C (annealed) d) 180°C (as-cast, heat-treated) e) 180°C (annealed).....112
55. FT-IR spectra of C=O stretching region of “annealed” and “as-cast, heat-treated” blends of 30/70 (w/w) blend of LCPU/PS-co-VPh(20). Curve (a) corresponds to sample at 30°C while the remaining curves are for samples heat-treated at b) 130°C (as-cast, heat-treated) c) 130°C (annealed) d) 160°C (as-cast, heat-treated) e) 160°C (annealed) f) 180°C (as-cast, heat-treated) g) 180°C (annealed).....113
56. FT-IR spectra of C=O stretching region of “annealed” and “as-cast, heat-treated” blends of 20/80 (w/w) blend of LCPU/PS-co-VPh(20). Curve (a) corresponds to sample at 30°C while the remaining curves are for samples heat-treated at b) 140°C (as-cast, heat-treated) c) 140°C (annealed) d) 180°C (as-cast, heat-treated) e) 180°C (annealed).....114
57. FT-IR spectra of C=O stretching region of “annealed” and “as-cast, heat-treated” blends of 80/20 (w/w) blend of LCPU-M/PS-co-VPh(40). Curve (a) corresponds to sample at 30°C while the remaining curves are for samples heat-treated at b) 140°C (as-cast, heat-treated) c) 140°C (annealed) d) 180°C (as-cast, heat-treated) e) 180°C (annealed).....115
58. FT-IR spectra of C=O stretching region of “annealed” and “as-cast, heat-treated” blends of 50/50 (w/w) blend of LCPU-M/PS-co-VPh(40). Curve (a) corresponds to sample at 30°C while the remaining curves are for samples heat-treated at b) 140°C (as-cast, heat-treated) c) 140°C (annealed) d) 180°C (as-cast, heat-treated) e) 180°C (annealed).....116
59. FT-IR spectra of C=O stretching region of “annealed” and “as-cast, heat-treated”

| | | |
|-----|---|-----|
| | blends of 45/55 (w/w) blend of LCPU-M/PS-co-VPh(40). Curve (a) corresponds to sample at 30°C while the remaining curves are for samples heat-treated at b) 130°C (as-cast, heat-treated) c) 130°C (annealed) d) 160°C (as-cast, heat-treated) e) 160°C (annealed) f) 180°C (as-cast, heat-treated) g) 180°C (annealed)..... | 117 |
| 60. | FT-IR spectra of C=O stretching region of “annealed” and “as-cast, heat-treated” blends of 40/60 (w/w) blend of LCPU-M/PS-co-VPh(40). Curve (a) corresponds to sample at 30°C while the remaining curves are for samples heat-treated at b) 140°C (as-cast, heat-treated) c) 140°C (annealed) d) 180°C (as-cast, heat-treated) e) 180°C (annealed)..... | 118 |
| 61. | Percent of intermolecular hydrogen bonding as a function of temperature for annealed and as-cast, heat-treated blends of 80/20 (w/w) LCPU/PS-co-VPh(20)..... | 121 |
| 62. | Percent of intermolecular hydrogen bonding as a function of temperature for annealed and as-cast, heat-treated blends of 40/60 (w/w) LCPU/PS-co-VPh(20)..... | 122 |
| 63. | Percent of intermolecular hydrogen bonding as a function of temperature for annealed and as-cast, heat-treated blends of 80/20 (w/w) LCPU-M/PS-co-VPh(40)..... | 123 |
| 64. | Percent of intermolecular hydrogen bonding as a function of temperature for annealed and as-cast, heat-treated blends of 50/50 (w/w) LCPU-M/PS-co-VPh(40)..... | 124 |
| 65. | Percent of intermolecular hydrogen bonding as a function of temperature for annealed and as-cast, heat-treated blends of 20/80 (w/w) LCPU/PS-co-VPh(20)..... | 125 |
| 66. | Percent of intermolecular hydrogen bonding as a function of temperature for annealed and as-cast, heat-treated blends of 40/60 (w/w) LCPU-M/PS-co-VPh(40)..... | 126 |
| 67. | Percent of intermolecular hydrogen bonding as a function of temperature for annealed and as-cast, heat-treated blends of 30/70 (w/w) LCPU/PS-co-VPh(20)..... | 130 |
| 68. | Percent of intermolecular hydrogen bonding as a function of temperature for annealed and as-cast, heat-treated blends of 45/55 (w/w) LCPU-M/PS-co-VPh(40)..... | 131 |
| 69. | Chemical specific repeat units of N-methyl liquid crystalline polyurethane | |

(LCPU-M) and poly (styrene-co-4-vinylphenol) [PS-co-VPh] copolymers.....150

70. Comparison of experimental data (IR spectroscopy) with theoretical curves for the one- and two-phase systems for plots of fraction of hydrogen bonded C=O ($f_{HB}^{C=O}$) versus blend composition of LCPU-M/PS-co-VPh(5) blends at 150°C: thick, continuous line (theory, single phase) and dashed line (lever rule, two phase).....160
71. Comparison of experimental data (IR spectroscopy) with theoretical curves for the one- and two-phase systems for plots of fraction of hydrogen bonded C=O ($f_{HB}^{C=O}$) versus blend composition of LCPU-M/PS-co-VPh(10) blends at 150°C.....161
72. Comparison of experimental data (IR spectroscopy) with theoretical curves for the one- and two-phase systems for plots of fraction of hydrogen bonded C=O ($f_{HB}^{C=O}$) versus blend composition of LCPU-M/PS-co-VPh(20) blends at 150°C.....162
73. Comparison of experimental data (IR spectroscopy) with theoretical curves for the one- and two-phase systems for plots of fraction of hydrogen bonded C=O ($f_{HB}^{C=O}$) versus blend composition of LCPU-M/PS-co-VPh(30) blends at 150°C.....163
74. Comparison of experimental data (IR spectroscopy) with theoretical curves for the one- and two-phase systems for plots of fraction of hydrogen bonded C=O ($f_{HB}^{C=O}$) versus blend composition of LCPU-M/PS-co-VPh(40) blends at 150°C.....164
75. Comparison of experimental data (IR spectroscopy) with theoretical curves for the one- and two-phase systems for plots of fraction of hydrogen bonded C=O ($f_{HB}^{C=O}$) versus blend composition of LCPU-M/PS-co-VPh(50) blends at 150°C.....165
76. Schematic representation of a typical phase diagram.....167
77. A plot of $\Phi_A f_{HB}$ versus Φ_A obtained for LCPU-M/PS-co-VPh(5) blends. $f_{HB}^{C=O}$ is obtained experimentally at 150°C from IR spectroscopy.....169
78. Comparison of theoretical (from association model) and experimental (from optical microscopy) phase diagrams of LCPU-M/PS-co-VPh(5).....173
79. Comparison of theoretical (from association model) and experimental (from optical microscopy) phase diagrams of LCPU-M/PS-co-VPh(10).....174
80. Comparison of theoretical (from association model) and experimental (from optical microscopy) phase diagrams of LCPU-M/PS-co-VPh(20).....175
81. Comparison of theoretical (from association model) and experimental (from optical microscopy) phase diagrams of LCPU-M/PS-co-VPh(30).....176

| | | |
|-----|--|-----|
| 82. | Comparison of theoretical (from association model) and experimental (from optical microscopy) phase diagrams of LCPU-M/PS-co-VPh(40)..... | 177 |
| 83. | Comparison of theoretical (from association model) and experimental (from optical microscopy) phase diagrams of LCPU-M/PS-co-VPh(50)..... | 178 |
| 84. | Van't Hoff plot for determining interassociation equilibrium constant at 25°C using data obtained at higher temperatures (see Table 10) for different copolymer compositions of 20/80 (w/w) LCPU-M/PS-co-VPh blends..... | 181 |
| 85. | A plot of interassociation equilibrium constant based on a common reference volume of 100 cm ³ /mol at 25°C (K_A^{STD}) versus molar volume between vinyl phenol units of PS-co-VPh copolymer (R_B) for miscible LCPU-M/PS-co-VPh blends. Error Bar in the plot corresponds to ± 0.3..... | 184 |
| 86. | GPC data of pure LCPU..... | 196 |
| 87. | GPC data of PS-co-VPh (5 mol% VPh)..... | 197 |
| 88. | GPC data of PS-co-VPh (10 mol% VPh)..... | 198 |
| 89. | GPC data of PS-co-VPh (20 mol% VPh)..... | 199 |
| 90. | GPC data of PS-co-VPh (30 mol% VPh)..... | 200 |
| 91. | GPC data of PS-co-VPh (40 mol% VPh)..... | 201 |
| 92. | GPC data of PS-co-VPh (50 mol% VPh)..... | 202 |
| 93. | GPC data of the N-methyl Liquid Crystalline Polyurethane (LCPU-M)..... | 203 |

Chapter 1

Introduction

1.1 Motivation and Objective

Over the last thirty years, the study of polymer blends has been one of the most important areas of industrial and academic research in polymer science. The growing history of polymer blend science and technology has been well documented in a number of review articles and monographs.¹⁻²³ The motivation behind the tremendous effort in scientific research and industrial development of blends may, in general, be categorized into four aspects: tailoring properties, improving processability, reducing product cost and recycling post-consumer polymers.

Tailoring properties is particularly attractive from two points of view. First, the pattern of the properties achieved by combining different polymers is often beyond the reach of the individual polymers involved. As an example, polymer substrates for ROM (Read Only Memory) optical disks require a combination of various properties. Low birefringence (optical homogeneity) and moisture sensitivity are essential. Poly(methyl methacrylate) (PMMA) has the advantage of low sensitivity to orientation birefringence but has the disadvantage of high water absorption. However, when PMMA is blended with poly(vinylidene fluoride) (a birefringence-negative and moisture-insensitive polymer) at an appropriate ratio, an excellent optical substrate results which is not only free of birefringence but also displays considerably reduced water absorption in comparison with pure PMMA.⁸⁻⁹

The poor processability of a highly viscous polymer can be overcome by blending the

polymer with others that have low viscosity. In this case, the less viscous polymers may be viewed as a permanent plasticizers.¹¹ A typical example is given by the miscible blend of poly(2,4-dimethyl phenylene oxide) (PPO) and polystyrene (PS). PPO is an amorphous engineering polymer with notable properties of high strength and heat distortion temperature. These superior properties are, however, accompanied by extremely poor flow properties which make the material very difficult to process. The addition of PS leads to a drastic reduction in melt viscosity, and the blend can be processed without difficulty while retaining the superior properties of PPO.

One of the initial incentives behind the development of polymer blend industries is cost reduction. A lot of attention has been given to attempt to achieve certain desired properties at affordable prices or, in other words, an economically more favorable price/performance ratio. Today, with increasing concern on environmental protection and increasing importance of multi-component systems such as multi-films and rigid packages, blending has inevitably become an indispensable tool for both post-consumer and inhouse recycling.¹⁵

These motivations clearly explain the rapid and continuing growth of the polymer blend literature. In particular, the pursuit of special properties for high technology and specific engineering applications represents a major challenge. The properties of polymer blends depend on how the individual constituents are dispersed in one another. For miscible blends, the properties generally follow relationships that are functions of composition although in some cases a synergistic effect is observed. Extensive studies have been undertaken to better understand the origin of polymer-polymer miscibility. The reasons for

this effort are obvious: high mechanical properties can be produced and the various properties required for specific applications can be achieved simply by altering the composition of the blend. For immiscible blends, on the other hand, the desirable properties cannot be achieved unless particular effort is made to carefully control the phase morphology and the level of interfacial adhesion (often through the use of a compatibilizer), in addition to the considerations of blend composition.

Liquid crystalline polymers (LCP) are an important class of materials with unique and desirable properties. These mesogenic fluids exhibit highly efficient molecular orientation in flow, display exceptional tensile properties and possess viscosities lower than that of conventional polymers of comparable molecular weight. LCPs have thus been found to have potential applications as high-strength fibers and plastics.²⁴⁻²⁸ However, the high cost of LCPs has kindled interest in many²⁹⁻³⁸ to investigate the feasibility of blending them with commodity amorphous polymers, and thereby forming rigid rod/flexible coil polymer blends that ideally would exhibit extraordinary mechanical properties and processability. Such a miscible polymer blend containing a rigid rod polymer and an amorphous coiled polymer is often termed a 'molecular composite' as the rod-like polymer will act as a reinforcing 'filler' of the coiled polymer with a high aspect ratio *if* the rod-like polymer is molecularly dispersed in the amorphous matrix. The research study described in this thesis work demonstrates the formation of such molecular composites with the LCP acting as the rod-like component.

1.2 Literature Review

Thermodynamics of Mixing in Polymer blends

The task of mixing two polymers is not trivial due to the fact that any phase

separation between the polymer components could lead to a weak interface and therefore poor blend properties. Unfortunately, most polymer pairs are incompatible and form two phases when mixed.³⁹⁻⁴¹ Phase separation in polymer blends arises due to insignificant contribution of the favorable combinatorial entropy of mixing and significant contribution of the unfavorable enthalpy of mixing to the Gibbs free energy of mixing two dissimilar polymers. The most common theoretical model that describes the change in Gibbs free energy of mixing is the Flory-Huggins theory³⁹, which is as follows:

$$\frac{\Delta G_m}{RT} = -\frac{\Phi_A}{M_A} \ln \Phi_A - \frac{\Phi_B}{M_B} \ln \Phi_B + \chi_{AB} \Phi_A \Phi_B \quad (1.1)$$

where Φ_A and Φ_B , and M_A and M_B are the volume fractions and degrees of polymerization of polymers A and B, respectively and χ_{AB} is the Flory interaction parameter. Some of the factors that could contribute to a positive Gibbs free energy of mixing two dissimilar polymers (meaning phase separation) are high molecular weight chains, dispersion forces among chains, and structural dissimilarity of chains. High molecular weight polymer chains in the blend lower the combinatorial entropy of mixing, which is represented by the first two terms of the Flory-Huggins equation, due to the limited number of possible molecular conformations of the chains.^{42,43} Dispersion forces among the polymer chains represent forces that are unfavorable to the free energy of mixing. These dispersion forces give rise to an enthalpy of mixing (the third term of the Flory-Huggins equation) that tends to be significantly positive, favoring phase separation.

In addition to the above considerations, when one of the polymers in the mixture is a rigid-rod and the other one is a random-coil, the tendency of the mixture to phase separate is

further intensified. Flory has shown that a rod/coil polymer blend dissolved in a solvent will separate into an isotropic phase which consists mainly of a coiled polymer solution and an anisotropic phase which consists mainly of the rod-like polymer.⁴⁴ The structural similarity of the rod-like chains provides an impetus for them to align relative to each other and exclude a structurally dissimilar coil-like chain. This tendency governs the phase behavior/miscibility behavior of rod/coil mixtures which is the subject of study of this work.⁴⁵ Although rod/coil mixing is thermodynamically unfavorable, it is economically desirable to create a molecular composite, i.e. a miscible blend containing a liquid crystalline polymer and an amorphous polymer. Fortunately, the formation of strong specific interactions between two polymers may enhance their miscibility. This makes polymer blends that allow strong intermolecular interactions an important and well-studied class of polymer blends. The presence of strong specific intermolecular interactions, such as hydrogen bonding, between two polymer chains may induce miscibility by creating sufficient favorable enthalpic interactions to result in a negative free energy of mixing. Flory-Huggins theory is based on the assumption that the polymer chains mix randomly in a blend.^{44,45} This assumption finds its limitation in the presence of strong, specific interactions such as hydrogen bonding in the system since the polymer chains are forced into non-random configurations by these interactions.

Painter and co-workers⁴⁶⁻⁴⁹ have studied this phenomenon extensively and have developed a theory to describe the thermodynamics of mixing two polymers that possess functional groups capable of strong intermolecular interactions such as hydrogen bonding. They write the theoretical expression for the change in free energy upon mixing as:

$$\frac{\Delta G_m}{RT} = \frac{\Phi_A}{M_A} \ln \Phi_A + \frac{\Phi_B}{M_B} \ln \Phi_B + \chi_{AB} \Phi_A \Phi_B + \frac{\Delta G_H}{RT} \quad (1.2)$$

where Φ_A , Φ_B , M_A , M_B , χ_{AB} have the same definition as in the original Flory-Huggins theory. This equation consists of the standard combinatorial entropy (first two terms) and the unfavorable ‘physical’ interactions represented by χ_{AB} , however it also incorporates a third contribution (ΔG_H) that accounts for the change of entropy and enthalpy that derives from the presence of strong intermolecular interactions.

The extent of intermolecular H-bonding (H-bonding between dissimilar polymer chains) is an important parameter in determining miscibility in the blend. The presence of any intramolecular H-bonding (H-bonding among similar polymer chains) will limit the number of hydrogen bonding functional groups available for intermolecular H-bonding. It is important to note that intramolecular H-bonding and intermolecular H-bonding have opposite effects on the free energy of mixing two polymers. Intramolecular H-bonding is considered as endothermic enthalpy of mixing and intermolecular H-bonding as exothermic enthalpy of mixing, since the former is unfavorable to the free energy of mixing two dissimilar chains and needs to be broken, while the latter being favorable, needs to be formed in order to achieve blend miscibility. Although strong, specific interactions can produce a favorable enthalpy of mixing in the blend, it is to be noted that such interactions tend to take their toll on the entropy of mixing by causing strong orientation effects in the polymer chains. This means that the mobility of chains is limited and the rotational freedom of the chains is hindered as a consequence. The polymer chains are forced to assume non-random configurations and thus find a decrease in entropy of mixing.

To account for the enthalpic contributions to the free energy of mixing, corresponding to both self and inter-molecular associations, and the entropic changes corresponding to loss of rotational freedom due to specific interactions, Painter et al.⁴⁶⁻⁴⁹ have developed an association model that correlates ΔG_H to the change in the number of hydrogen bonded species with concentration and temperature. This model accounts for the fact that hydrogen bonds are in a state of dynamic equilibrium and thus exist as a distribution of free (non-hydrogen bonded) and hydrogen bonded species at any instant at a given temperature, and therefore must be characterized by a suitable equilibrium constant. An extensive description of this model for better understanding of the concepts and its applicability in this study has been provided in Chapter 5 of this thesis.

Hydrogen Bonded Rod/Coil Polymer Blends

The presence of rigid rod-like polymer dispersed on a molecular level in a flexible coil-like polymer matrix was first proposed by Helminiak and co-workers.⁵⁰ The high aspect ratio of the rigid rod-like polymer can be advantageously used to bring high modulus and strength to the blend. The miscibility of the blend made out of a rod-like and a random coil-like polymers to form a polymeric composite is however not an easy task since the mixing is limited by the small entropy of mixing.³⁹ The extent of mixing between the two polymers is a crucial factor in determining the overall strength and mechanical properties of the composite. Flory⁴² predicted that a blend of rod-like and coil-like polymers dissolved in a solvent will separate into an anisotropic phase of the rod polymer and an isotropic phase which consists mainly of a solution of the coiled polymer, as discussed in the previous section.

Elsewhere, Ballauff⁵¹ suggested that the miscibility in a rod/coil polymer blend can be

promoted by specific interactions such as hydrogen bonding or by attaching flexible side chains to rods. Coleman et al.⁵² theoretically predicted the phase diagram for rod/coil polymer blends that have hydrogen bonding interactions in them, by which, they concluded that a single phase rod/coil polymer blend can be found in the presence of very strong, specific interactions between a rod polymer and a coil polymer. As per these theoretical predictions, the phase behavior of lyotropic liquid crystal poly(γ -alkyl-L-glutamates) such as poly(γ -methyl-L-glutamate) (PMLG), poly(γ -ethyl-L-glutamate) (PELG) and poly(γ -butyl-L-glutamate) (PBLG) blended with poly(vinylphenol) (PVPh) were investigated.⁵³ The calculation of the phase diagram in these blends predicted the possibility of forming single phase rod/coil polymer mixtures with a very small biphasic gap between the isotropic and the anisotropic phases in appropriate compositions. The formation of a miscible blend between PVPh and PELG was also confirmed by determining the blend phase behavior by DSC and optical microscopy. The experimentally determined phase behavior was found to be consistent with that predicted theoretically.

Elsewhere, Green et al.⁵⁴ have attempted to prepare a molecular composite based on rod-like side chain functionalized polyisocyanates with ether, ester and ketone groups i.e., poly(3-(benzyloxy)-n-propyl isocyanate) (PIET), poly(3-(benzyloxycarbonyl)-n-propyl isocyanate) (PIES) and poly(3-oxobutyl isocyanate) (PIK) with hydrogen bonding donor random coil poly(styrene-co-4-vinylphenol). Thermodynamically stable miscible blends were reported for copolymer composition containing 9 mol% vinyl phenol, suggesting the possibility of forming molecular composites. However, an extensive study was not attempted to provide guidelines by which miscible rod/coil polymer blends may be created.

Functional Group Accessibility in Polymer blends

The formation of intermolecular hydrogen bonds between two polymers in a blend plays an integral role in the blend miscibility, and therefore, the extent of intermolecular hydrogen bonds that can occur between two polymers is an important parameter in determining the thermodynamics of such blends. Moreover, there are many factors that impact the extent of intermolecular hydrogen bonding that can exist between two polymers. For instance, if one polymer can undergo intramolecular hydrogen bonding with itself, then the presence of this intramolecular hydrogen bonding will limit the number of hydrogen bonding moieties that are available to participate in intermolecular hydrogen bonding. Intramolecular hydrogen bonding that occurs between similar polymer chains in a polymer blend is not the only factor that can impact the extent of intermolecular hydrogen bonding. The accessibility of functional groups that participate in intermolecular interactions also plays an important role in the formation of interchain contacts. For example, factors such as steric shielding of the functional moieties due to the presence of neighboring bulky groups or steric crowding of hydrogen bonding groups due to limited spacing between functional groups in a chain can inhibit the ability of functional groups to form specific interactions with other chains. Coleman and Painter have shown how such factors affect the accessibility of functional groups to interact between different chains by correlating the extent of interchain contacts to steric accessibility of a hydrogen bonding functional group and spacing between functional groups in a polymer chain. More specifically, they monitored the extent of intermolecular hydrogen bonding that can occur in a variety of blends consisting of a wide range of carbonyl containing (co)polymers and hydroxyl containing (co)polymers. As an

example, they studied blends containing poly(*n*-alkyl methacrylate) (PAMA) having different side chain lengths and poly(2,3-dimethyl butadiene-stat-4-vinylphenol) (DMBVPh) containing 24 wt.% VPh.⁵⁵ This study shows that steric shielding of the carbonyl due to the *n*-alkyl side chain decreases the intermolecular interactions. Using the interassociation equilibrium constant (K_A) as an indicator of intermolecular hydrogen bonding, they have shown that a decrease in the side chain length in the PAMA results in an increase in K_A , which correlates to an increase in intermolecular hydrogen bonding. In these studies, the poly(*n*-alkyl methacrylates) poly(methyl methacrylate) (PMMA), poly(ethyl methacrylate) (PEMA), poly(*n*-butyl methacrylate) (PBMA), poly(*n*-hexyl methacrylate) (PHMA), poly(*n*-decyl methacrylate) (PDMA), poly(*n*-lauryl methacrylate) (PLMA) were examined.

In another set of experiments, Coleman and Painter examined blends of PAMA and DMVBPh with various copolymer compositions (24, 48 and 72 wt.% VPh).⁵⁵ This study elucidated the effect of spacing the hydroxyl groups in the DMVBPh chain on the amount of intermolecular H-bonding that occurs in these blends. Their experiments showed an increase in interchain H-bonding as the amount of VPh was decreased from 72 to 24 wt.% in DMVBPh (and thus increased the spacing between the –OH groups on the chain), regardless of the steric shielding in PAMA. The authors interpreted these results as evidence that the spacing of hydroxyl groups on a copolymer chain can dramatically affect the amount of intermolecular H-bonding in polymer blends. They attribute this trend to the fact that spacing hydroxyl groups apart allows these groups to rotate independently with respect to one another, thus allowing them to reorient themselves in such a way that they are readily available for hydrogen bonding. However, the spacing effect does not provide any further

increase in interchain H-bonding below 24 wt.% VPh, as the number of VPh groups in the copolymer becomes so low as to limit the number of possible intermolecular H-bonds that can be formed.

Further experiments by Coleman et al. provide further evidence of the importance of spacing groups along the chain on the extent of intermolecular hydrogen bonding by examining blends that contain DMBVPh and poly(ethylene-co-vinylacetate) (EVAc).⁵⁶ These results show an increased accessibility of the VAc carbonyl groups to form interchain H-bonds as the spacing between the carbonyl groups in EVAc increases. This trend continues until 18 wt.% VAc in EVA, below which there is a decrease in interchain H-bonding, due to a decrease in the possible number of H-bonds that can be formed. Coleman and Painter have also studied other systems to examine the effect of functional group spacing and steric crowding on the extent of intermolecular hydrogen bonding. Each of these studies have shown that an increased spacing between functional groups on a chain increases the amount of intermolecular hydrogen bonding, however the optimum spacing seems to be system dependent.^{57,58} These results also verify that steric crowding can limit access of functional groups to participate in intermolecular hydrogen bonding.

Elsewhere, Radmard et al.⁵⁹ have studied the effect of functional group spacing along a polymer chain on the amount of intermolecular H-bonding that forms between a rigid and a flexible polymer. They studied a blend containing a rigid liquid crystalline polyether (DHMS-7,9) and flexible poly(styrene-co-4-vinylphenol) (PS-co-VPh). An increase in the amount of intermolecular hydrogen bonding as the amount of VPh in the PS-co-VPh decreases (and the spacing of the –OH groups increases) is observed in blends that consist of

7,9-dihydroxy methyl stilbene and PS-co-VPh copolymers that contain 10, 20, and 100 mole% VPh. Their results are in agreement with those of Coleman and Painter indicating that, even for systems with chains that differ in stiffness, spacing the hydroxyl groups apart on the copolymer chain produces a significant amount of, and may optimize the extent of, intermolecular H-bonding.

Coleman and Painter have also identified another important factor that affects the formation of intermolecular interactions. A flexible chain can bend back upon itself to avoid intermolecular interactions, thus inhibiting the formation of intermolecular interactions. This effect has been termed intramolecular screening. Coleman et al. have developed a method to account for this effect by correlating the screening effect caused by intrachain contacts to chain connectivity and chain flexibility.^{60,61} By introducing this screening parameter γ , they have shown improved agreement between theoretical and experimental phase diagrams relative to theoretical calculations that do not include the screening parameter. For example, their studies on blends containing poly(ethyl methacrylate-stat-4-vinylphenol) (EMAVPh, 55 wt.% VPh) and poly(ethylene oxide) (PEO) shows a larger disparity between the theoretical and experimental phase diagrams when the screening parameter is excluded from theoretical estimations than when it is included.⁶¹ They have obtained similar results examining EMAVPh blends with poly(ethylene oxide-stat-propylene oxide) copolymer. A recent work by Coleman and Painter has also examined the intramolecular screening effect in systems containing dendrimers.⁶² They have shown that intramolecular screening is less significant in hyperbranched polyesters with 2 generations than it is in hyperbranched polyesters with 5 generations.

1.3 Goals and Justifications

Polymer blends containing a liquid crystalline polymer and an amorphous polymer have a propensity to phase separate, but sufficient hydrogen bonding between two immiscible polymers may induce miscibility. Moreover, there exist a significant number of parameters that can be manipulated to optimize the extent of intermolecular hydrogen bonding, and thus the phase behavior of these mixtures. Therefore, in the quest to design and create a molecular composite reproducibly, an understanding of the relationship between these controllable parameters, the extent of intermolecular hydrogen bonding *and* the phase behavior of the mixtures containing an amorphous polymer and a LCP must be more clearly understood. Is it possible to form a miscible blend containing a LCP (rod-like) and an amorphous polymer (coil-like) by incorporating hydrogen bonding between the two components? If so, under what conditions might this be feasible? Previously, Painter et al.^{33,63} and Green et al.⁵⁴ have showed that a thermodynamically stable molecular composite can be found by incorporating hydrogen bonding between the LCP and amorphous polymer. However, a detailed study has not been attempted to provide guidelines by which miscible blends of LCP and amorphous polymers may be *designed* and created. Clearly, there should be a correlation between the extent of hydrogen bonding between two polymers and the phase behavior of their blend. This study presents data and experimental results that make this correlation.

To accomplish our goals, we have done a detailed study on a polymer mixture containing a liquid crystalline polyurethane (LCPU) and poly (styrene-co-4-vinyl phenol) (PS-co-VPh).^{64,65} We have shown how intermolecular H-bonding can be optimized between

the two polymers by systematically varying the PS-co-VPh copolymer composition. To be more specific, the amount of VPh units in the copolymer was varied to control the number of hydroxyl functional groups in the blend. By controlling the space between the hydroxyl groups along the copolymer chain, we have determined, using FT-IR technique, the amount of VPh in the copolymer that provides the optimum amount of intermolecular H-bonding in the blend. Using this information, it was demonstrated that the system with the optimum amount of intermolecular hydrogen bonding is also the system with the broadest miscible window.

Furthermore, we have extended the idea of optimizing intermolecular hydrogen bonding further by means of eliminating intramolecular H-bonding among the LCPU chains. This was accomplished by converting the N-H groups of the LCPU chains to N-CH₃ groups, thereby forming a N-methyl counterpart of the liquid crystalline polyurethane (LCPU-M).⁶⁶ This step helps to eliminate the possibility of C=O --- H-N hydrogen bonding among the LCP chains, and thereby, increases the number of C=O groups in the LCP available for intermolecular H-bonding. Therefore, this thesis will also present results of LCPU-M/PS-co-VPh blends and compare them to those of LCPU/PS-co-VPh blends to illustrate the effect of eliminating intramolecular H-bonding in LCP chains on the amount of intermolecular H-bonding and on the blend phase behavior. Finally, we have applied the association model developed by Painter et al. to these rod/coil polymer blends to demonstrate the correlation of theoretical phase diagrams determined by this model and experimental phase diagrams obtained by optical microscopy and DSC measurements.

Chapter 2

Creating Miscible Liquid Crystalline Polyurethane/

Poly(Styrene-co-4-Vinyl phenol) Blends

2.1 Introduction

In this chapter, a blend containing a liquid crystalline polyurethane (LCPU) and an amorphous copolymer that contains a monomer that can participate in hydrogen bonding (vinyl phenol, VPh) and one that cannot (styrene) has been examined [poly(styrene-co-4-vinylphenol) denoted as PS-co-VPh]. FT-IR has been used to determine the extent of intermolecular hydrogen bonding that occurs in the blend as a function of the spacing of the hydrogen bonding functional groups (as controlled by the composition of the copolymer). This data will then be related to the phase behavior of the blends to illustrate the correlation between the extent of intermolecular hydrogen bonding and blend miscibility of a molecular composite and provide guidelines by which these materials can be designed and produced.

2.2 Experimental

Materials

4,4-Biphenol and 2,4-toluene diisocyanate (TDI) were obtained from TCI America Inc, styrene, 4-acetoxystyrene and hydrazine hydrate were purchased from Aldrich Chemical Company, azobisisobutyronitrile (AIBN) was purchased from Dojac Inc, and sodium hydroxide, 6-chlorohexanol, methanol, dioxane, N,N'-dimethyl formamide (DMF), and 1-butanol were purchased from Fisher-Acros. Poly(4-vinylphenol) [PVPh] was purchased from

Polysciences Inc. In the polymerization of the liquid crystalline polyurethane (LCPU), DMF, 1-butanol and TDI were purified by vacuum distillation before use. All other chemicals were used as received.

Experimental Techniques

Molecular weights of the synthesized polymers were determined using a Waters Gel Permeation Chromatograph equipped with ultrastyrigel columns with a refractive index detector. DMF was used as elution solvent for the LCPU and tetrahydrofuran (THF) for the styrenic copolymers (PS-co-VPh). Narrowly dispersed polystyrene was used as calibration standard for both. Differential Scanning Calorimetry (DSC) measurements were completed to determine thermal properties of the polymers and blends and were run at 10 °C/min using a Mettler DSC 821 calibrated with Indium.

Structure and compositions of the LCPU and PS-co-VPh copolymers were determined by proton NMR spectroscopy on a 250 MHz Bruker NMR using TMS as an internal standard. The solvents for these NMR experiments were deuterated dimethylsulfoxide for the LCPU and deuterated chloroform for the PS-co-VPh copolymers.

Infrared spectra were obtained on a Biorad FTS-60A Fourier Transform Infrared (FT-IR) spectrometer purged with dried air using a minimum of 64 scans at a resolution of 2 cm⁻¹. The frequency scale was calibrated internally with a He-Ne reference to an accuracy of 0.2 cm⁻¹ and externally with polystyrene. Samples for FT-IR studies were obtained by solvent casting blends of LCPU and PS-co-VPh from DMF (2% w/v) on KBr disks at room temperature. The KBr disks were placed on a horizontal holder in a dessicator to reduce the evaporation rate and to avoid film cracking. After evaporating most of the solvent at room

temperature, the disks were subsequently dried in a vacuum oven at 60 °C for 3 days to remove residual solvent and moisture. The absence of solvent in the sample was verified by the absence of the C=O peak of DMF which occurs at 1650 cm⁻¹ in the IR curve, which occurs at a lower wavenumber than the C=O peak of the LCPU (1730 cm⁻¹). The films prepared for FT-IR were adequately thin to be within an absorbance range where the Beer-Lambert law is satisfied. High temperature spectra were obtained using a cell mounted in the spectrometer connected to a temperature controller. The temperature was controlled to an accuracy of 0.5°C. The samples were kept constant at the set temperature for 15 min., in order for the sample to attain that temperature, before obtaining the “as-cast, heat-treated” data.

Phase behavior data of the blends was obtained by preparing 2% (w/v) solutions of the blend in DMF and spotting them on a microscope slide. The solvent was allowed to evaporate in a dessicator first and then overnight in a vacuum oven at 60°C to remove residual solvent. The phase behavior of the blends were monitored by phase contrast and polarized optical microscopy using an Olympus BH-2 optical microscope equipped with a Mettler FP82HT hot stage.

Polymer Synthesis and Characterization

The liquid crystalline polyurethane was synthesized by the condensation of 4,4'-bis(6-hydroxyhexoxy) biphenyl (BHHBP) and 2,4-toluene diisocyanate (2,4-TDI) (see Figure 1).⁶⁷ The procedure for the synthesis of the liquid crystalline polyurethane are shown below:

Synthesis of the Diol (BHHBP)

Sodium hydroxide (32.00 g, 0.800 mol) and 4,4'-dihydroxybiphenyl (37.2 g, 0.200

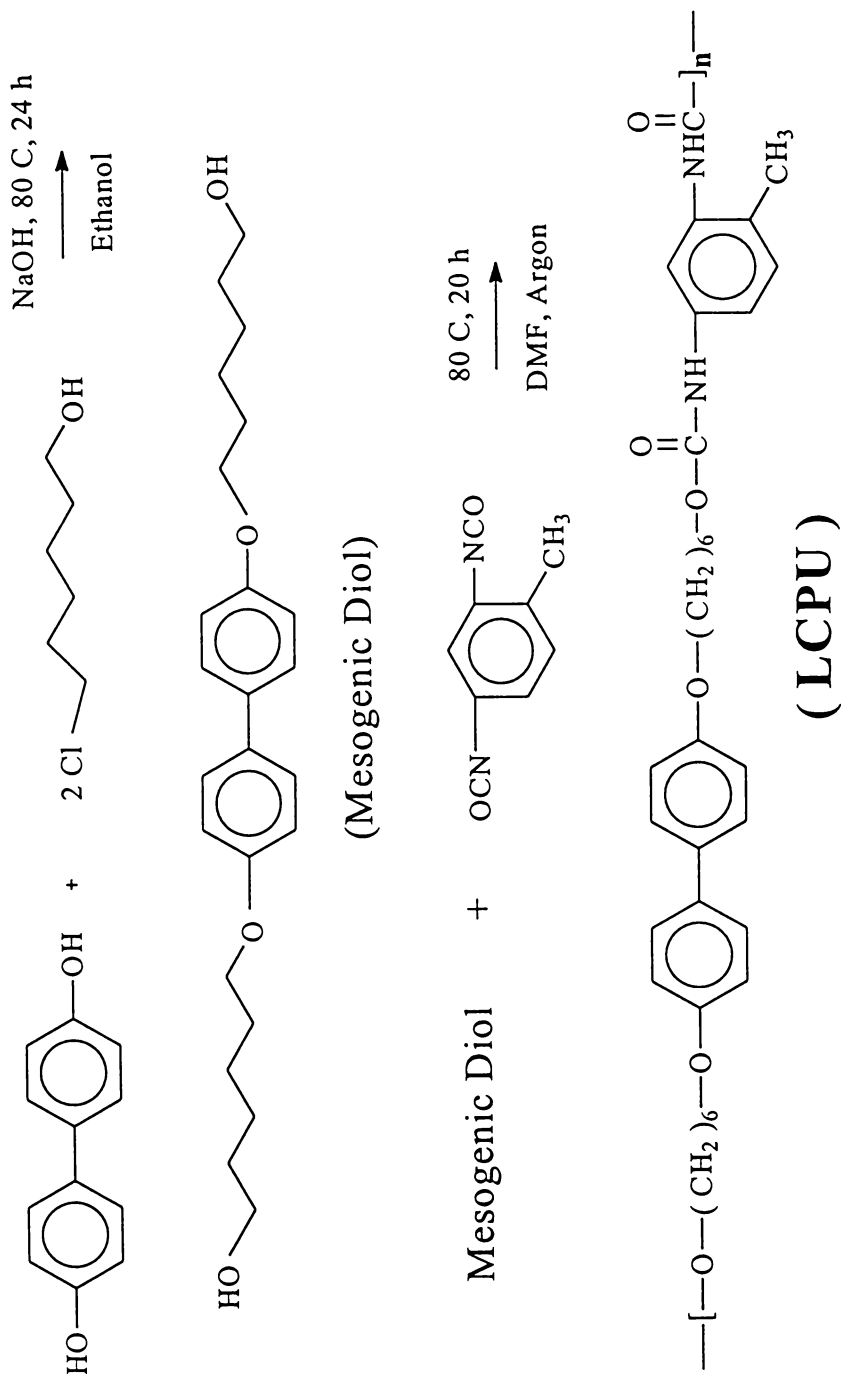


Figure 1. Synthesis of the Liquid Crystalline Polyurethane (LCPU) used in this study

mol) were stirred into 400 mL of ethanol. The resulting slurry was heated under reflux, and 6-chlorohexanol (120.2 g, 0.880 mol) was added dropwise. The reaction mixture was refluxed for 24 h and poured into cold water. The precipitated solid was filtered and recrystallized twice, first from a 3:1 mixture of ethanol and DMF and then from 1-butanol, to give 70.8 g BHHBP, yield 89%, mp 152°C.

Synthesis of the Liquid Crystalline Polyurethane (LCPU)

LCPU was synthesized by the reaction of BHHBP with 2,4-TDI. A slight excess (0.5-1.0%) of the latter was used to compensate for side reactions involving isocyanate groups. BHHBP (67.98 g, 0.1759 mol) was dissolved in 200 mL of DMF in a heat-dried five-necked round-bottom flask with a condenser, mechanical stirrer, thermometer, and additional funnels charged with DMF and 2,4-TDI. Nitrogen was kept flowing through the system continuously. 2,4-TDI (30.90 g, 0.1774 mol) was added dropwise to the solution, and the temperature was raised to 80°C and held there for 20 h. As the reaction proceeded, DMF was added as needed to keep the solution viscosity low enough to allow stirring. By the end of the reaction period, 500 mL of additional DMF had been added. The hot viscous solution was poured into cold methanol to precipitate the polymer in the form of a white, fibrous material. The polymer was filtered, washed with fresh methanol, and subsequently dried under vacuum at 90°C for 72 h. The yield was 80.7 g (82.5%). ¹H NMR (see Figures 2 and 3) (reported as chemical shift, multiplicity, integration, assignment) [δ 9.51 (s, 1H, a), 8.75 (s, 1H, b), 7.47 (m, 5H, c), 6.96 (m, 6H, d), 3.96 (m, 8H, e), 2.09 (s, 3H, f), 1.65 (m, 8H, g), 1.40 (m, 8H, h)]. IR peaks (see Figure 4): ν N-H (~3200 cm⁻¹), ν C=O (~1730 cm⁻¹), δ N-H (~1500 cm⁻¹).

Synthesis of Poly(styrene-co-4-vinyl phenol) copolymers

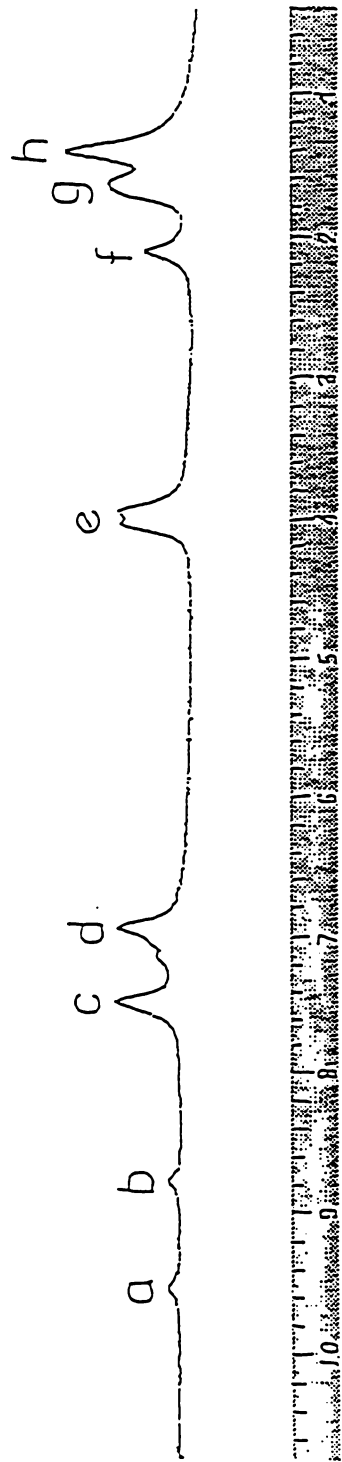


Figure 2. Characteristic Proton NMR spectra of pure LCPU. Lower case letters refer to Proton NMR results (see also Figure 3)

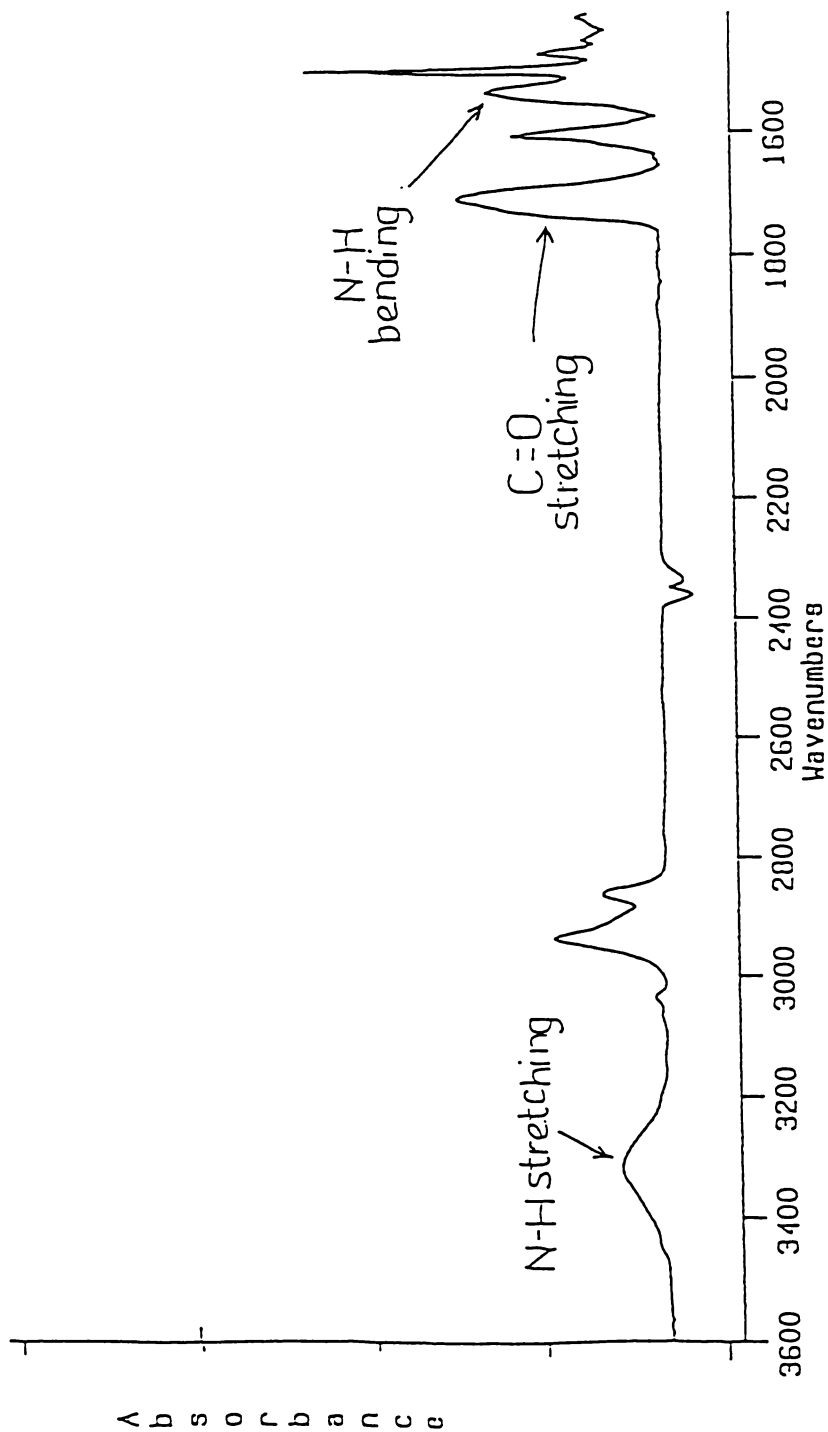


Figure 4. FT-IR spectra of pure LCPU measured at 30°C upon cooling from the melt

Poly(styrene-co-4-vinyl phenol) (PS-co-VPh) random copolymers were prepared by the free radical polymerization of styrene and 4-acetoxy styrene using AIBN as the initiator followed by the hydrolysis of the acetoxy groups using hydrazine hydrate according to the procedure of Green and Khatri⁵⁴ (see Figure 5). Copolymers containing 5, 10, 20, 30, 40 and 50 mole percent vinyl phenol were synthesized and utilized in this study. Hereinafter, PS-co-VPh(*n*) denotes a PS-co-VPh copolymer with *n* mole % VPh. As an example, the procedure for the synthesis of PS-co-VPh(10) is shown below.

Synthesis of PS-co-VPh(10)

First, styrene (2.7 mL, 23.56 mmole), 4-acetoxy styrene (0.4 mL, 2.62 mmole) and AIBN (0.0104 g) were transferred into a 3-neck round-bottom flask filled with dioxane (50 mL) under a mild flow of argon. The flask equipped with a water-jacketed condenser was heated at 60°C for 18 h. The solution was then poured into methanol to precipitate the poly(styrene-co-4-acetoxy styrene) as the product. The polymer was dried in a vacuum oven for a day (yield 82%). ¹H NMR spectra of the different copolymer compositions of poly(styrene-co-4-acetoxy styrene) are shown in Figures 6-11. ¹H NMR peak assignments: 1.4 ppm (2H, d, CH₂); 1.7 ppm (1H, t, CH); 2.2 ppm (3H, s, CH₃); 6.2-7.2 ppm (9H, m, aromatic H). Acetoxy styrene groups are randomly distributed in the copolymer chain as the reactivity ratios of styrene and 4-acetoxy styrene are $r_1 = 0.8$ and $r_2 = 1.02$.⁵⁵

Next, the hydrolysis of acetoxy groups to hydroxyl groups was carried out by the dissolution of 2 g of poly(styrene-co-4-acetoxy styrene) in dioxane (40 mL) in a round-bottom flask.⁶⁸ Hydrazine hydrate (6 mL) was then added to this solution and stirred for 40 h at room temperature. The polymer was precipitated into methanol and dried in a vacuum

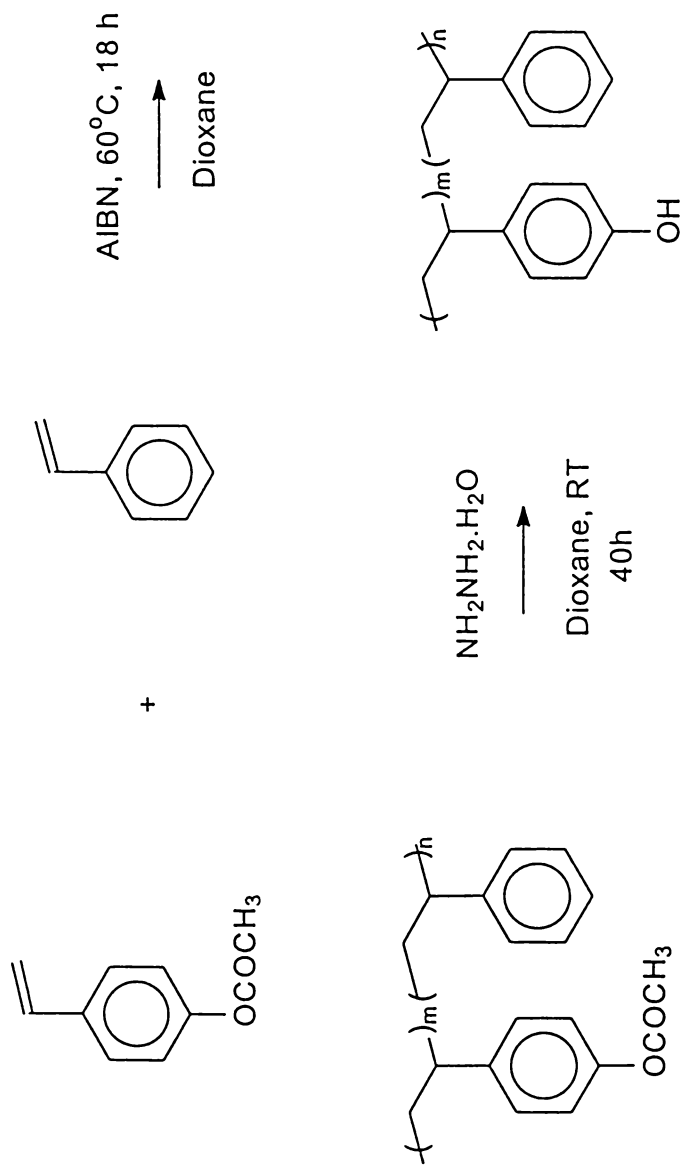


Figure 5. Synthesis of Poly(Styrene-co-4-Vinyl phenol) (PS-co-VPh) copolymer used in this study

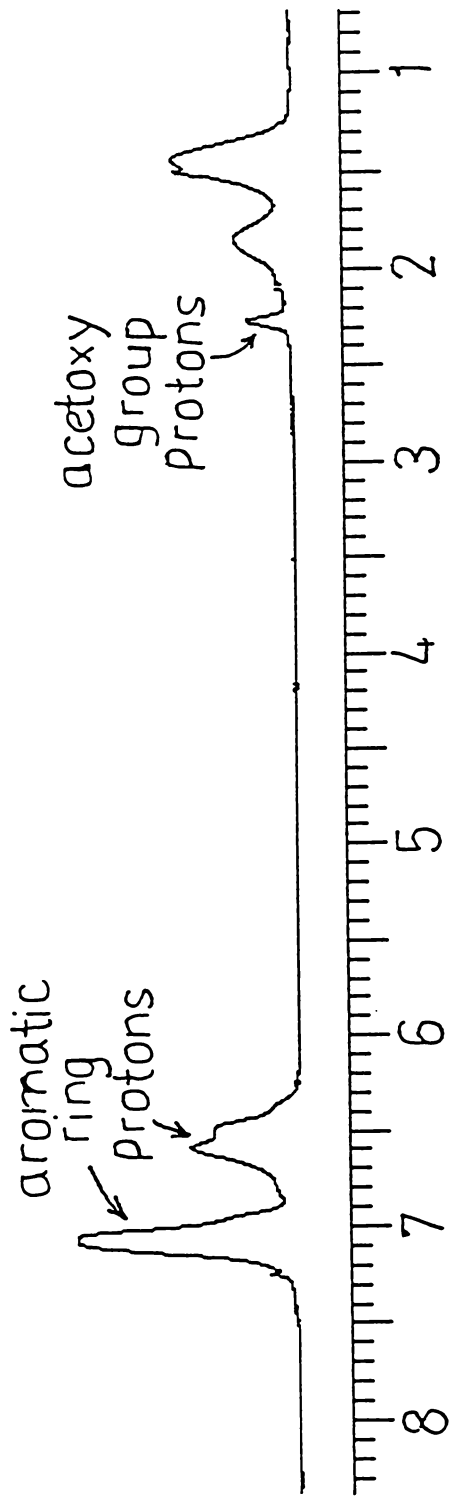


Figure 6. Characteristic $^1\text{H-NMR}$ spectra of Poly(Styrene-co-4-Acetoxystyrene) containing 5 mol% 4-acetoxy styrene.

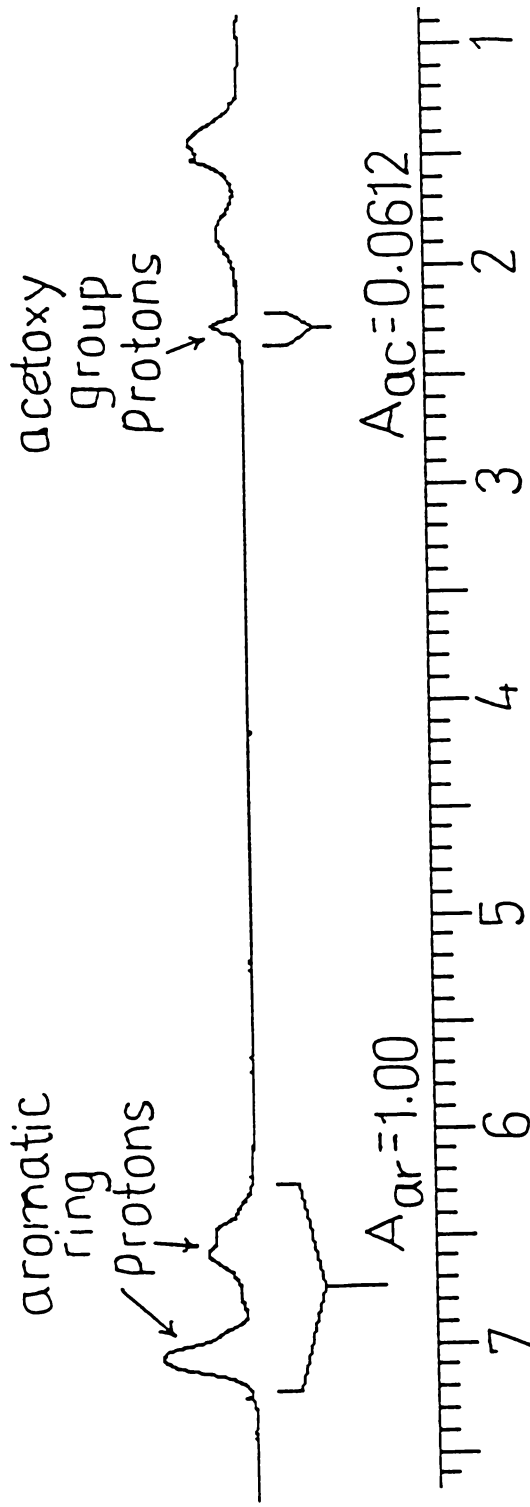


Figure 7. Characteristic $^1\text{H-NMR}$ spectra of Poly(Styrene-co-4-Acetoxy styrene) containing 10 mol% 4-acetoxy styrene.

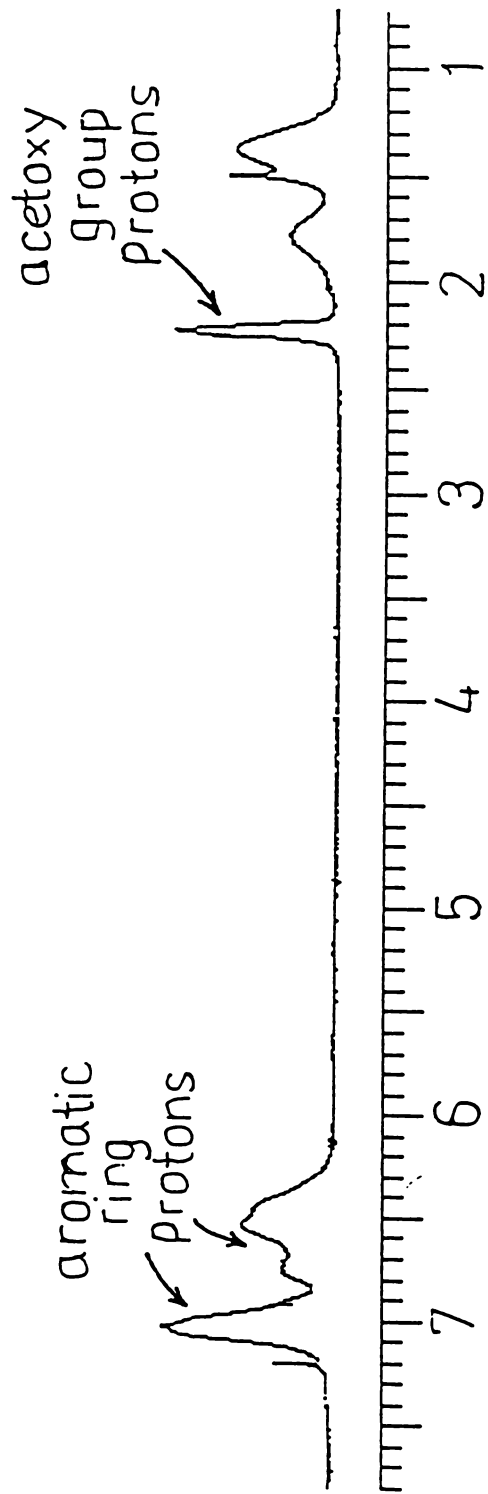


Figure 8. Characteristic ¹H-NMR spectra of Poly(Styrene-co-4-Acetoxystyrene) containing 20 mol% 4-acetoxy styrene.

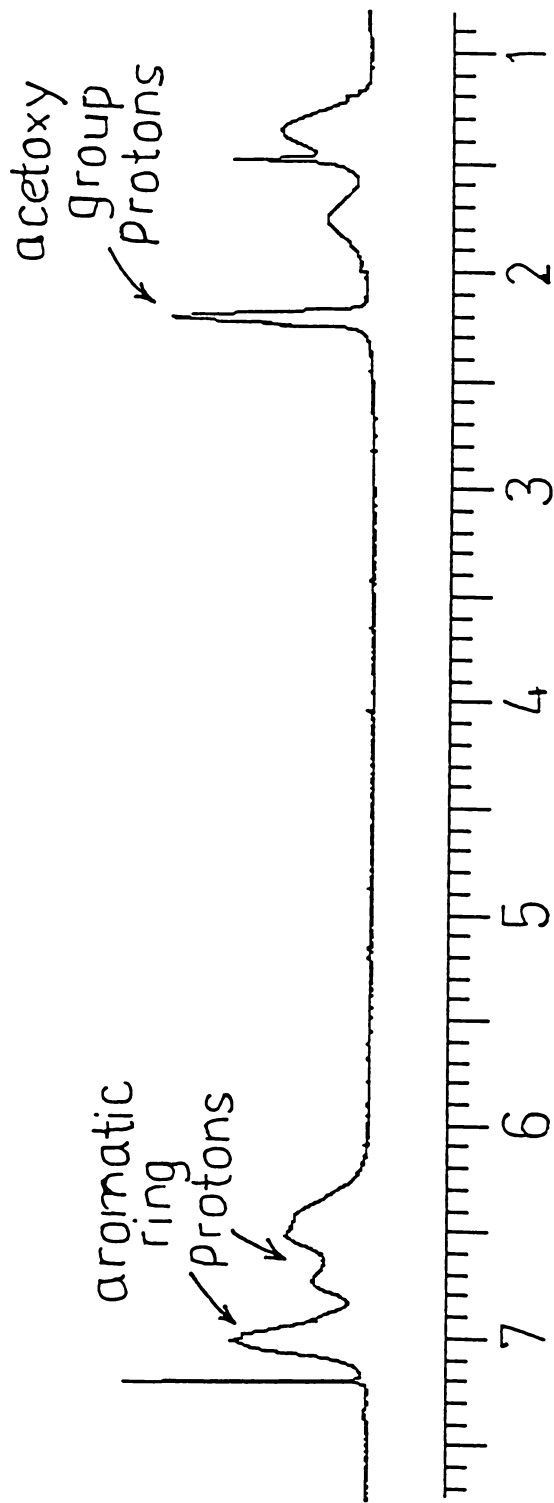


Figure 9. Characteristic $^1\text{H-NMR}$ spectra of Poly(styrene-co-4-Acetoxystyrene) containing 30 mol% 4-acetoxystyrene.

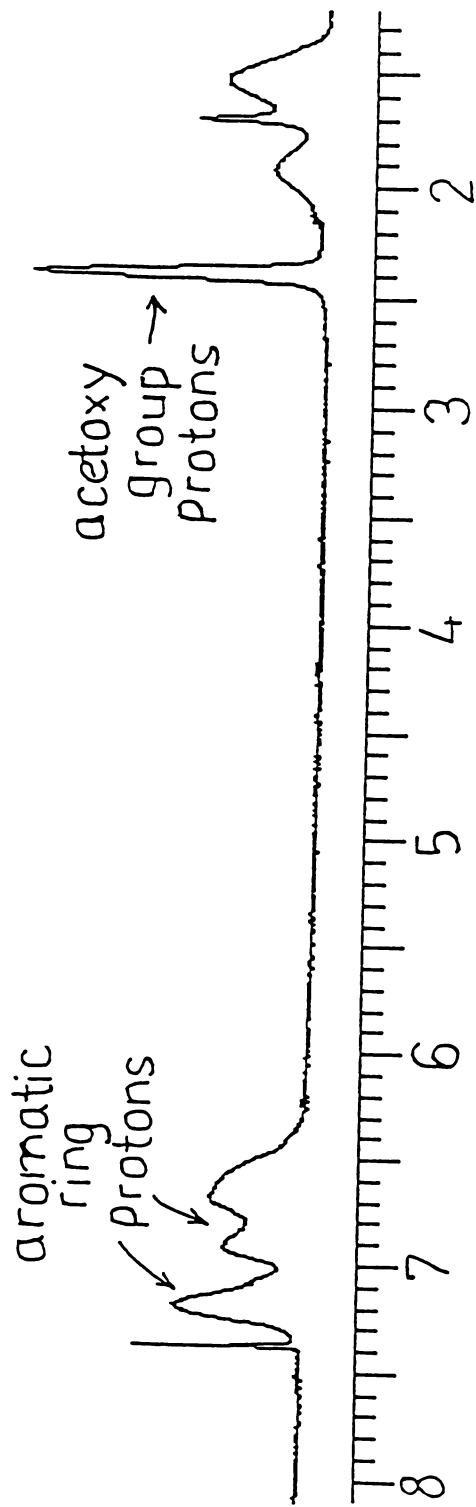


Figure 10. Characteristic $^1\text{H-NMR}$ spectra of Poly(styrene-co-4-Acetoxystyrene) containing 40 mol% 4-acetoxy styrene.

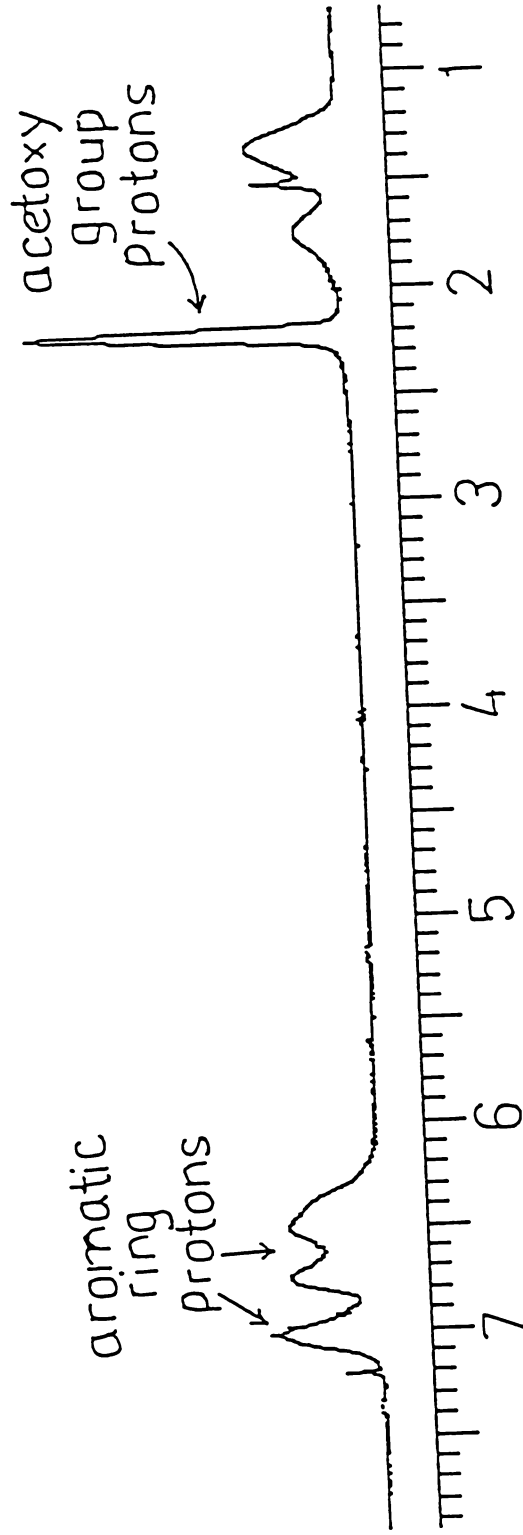


Figure 11. Characteristic $^1\text{H-NMR}$ spectra of Poly(styrene-co-4-Aceloxystyrene) containing 50 mol% 4-accloxy styrene.

oven for 24 h. The completion of hydrolysis was verified by the disappearance of the methyl peak of acetoxy group at 2.2 ppm in the NMR spectrum (see Figure 12).

The composition of PS-co-VPh(10) copolymer is then determined by integration of NMR spectra shown in Figure 7, using the method of Coleman et al.⁶⁹ and Radmard.⁷⁰ In this procedure, the area of the methyl group in the acetoxy group (ca. 2.2 ppm) is compared to the area of the aromatic hydrogens (ca. 6.2-7.2 ppm). The NMR line at 2.2 ppm corresponds to the 3 protons present in the methyl substituent of the acetoxy group. Therefore, the normalized area per proton corresponding to the acetoxy styrene chemical repeat may be determined as:

$$A_{ac} = \text{Area of 2.2 ppm line} / 3 \quad (2.1)$$

Now, the normalized area per proton corresponding to the styrene chemical repeat is required. But there is no isolated NMR line in the spectrum that is solely characteristic of styrene repeat unit, since the relatively broad peak appearing between 6.2 and 7.2 ppm corresponds to the aromatic protons that occur in styrene and acetoxy styrene units which is designated as A_{ar} . To solve this problem, the total area (which reflects the contribution from the 5 aromatic protons of the styrene repeat and the 4 aromatic protons of the acetoxy styrene repeat) is measured, the contribution from the acetoxy styrene repeat (i.e., 4 times the normalized area per proton calculated as A_{ac}) is subtracted out from this total area and then the obtained value is divided by 5 (the number of aromatic protons in the styrene repeat). This corresponds to the normalized area per proton of styrene chemical repeat.

$$A_{sty} = [A_{ar} - 4 A_{ac}] / 5 \quad (2.2)$$

Thus, the mole fraction of styrene in the copolymer is simply given by:

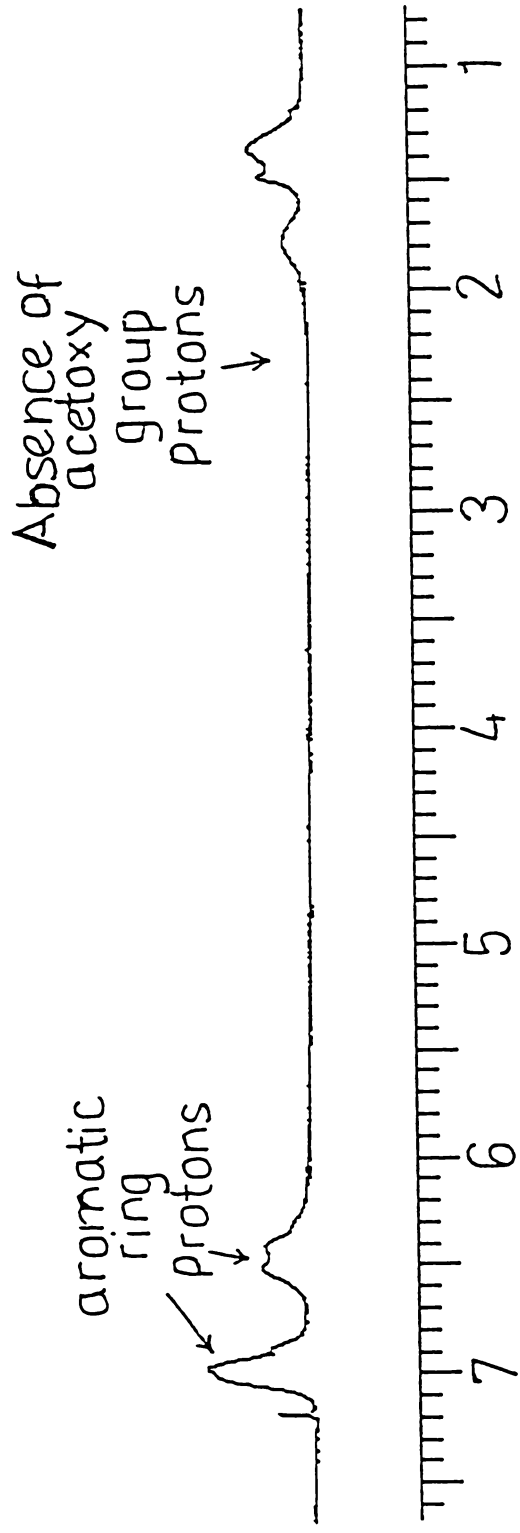


Figure 12. Characteristic ¹H-NMR spectra of Poly(styrene-co-4-Vinylphenol).

$$\pi_{sty} = \frac{A_{sty}}{A_{sty} + A_{ac}} \quad (2.3)$$

The NMR spectra, after the hydrolysis step, indicate that the acetoxy styrene units in the copolymer chain have been completely converted to vinyl phenol units. Therefore, it is reasonable to assume the mole fraction of acetoxy styrene in the copolymer for the mole fraction of vinyl phenol units, which is $(1 - \pi_{sty})$. The mole percent of vinyl phenol in the synthesized PS-co-VPh(10) copolymer, calculated this way, was found to be 10.01% (yield 80%).

DSC results of the LCPU and PS-co-VPh are shown in Figure 13 and Figure 14, respectively, and GPC data are shown in the Appendix. The molecular weight and the phase transition temperatures of the LCPU and the different PS-co-VPh copolymer compositions are reported in Table 1.

2.3 Results and Discussion

FT-IR Studies

The aim of this study is to understand the correlation between the copolymer composition, the extent of intermolecular hydrogen bonding in a blend containing a liquid crystalline polymer and an amorphous copolymer, and the phase behavior of that blend. The structure of the LCPU and PS-co-VPh are already shown in Figures 3 and 5 and the scheme of hydrogen bonding in LCPU/PS-co-VPh blends is shown in Figure 15. To determine the amount of intermolecular H-bonding between the two blend components, FT-IR was used to evaluate the carbonyl stretching vibration around 1700 cm^{-1} . The deconvolution of the absorbance IR peaks was performed by Peakfit software version 3.0 with baseline correction.

Table 1. Molecular weights and Phase Transitions of Liquid Crystalline Polyurethane (LCPU), N-methyl Liquid Crystalline Polyurethane (LCPU-M) and Poly(Styrene-co-4-Vinyl phenol) (PS-co-VPh) Copolymers.

| Polymer | Molecular weight (g/mol) | | Phase Transition Temperature (°C) | | |
|---------------|-----------------------------|--------|--------------------------------------|-----|-----|
| | Mn | Mw | Tg | Tm | Ti |
| Pure LCPU | 35,000 | 53,600 | 87 | 132 | 160 |
| Pure LCPU-M | 37,000 | 56,700 | 72 | 117 | 134 |
| PS-co-VPh(5) | 13,700 | 21,300 | 101 | - | - |
| PS-co-VPh(10) | 20,700 | 34,500 | 103 | - | - |
| PS-co-VPh(20) | 47,100 | 90,100 | 105 | - | - |
| PS-co-VPh(30) | 22,100 | 32,400 | 108 | - | - |
| PS-co-VPh(40) | 31,300 | 61,100 | 114 | - | - |
| PS-co-VPh(50) | 34,100 | 65,200 | 116 | - | - |
| Pure PVPh | 22,000 | - | 147 | - | - |

T_m = crystalline melt temperature, T_i = nematic to isotropic transition temperature

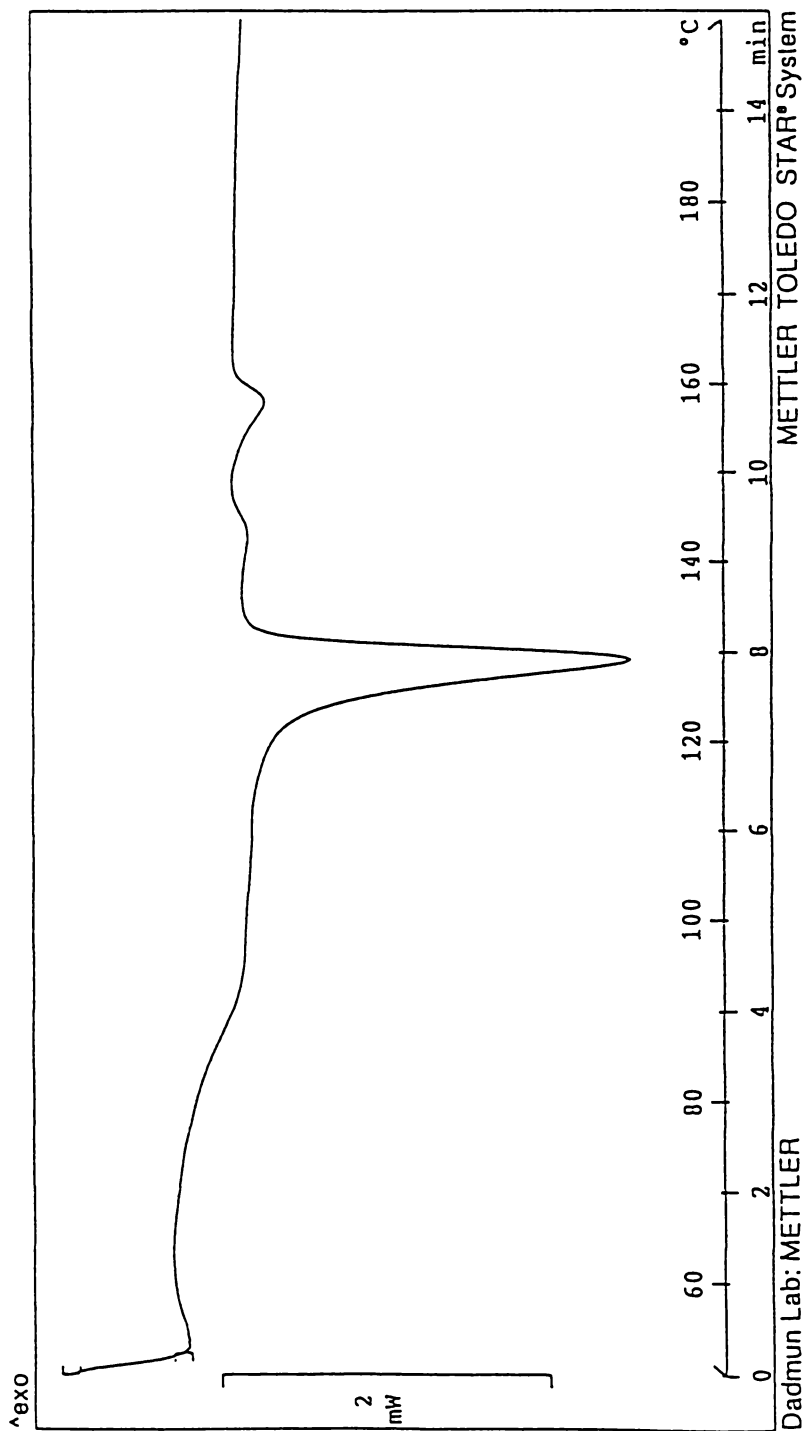


Figure 13. DSC curve of pure LCPU.

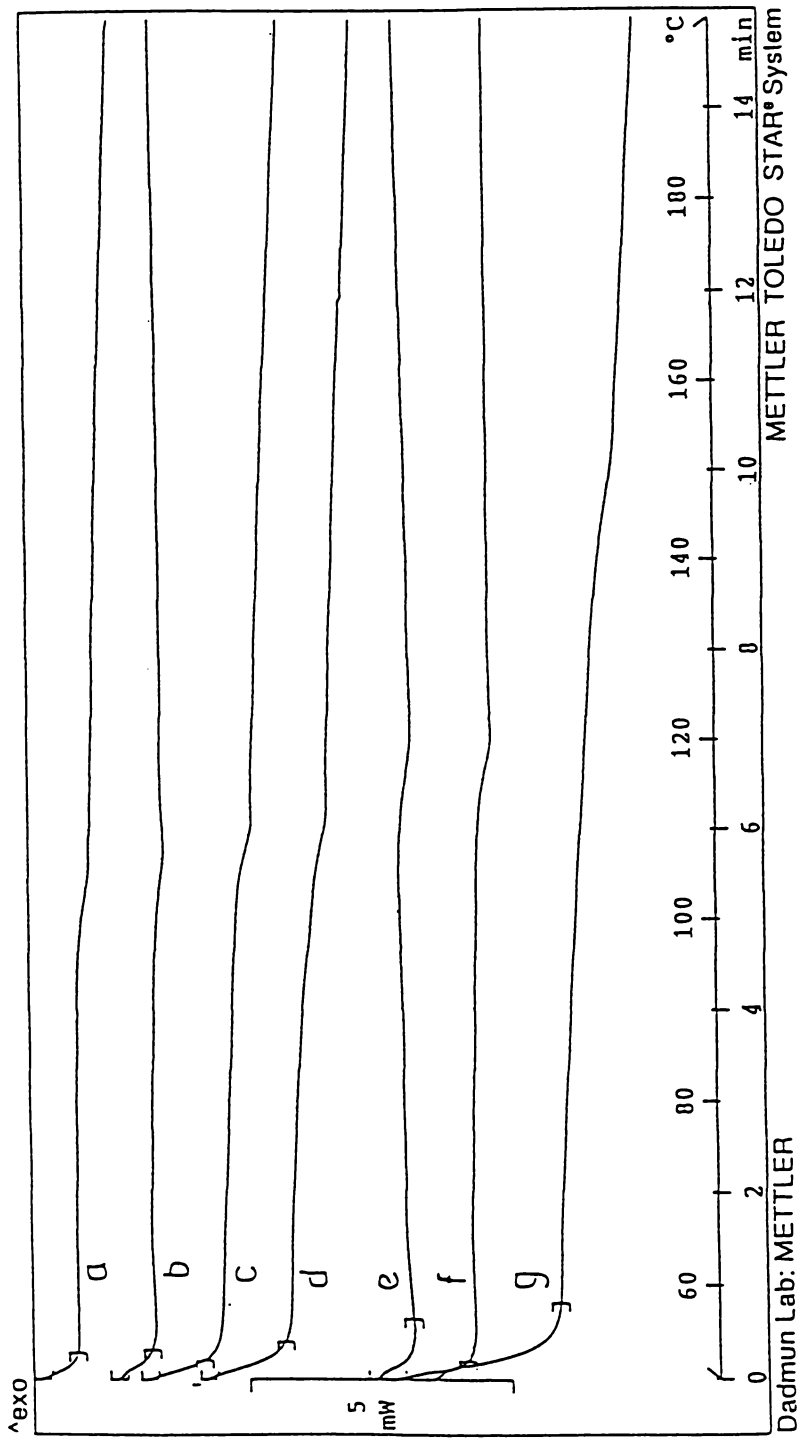
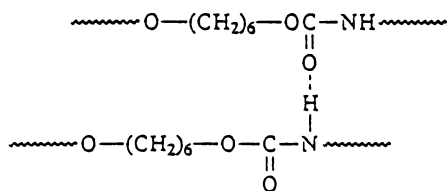


Figure 14. DSC curves of (a) PS-co-VPh (5 mol% VPh) (b) PS-co-VPh (10 mol% VPh) (c) PS-co-VPh (20 mol% VPh) (d) PS-co-VPh (30 mol% VPh) (e) PS-co-VPh (40 mol% VPh) (f) PS-co-VPh (50 mol% VPh) (g) pure PVPh.

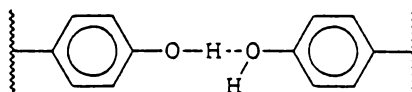
Hydrogen Bonding in
LCPU/PS-co-VPh Blends

Intramolecular H-bonding
in LCPU

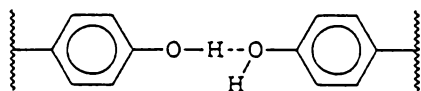


Hydrogen Bonding in
LCPU-M/PS-co-VPh Blends

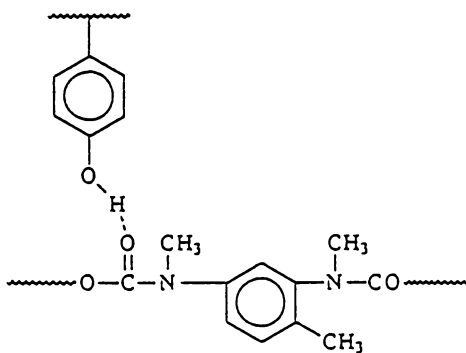
Intramolecular H-bonding
in copolymer



Intramolecular H-bonding
in copolymer



Intermolecular H-bonding in
N-methyl LCPU/copolymer blends



Intermolecular H-bonding
in LCPU/Copolymer blends

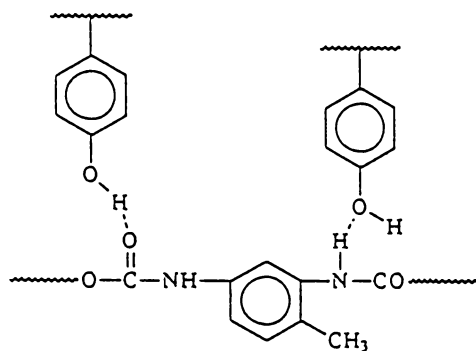


Figure 15. Possible hydrogen bonding associations in LCPU/PS-co-VPh blends and LCPU-M/PS-co-VPh blends.

It is well known that the C=O bond strength decreases upon hydrogen bonding. In order to interpret the deconvolution peaks that comprise the C=O stretching band of the LCPU/PS-co-VPh blends, a prior understanding of the C=O stretching band of pure LCPU is required. Deconvolution of the C=O stretching band of pure LCPU at 30°C reveals three peaks that are assigned to free C=O groups (around 1730 cm⁻¹), disordered (amorphous) domain (around 1690 cm⁻¹) and ordered (crystalline) domain (around 1670 cm⁻¹) of hydrogen bonded C=O groups (to N-H groups). Temperature studies of the pure LCPU and its blends were carried out from 30°C to 180°C (heating cycle) and back to 30°C (cooling cycle) in order to study their thermal response. IR plots showing the representative curves of heating and cooling cycles of the pure LCPU are shown in Figure 16. Deconvolution of the heating cycle curve of pure LCPU reveals: an increase in the free C=O peak, a decrease in disordered H-bonded C=O peak (along with a wavenumber shift from 1690 cm⁻¹ to 1695 cm⁻¹) and a decrease in ordered H-bonded C=O peak (that disappears above 130°C, giving way to a broad band composed of free and disordered H-bonded C=O peaks). Deconvolution of the cooling cycle curve shows a reversed trend except for the ordered H-bonded component which appears at about 120°C. Deconvolution of the curves of the pure LCPU sample at 180°C and the cooled-from-melt sample at 30°C are shown in Figure 17. Deconvolution results of the cooling cycle curve of pure LCPU are shown as a temperature versus area plot in Figure 18. This plot shows a decrease in the free C=O area at the expense of an increase in the H-bonded C=O area, and the appearance of an ordered H-bonded C=O at 120°C indicating crystallization of the sample at this temperature.

Deconvolution of the C=O stretching band of LCPU/PS-co-VPh blends was

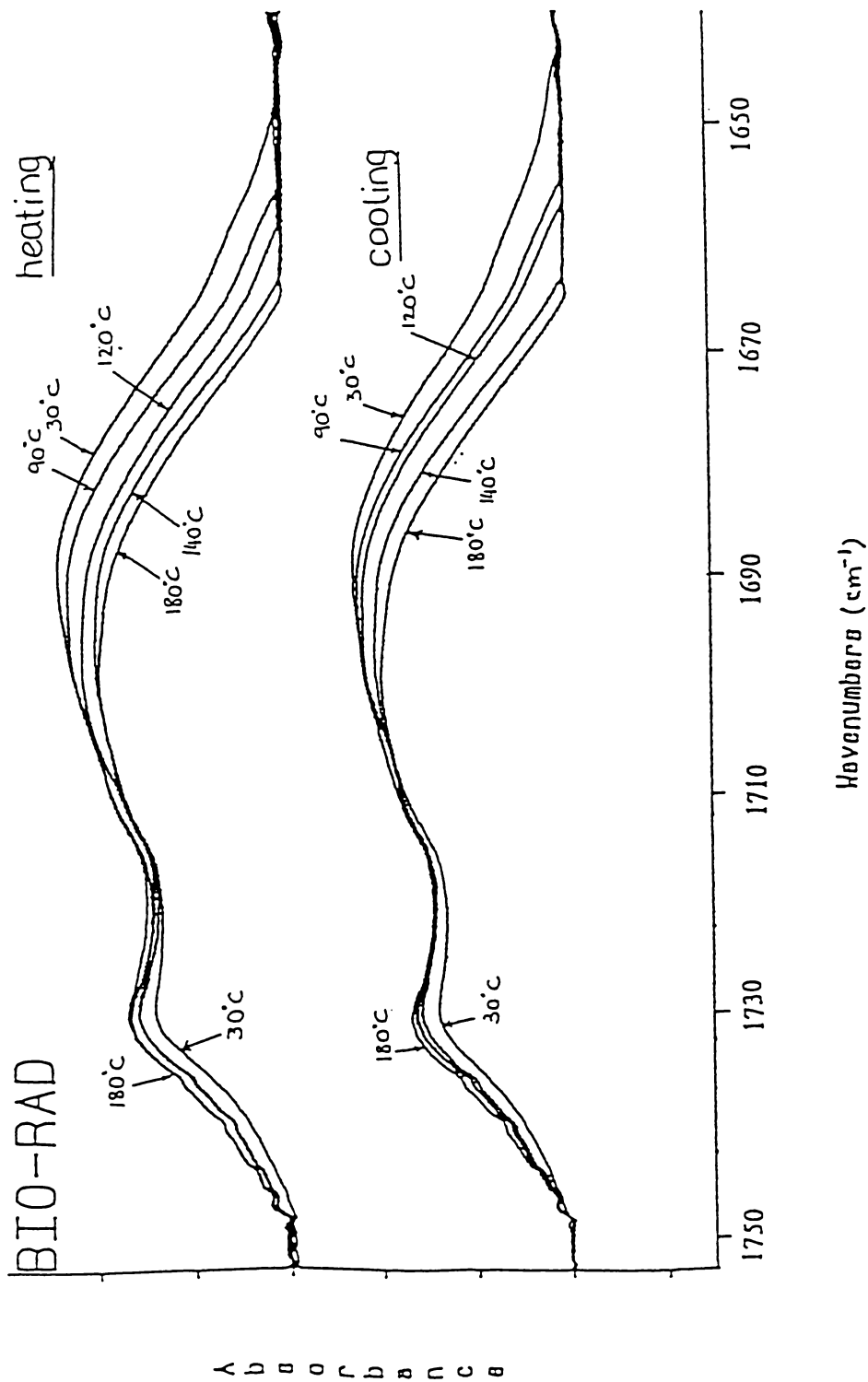


Figure 16. FT-IR spectra of C=O stretching region for pure LCPU as a function of temperature.

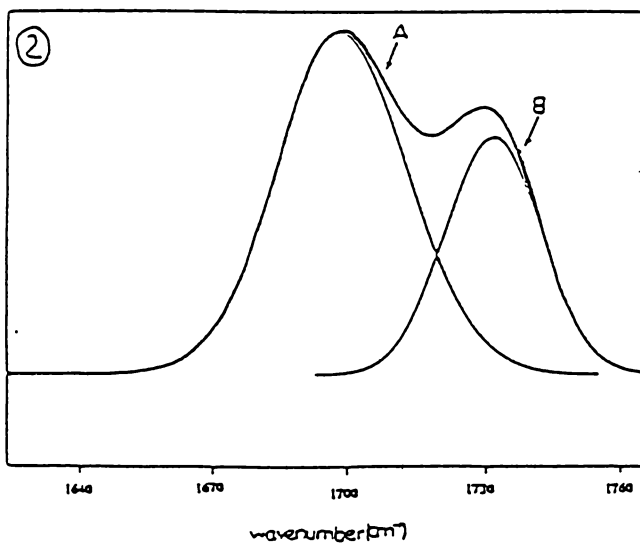
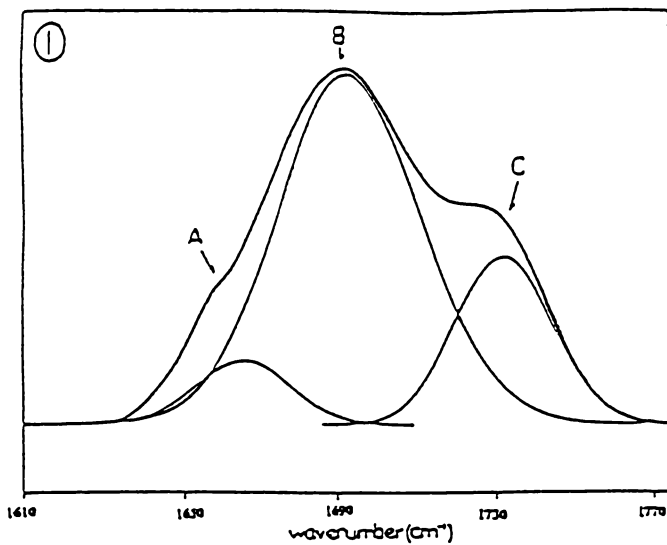


Figure 17. Example of results of the deconvolution procedure for the carbonyl stretching regime of FT-IR spectra of pure LCPU measured at 1) 30°C (upon cooling) 2) 180°C.

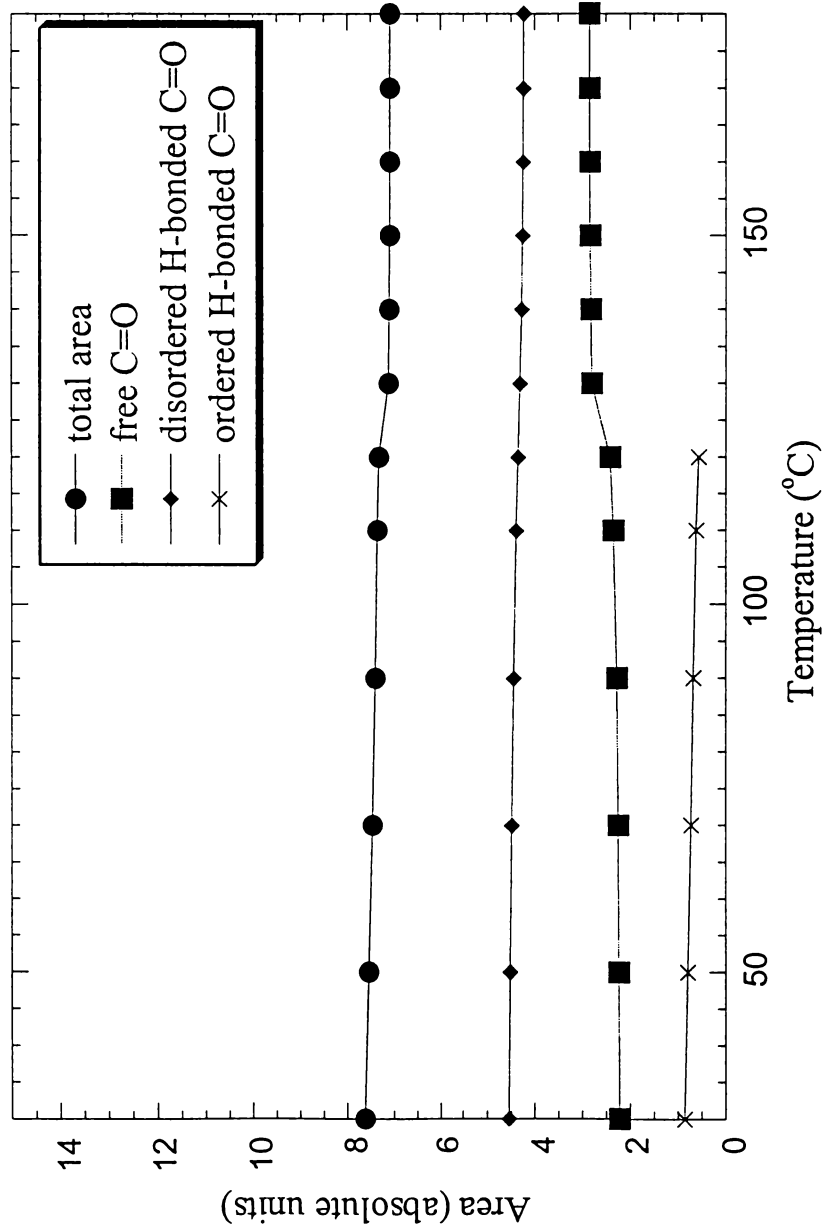


Figure 18. Area plots corresponding to the contributing peaks of pure LCPU obtained from deconvolution of C=O stretching band of the FT-IR spectra upon cooling from 180°C to 30°C

completed for samples at 180°C. It is well known that blends that are formed by solvent casting often don't represent equilibrium structures due to varying polymer-solvent interactions among the blend constituents. By obtaining data at 180°C (above the T_g and T_m of the blend components), the samples were allowed to reach equilibrium conditions, in contrast to the non-equilibrium condition that would exist in as-cast samples. Deconvoluted peaks thus obtained show three peaks that are assigned to free (non-hydrogen bonded) carbonyl groups [around 1730 cm^{-1}], intermolecularly hydrogen bonded C=O groups (to O-H groups) [around 1715 cm^{-1}] and intramolecularly hydrogen bonded C=O groups (to N-H groups) [around 1695 cm^{-1}]. Analysis of these peaks provides a mechanism to determine the percentage of carbonyl groups in the system that participate in intermolecular hydrogen bonding.⁷¹ However, the percentage of hydroxyl groups on the styrenic copolymer that intermolecularly hydrogen bond to the LCPU can not be quantitatively determined by deconvoluting the O-H stretching band at 3300 cm^{-1} . This is primarily due to the hydroxyl region not being as easily amenable for quantitative evaluation because of vibration overlap of all the contributing peaks thus giving rise to a very broad O-H peak.⁷¹ Also, this O-H peak is plagued by the presence of the overtone of the fundamental C=O stretching vibration.⁷² In addition to these, in LCPU blends there is the presence of the overlap between the N-H and the O-H stretching bands. Therefore, the amount of OH that is participating in intermolecular hydrogen bonding is determined stoichiometrically as described below.

Stoichiometric Estimation of Percent O-H Intermolecularly Hydrogen Bonded to C=O

First, the number of carbonyl and hydroxyl units in the blend is estimated from the molecular weights of LCPU and PS-co-VPh and the composition of the LCPU/PS-co-VPh

blend system. It is important to note here that the molecular weights of the copolymers used in this study are different for different copolymer compositions (see Table 1). Therefore, the number of C=O and O-H units in the blend is determined individually for every set of blend composition and copolymer composition. The percentage of hydroxyl groups that participate in intermolecular hydrogen bonding is then determined by dividing the percentage of carbonyl groups participating in hydrogen bonding by the ratio of the number of hydroxyl groups to carbonyl groups present in the blend. This procedure is shown mathematically as

$$\Gamma(\text{OH}) = \Gamma(\text{C=O}) / (N_{\text{OH}}/N_{\text{C=O}}) \quad (2.4)$$

where $\Gamma(\text{OH})$ is the percentage of hydroxyl groups that are participating in intermolecular hydrogen bonding, $\Gamma(\text{C=O})$ is the percentage of carbonyl groups that are participating in intermolecular hydrogen bonding, N_{OH} is the total number of hydroxyl groups present in the blend and $N_{\text{C=O}}$ is the total number of carbonyl groups present in the blend.

Stoichiometric Estimation of $N_{\text{OH}}/N_{\text{C=O}}$

a) $N_{\text{C=O}}$ Estimation:

The number of C=O groups per unit weight of the LCPU/PS-co-VPh blend, $N_{\text{C=O}}$, is given by

$$N_{\text{C=O}} = (\phi_{\text{C=O}} \cdot \phi_{\text{LCPU}}) \quad (2.5)$$

where ϕ_{LCPU} is the number of LCPU chains per unit weight of the blend and $\phi_{\text{C=O}}$ is the number of C=O groups per LCPU chain.

The number of LCPU chains per unit weight of the blend (ϕ_{LCPU}) is given by

$$\phi_{\text{LCPU}} = \left(\frac{W_1}{M_{\text{LCPU}}} \right) \quad (2.6)$$

where W_1 is the weight fraction of the LCPU in the blend (i.e., blend composition) and M_{LCPU} is the molecular weight of the LCPU.

The number of C=O groups per LCPU chain ($\phi_{C=O}$) is given by

$$\phi_{C=O} = (\phi_{C=O}^* \cdot \phi_{monomer}) \quad (2.7)$$

where $\phi_{C=O}^*$ is the number of C=O groups per LCPU monomer and $\phi_{monomer}$ is the number of LCPU monomers per LCPU polymer chain.

Substituting Equations 2.6 and 2.7 in Equation 2.5,

$$N_{C=O} = \left(\frac{W_1}{M_{LCPU}} \right) (\phi_{C=O}^* \cdot \phi_{monomer}) \quad (2.8)$$

b) N_{O-H} Estimation:

The number of O-H groups per unit weight of the blend, N_{O-H} , is given by

$$N_{O-H} = (\phi_{PS-co-VPh} \cdot \phi_{O-H}) \quad (2.9)$$

where $\phi_{PS-co-VPh}$ is the number of PS-co-VPh chains per unit weight of the blend and ϕ_{O-H} is the number of O-H groups per PS-co-VPh.

The number of PS-co-VPh chains per unit weight of the blend ($\phi_{PS-co-VPh}$) is given by

$$\phi_{PS-co-VPh} = \left(\frac{W_2}{M_{PS-co-VPh}} \right) \quad (2.10)$$

where W_2 is the weight fraction of PS-co-VPh in the blend ($W_2 = 1 - W_1$) and $M_{PS-co-VPh}$ is the molecular weight of PS-co-VPh.

Since the number of hydroxyl (O-H) groups, ϕ_{O-H} is the same as the number of 4-vinyl phenol (VPh) groups, ϕ_{VPh} in every PS-co-VPh chain, we refer to ϕ_{VPh} as ϕ_{O-H} here for

the sake of convenience. ϕ_{O-H} is given by

$$\phi_{O-H} = \left(\frac{\psi_{VPh} \cdot M_{PS-co-VPh}}{M_{VPh}} \right) \quad (2.11)$$

where ψ_{VPh} is the weight fraction of 4-vinyl phenol in PS-co-VPh, $M_{PS-co-VPh}$ is the molecular weight of PS-co-VPh and M_{VPh} is the molecular weight of 4-vinyl phenol.

The weight fraction of 4-vinyl phenol (ψ_{VPh}) can be determined from the mole fraction of styrene in PS-co-VPh (π_{sty}) as shown in the equation below. The determination of π_{sty} of the copolymer using Proton-NMR characterization technique has already been discussed in the experimental part of this chapter.

$$\psi_{VPh} = \frac{M_{VPh} (1 - \pi_{sty})}{M_s \pi_{sty} + M_{VPh} (1 - \pi_{sty})} \quad (2.12)$$

where M_s is the molecular weight of Styrene (104 g/mol) and M_{VPh} is the molecular weight of 4-vinyl phenol (120 g/mol).

Substituting Equations 2.10 and 2.11 in Equation 2.9,

$$\begin{aligned} N_{O-H} &= \left(\frac{W_2}{M_{PS-co-VPh}} \right) \left(\frac{\psi_{VPh} \cdot M_{PS-co-VPh}}{M_{VPh}} \right) \\ &= \left(\frac{W_2}{M_{PS-co-VPh}} \right) \left(\frac{M_{VPh} (1 - \pi_{sty})}{M_s \pi_{sty} + M_{VPh} (1 - \pi_{sty})} \right) \left(\frac{M_{PS-co-VPh}}{M_{VPh}} \right) \end{aligned} \quad (2.13)$$

Thus, using Equations 2.8 and 2.13, $N_{OH}/N_{C=O}$ ratio can be determined stoichiometrically.

Figure 19 shows the FT-IR curves in the C=O stretching region (1800-1650 cm^{-1}) for a blend containing PS-co-VPh and LCPU (20 wt.% LCPU) for differing copolymer compositions measured at 180°C. This figure illustrates that there is an increase in the

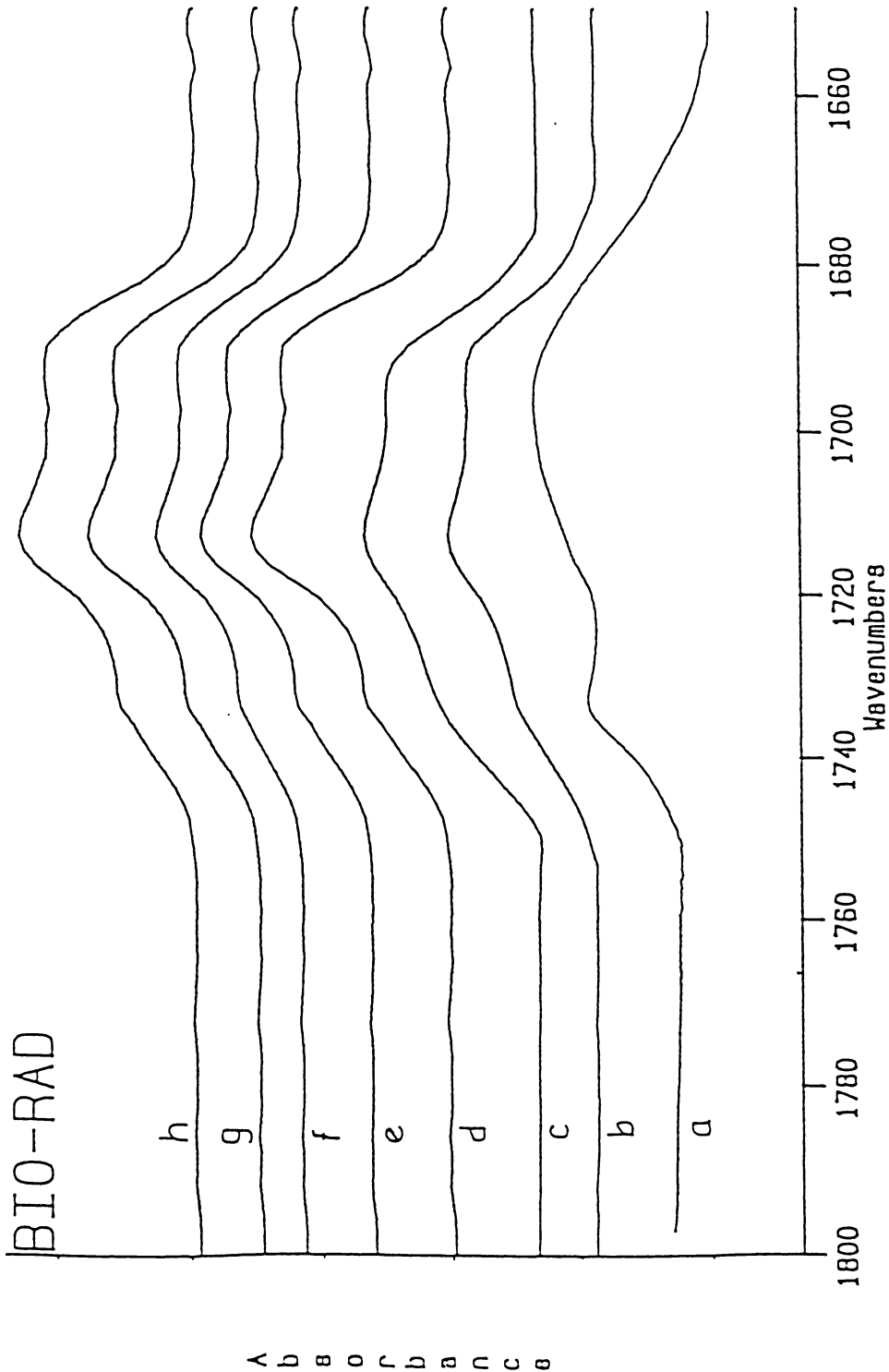


Figure 19. FT-IR spectra of C=O stretching region for blends measured at 180°C. Compositions of blends are 80 wt. % PS-co-VPh and 20 wt. % LCPU. Curve (a) is the pure LCPU, while the remaining curves are for blends containing PS-co-VPh with b) 5 mole % c) 10 mole % d) 20 mole % e) 30 mole % f) 40 mole % g) 50 mole % h) 100 mole % VPh

amount of intermolecular hydrogen bonding as the amount of VPh in the copolymer increases from 0 to 20% (curves *b-d*), as is demonstrated by the increase in the carbonyl peak at 1710 cm^{-1} . However, very little change is observed in this peak above 20% VPh in the copolymer (curves *e-h*). FT-IR curves of the C=O stretching region of blends that contain LCPU and PS-co-VPh(20) of various composition measured at 180°C are shown in Figure 20. This figure shows an increase in the extent of intermolecularly H-bonded C=O groups as the amount of PS-co-VPh(20) in the blend increases from 0 to 80 wt.%, illustrated by an increase in the peak at around 1710 cm^{-1} . A more quantitative understanding of the extent of intermolecular hydrogen bonding in these blends can be obtained by deconvoluting the C=O absorbance peaks in these IR curves. Parameters obtained from the deconvoluting procedure of the C=O stretching region for the free C=O, intermolecularly H-bonded C=O and intramolecularly H-bonded C=O bands are listed in Table 2.

At this point, a digression is warranted. A trend that is found commonly in hydrogen bonded systems is that the frequency shift in the bands associated with non-hydrogen bonded species is negligible with change in temperature and/or blend composition while that associated with hydrogen bonded species is significant and is much greater than the corresponding non-hydrogen bonded species. Results published previously by other authors^{73,74} establish this and suggest that it is reasonable to assume here that the frequency of the non-hydrogen bonded peak does not change with temperature and/or blend composition. On this basis, during deconvolution, the position of the free C=O vibration in the blend was kept fixed at the same position, whereas those of the hydrogen bonded vibrations were allowed to vary. The hydrogen bonded C=O peak position was allowed to

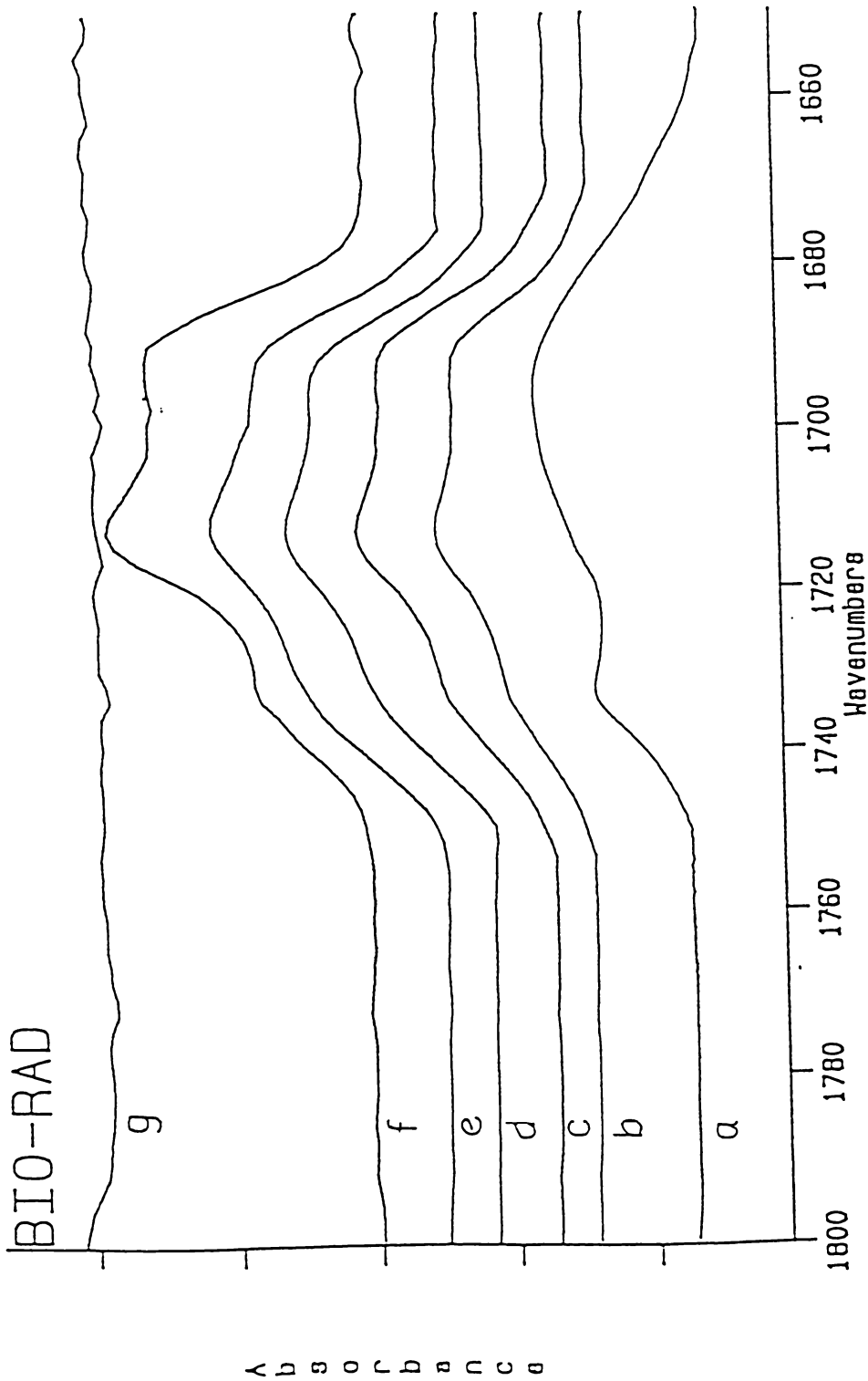


Figure 20. FT-IR spectra of C=O stretching region for blends containing PS-co-VPh(20) measured at 180°C. The curves correspond to blends with a composition of (LCPU/PS-co-VPh wt/wt) a) 100/0 b) 80/20 c) 60/40 d) 50/50 e) 40/60 f) 20/80 g) 0/100

Table 2. Results of the Deconvolution of the C=O stretching band for pure LCPU and blends containing 80 wt.% PS-co-VPh copolymer for various copolymer compositions measured at 180°C

| % VPh in PS-co-VPh | Free C=O | | | Intermolecularly H-bonded C=O | | | Intramolecularly H-bonded C=O | | | % C=O intermolecularly H-bonded |
|--------------------|--------------------------|----------------------------|-------|-------------------------------|----------------------------|-------|-------------------------------|----------------------------|-------|---------------------------------|
| | ν^* cm^{-1} | $W_{1/2}$ cm^{-1} | A_1 | ν cm^{-1} | $W_{1/2}$ cm^{-1} | A_2 | ν cm^{-1} | $W_{1/2}$ cm^{-1} | A_3 | |
| Pure LCPU | 1732 | 24.0 | 2.854 | - | - | - | 1695.4 | 32.1 | 4.225 | - |
| 5 | 1732 | 22.8 | 2.152 | 1714.8 | 23.7 | 0.967 | 1694.9 | 27.7 | 3.880 | 11.96 |
| 10 | 1732 | 23.5 | 2.023 | 1714.3 | 24.0 | 1.703 | 1695.5 | 25.4 | 3.837 | 19.69 |
| 20 | 1732 | 23.2 | 1.426 | 1713.7 | 24.8 | 2.845 | 1694.4 | 24.2 | 3.090 | 35.00 |
| 30 | 1732 | 22.7 | 1.493 | 1713.7 | 24.6 | 3.096 | 1694.7 | 24.5 | 3.181 | 36.10 |
| 40 | 1732 | 23.2 | 1.493 | 1713.6 | 24.5 | 3.161 | 1694.9 | 23.9 | 3.213 | 36.50 |
| 50 | 1732 | 22.9 | 1.356 | 1713.5 | 24.7 | 2.972 | 1694.6 | 24.2 | 2.970 | 37.00 |
| 100 | 1732 | 22.5 | 1.373 | 1713.5 | 24.8 | 3.075 | 1694.9 | 23.7 | 3.100 | 37.10 |

* Fixed during curve fitting. Absorptivity Coefficient Ratio (K) = $1.54 = K_1 = K_2$; $A_2' = A_2/K_1$; $A_3' = A_3/K_2$; $A_T = A_1 + A_2' + A_3'$

% C=O intermolecularly H-bonded = $(A_2'/A_T) * 100$

deviate to account for the fact that hydrogen bond geometry distribution and strength can be a function of temperature and/or blend composition.⁷²⁻⁷⁴ In all cases, a Gaussian bandshape was assumed.

Suppose, for example, that the hydrogen bonded system is analyzed in its heating cycle. Two major effects are observed and both are relevant to the subject of miscibility and phase behavior. The first effect is that the fraction of hydrogen bonded groups decreases with increasing temperature as determined by quantitative analysis of the IR peak. The second is that the average overall strength of the hydrogen bonding interactions decreases which is indicated by the increase in frequency of the hydrogen-bonded band (see Table 2). On an average, at a given temperature, quantitative analysis of the infrared spectrum reflects only the first effect and this would give rise to erroneous results. By logic, the decrease in the hydrogen bonded peak should be accompanied by an equal increase in the non-hydrogen bonded peak which is not what we observe in hydrogen bonded systems. In other words, the decrease in the area of the hydrogen bonded peak with increasing temperature is not simply a result of hydrogen bonded groups transforming to non-hydrogen bonded groups but is also due to different absorption coefficients of the non-hydrogen bonded (free) and hydrogen bonded peaks which is a result of decreasing overall strength of hydrogen bonding interactions.

Determination of Absorption Coefficient Ratio

To correct for the difference in absorption coefficients of free and hydrogen bonded peaks in order to obtain a more accurate proportions of these peaks as mentioned above, a knowledge of the respective absorption coefficients, a_1 and a_2 of the free and hydrogen

bonded peaks, or at least the ratio of the two absorption coefficients ($K = a_2/a_1$) is required. The absorption intensity of the H-bonded band is corrected for the difference in absorption coefficients of the H-bonded and non-hydrogen bonded bands by dividing the experimentally determined area of the hydrogen bonded peak by the K value. The percent of intermolecularly hydrogen bonded groups is obtained using this corrected value of the area of the hydrogen bonded peak. The absorption coefficient ratio is estimated by using the method of Coleman and Painter^{71,75,77,77} which employs the following equation:

$$K = [A_{HB}^{T2} - A_{HB}^{T1}] / [A_F^{T1} - A_F^{T2}] \quad (2.14)$$

where A_{HB}^{T1} and A_{HB}^{T2} are hydrogen bonded absorption intensities at temperatures T_1 and T_2 and A_F^{T1} and A_F^{T2} are non-hydrogen bonded absorption intensities at temperatures T_1 and T_2 .

The success of the ‘absorption coefficient ratio determination’ method requires that:

1) the change in absorption coefficient with temperature must be insignificant and 2) there must be a large transformation between free and hydrogen bonded groups in order to minimize errors. The immediate question is: How is the application of this method to the blend system discussed in this work justified? First, it is important to note that, unlike the N-H or the O-H stretching band which are highly sensitive to temperature (frequency shifts of hydrogen bonded peaks are usually about 50-70 cm^{-1}), the C=O stretching band is far less sensitive to temperature (frequency shifts of hydrogen bonded peaks usually less than 5 cm^{-1}). In other words, unlike the N-H or O-H stretching mode, the absorption coefficients of the hydrogen bonding and non-hydrogen bonding peaks of the carbonyl stretching band do not change appreciably with temperature and/or blend composition. That is, the absorption coefficient ratio of the H-bonded C=O band to the free C=O band in the

C=O stretching mode remains low (usually between 1.0 and 1.7) and almost a constant with temperature and/or blend composition which makes it convenient for quantitative analysis. Second, a temperature range used for the K value determination was carefully chosen so as to include a large transformation between free and hydrogen bonded groups. For the blends studied here, this large transformation was found to be in the cooling cycle between 140°C and 70°C which happens to include the crystallization and glass transition temperatures of the blends. The value of K was determined for multiple samples of the same blend composition and, in this manner, for several blend and copolymer compositions and finally averaged as a whole.

The areas under the three peaks that contribute to C=O stretching vibration band of the spectrum in the LCP/PS-co-VPh blends are determined from the fitting procedure; A_1 is the area of the free carbonyl peak, A_2 is the area of the peak associated with the intermolecularly hydrogen bonded carbonyls, and A_3 is the area of the intramolecularly hydrogen bonded carbonyls peak. Table 3 gives the values of the different parameters used to determine K of multiple samples of 20:80 LCP/PS-co-VPh(5) blends as an example. This whole procedure was then repeated for over twenty randomly chosen blends which include different PS-co-VPh copolymer compositions and LCP/PS-co-VPh blend compositions. Finally, an average K value was determined which was found to be 1.54 ± 0.03 for intermolecular hydrogen bonding (K_1) and 1.54 ± 0.06 for intramolecular hydrogen bonding (K_2). The absorption intensities of the H-bonded C=O bands (A_2 and A_3) were then corrected for the difference in absorption coefficients of the H-bonded and free C=O bands by division of their experimentally determined areas by their respective K values ($A_2' = A_2 /$

Table 3. Deconvolution results of the C=O stretching region for multiple samples of LCP/PS-co-VPh blends containing 80 wt.% PS-co-VPh(5) copolymer measured at 140°C and 70°C (for determining Absorption Coefficient Ratio)

| Sample No. | Temp. (°C) | Free C=O | | | Intermolecularly H-bonded C=O | | | Intramolecularly H-bonded C=O | | | K ^{Inter} | K ^{Intra} |
|-------------|------------|-----------------------------|-------------------------------|----------------|-------------------------------|-------------------------------|----------------|-------------------------------|-------------------------------|----------------|--------------------|--------------------|
| | | ν^* cm ⁻¹ | $W_{1/2}$ cm ⁻¹ | A ₁ | ν cm ⁻¹ | $W_{1/2}$ cm ⁻¹ | A ₂ | ν cm ⁻¹ | $W_{1/2}$ cm ⁻¹ | A ₃ | | |
| 1 | 140 | 1732 | 22.2 | 2.505 | 1714.2 | 22.3 | 0.917 | 1693.7 | 26.3 | 4.778 | 1.531 | 1.521 |
| | 70 | 1732 | 21.8 | 2.095 | 1713.0 | 22.2 | 1.555 | 1691.8 | 25.8 | 5.402 | | |
| 2 | 140 | 1732 | 21.7 | 2.383 | 1714.2 | 21.8 | 0.910 | 1694.0 | 26.0 | 4.750 | 1.556 | 1.558 |
| | 70 | 1732 | 21.7 | 1.973 | 1713.1 | 21.9 | 1.548 | 1691.8 | 25.8 | 5.389 | | |
| 3 | 140 | 1732 | 22.3 | 2.603 | 1714.2 | 22.3 | 0.942 | 1694.1 | 25.9 | 4.800 | 1.529 | 1.531 |
| | 70 | 1732 | 22.5 | 2.193 | 1713.0 | 22.0 | 1.569 | 1691.5 | 26.0 | 5.428 | | |
| Average K = | | | | | | | | | | 1.539 | 1.536 | |

* Fixed during curve fitting. K^{Inter}, K^{Intra} are Absorption Coefficient Ratios of Intermolecularly Hydrogen Bonded C=O groups and Intramolecularly Hydrogen Bonded C=O groups, respectively.

K_1 and $A_3' = A_3 / K_2$). Finally, the percent of carbonyl groups that participate in intermolecular hydrogen bonding is then calculated by:

$$\% \text{ C=O} = \frac{A_2'}{A_1 + A_2 + A_3} \quad (2.15)$$

The results of the fitting procedures for neat LCPU and LCPU/PS-co-VPh blends containing 80 wt.% PS-co-VPh copolymer for various copolymer compositions measured at 180°C are listed in Table 2. Figure 21 shows the results of this analysis by documenting the percent of carbonyl (%C=O) groups that are intermolecularly H-bonded with the composition of the PS-co-VPh for various blend compositions measured at 180°C. For each blend, as the amount of hydroxyl containing monomer (VPh) increases up to 20 mol%, the amount of C=O that participates in intermolecular hydrogen bonding increases. However, above 20 mol% VPh, the percent of carbonyl groups that participate in intermolecular hydrogen bonding changes little. Thus, adding more hydroxyl groups does not increase the extent of intermolecular hydrogen bonding above 20 mol% VPh in the copolymer. A logical interpretation of this trend is that as the amount of –OH increases from 0 to 20%, more hydroxyl groups are introduced that can H-bond with C=O groups, more carbonyl groups find available –OH groups to create intermolecular hydrogen bonds, and this curve increases. However, above 20% VPh in the copolymer, the additional –O-H groups are not usually able to find suitably oriented or positioned carbonyl groups with which to form an intermolecular H-bond, and this curve remains flat. This interpretation is corroborated by examining the percentage of hydroxyl groups that participate in intermolecular H-bonding with C=O. Figure 22 shows these data and demonstrates that this parameter doesn't change much up to 20% VPh in the

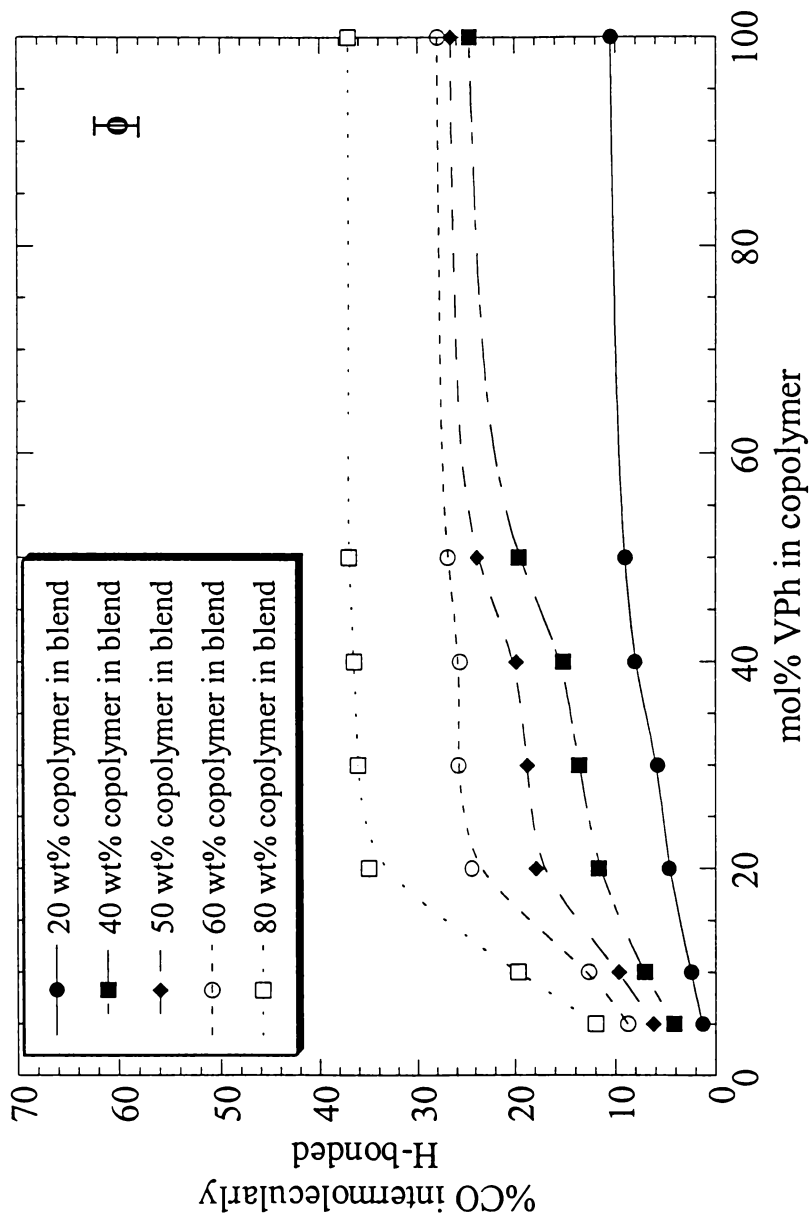


Figure 21. Percent of carbonyl groups participating in intermolecularly hydrogen bonding as a function of PS-co-VPh copolymer composition for different blend compositions of LCP/PS-co-VPh measured at 180°C. Error Bar in the plot corresponds to $\pm 2\%$

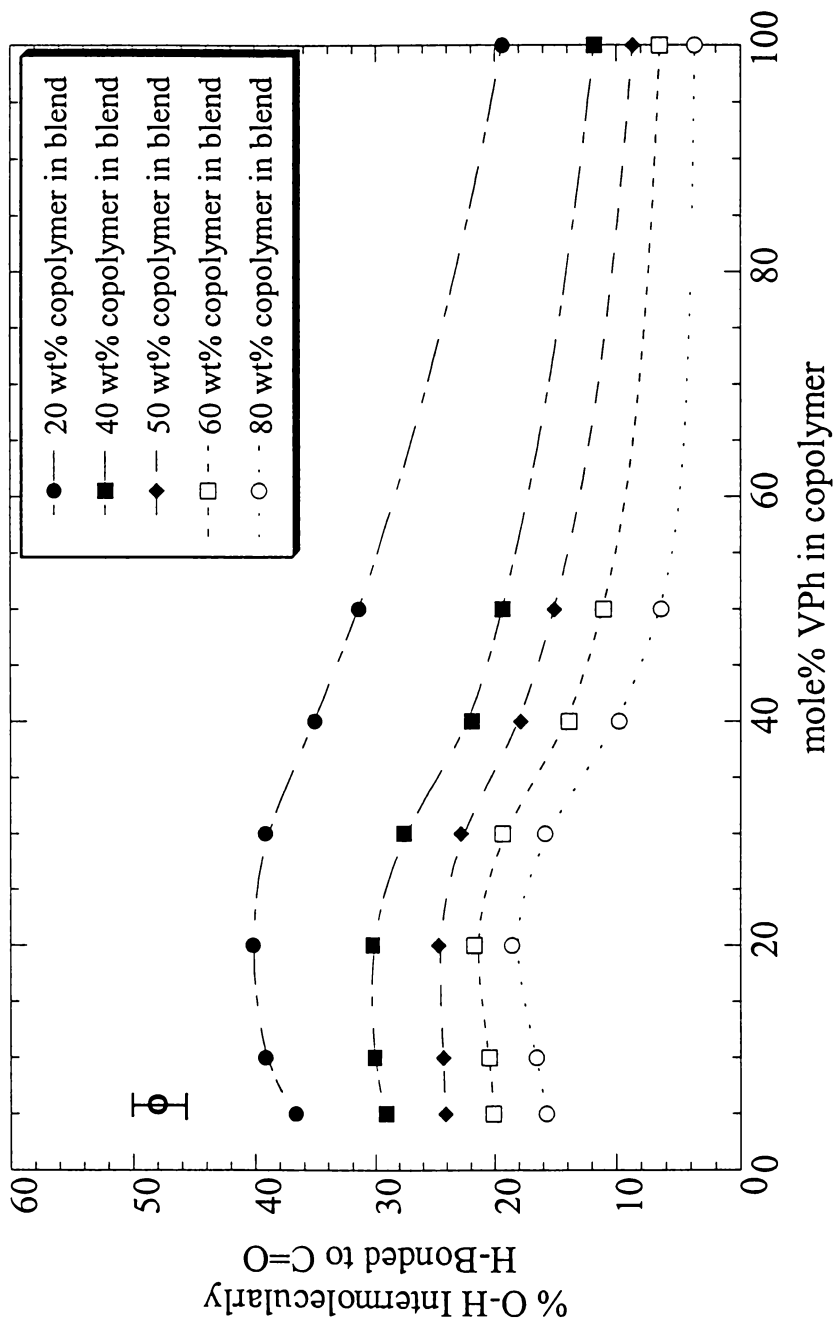


Figure 22. Percent of hydroxyl groups participating in intermolecularly hydrogen bonding as a function of PS-co-VPh copolymer composition for different blend compositions of LCPU/PS-co-VPh measured at 180°C. Error Bar in the plot corresponds to $\pm 2\%$

copolymer, but decreases as more hydroxyl groups are included on the copolymer chain. These observations indicate that when the amorphous copolymer contains 20 mol% VPh, the percent of hydroxyl groups that participate in intermolecular hydrogen bonding is maximized and the amount of carbonyl groups that engage in intermolecular hydrogen bonding is also maximized. Thus, this composition of the copolymer denotes the system where the extent of intermolecular hydrogen bonding between these two polymers is optimized. This is in agreement with the work of Radmard and co-workers who showed that the extent of intermolecular hydrogen bonding between the two polymers with dissimilar rigidities is maximized when the hydroxyl groups along the copolymer chain are significantly separated along the chain.⁵⁹

As mentioned earlier, the reason for this trend is related to the proximity of the hydroxyl groups on the amorphous copolymer to other hydroxyl groups. The separation of the hydroxyl groups on the chain provides each hydroxyl group with sufficient rotational freedom to enable the independent reorientation of the individual hydroxyl groups that allows more groups to orient themselves correctly near other functional groups to form intermolecular hydrogen bonding. Additionally, the separation of the hydroxyl groups along the chain also decreases the probability of forming *intra*-molecular (hydroxyl to hydroxyl) hydrogen bonding.

Our FT-IR results indicate that there is no significant change in the percent of carbonyl groups participating in intermolecular H-bonding above 20 mole% VPh in the copolymer in LCPU/PS-co-VPh blends (Figure 21). Therefore, a significant decrease in the percent of hydroxyl groups participating in intermolecular H-bonding is expected as a result

of the limited number of carbonyl groups participating in intermolecular H-bonding as more O-H groups are incorporated into the blend. On the contrary, our FT-IR results indicate only a modest decrease in the percent of hydroxyl groups that participate in intermolecular H-bonding above 20 mole% VPh in the copolymer (see Figure 22).

As discussed previously in this chapter, the percentage of hydroxyl groups that participate in intermolecular hydrogen bonding with C=O groups is estimated stoichiometrically by dividing the percentage of carbonyl groups participating in hydrogen bonding by the ratio of the number of hydroxyl groups to carbonyl groups present in the blend. The number of carbonyl and hydroxyl units in the blend is in turn estimated from the molecular weights of LCPU and PS-co-VPh and the composition of the LCPU/PS-co-VPh blend system. Since the molecular weights of the copolymers used in this study are different for different copolymer compositions (see Table 1), the number of C=O and O-H units in the blend is estimated individually for every set of blend composition and copolymer composition. It is to be noted that the ratio of the number of hydroxyl groups to carbonyl groups present in the blend in turn increases with an increase in the molecular weight of the copolymer and/or an increase in the mole% VPh in the copolymer. Thus we cannot merely correlate the data in Figures 21 and 22 by considering the composition of the copolymer since one must also consider the changes in the molecular weight of the copolymer.

As an example, in Figure 22, we find a modest decrease in the percent of hydroxyl groups participating in intermolecular H-bonding as the mole% VPh in the copolymer increases from 50 to 100, although a halving is expected due to the doubling in mole% VPh in the copolymer if only the composition of the copolymer is considered. The molecular

weights of the PS-co-VPh(50) (34,100 g/mol) and Pure PVPh (22,000 g/mol) used in this study are significantly different and, therefore, also impacts the correlation between Figures 21 and 22.

Thermal and Optical Phase Behavior Studies

To correlate the extent of intermolecular hydrogen bonding to the phase behavior of these blends, the phase diagrams of blends containing LCPU and copolymers that consist of 10%, 20% and 30% VPh [PS-co-VPh(10), PS-co-VPh(20), PS-co-VPh(30)] were determined using DSC and optical microscopy. Figures 23, 24 and 25 show the DSC curves of LCPU/PS-co-VPh(10), LCPU/PS-co-VPh(20) and LCPU/PS-co-VPh(30) blends, respectively, for various blend compositions. A single glass transition is observed for blend compositions above 60 wt.% PS-co-VPh(20) for LCPU/PS-co-VPh(20) and above 80 wt.% PS-co-VPh for LCPU/PS-co-VPh(10) and LCPU/PS-co-VPh(30), suggesting miscibility in these blends in these regimes. Figures 26, 27, and 28 provide further evidence of miscibility by showing the dependence of the blend T_g (as determined by DSC) on blend composition for blends of LCPU/PS-co-VPh(10), LCPU/PS-co-VPh(20) and LCPU/PS-co-VPh(30), respectively. These figures also include the expected T_g of miscible blends as calculated from the Fox equation and show that the experimental single T_g values agree very well with the theoretical Fox equation in the miscible region, suggesting that these systems do indeed exhibit miscibility in this window. The Fox equation⁷⁸ that relates the T_g of the mixture to that of its components is shown as follows:

$$\frac{1}{T_g} = \frac{W_1}{T_{g1}} + \frac{W_2}{T_{g2}} \quad (2.16)$$

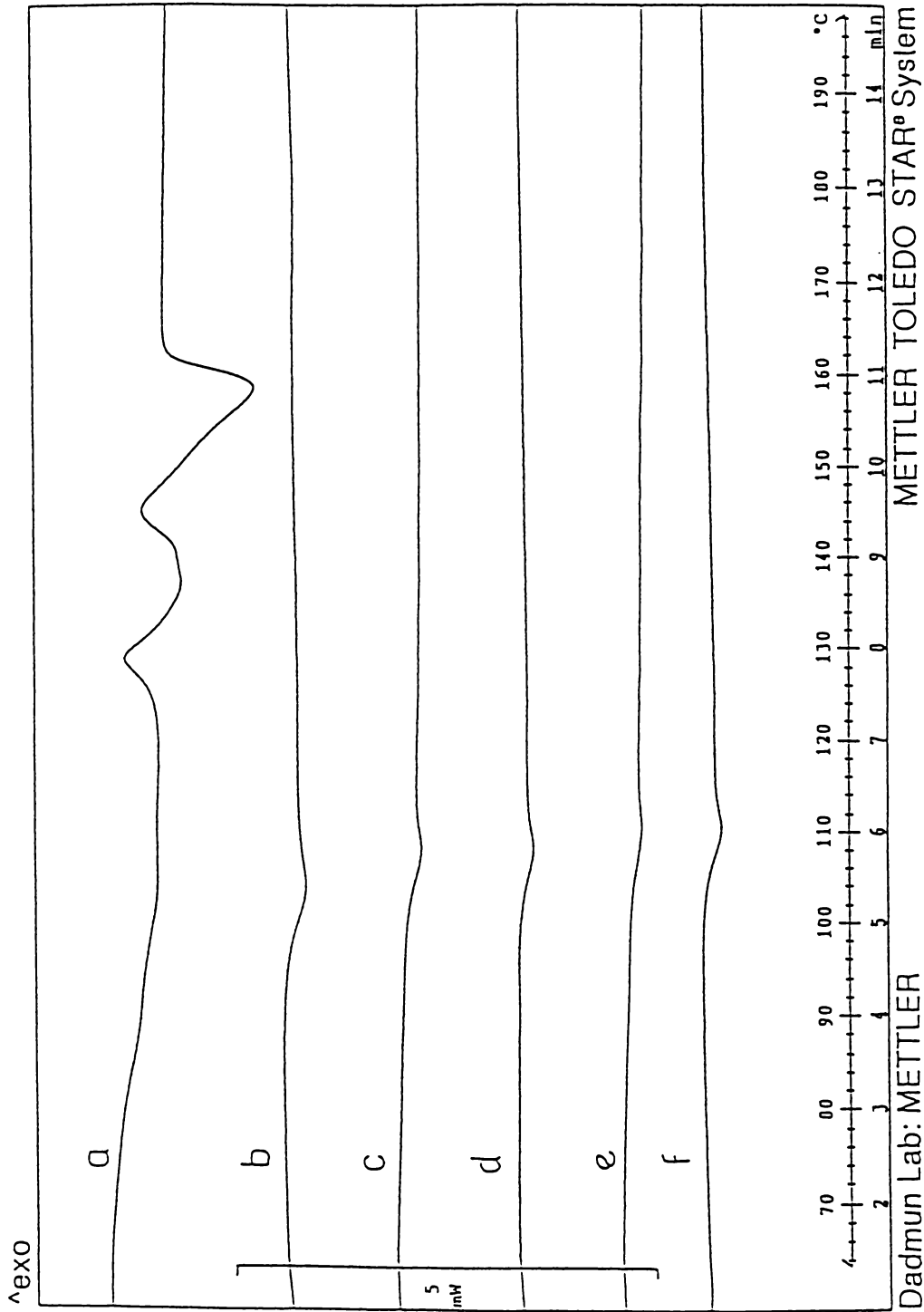


Figure 23. Representative DSC curves of blends containing LCPU and PS-co-VPh(10). Compositions of the blends are (LCPU/PS-co-VPh(10) wt/wt) a) 25/75 b) 20/80 c) 15/85 d) 10/90 e) 5/95 f) 0/100

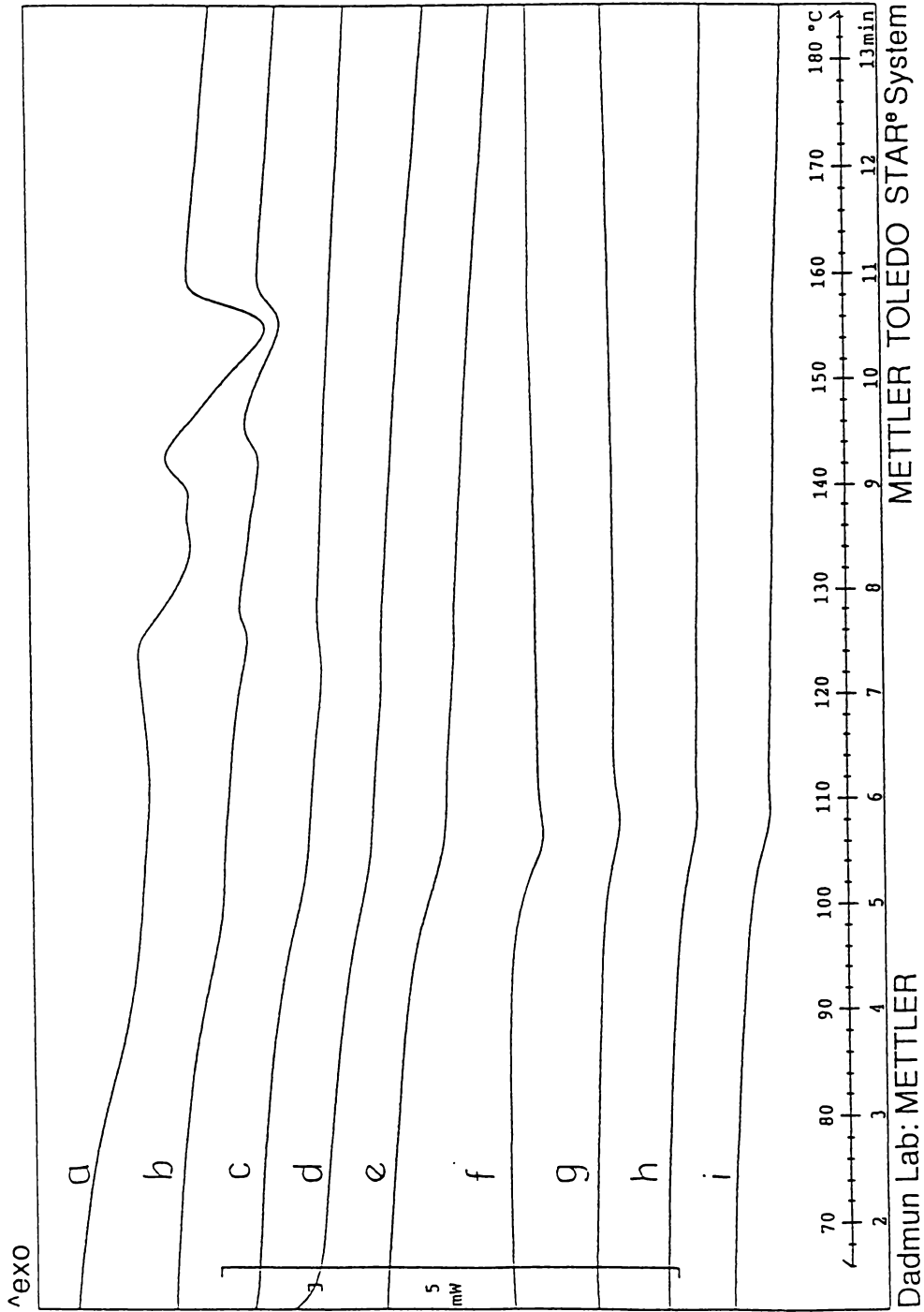


Figure 24. Representative DSC curves of blends containing LCPU and PS-co-VPh(20). Compositions of the blends are (LCPU/PS-co-VPh(20) wt/wt) a) 40/60 b) 35/65 c) 30/70 d) 25/75 e) 20/80 f) 15/85 g) 10/90 h) 5/95 i) 0/100

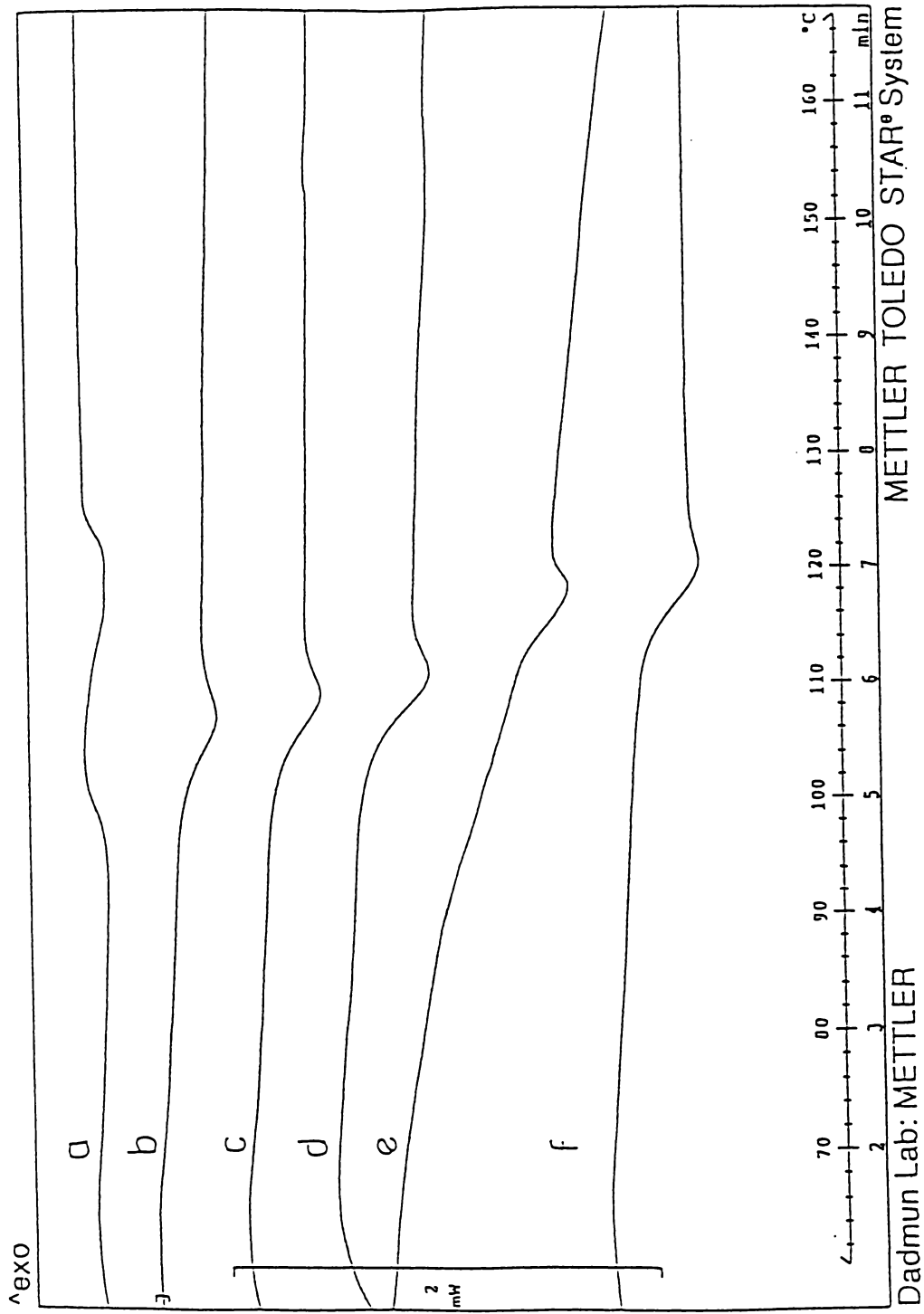


Figure 25. Representative DSC curves of blends containing LCPU and PS-co-VPh(30). Compositions of the blends are (LCPU/PS-co-VPh(30) wt/wt) a) 25/75 b) 20/80 c) 15/85 d) 10/90 e) 5/95 f) 0/100

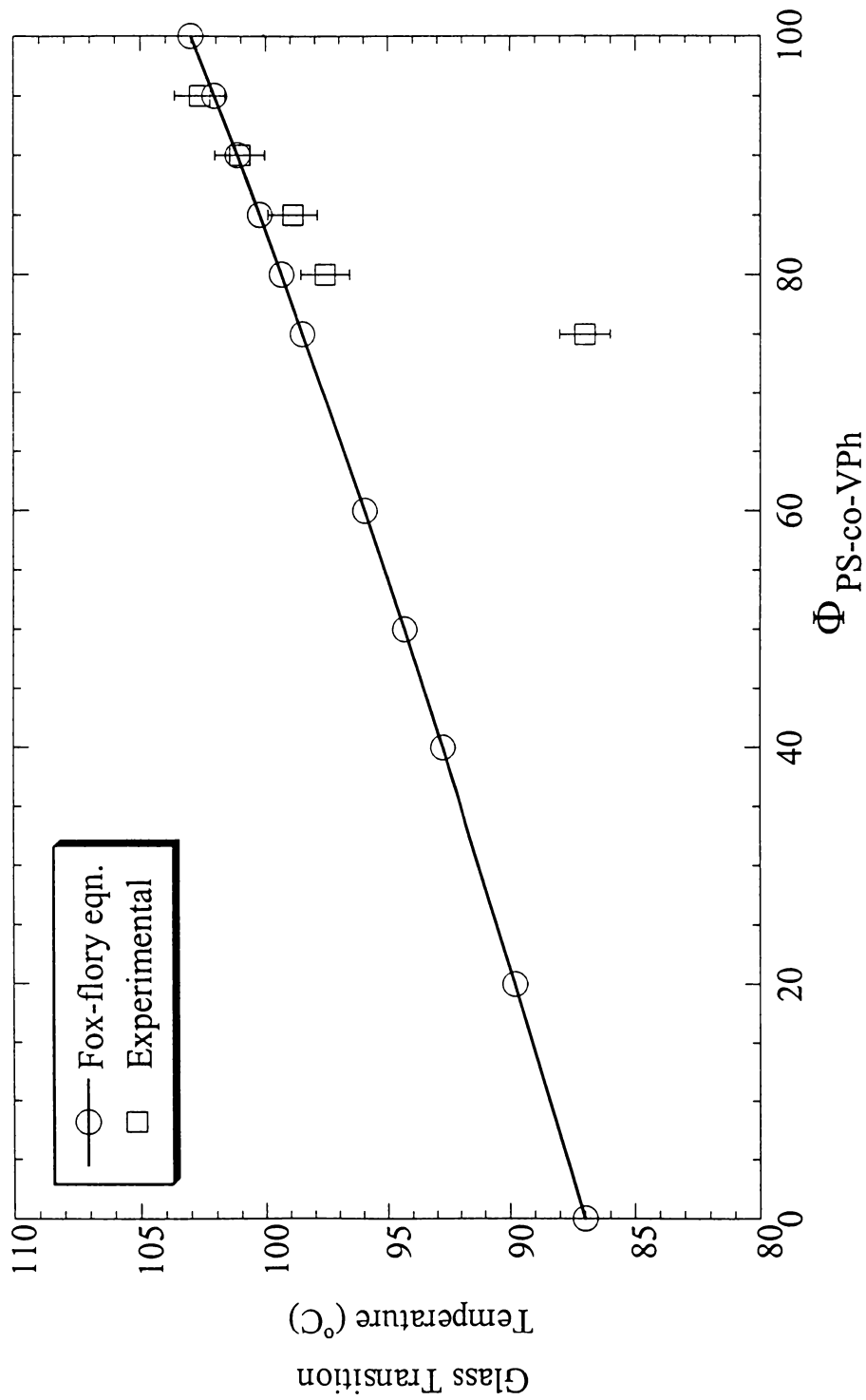


Figure 26. Experimental and theoretical glass transition temperatures of blends containing PS-co-VPh(10) and LCPU

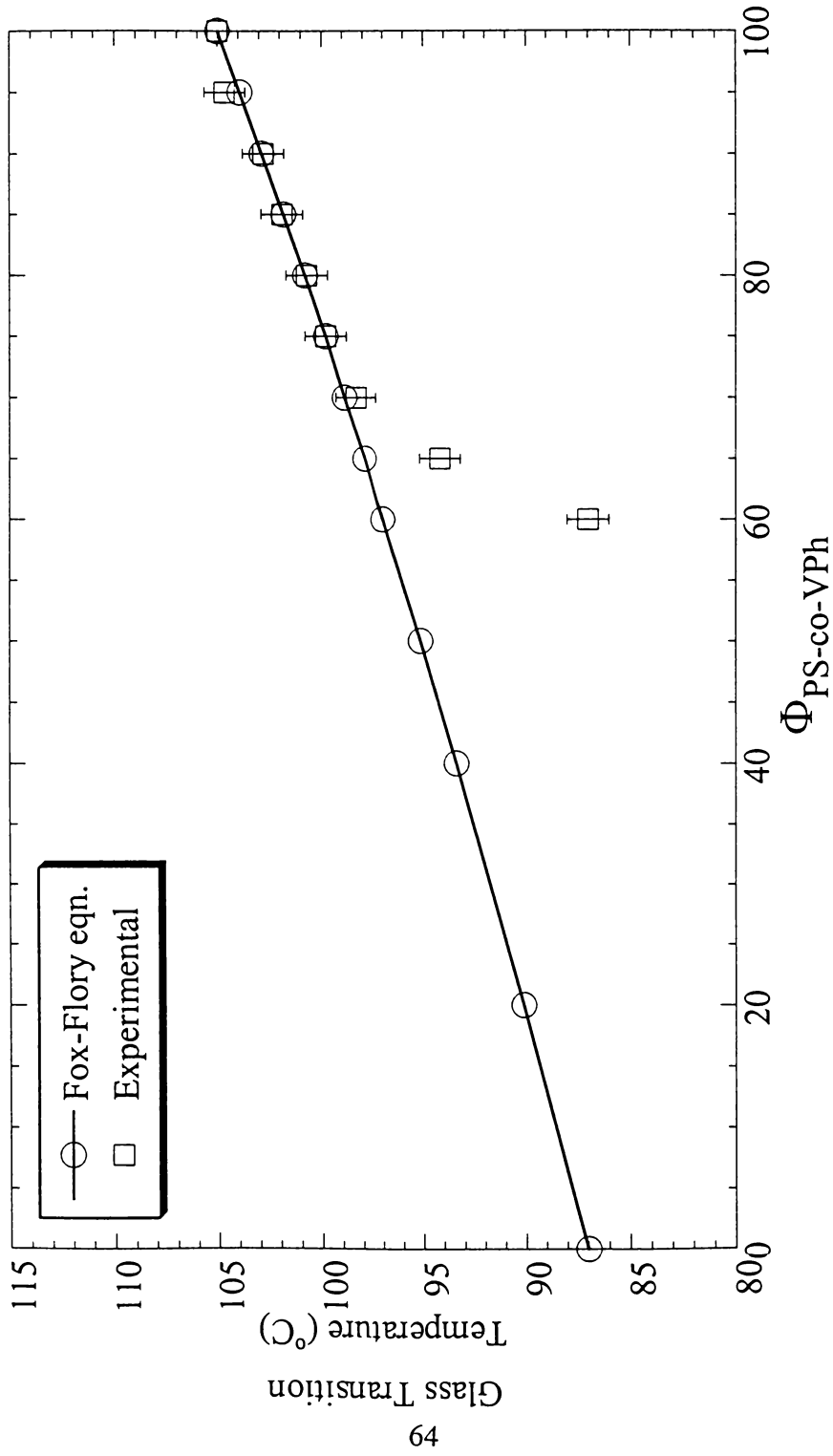


Figure 27. Experimental and theoretical glass transition temperatures of blends containing PS-co-VPh(20) and LCPU

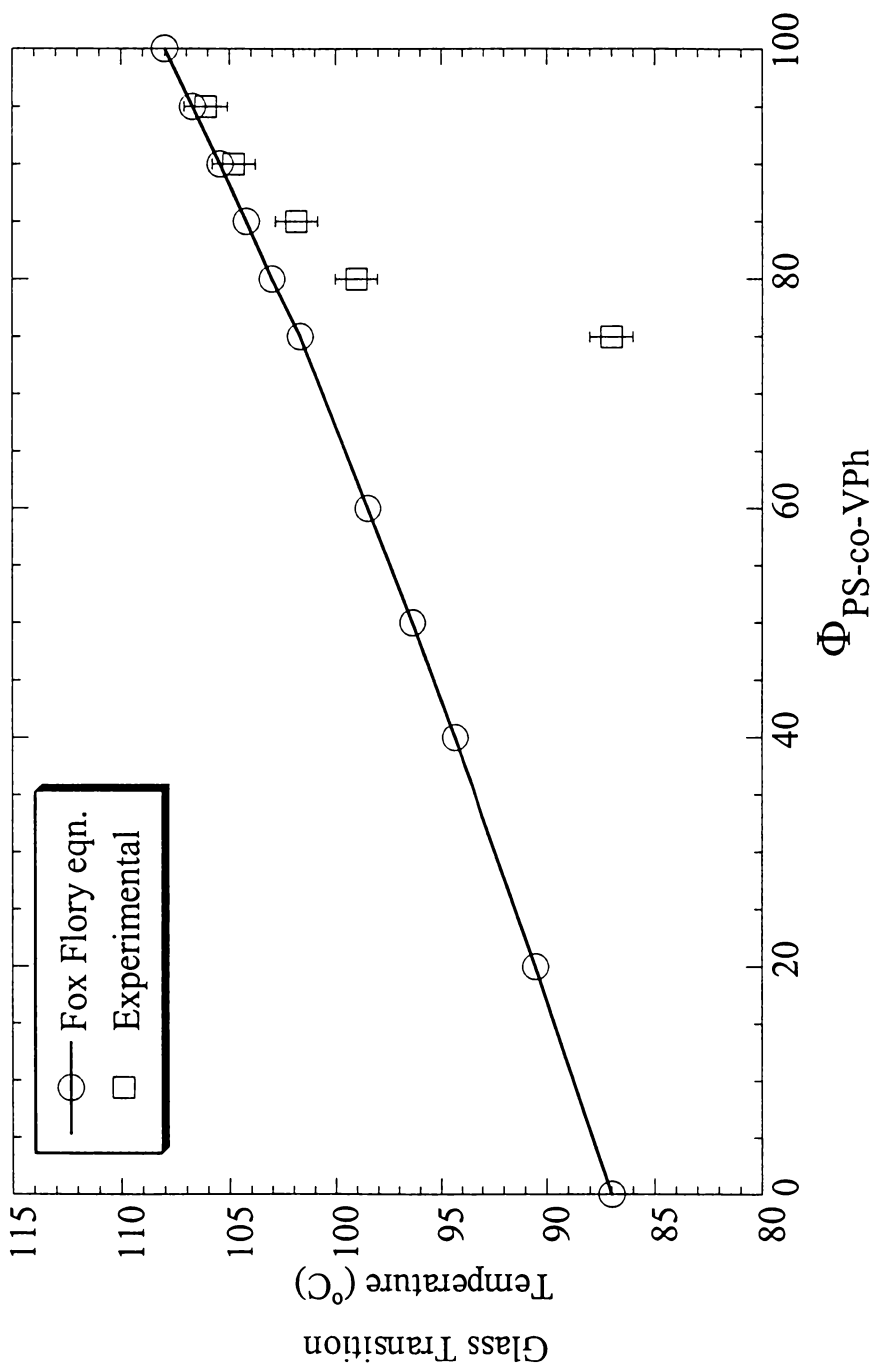


Figure 28. Experimental and theoretical glass transition temperatures of blends containing PS-co-VPh(30) and LCPU

where T_{g_1} and T_{g_2} are the T_g 's of the pure components and W_1 and W_2 are the respective weight fractions present in the mixture.

Lastly, phase-contrast optical microscopy was used to determine the temperature-composition phase diagrams of the three blends, LCPU/PS-co-VPh(10), LCPU/PS-co-VPh(20) and LCPU/PS-co-VPh(30) and these phase diagrams are shown in Figure 29. There clearly is a miscibility window for these three systems, which demonstrates that the presence of significant hydrogen bonding can indeed induce miscibility in a rod/coil polymer blend. Moreover, comparison of the miscibility windows of these three systems shows that the system with the optimized extent of intermolecular hydrogen bonding (LCPU/ PS-co-VPh(20)) is also the system with the largest miscibility window.

A very specific observation which is interesting to note here is the difference in the miscibility window of LCPU/PS-co-VPh(20) and LCPU/PS-co-VPh(30) in the phase diagram determined by optical microscopy (see Figure 29). It can be seen that the increase in the mole percentage of vinyl phenol (VPh) in the copolymer from 20 to 30 causes a dramatic narrowing of the miscibility window. We believe that a plausible explanation for this phenomenon can be provided in terms of the solubility parameters of the mixing polymers assuming the absence of any effects of hydrogen bonding in the blend.

A discussion of the estimation of solubility parameter is relevant here. A calculation based on group contributions assumes that a molecule can be “broken down” into a set of functional groups (e.g., methyl, methylene, esters) and the interactions between the functional groups are largely non-polar. Based on the molar volume constant (V) and the molar attraction constant (F) of the functional groups that constitute the repeat unit of a

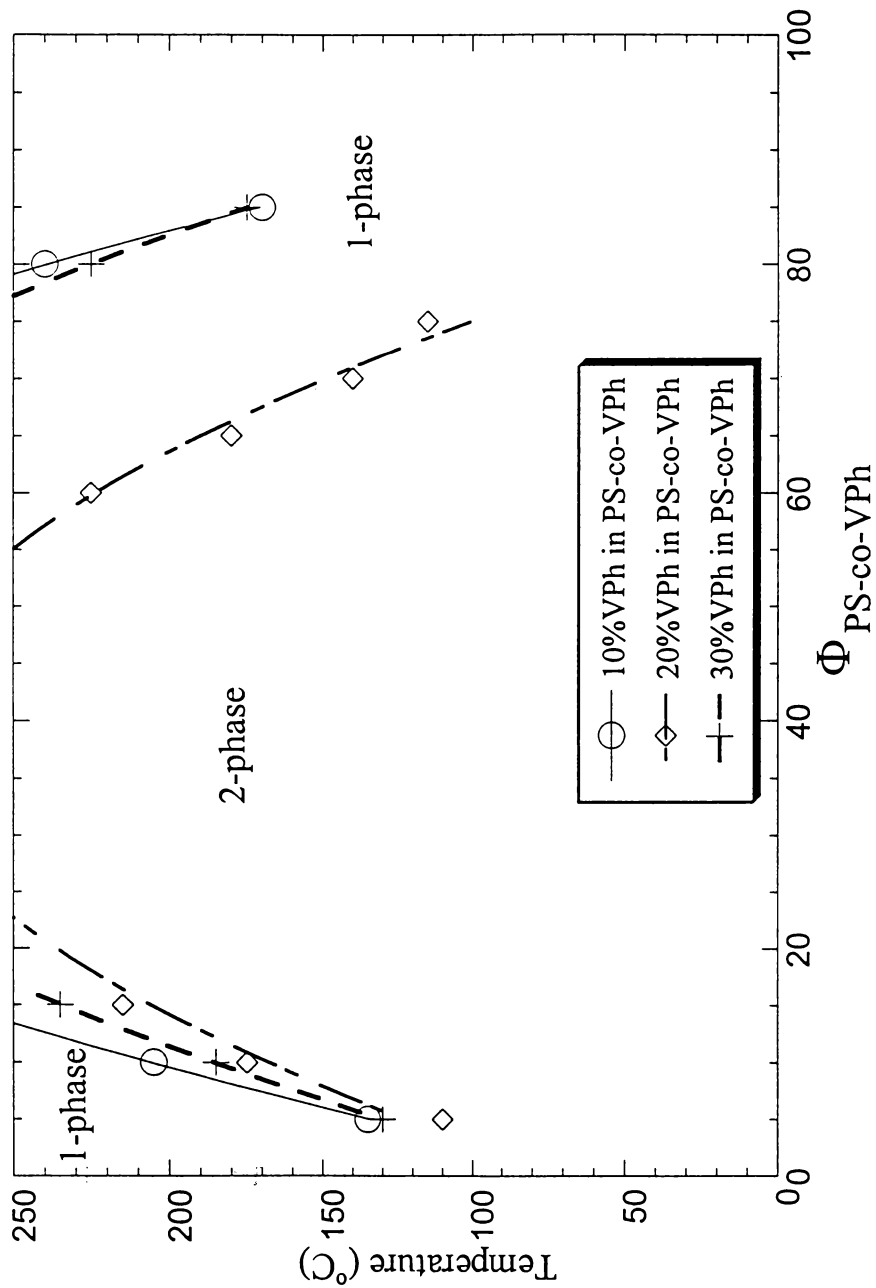


Figure 29. Phase diagram of blends containing PS-co-VPh(10), PS-co-VPh(20) and PS-co-VPh(30) as determined from phase contrast optical microscopy

polymer, the solubility parameter of a polymer can be found using the following relationship.

$$\delta = \frac{\sum_i F_i}{\sum_i V_i} (\text{cal.cm}^{-3})^{0.5} \quad \text{where } i \text{ denotes the } i\text{th functional group.} \quad (2.17)$$

The values of the molar volume constant and the molar attraction constant of the different functional groups can be obtained from the work of Coleman and Painter.⁶⁹

By following the above procedure, we obtain a solubility parameter of 7.52 for the LCPU, 9.5 for styrene and 10.6 for vinyl phenol. It is apparent that the difference in solubility parameters of the LCPU and Polystyrene ($9.5-7.52 = 1.98$) is less than that of the LCPU and Poly(vinyl phenol) ($10.6-7.52 = 3.08$). We can easily conclude that, in the absence of the effects of hydrogen bonding in the blend, the LCPU is more inclined to mix with styrene molecules than with vinyl phenol molecules. This brings about a decrease in the mixing propensity between the LCPU and the copolymer in the blend when the %VPh in the copolymer is increased from 20 to 30. Thus, we interpret the decrease in the mixing propensity of the LCPU with the copolymer (as indicated by the difference in solubility parameter), with increase in % VPh in the copolymer, as a possible cause for the dramatic narrowing of the miscibility window in LCPU/PS-co-VPh(50) relative to LCPU/PS-co-VPh(40).

2.4 Summary

Clearly, these results demonstrate that optimizing the extent of intermolecular hydrogen bonding between two polymers will provide a great opportunity to induce miscibility in a polymer blend. Moreover, these and other recent results suggest that this optimal amount of intermolecular hydrogen bonding can be attained when the hydrogen

bonding moieties are sufficiently separated along the polymer chain.

Thus, these results provide guidelines by which true molecular composites, i.e. miscible blends of a liquid crystalline polymer and an amorphous polymer, can be designed and reproducibly created. This is accomplished by mixing a LCP with an amorphous polymer that has been modified to include well-separated functional groups that can form strong intermolecular interactions with the LCP. It is worth emphasizing that this separation of hydrogen bonding moieties means that the functional group is present as a minor component in the amorphous copolymer and thus the modification of the amorphous polymer (and its properties) is minimal.

Chapter 3

Creating Miscible N-methyl Liquid Crystalline Polyurethane/ Poly(Styrene-co-4-Vinyl phenol) Blends

3.1 Introduction

Chapter 2 showed that intermolecular H-bonding can be optimized in a polymer mixture containing a liquid crystalline polyurethane (LCPU) and poly (styrene-co-4-vinyl phenol) (PS-co-VPh) by systematically varying the PS-co-VPh copolymer composition. By controlling the distance between the hydroxyl groups along the PS-co-VPh chain, the amount of VPh in the copolymer that would give the optimum amount of intermolecular H-bonding in the blend is determined. Using this information, it was demonstrated that the system with optimum amount of intermolecular hydrogen bonding reflects itself as the broadest miscible window in the phase diagram.

In this chapter, the extent of intermolecular hydrogen bonding was further optimized by eliminating intramolecular H-bonding between the LCPU chains. To be more specific, a N-methyl liquid crystalline polyurethane (LCPU-M) was formed from the LCPU by converting the N-H groups of the LCPU chains to N-CH₃ groups. This step eliminates the possibility of C=O --- H-N hydrogen bonding among the LCP chains, which should increase the number of C=O groups in the LCP available for intermolecular H-bonding. This chapter will therefore present FT-IR and phase behavior data of LCPU-M/PS-co-VPh blends and compare them to the results obtained for LCPU/PS-co-VPh blends to illustrate the effect of

eliminating intramolecular H-bonding in LCP chains on the amount of intermolecular H-bonding in the blend and on the blend phase behavior.

3.2 Experimental

All the chemicals required for the synthesis of LCPU and PS-co-VPh copolymers are the same as those listed in Chapter 2 of this dissertation. The chemicals required for the synthesis of LCPU-M, sodium hydride and methyl iodide were purchased from Aldrich Chemical Co. and N, N-dimethyl formamide (DMF) and methanol from Fisher-Acros Co. DMF was purified by vacuum distillation before use.

The liquid crystalline polyurethane (LCPU) was synthesized by the condensation of 4,4'-bis(6-hydroxyhexoxy) biphenyl (BHHBP) and 2,4-toluene diisocyanate (TDI) by following the procedure described in the previous chapter. The N-methyl liquid crystalline polyurethane (LCPU-M) was prepared by reacting the LCPU with sodium hydride and methyl iodide using the method of Mihara and Koide⁷⁹ (see Figure 30) as described below.

Synthesis and Characterization of LCPU-M:

In an atmosphere of nitrogen, sodium hydride (0.053 g, 0.0022 mol) suspended in 2 mL of DMF was stirred in a chilled reaction vessel. A DMF solution of LCPU (0.4 g, 0.00066 mol) was added to the suspension of sodium hydride. After the reaction mixture was stirred for 30 min, methyl iodide (0.2 mL, 0.0032 mol) was added dropwise to the mixture. Following stirring of the reaction mixture for 2 h, excess sodium hydride was removed by filtration. The filtrate was concentrated and poured into a large amount of methanol and the obtained precipitate was washed with methanol (yield 75%). ¹H NMR (see Figures 31 and 32) (reported as chemical shift, multiplicity, integration, assignment) [δ 7.47 (m, 5H, a), 6.96

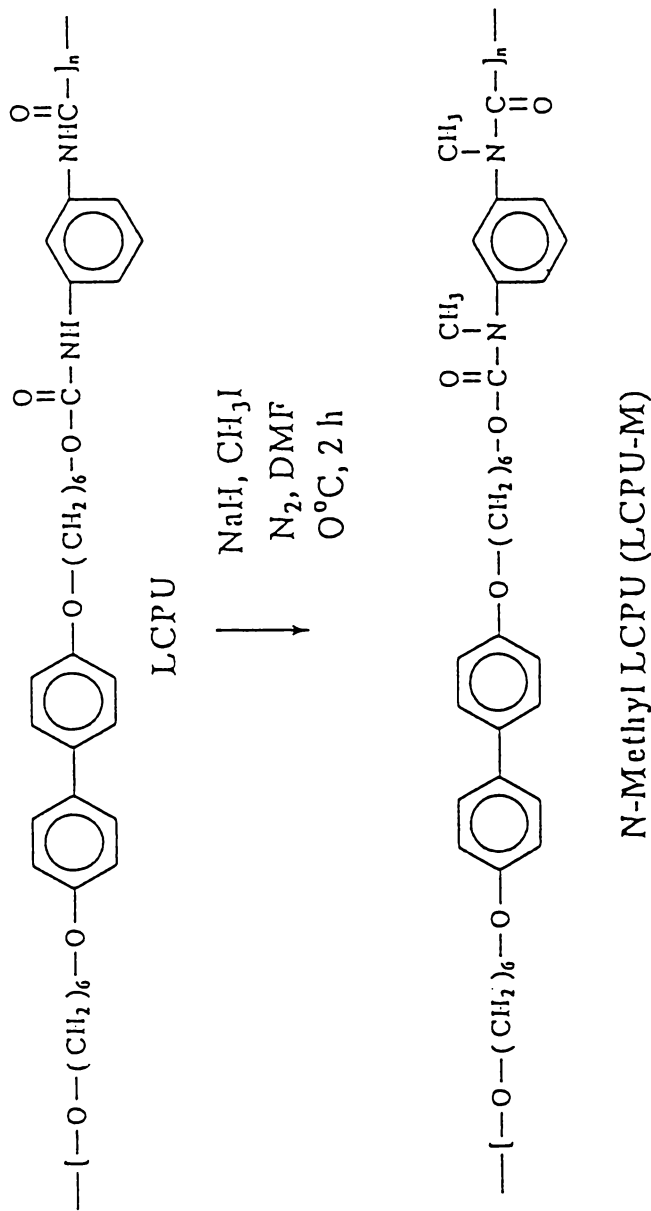


Figure 30. Synthesis of the N-methyl Liquid Crystalline Polyurethane (LCPU-M) used in this study

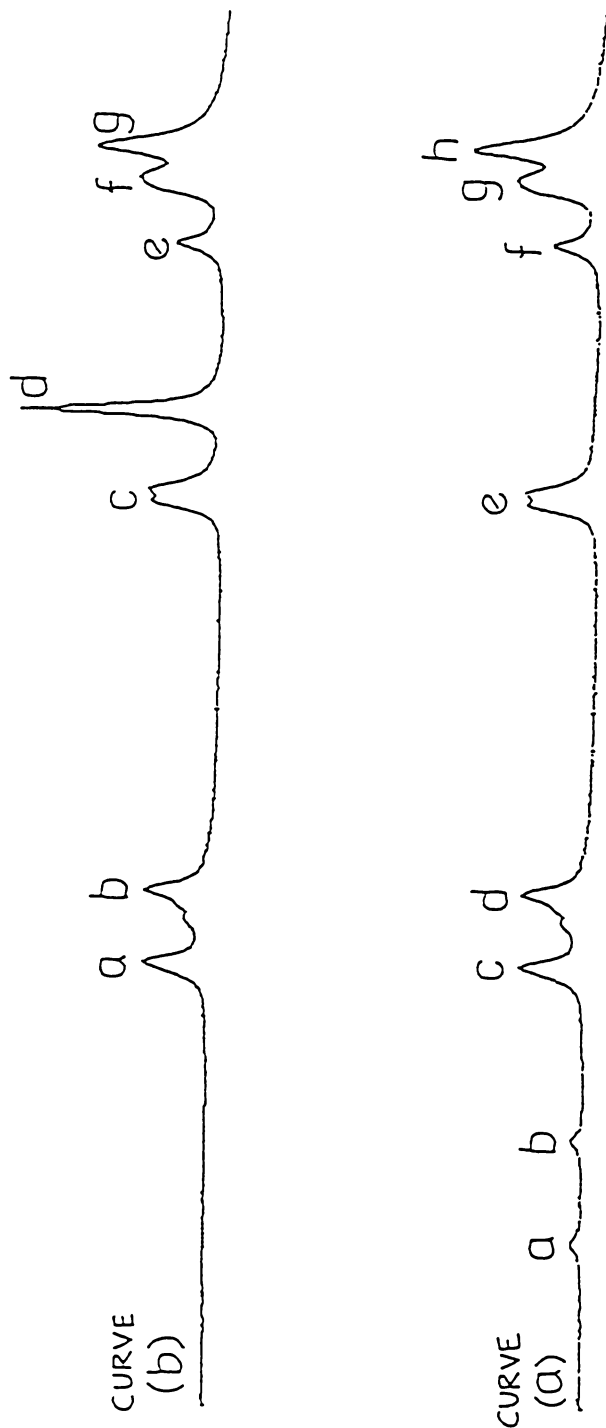


Figure 31. Characteristic Proton NMR spectra of pure LCPU (curve a) and pure LCPU-M (curve b). Lower case letters refer to Proton NMR results (see also Figure 32)

(m, 6H, b), 3.96 (m, 8H, c), 3.4 (s, 6H, d), 2.09 (s, 3H, e), 1.65 (m, 8H, f), 1.40 (m, 8H, g)]. DSC results of the LCPU-M are shown in Figure 33 and the phase transition temperatures of the LCPU-M are provided in Table 1. GPC data are provided in the Appendix and the molecular weight of the LCPU-M is reported in Table 1.

FT-IR and proton NMR characterization of the LCPU-M were completed and the results were compared to those of LCPU to verify the complete conversion of LCPU to LCPU-M. Curve (a) and curve (b) in Figure 34 represent FT-IR spectra of pure LCPU and pure LCPU-M measured at 30°C upon cooling from the melt. The N-H stretching vibration at 3300 cm^{-1} and N-H bending vibration at 1500 cm^{-1} , in Figure 34, completely disappear in the LCPU-M, suggesting the absence of N-H groups in LCPU-M. In addition the appearance of a sharp, strong C=O peak at around 1705 cm^{-1} in LCPU-M suggests the absence of hydrogen bonded C=O groups in LCPU-M when compared to the relatively broader C=O peak in LCPU. The sharp C=O peak in LCPU-M corresponds to free C=O groups at around 1705 cm^{-1} and the broad C=O peak in pure LCPU corresponds to free C=O groups at around 1730 cm^{-1} , disordered (amorphous) hydrogen bonded C=O groups (to N-H groups) at around 1690 cm^{-1} , and ordered (crystalline) hydrogen bonded C=O groups (to N-H groups) at around 1670 cm^{-1} . The decrease in wave number of the free C=O peak from 1730 cm^{-1} (in LCPU) to 1705 cm^{-1} (in LCPU-M) is because the electron donating methyl group in N-CH₃ (in LCPU-M) decreases the electro-negativity of the nitrogen atom. This causes an increase in the C=O bond length and a corresponding decrease in its bond strength, which results in a lower wave number. Proton NMR characterization (Figure 31) indicates the disappearance of the two N-H proton peaks of LCPU (curve a) at 9.5 ppm (1H) and 8.75 ppm (1H) and the appearance of

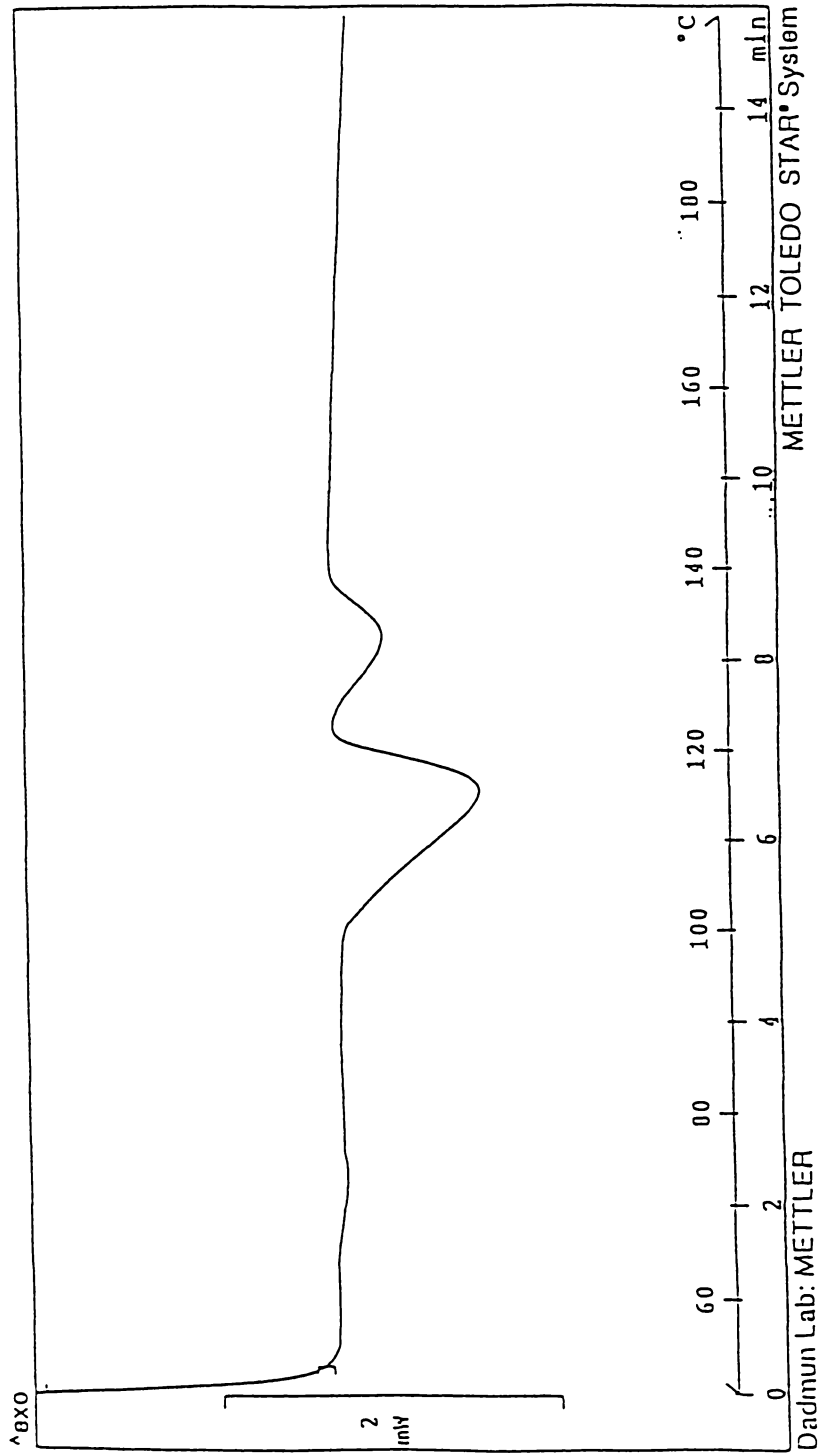


Figure 33. DSC curve of the N-methyl Liquid Crystalline Polyurethane (LCPU-M)

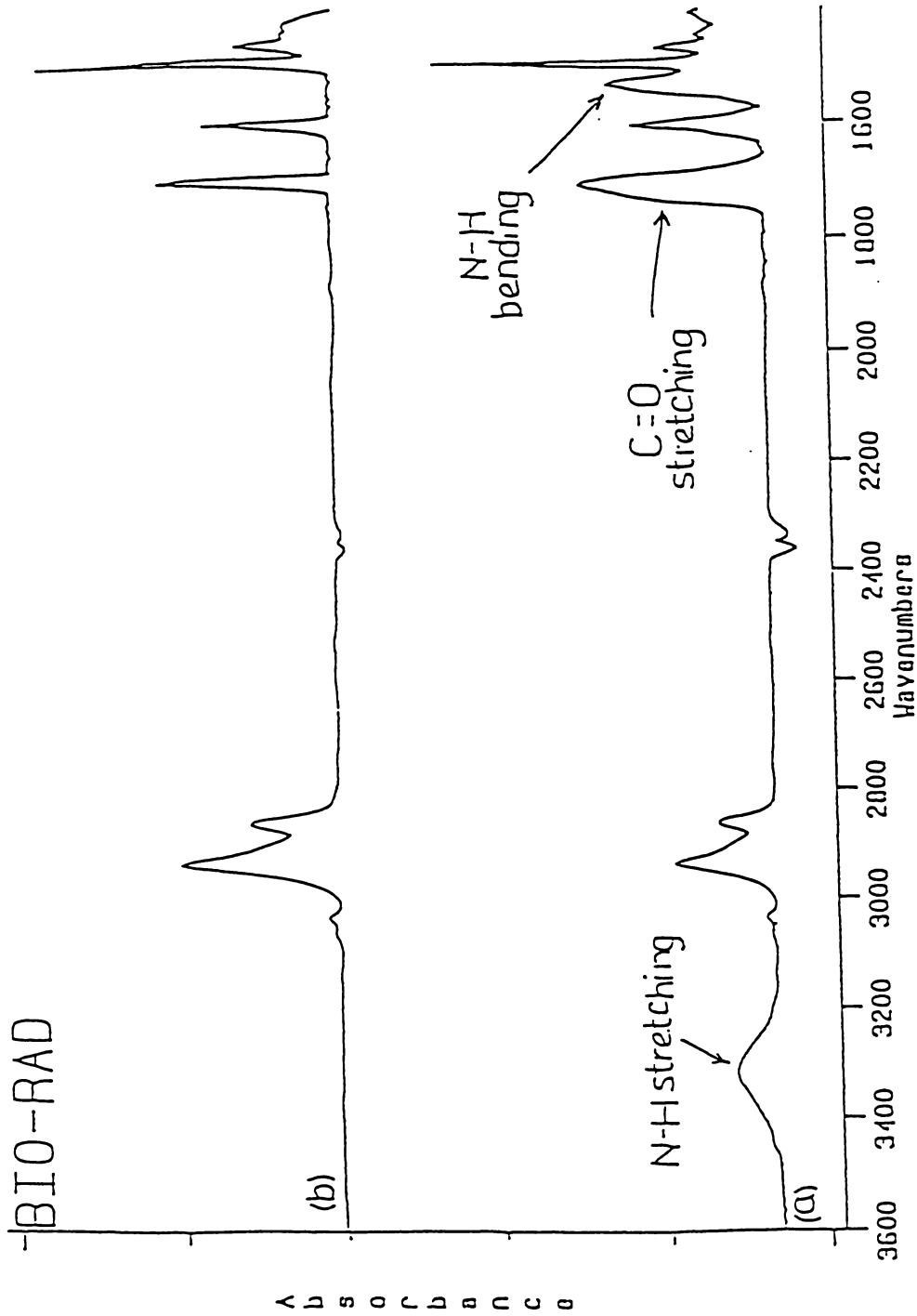


Figure 34. FT-IR spectra of pure LCPU (curve a) and LCPU-M (curve b) measured at 30°C upon cooling from the melt

the N-CH₃ proton peak in LCPU-M (curve b) at 3.4 ppm (6H). This again provides evidence for the complete conversion of LCPU to LCPU-M.

3.3 Results and Discussion

FT-IR Studies

The aim of this study is to understand the correlation between the liquid crystalline polymer composition, the copolymer composition, the extent of intermolecular H-bonding in a blend containing the LCP and the copolymer, and the phase behavior of that blend. In Chapter 2 of this dissertation, it is shown that miscible LCPU/PS-co-VPh blends can indeed be created by optimizing the amount of intermolecular hydrogen bonding by varying the PS-co-VPh composition (i.e., spacing out the hydroxyl groups along the copolymer chain). In this chapter, a further improvement in blend miscibility is sought by structural manipulation of the LCP (achieved by eliminating H-bonding among the LCP chains, thereby converting LCPU to LCPU-M) in addition to that of the PS-co-VPh. The immediate logical question is: How do we know if improvement in blend miscibility occurs through this LCP structural manipulation? A simple answer is to compare the results obtained by structural modification of the LCP as well as the amorphous copolymer (LCPU-M/PS-co-VPh blends) with those obtained from structural modification of the amorphous copolymer alone (LCPU/PS-co-VPh blends). The scheme of hydrogen bonding associations in LCPU-M/PS-co-VPh blends is shown in Figure 15.

In LCPU/PS-co-VPh blends, the extent of intermolecular hydrogen bonding between the two polymer components was quantitatively estimated using FT-IR. Likewise, in LCPU-M/PS-co-VPh blends, the same procedure of deconvoluting (using Peakfit software version

3.0) the carbonyl stretching vibration (around 1700 cm^{-1}) of the FT-IR curve has been applied to determine the percentage of carbonyl groups in the system participating in intermolecular H-bonding between the two blend components. In LCPUs blends, we have contributions to the C=O stretching band from free C=O groups (around 1730 cm^{-1}), intermolecularly hydrogen bonded C=O groups (around 1710 cm^{-1}), and intramolecularly H-bonded C=O groups (around 1690 cm^{-1}). However, in the LCPUs-M blends, contributions to this C=O stretching band envelope are assigned to free (non-hydrogen bonded) C=O groups (around 1705 cm^{-1}) and intermolecularly H-bonded C=O groups (to O-H groups) (around 1680 cm^{-1}). As mentioned in the previous chapter, the percentage of O-H groups on the copolymer that is intermolecularly H-bonded to C=O cannot be determined quantitatively by deconvoluting the O-H stretching band at 3300 cm^{-1} . This is primarily due to the difficulty of quantitative analysis of hydroxyl region due to overlap of all the contributing peaks thus giving rise to a very broad O-H peak.⁷¹ Also, this O-H peak is plagued by the presence of the overtone of the fundamental C=O stretching vibration.⁷² In addition to these factors, in LCPUs blends there is the presence of the overlap between the N-H and the O-H stretching bands. Therefore, the amount of O-H groups that is involved in intermolecular H-bonding was estimated stoichiometrically. The percent of O-H groups that participate in intermolecular H-bonding is estimated by dividing the experimentally determined percent of C=O groups participating in hydrogen bonding by the ratio of the number of O-H groups to C=O groups present in the blend. More details about the estimation of the percent of O-H groups involved in intermolecular H-bonding have been provided in Chapter 2.

Figure 35 shows the FT-IR curves in the C=O stretching region ($1800-1650\text{ cm}^{-1}$) for

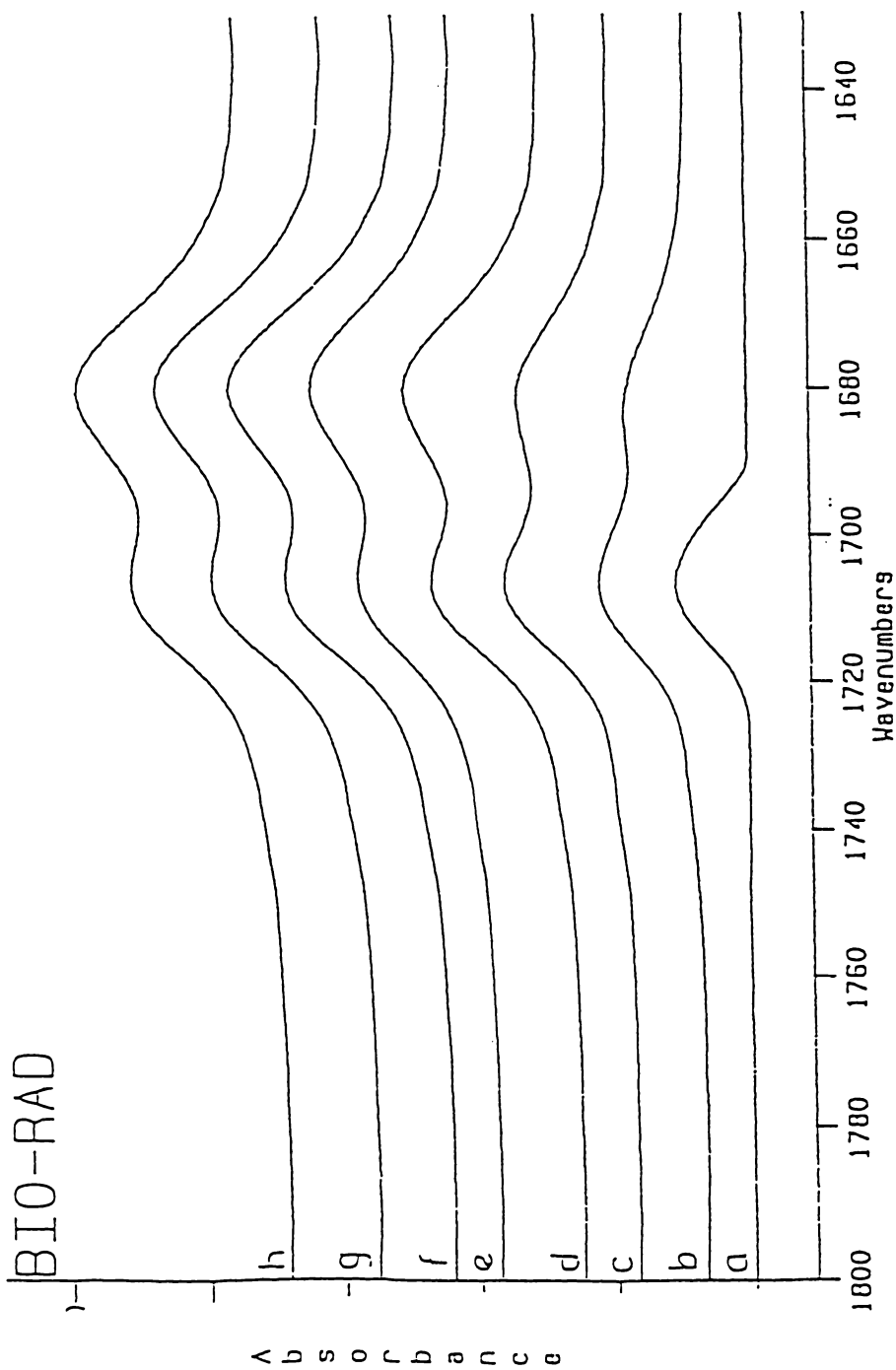


Figure 35. FT-IR spectra of C=O stretching region for blends containing 80 wt.% PS-co-VPh and 20 wt.% LCPU-M measured at 180°C. Curve (a) is the pure LCPU-M, while the remaining curves are for blends containing PS-co-VPh with b) 5 mole % c) 10 mole % d) 20 mole % e) 30 mole % f) 40 mole % g) 50 mole % h) 100 mole % VPh

a blend containing LCPU-M and PS-co-VPh (80 wt.% PS-co-VPh) for various copolymer compositions measured at 180°C. This figure demonstrates the increase in the amount of intermolecular H-bonding with increase in the amount of VPh in the copolymer from 0 to 40% (curves b-f), as is shown by the increase in the C=O peak at 1680 cm⁻¹. However, there is no significant change observed in this peak above 40% VPh in the copolymer (curves f-h). FT-IR curves of the C=O stretching region of blends that contain LCPU-M and PS-co-VPh(40) of various composition measured at 180°C are shown in Figure 36. This figure shows an increase in the extent of intermolecular H-bonded C=O groups with increase in the amount of PS-co-VPh(40) in the blend from 0 to 80 wt.%, which is clearly illustrated by an increase in the peak at around 1680 cm⁻¹. A better understanding of these curves can be obtained by quantitatively estimating the extent of intermolecular H-bonding in these blends by deconvoluting the C=O stretching peaks of these IR curves. The parameters obtained as a result of deconvoluting LCPU-M/PS-co-VPh(40) blends are shown in Table 4. During deconvolution, a Gaussian band shape was used. We allowed variations only in hydrogen bonded C=O frequency and kept the free C=O vibration position fixed. This is due to the fact that hydrogen bond geometry distribution and strength varies as a function of temperature.⁷² The area under the two peaks that contribute to the C=O stretching vibration are determined from the deconvolution procedure; A₁ is the area of the free carbonyl peak and A₂ is the area of the peak associated with the intermolecularly hydrogen bonded carbonyls. As explained earlier, the absorption coefficient of the hydrogen bonded band is different than that of free band. To account for this difference in absorption coefficients, a ratio of the absorption coefficients of these bands is required. The absorption coefficient ratio (K) was found using

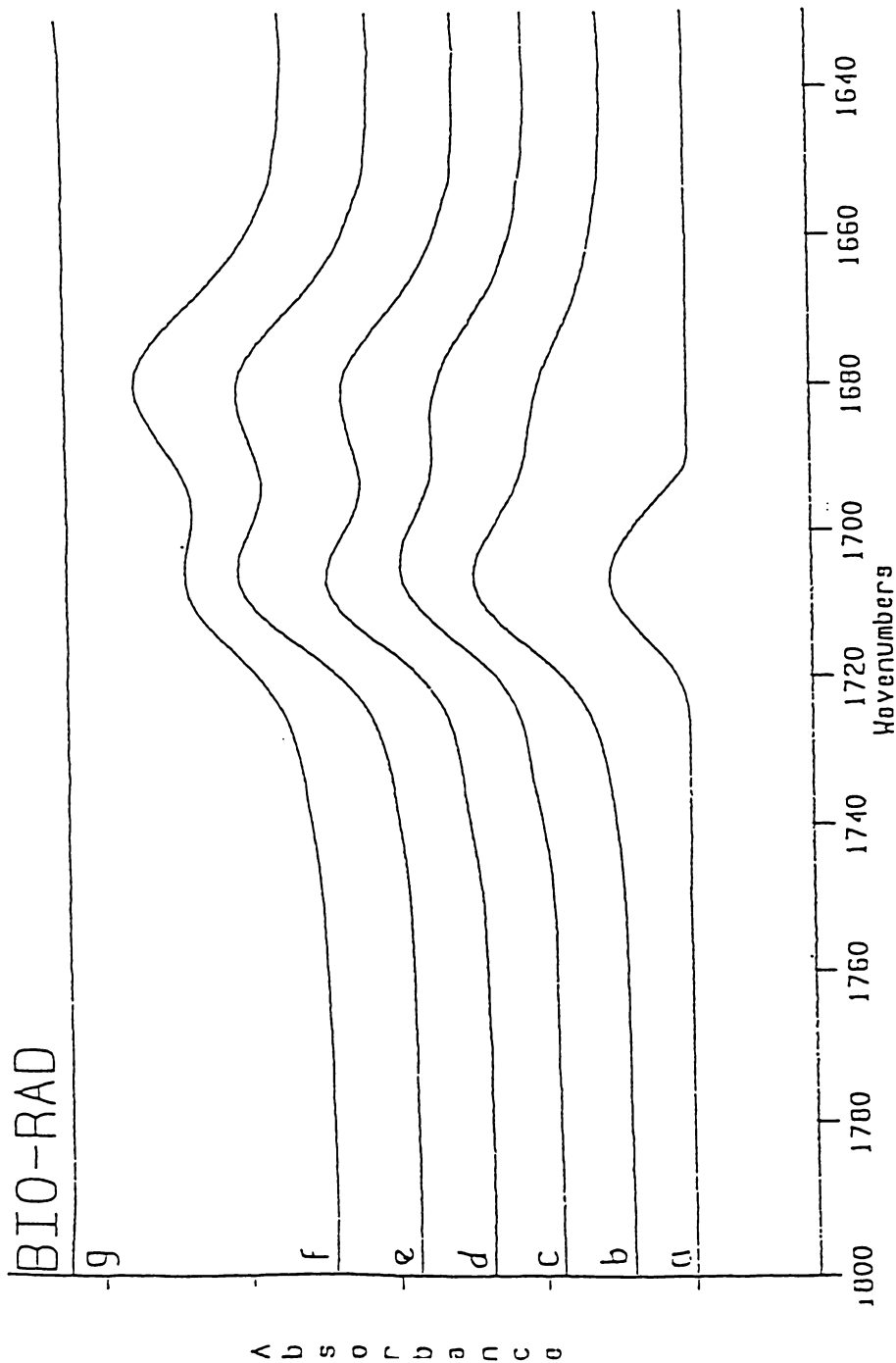


Figure 36. FT-IR spectra of C=O stretching region for blends containing PS-co-VPh(40) measured at .180°C. The curves correspond to blends with a composition of (LCPU-M/PS-co-VPh wt/wt) a) 100/0 b) 80/20 c) 60/40 d) 50/50 e) 40/60 f) 20/80 g) 0/100

Table 4. Deconvolution results of the C=O stretching region for pure LCPU-M and blends containing 80 wt.% PS-co-VPh copolymer for various copolymer compositions measured at 180°C.

| %VPh in PS-co-VPh | Free C=O | | | Intermolecularly H-bonded C=O | | | % C=O intermolecularly H-bonded |
|-------------------|--------------------------|----------------------------|-------|-------------------------------|----------------------------|-------|---------------------------------|
| | ν^* cm ⁻¹ | $W_{1/2}$ cm ⁻¹ | A_1 | ν cm ⁻¹ | $W_{1/2}$ cm ⁻¹ | A_2 | |
| Pure LCPU-M | 1707 | 18.0 | 7.382 | - | - | - | - |
| 5 | 1707 | 18.1 | 5.750 | 1682.2 | 30.2 | 1.538 | 14.8 |
| 10 | 1707 | 18.1 | 4.473 | 1680.3 | 30.6 | 2.827 | 29.1 |
| 20 | 1707 | 18.2 | 4.075 | 1679.5 | 30.5 | 3.961 | 38.7 |
| 30 | 1707 | 18.0 | 3.562 | 1679.0 | 30.8 | 3.843 | 41.2 |
| 40 | 1707 | 18.0 | 3.284 | 1678.8 | 31.0 | 3.957 | 43.9 |
| 50 | 1707 | 18.2 | 3.275 | 1678.8 | 31.0 | 3.995 | 44.2 |
| 100 | 1707 | 18.2 | 3.312 | 1678.8 | 31.0 | 4.106 | 44.6 |

* Fixed during curve fitting

Absorptivity Coefficient (K) = 1.54; $A_2' = A_2/K$; $A_T = A_1 + A_2'$

% C=O intermolecularly H-bonded = $(A_2'/A_T) * 100$

the method of Coleman and Painter^{72,75-77} to account for this differing absorptivity coefficients.

$$K = [A_{\text{HB}}^{\text{T}2} - A_{\text{HB}}^{\text{T}1}] / [A_{\text{F}}^{\text{T}1} - A_{\text{F}}^{\text{T}2}] \quad (3.1)$$

where $A_{\text{HB}}^{\text{T}1}$ and $A_{\text{HB}}^{\text{T}2}$ are hydrogen bonded carbonyl absorption intensities at temperatures T_1 and T_2 and $A_{\text{F}}^{\text{T}1}$ and $A_{\text{F}}^{\text{T}2}$ are free C=O absorption intensities at temperatures T_1 and T_2 .

The absorption intensities of the hydrogen bonded C=O band (A_2) was corrected for the difference in absorptivity coefficients by dividing this area by K ($A_2' = A_2 / K$). Finally, the percent of C=O groups involved in intermolecular H-bonding is calculated by:

$$\% \text{ C=O} = A_2' / (A_1 + A_2') \quad (3.2)$$

The deconvolution results for LCPU-M/PS-co-VPh blends containing 80 wt.% PS-co-VPh for various copolymer compositions measured at 180°C are listed in Table 4.

Figures 21 and 37 show the percent C=O intermolecularly hydrogen bonded to O-H as a function of mole% VPh in the copolymer for various blend compositions of LCPU/PS-co-VPh and LCPU-M/PS-co-VPh blends respectively measured at 180°C. In LCPU blends, the amount of C=O that participates in intermolecular H-bonding increases up to 20 mole% VPh, but levels off above 20%. The logical interpretation of this curve is that as the amount of VPh increases from 0 to 20%, more hydroxyl groups are introduced that can H-bond with C=O groups and thus the curve increases. However, above 20% VPh in the copolymer, there is very little increase in the amount of intermolecular H-bonding, suggesting that additional O-H groups are unable to find suitably oriented or positioned C=O groups with which to form an intermolecular H-bond. In LCPU-M blends, the curve increases up to 40 mole% and levels off after that. An important observation is that the LCPU-M blends show an increased

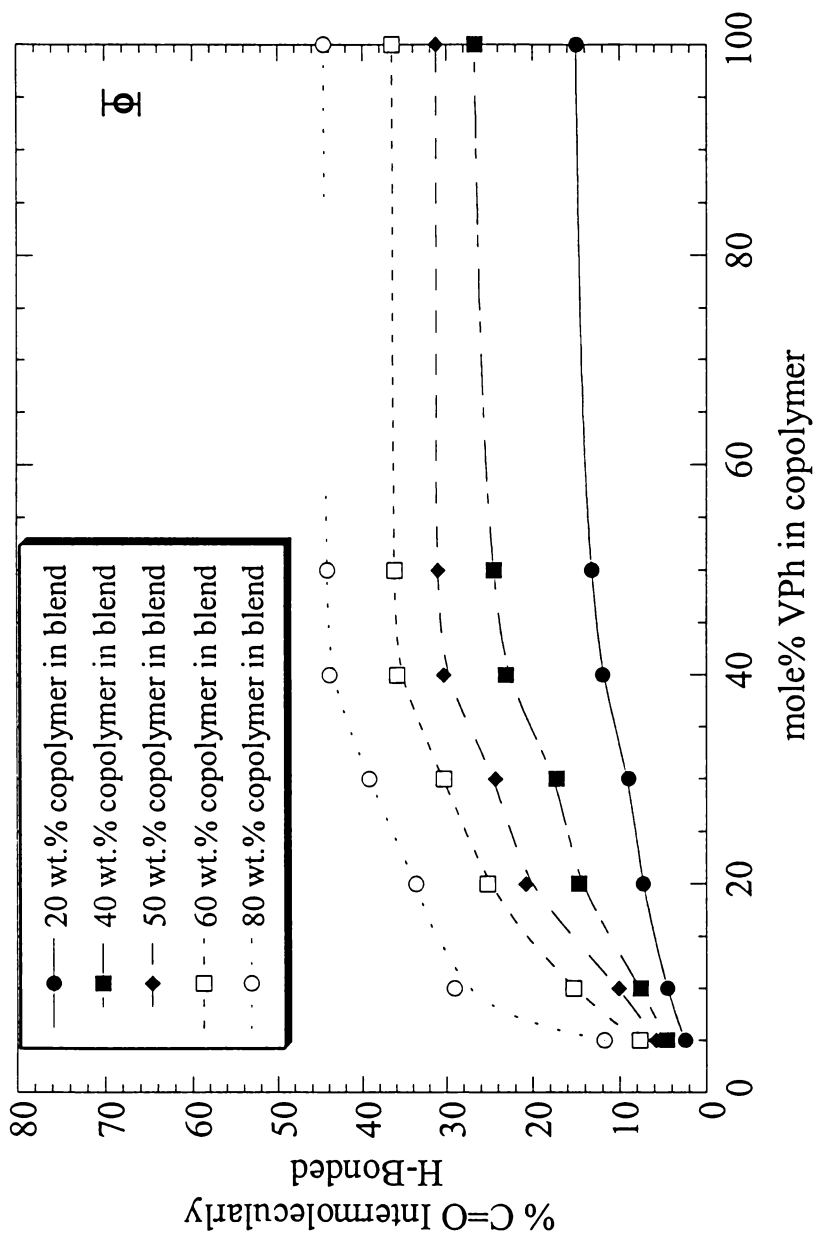


Figure 37. Percent of carbonyl groups participating in intermolecularly hydrogen bonding as a function of PS-co-VPh copolymer composition for different blend compositions of LCP-U-M and PS-co-VPh measured at 180°C. Error Bar in the plot corresponds to $\pm 2\%$

percent of C=O intermolecular H-bonding than the LCPU blends for all copolymer compositions studied, which verifies that a greater fraction of C=O groups participate in intermolecular H-bonding for LCPU-M.

Figures 22 and 38 show the percent O-H intermolecularly H-bonded to C=O as a function of mole% VPh in the copolymer for various blend compositions of LCPU/PS-co-VPh and LCPU-M/PS-co-VPh blends, respectively, measured at 180°C. In LCPU blends, the percentage of O-H that participate in intermolecular hydrogen bonding does not change much up to 20 mole% VPh in the copolymer, but decreases as more O-H groups are included on the copolymer chain. These results show that, in general, decreasing the distance between O-H groups increases the probability of intramolecular H-bonding which, in turn, decreases the number of O-H groups that can participate in intermolecular hydrogen bonding. In LCPU-M blends, the curves does not change much up to 40 mole% before they start to decrease. More importantly, there is a greater % O-H intermolecularly hydrogen bonded to C=O in LCPU-M blends than in LCPU blends for all copolymer compositions. This is presumably due to a larger number of C=O groups available for intermolecular hydrogen bonding in LCPU-M blends.

Thus, FT-IR results suggest that optimum intermolecular hydrogen bonding occurs for a copolymer with 20 mole% VPh for LCPU blends and 40 mole% VPh for LCPU-M blends. It is clear that, at every copolymer composition studied in this work, an increased amount of intermolecular hydrogen bonding is obtained in LCPU-M blends compared to LCPU blends. In addition, it is quite obvious that optimum amount of intermolecular hydrogen bonding occurs for a copolymer with a larger mole% VPh for LCPU-M blends

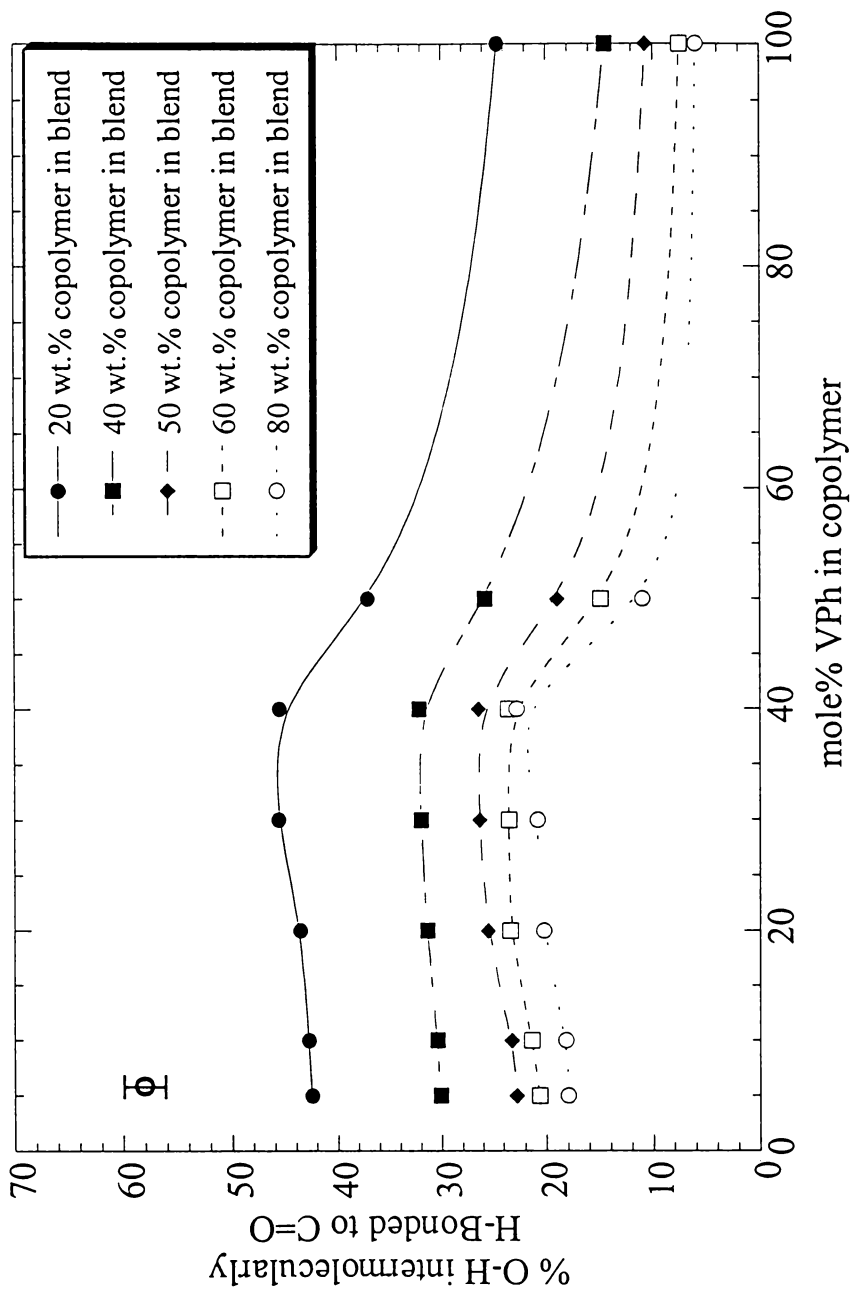


Figure 38. Percent of hydroxyl groups participating in intermolecularly hydrogen bonding as a function of PS-co-VPh copolymer composition for different blend compositions of LCPU-M and PS-co-VPh measured at 180°C. Error Bar in the plot corresponds to $\pm 2\%$

relative to that for LCPUs blends. These observations signify an increased amount of C=O groups that participate in intermolecular hydrogen bonding in LCPUs-M blends. The increased availability of C=O groups is due to the absence of hydrogen bonding between LCP chains. Furthermore, the spacing between O-H groups in the copolymer chains in LCPUs-M blends seem to show an effect similar to that in the LCPUs blends. The results of this “spacing effect” study are in agreement with similar work by Coleman et al.⁵²⁻⁵⁸ and Radmard et al.⁵⁹, all of which indicate that the extent of intermolecular H-bonding is an optimum when the hydroxyl groups are distanced apart on the copolymer chain. This increased spacing contributes to improvement in the rotational freedom of the functional groups and causes a decrease in the chance of H-bonding between neighboring O-H groups, thereby improving the accessibility and availability of O-H for intermolecular hydrogen bonding with C=O. However, this increasing trend lasts only until a certain amount of VPh in the copolymer (40 mole% and 20 mole% in LCPUs-M and LCPUs blends respectively) below which the number of hydroxyl groups in the copolymer becomes so low that it limits the number of possible intermolecular H-bonds that can be formed.

Our FT-IR results indicate that there is no significant change in the percent of carbonyl groups participating in intermolecular H-bonding above 40 mole% VPh in the copolymer in LCPUs-M/PS-co-VPh blends (Figure 37). Therefore, a significant decrease in the percent of hydroxyl groups participating in intermolecular H-bonding is expected as a result of the limited number of carbonyl groups participating in intermolecular H-bonding as more O-H groups are incorporated into the blend. On the contrary, our FT-IR results indicate only a modest decrease in the percent of hydroxyl groups that participate in intermolecular H-

bonding above 40 mole% VPh in the copolymer (see Figure 38).

As discussed previously in this chapter, the percentage of hydroxyl groups that participate in intermolecular hydrogen bonding with C=O groups is estimated stoichiometrically by dividing the percentage of carbonyl groups participating in hydrogen bonding by the ratio of the number of hydroxyl groups to carbonyl groups present in the blend. The number of carbonyl and hydroxyl units in the blend is in turn estimated from the molecular weights of LCPU-M and PS-co-VPh and the composition of the LCPU-M/PS-co-VPh blend system. Since the molecular weights of the copolymers used in this study are different for different copolymer compositions (see Table 1), the number of C=O and O-H units in the blend is estimated individually for every set of blend composition and copolymer composition. It is to be noted that the ratio of the number of hydroxyl groups to carbonyl groups present in the blend in turn increases with an increase in the molecular weight of the copolymer and/or an increase in the mole% VPh in the copolymer. Thus we cannot merely correlate the data in Figures 37 and 38 by considering the composition of the copolymer since one must also consider the changes in the molecular weight of the copolymer.

As an example, in Figure 38, we find a modest decrease in the percent of hydroxyl groups participating in intermolecular H-bonding as the mole% VPh in the copolymer increases from 50 to 100, although a halving is expected due to the doubling in mole% VPh in the copolymer if only the composition of the copolymer is considered. The molecular weights of the PS-co-VPh(50) (34,100 g/mol) and Pure PVPh (22,000 g/mol) used in this study are significantly different and, therefore, also impacts the correlation between Figures 37 and 38.

Thermal and Optical Phase Behavior Studies

In order to correlate the extent of intermolecular hydrogen bonding to the phase behavior of these blends, the phase diagrams of blends containing LCPU-M and PS-co-VPh that consist of 5%, 10%, 20%, 30%, 40% and 50% VPh [PS-co-VPh(5), PS-co-VPh(10), PS-co-VPh(20), PS-co-VPh(30), PS-co-VPh(40), PS-co-VPh(50)] were determined using DSC and optical microscopy. Figures 39-44 show the DSC curves of LCPU-M/PS-co-VPh(n) blends (n = 5, 10, 20, 30, 40, and 50 in that order) for various blend compositions. A single glass transition temperature is observed for blend compositions above 50 wt.% LCPU/PS-co-VPh(40), above 55 wt.% LCPU/PS-co-VPh(30) and LCPU/PS-co-VPh(20), above 65 wt.% LCPU/PS-co-VPh(10), and above 75 wt.% LCPU/PS-co-VPh(5) and LCPU/PS-co-VPh(50), which suggests miscibility in these regimes. Figures 45-50 compares the experimental T_g to the expected T_g of miscible blends as calculated from the theoretical Fox equation⁷⁸ and provides further evidence of miscibility in these blends. This comparison shows an agreement of experimental and theoretical T_g values in the same regions, suggesting miscibility in this window. The DSC plots of miscible LCPU blends with PS-co-VPh have already been reported in the previous chapter. With the data obtained from phase contrast optical microscopy, phase diagrams were mapped as temperature–composition plots for the blends of LCPU-M with PS-co-VPh and are shown in Figure 51. It was determined previously by FT-IR analysis that LCPU-M/PS-co-VPh(40) blend system gives an optimum (maximum) amount of intermolecular H-bonding among all the LCPU-M/PS-co-VPh blends studied in this work. Furthermore, our phase behavior data demonstrate the broadest miscibility window for LCPU-M/PS-co-VPh(40) blend system. A logical conclusion thereby

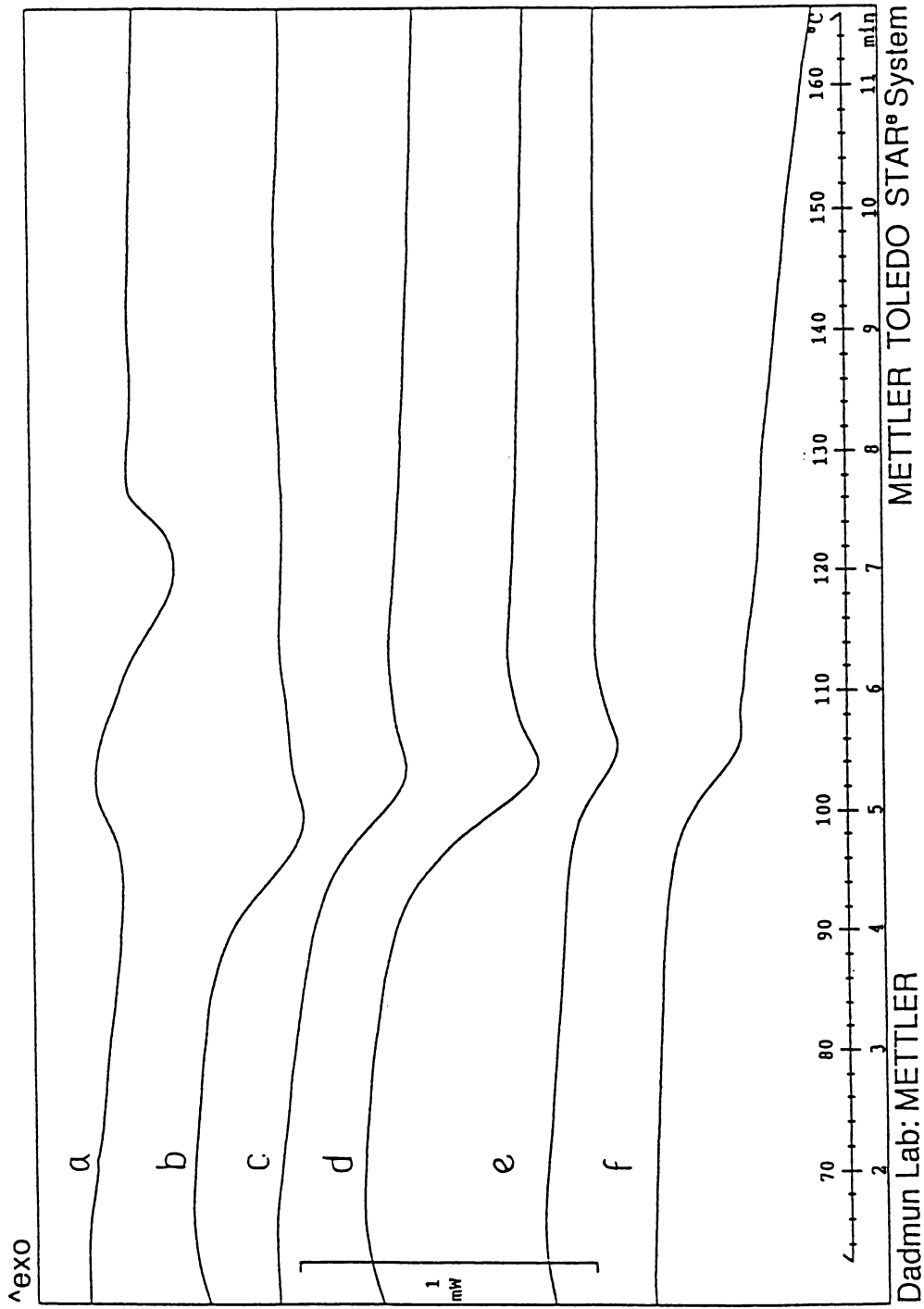


Figure 39. Representative DSC curves of blends containing LCPU-M and PS-co-VPh(5). Compositions of the blends are (LCPU-M/PS-co-VPh(5) wt/wt) a) 25/75 b) 20/80 c) 15/85 d) 10/90 e) 5/95 f) 0/100

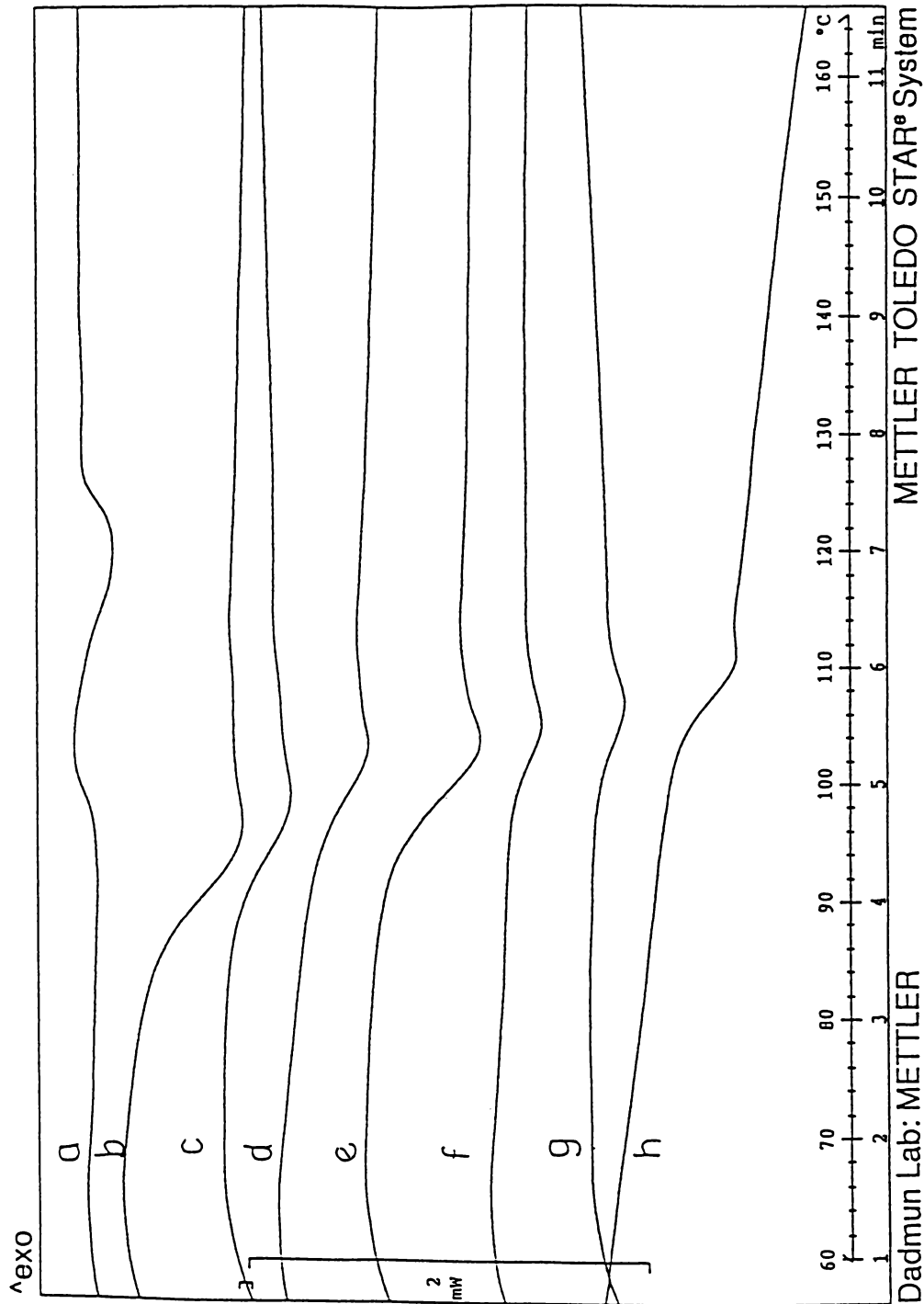


Figure 40. Representative DSC curves of blends containing LCPU-M and PS-co-VPh(10). Compositions of the blends are (LCPU-M/PS-co-VPh(10) wt/wt) a) 35/65 b) 30/70 c) 25/75 d) 20/80 e) 15/85 f) 10/90 g) 5/95 h) 0/100

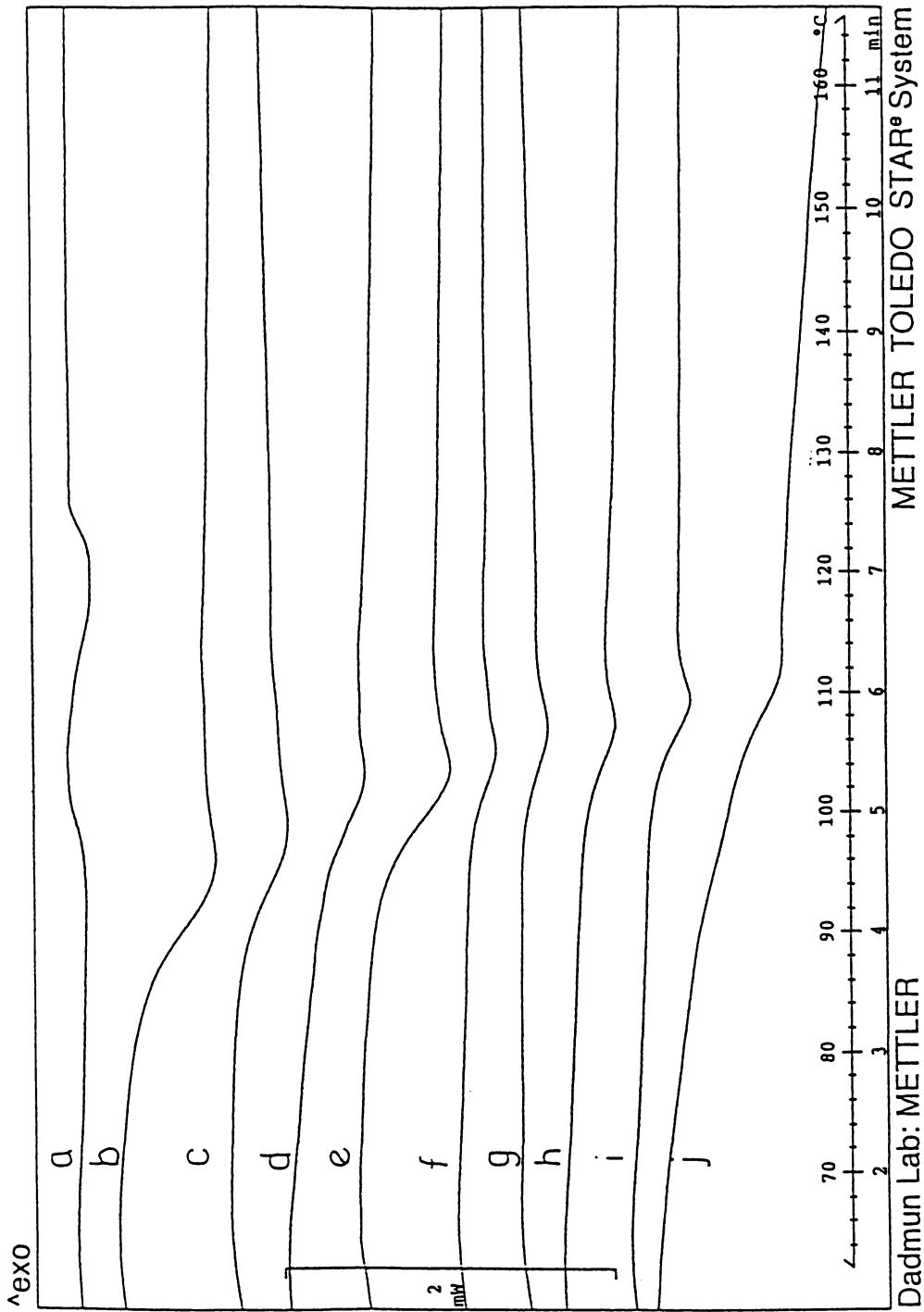
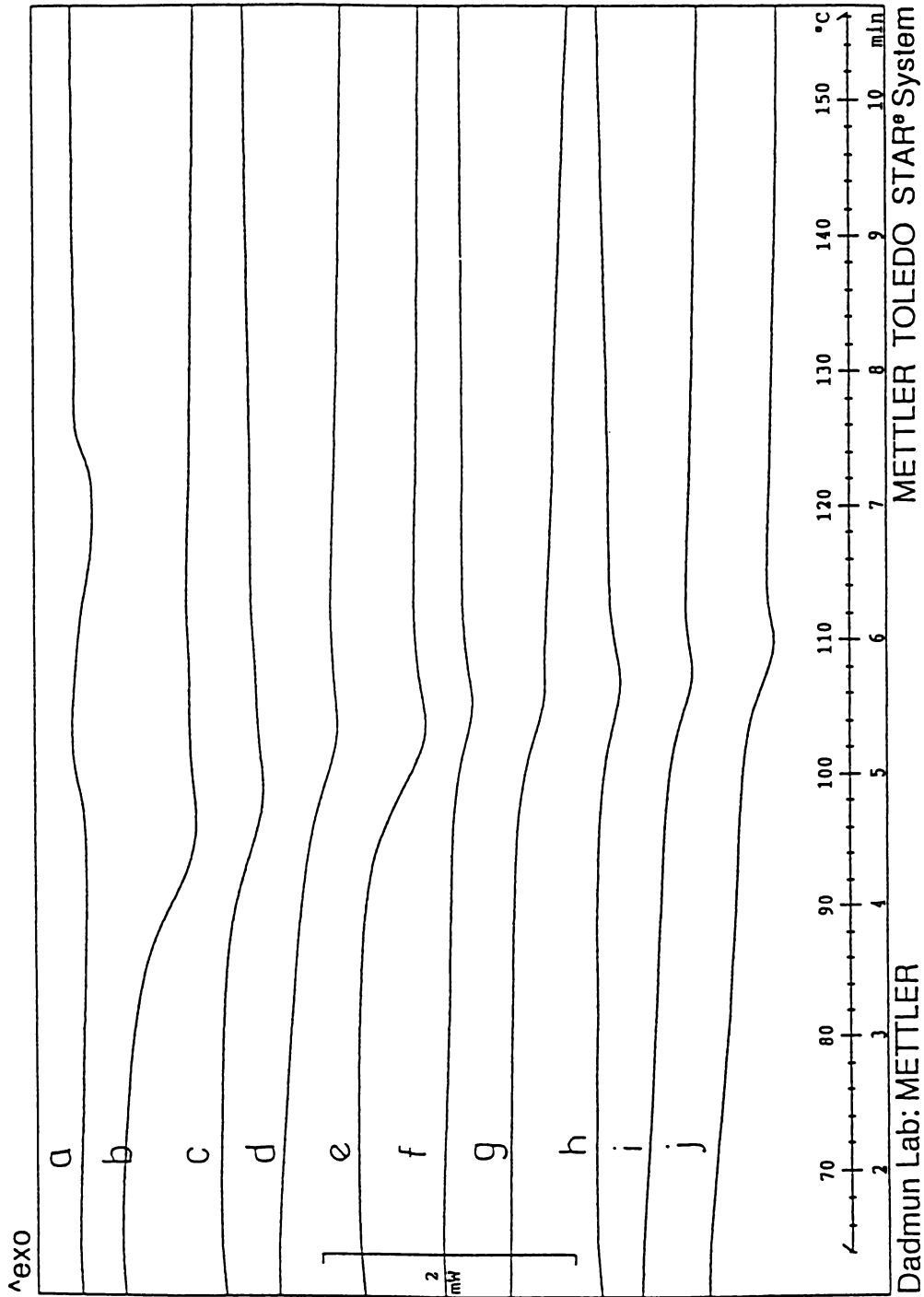


Figure 41. Representative DSC curves of blends containing LCPUs-M and PS-co-VPh(20). Compositions of the blends are (LCPUs-M/PS-co-VPh(20) wt/wt) a) 45/55 b) 40/60 c) 35/65 d) 30/70 e) 25/75 f) 20/80 g) 15/85 h) 10/90 i) 5/95 j) 0/100



Dadmun Lab: METTLER

METTTLER TOLEDO STAR® System

Figure 42. Representative DSC curves of blends containing LCPU-M and PS-co-VPh(30). Compositions of the blends are (LCPU-M/PS-co-VPh(30) wt/wt) a) 45/55 b) 40/60 c) 35/65 d) 30/70 e) 25/75 f) 20/80 g) 15/85 h) 10/90 i) 5/95 j) 0/100

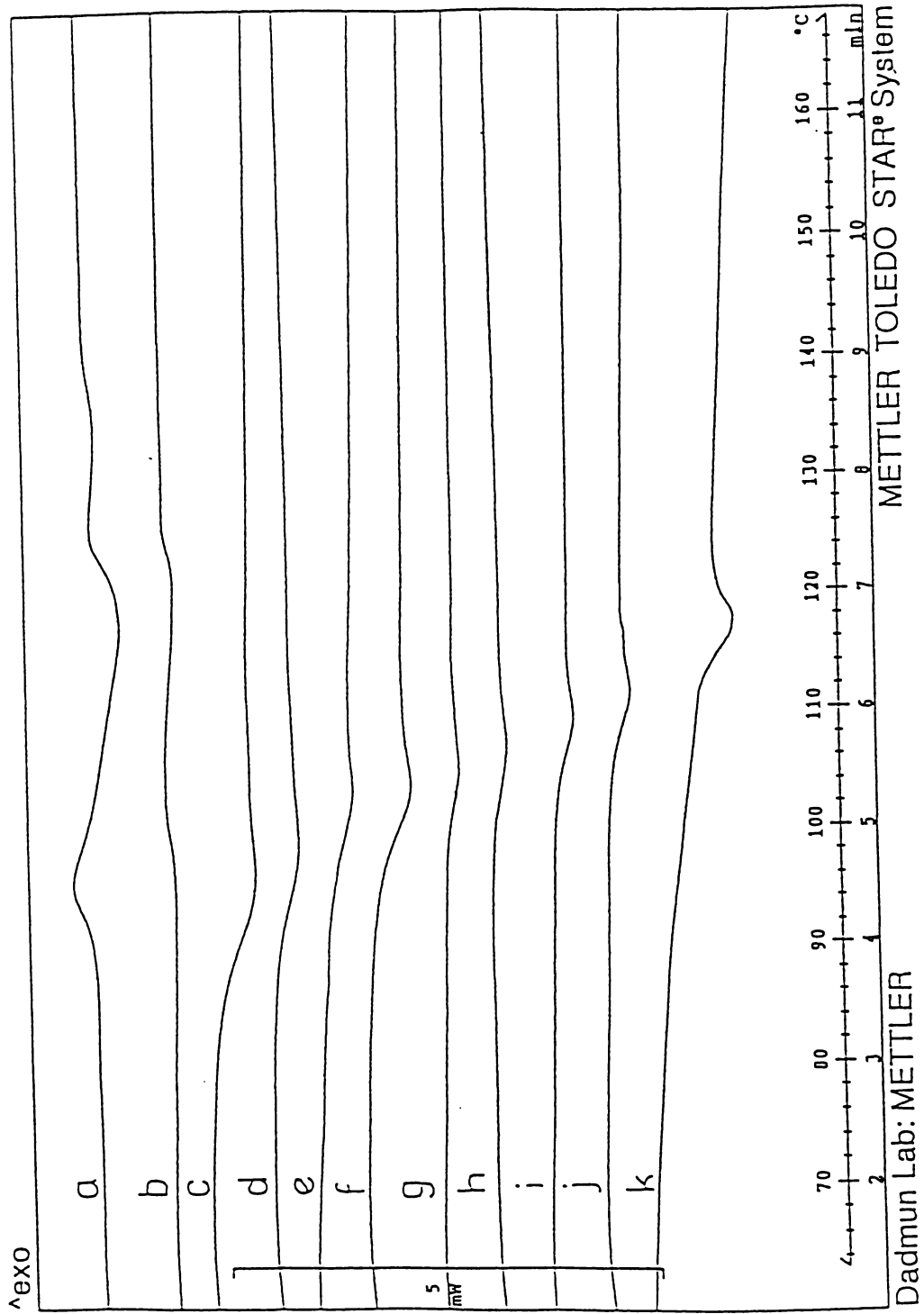


Figure 43. Representative DSC curves of blends containing LCPU-M and PS-co-VPh(40). Compositions of the blends are (LCPU-M/PS-co-VPh(40) wt/wt) a) 50/50 b) 45/55 c) 40/60 d) 35/65 e) 30/70 f) 25/75 g) 20/80 h) 15/85 i) 10/90 j) 5/95 k) 0/100

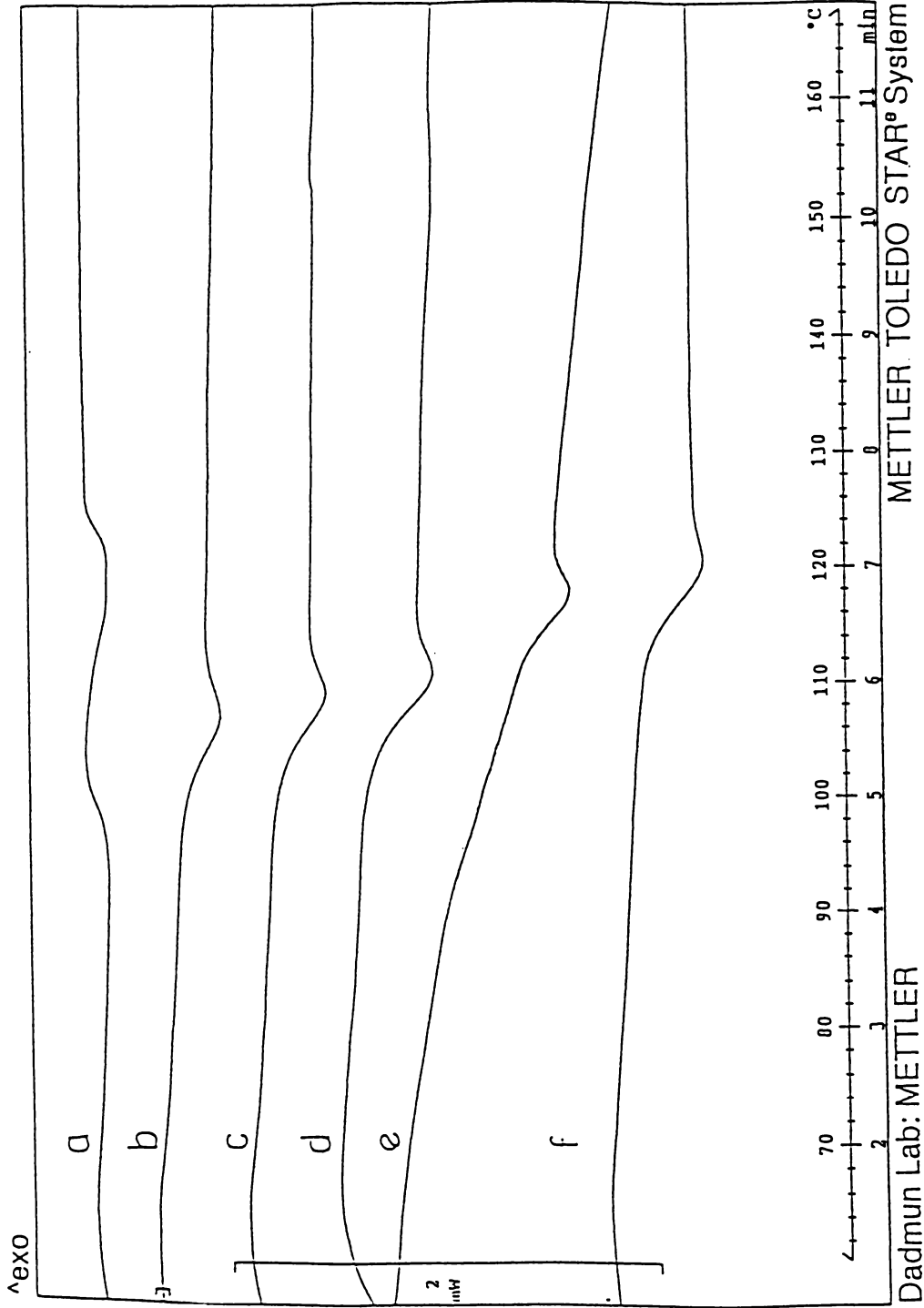


Figure 44. Representative DSC curves of blends containing LCPU-M and PS-co-VPh(50). Compositions of the blends are (LCPU-M/PS-co-VPh(50) w/wt) a) 25/75 b) 20/80 c) 15/85 d) 10/90 e) 5/95 f) 0/100

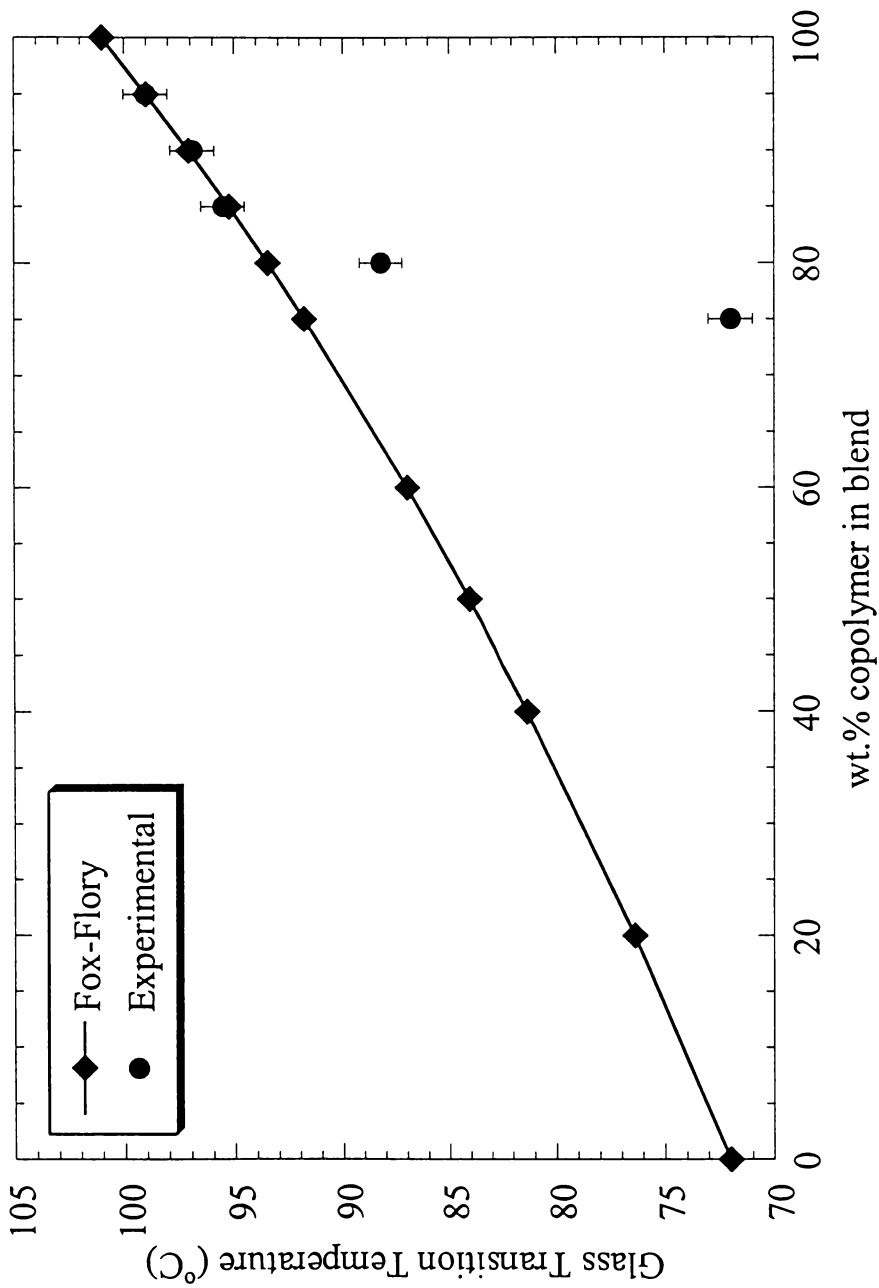


Figure 45. Experimental and theoretical glass transition temperatures of blends containing PS-co-VPh(5) and LCPU-M

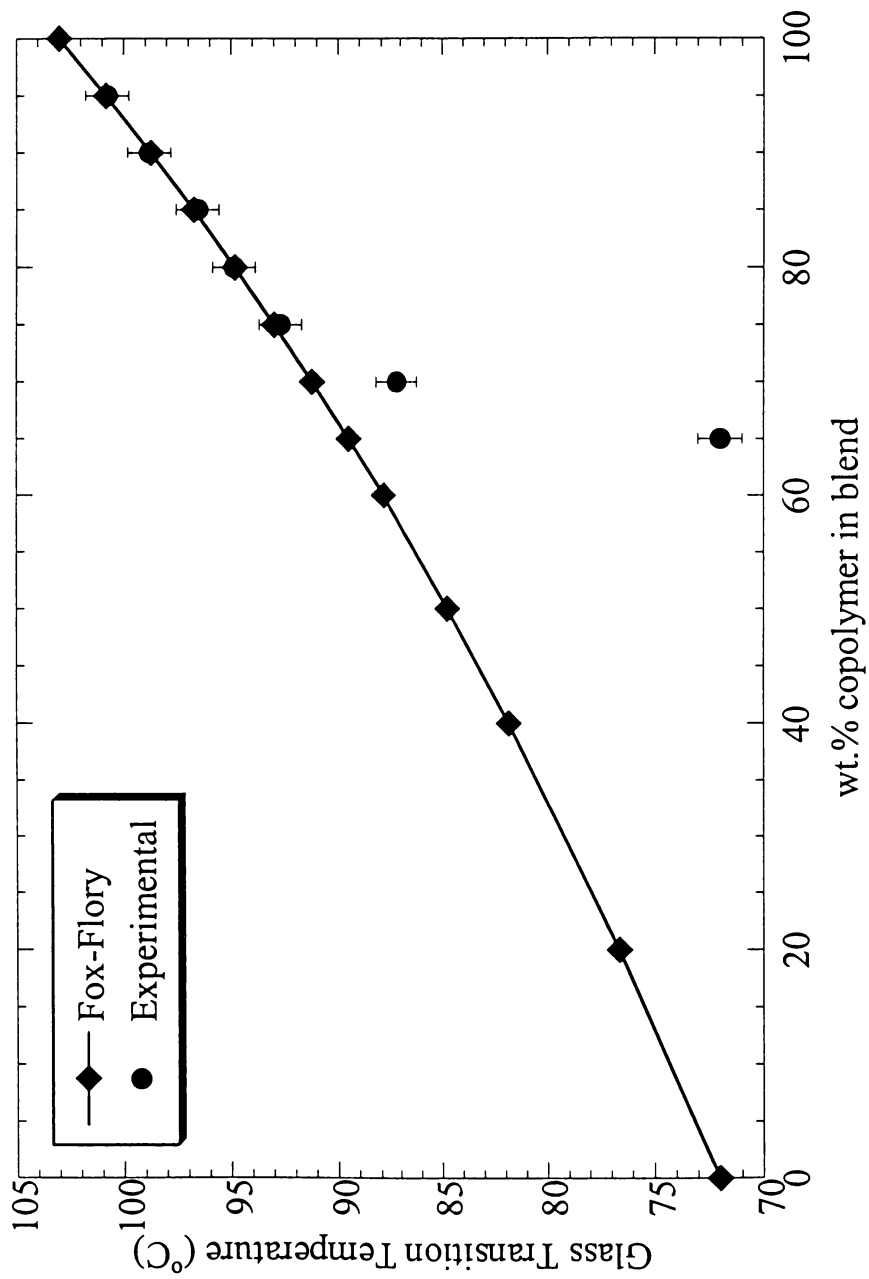


Figure 46. Experimental and theoretical glass transition temperatures of blends containing PS-co-VPh(10) and LCPU-M

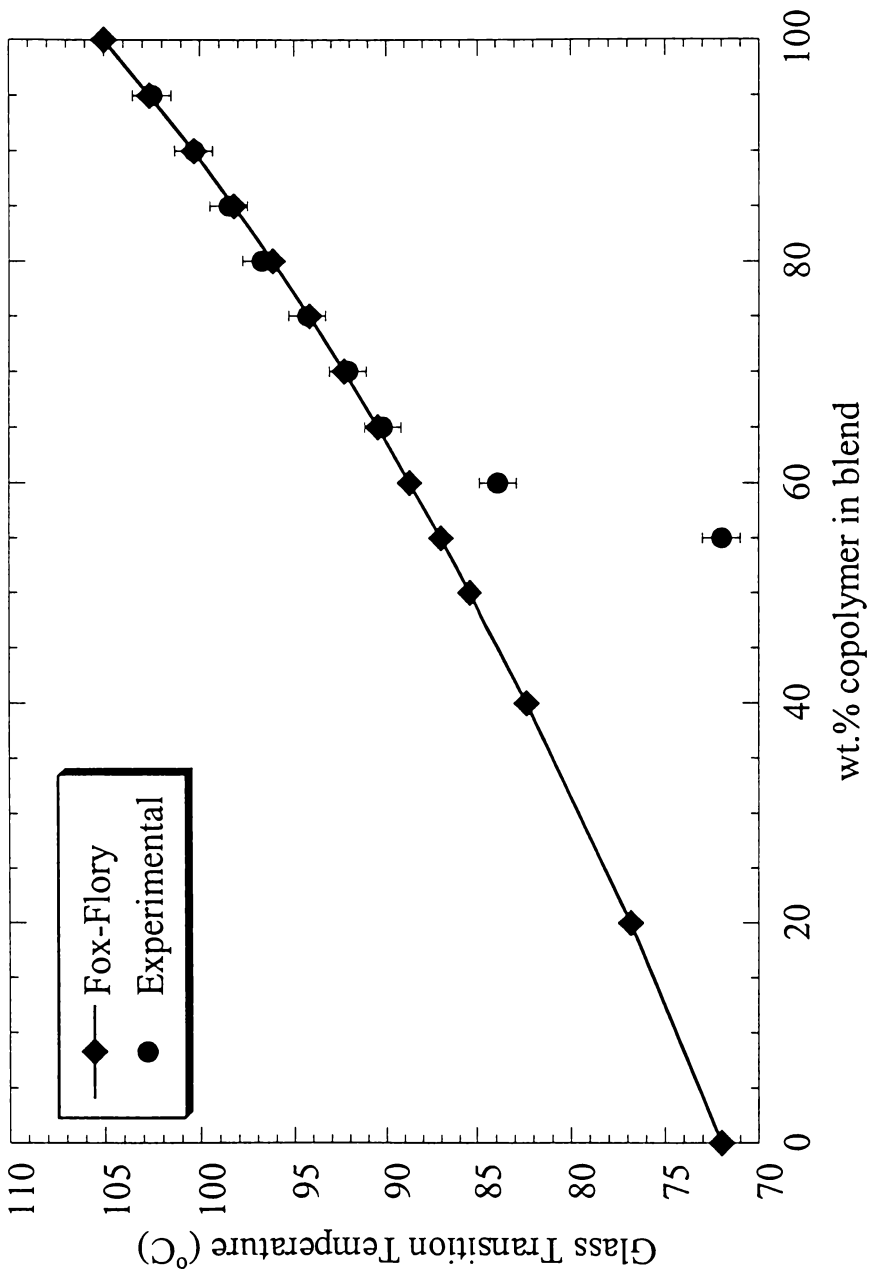


Figure 47. Experimental and theoretical glass transition temperatures of blends containing PS-co-VPh(20) and LCP-U-M

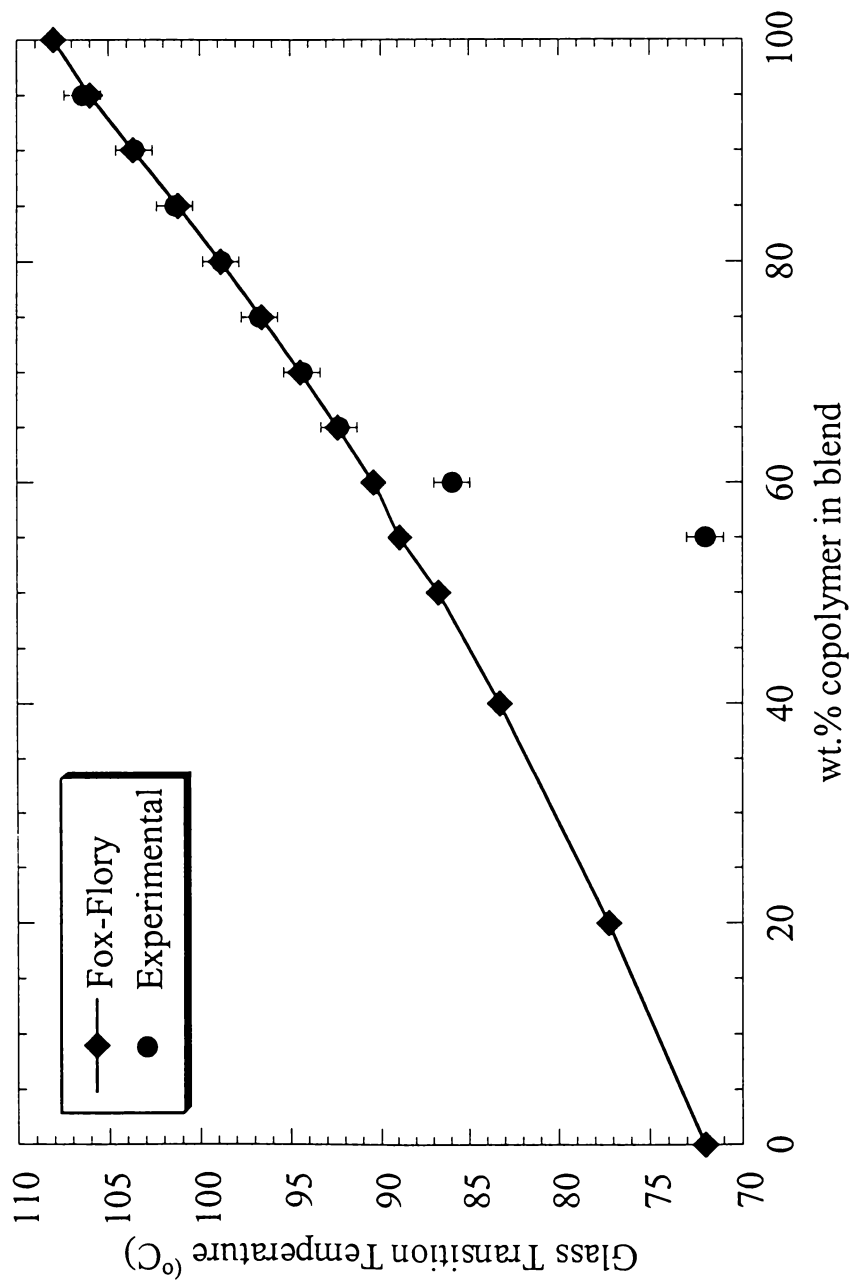


Figure 48. Experimental and theoretical glass transition temperatures of blends containing PS-co-VPh(30) and LCPU-M

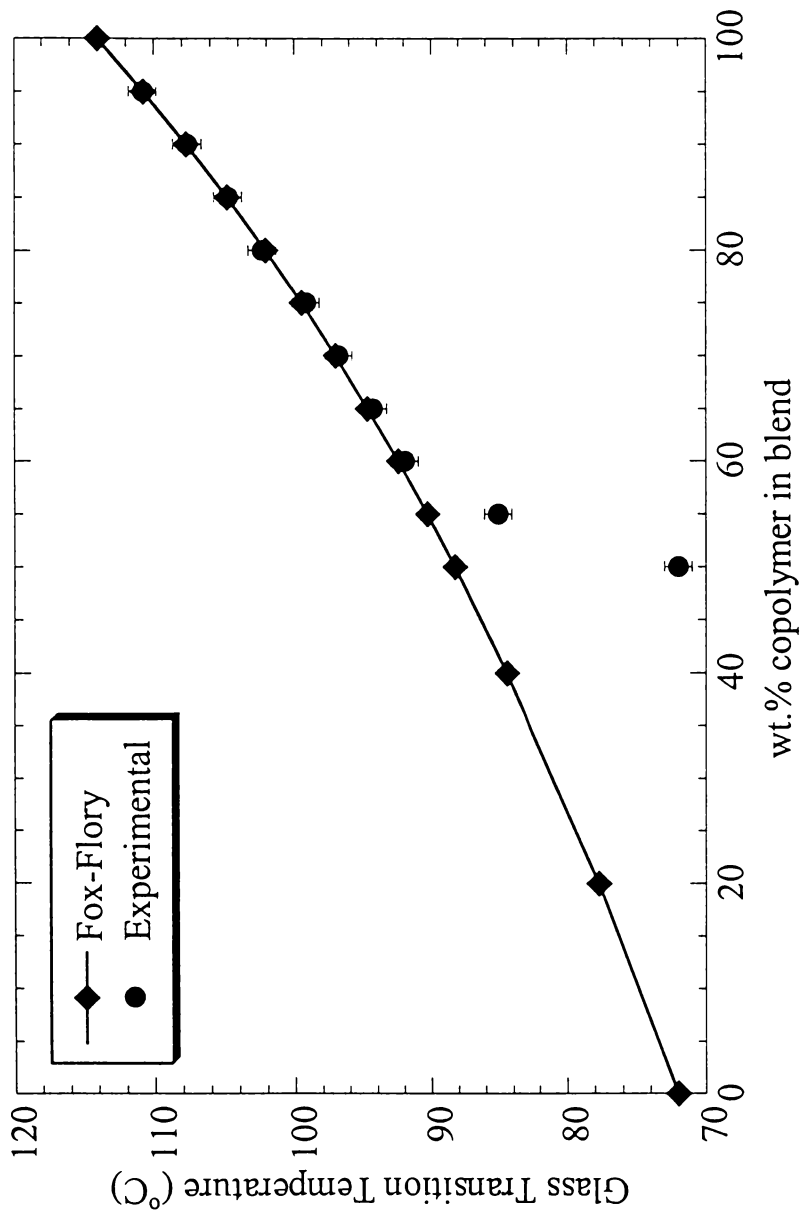


Figure 49. Experimental and theoretical glass transition temperatures of blends containing PS-co-VPh(40) and LCPU-M

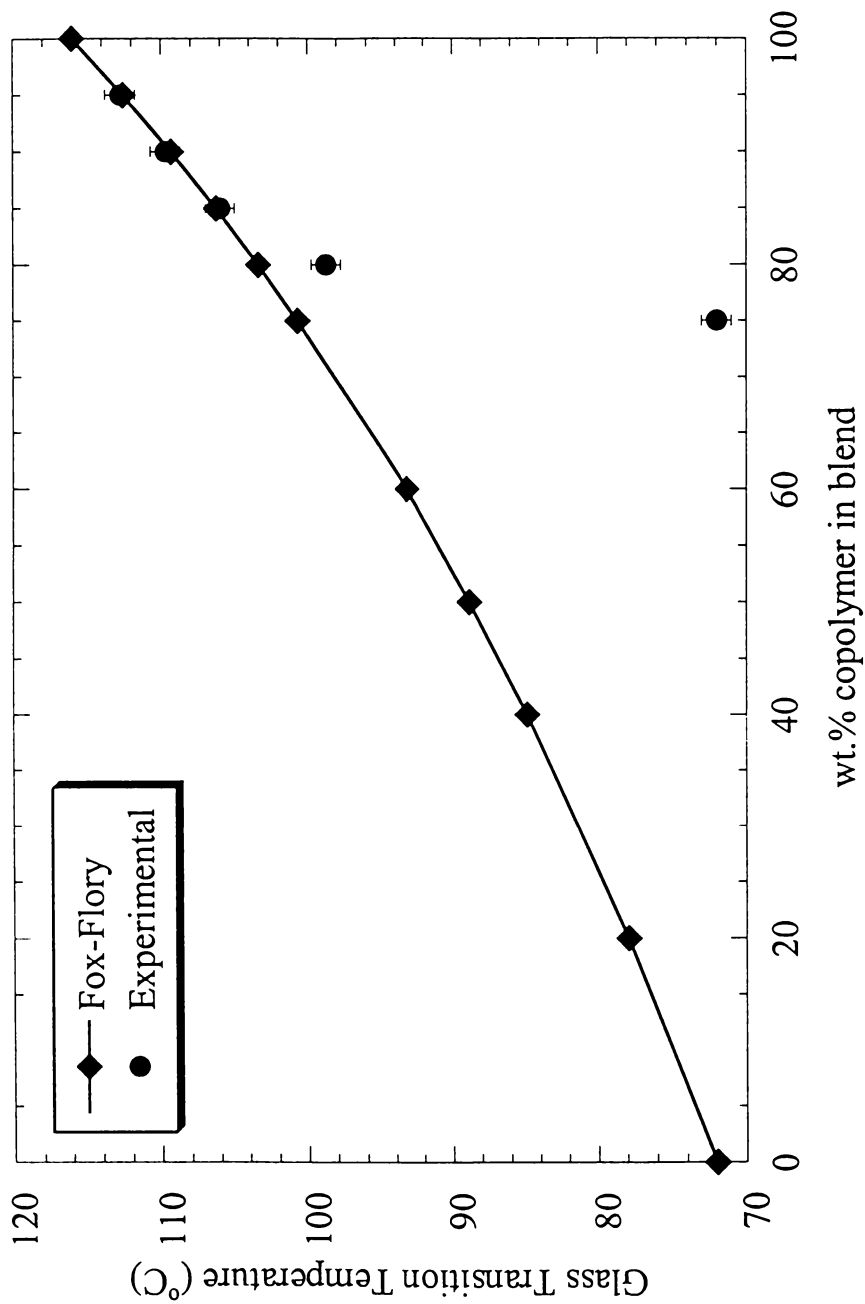


Figure 50. Experimental and theoretical glass transition temperatures of blends containing PS-co-VPh(50) and LCPU-M

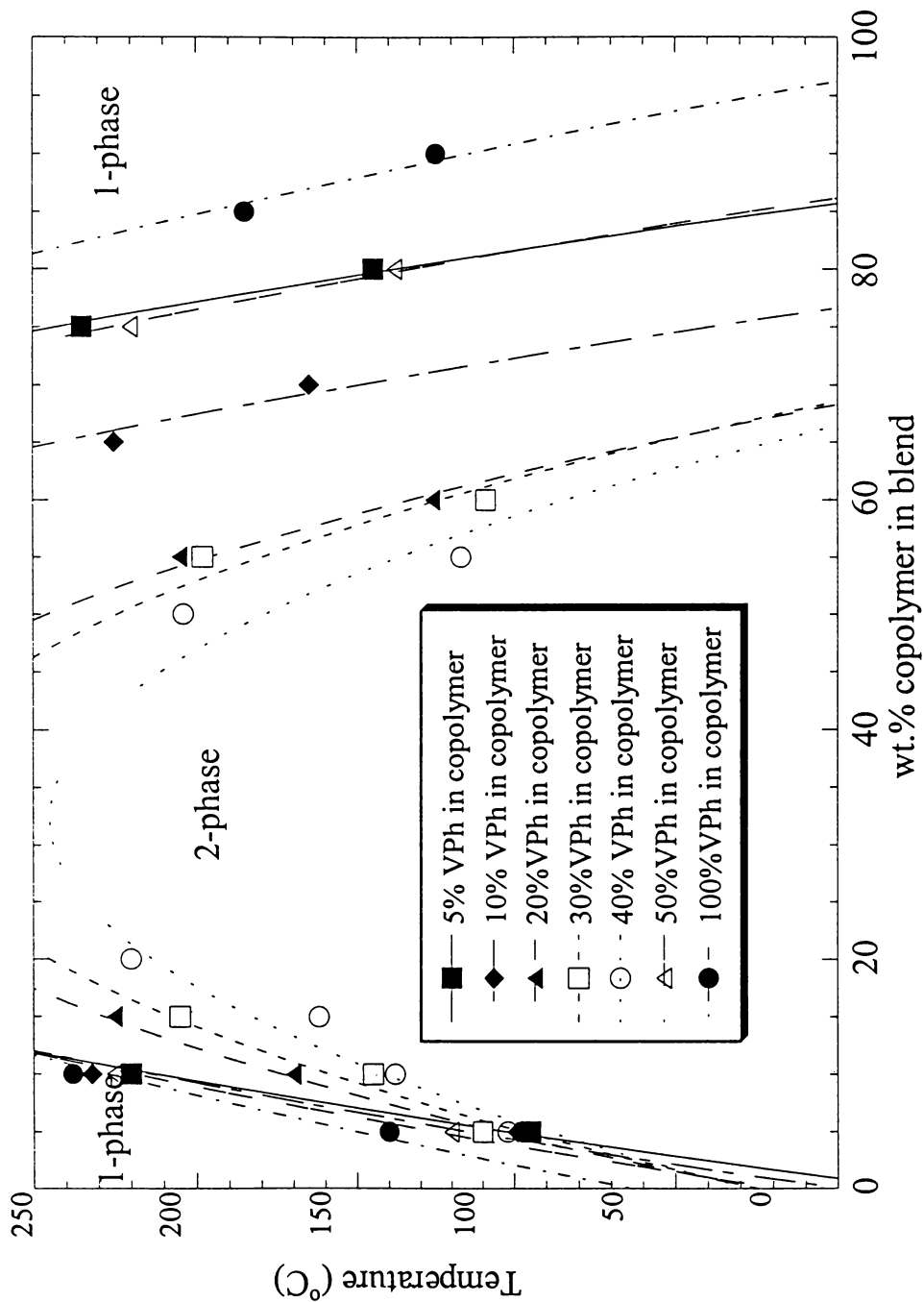


Figure 51. Phase diagram of blends containing LCP-U-M and PS-co-VPh as determined from phase contrast optical microscopy

is that the blend system with an optimum amount of intermolecular H-bonding is also the system with the broadest miscibility window (i.e., LCPU-M/PS-co-VPh(40) in this case).

A very specific observation which is interesting to note here is the difference in the miscibility window of LCPU-M/PS-co-VPh(40) from that of LCPU-M/PS-co-VPh(50) in the phase diagram determined by optical microscopy (see Figure 51). It can be seen that the increase in the mole percentage of vinyl phenol (VPh) in the copolymer from 40 to 50 causes a dramatic narrowing of the miscibility window. We believe that a plausible explanation for this phenomenon can be provided in terms of the solubility parameters of the mixing polymers assuming the absence of any effects of hydrogen bonding in the blend.

A discussion of the estimation of solubility parameter has already been provided in Chapter 2 of this thesis. We obtain a solubility parameter of 7.25 for the LCPU-M, 9.5 for styrene and 10.6 for vinyl phenol. It is apparent that the difference in solubility parameters of the LCPU-M and Polystyrene ($9.5 - 7.25 = 2.25$) is less than that of the LCPU-M and Poly(vinyl phenol) ($10.6 - 7.25 = 3.35$). We can easily conclude that, in the absence of the effects of hydrogen bonding in the blend, the LCPU-M is more inclined to mix with styrene molecules than with vinyl phenol molecules. This brings about a decrease in the mixing propensity between the LCPU-M and the copolymer in the blend as the % VPh in the copolymer increases from 40 to 50. Thus, we interpret the decrease in the mixing propensity of the LCPU-M with the copolymer (as indicated by the difference in solubility parameter), with increase in % VPh in the copolymer, as a possible cause for the dramatic narrowing of the miscibility window in LCPU-M/PS-co-VPh(50) relative to LCPU-M/PS-co-VPh(40).

3.4 Summary

It is clear from these results that the best way to find miscibility in polymer blends is by optimizing the amount of intermolecular H-bonding in the blend and relating this data to the blend phase behavior. Our studies on LCPU-M/PS-co-VPh blend system indicate that by spacing out the functional group along the copolymer chain, blends with optimal amount of intermolecular H-bonding can be reproducibly created. This is similar to the trend found in LCPU/PS-co-VPh blends reported in Chapter 2. Importantly, FT-IR results and phase diagrams of LCPU/PS-co-VPh blends and LCPU-M/PS-co-VPh blends indicate that, for every copolymer composition studied in this work, a greater amount of intermolecular H-bonding and a broader miscibility window are obtained for LCPU-M blends relative to those for LCPU blends. Also, an optimum amount of intermolecular H-bonding occurs for a copolymer with a larger mol% VPh for LCPU-M blends compared to that for LCPU blends. These observations indicate a greater availability and an increased participation of C=O groups in intermolecular H-bonding in LCPU-M blends.

Chapter 4

Thermal History Effects in Liquid Crystalline Polymer Blends

In the previous chapters of this dissertation, guidelines for creating miscible blends of a LCP and an amorphous copolymer have been presented. The results reveal that, by structural modification of the polymer chains, the extent of intermolecular H-bonding can be optimized and thereby the interactions among the components in a polymeric composite can be engineered to achieve mixing of the blend components. Correlation of these results to the response of the examined blends to thermal annealing may provide additional insight into the structure and thermodynamics of these blends.

Blends formed by solvent casting often don't immediately attain their equilibrium structures due to preferential solvent-polymer interactions in a particular blend component. When this is true, high-temperature annealing allows the polymer chains to relax to their equilibrium state and a change in the dispersion of the blend may occur due to either phase mixing or phase separation. To examine this phenomenon in the blends studied in this thesis, the LCP/PS-co-VPh blends were annealed at temperatures above 130°C (above the glass transition and crystalline melting temperatures of the blend constituents) and the effect of this thermal processing on the extent of intermolecular H-bonding is examined using FT-IR.

For this study, we have particularly chosen blend compositions that lie near the miscible-immiscible transition (as determined by optical microscopy) to encompass the different states of mixing, namely, miscible, "partially" miscible and immiscible. A miscible polymer blend can be defined as a homogeneous single-phase material for all temperatures

studied. If the two components of the blend are miscible only over a certain composition or temperature range, then we refer to that as a “partially” miscible blend. An immiscible blend is a two or more phase heterogeneous material for all temperatures studied. The morphology and properties of the polymer blends are controlled by miscibility and the thermodynamics of the mixture. In most of the partially miscible systems, varying the temperature or composition of the blend may alter the observed miscibility of the system.

In this chapter, we will analyze blends of LCPU/PS-co-VPh(20) with compositions 20/80 (classified as miscible by optical microscopy), 80/20 and 40/60 (immiscible) and 30/70 (partially miscible) (w/w) (see Figure 52); and blends of LCPU-M/PS-co-VPh(40) with compositions of 40/60 (miscible), 80/20 and 50/50 (immiscible) and 45/55 (partially miscible) (w/w) (see Figure 52). A miscible blend here refers to a blend composition that is miscible throughout the temperature range studied (30°C to 250°C), an immiscible blend is one that is immiscible throughout this temperature range and a partially miscible blend is one that transitions from immiscible to miscible with increased temperature.

High temperature annealing studies were conducted on a Biorad FTS-60A Fourier Transform Infrared (FT-IR) spectrometer purged with dried air using a minimum of 64 scans at a resolution of 2 cm^{-1} . The frequency scale was calibrated internally with a He-Ne reference to an accuracy of 0.2 cm^{-1} and externally with polystyrene. Samples for FT-IR studies were obtained by solvent casting blends of LCPU and PS-co-VPh from DMF (2% w/v) on KBr disks at room temperature. The KBr disks were placed on a horizontal holder in a dessicator to reduce the evaporation rate and to avoid film cracking. After evaporating most of the solvent at room temperature, the disks were subsequently dried in a vacuum oven at 60

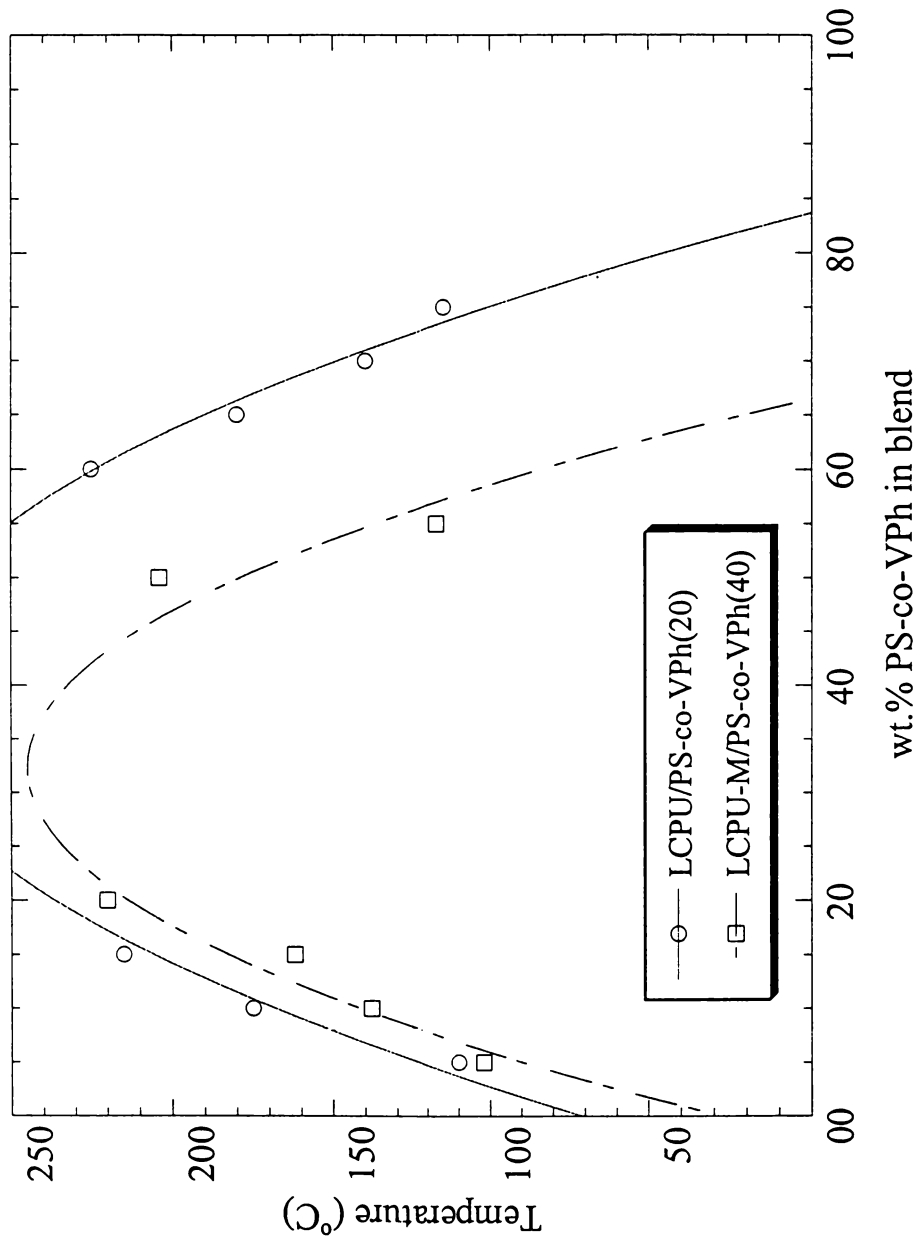


Figure 52. Phase diagram of LCPU/PS-co-VPh(20) and LCPU-M/PS-co-VPh(40) blends as determined from phase contrast optical microscopy

°C for 3 days to remove residual solvent and moisture. The absence of solvent in the sample was verified by the absence of the C=O peak of DMF which occurs at 1650 cm^{-1} in the IR curve, which occurs at a lower wavenumber than the C=O peak of the LCPU (1730 cm^{-1}). The films prepared for FTIR were adequately thin to be within an absorbance range where the Beer-Lambert law is satisfied. High temperature FT-IR spectra were obtained using a cell mounted in the spectrometer connected to a temperature controller. The temperature was controlled to an accuracy of 0.5°C . First, FT-IR data were obtained for the sample at room temperature ($\cong 30^\circ\text{C}$) and is referred to as “as-cast” here. The sample was then raised to a higher temperature and was kept constant for 15 min. at this temperature, in order for the sample to attain that temperature, before obtaining the “as-cast, heat-treated” data. This data provides an indication of changes in intermolecular interactions with a change in temperature. The sample was then allowed to anneal at this temperature for 1 h before obtaining the ‘annealed, before quenching’ data. These data provides evidence of a change in intermolecular interactions among the blend components as they approach equilibrium at this temperature. Once annealed, the sample was air-quenched back to room temperature ($\cong 30^\circ\text{C}$) before obtaining the ‘annealed, after quenching’ data. To demonstrate the effects of annealing, we have compared the percent of C=O intermolecularly H-bonded (to O-H) determined for the ‘annealed’ sample to those of the ‘as-cast’ and ‘as-cast, heat-treated’ samples. Throughout this study, our results indicate very little change in the extent of intermolecular H-bonding between the ‘annealed, before quenching’ and ‘annealed, after quenching’ data (much less than the error in the data itself), and therefore, we consider the effect of sample quenching on intermolecular H-bonding to be negligible. In this dissertation,

we have reported the ‘annealed, after quenching’ data as ‘annealed’ sample data.

Figures 53-60 show the FT-IR curves in the C=O stretching region of the ‘as-cast’, the ‘as-cast, heat-treated’, and the ‘annealed’ samples of the LCPU/PS-co-VPh and LCPU-M/PS-co-VPh blends. In the immiscible [80/20 and 40/60 (w/w) LCPU/PS-co-VPh(20) and 80/20 and 50/50 (w/w) LCPU-M/PS-co-VPh(40)] as well as the partially miscible [30/70 (w/w) LCPU/PS-co-VPh(20) and 45/55 (w/w) LCPU-M/PS-co-VPh(40)] blends, there is very little change in the curves with heat treatment. For the miscible blends [20/80 (w/w) LCPU/PS-co-VPh and 40/60 (w/w) LCPU-M/PS-co-VPh], the intermolecular H-bonding (around 1715 cm^{-1} in 20/80 LCPU/PS-co-VPh and around 1680 cm^{-1} in 40/60 LCPU-M/PS-co-VPh) clearly decreases in the ‘as-cast, heat-treated’ samples as the temperature is brought up from 30°C (curve a) through 140°C (curve b) to 180°C (curve d). However, the annealed samples show an increase in intermolecular H-bonding at 140°C (curve c) and at 180°C (curve e) relative to the ‘as-cast’ sample.

Quantitative analysis of the C=O absorption peaks of these IR curves was completed by the same deconvolution procedure as previously described to obtain the extent of intermolecular H-bonding in the blend. As an example, deconvolution parameters obtained for the free C=O and intermolecular H-bonded C=O bands of the C=O stretching region of the ‘as-cast’, the ‘as-cast, heat-treated’ and the ‘annealed’ samples of the 40/60 (w/w) LCPU-M/PS-co-VPh(40) are listed in Table 5. The areas under the two peaks that contribute to this portion of the spectrum are A_1 , the area of the free C=O peak, and A_2 the area of the intermolecularly H-bonded C=O peak. The absorption intensity of the H-bonded C=O band (A_2) is corrected to account for the difference in absorption coefficients of free and H-

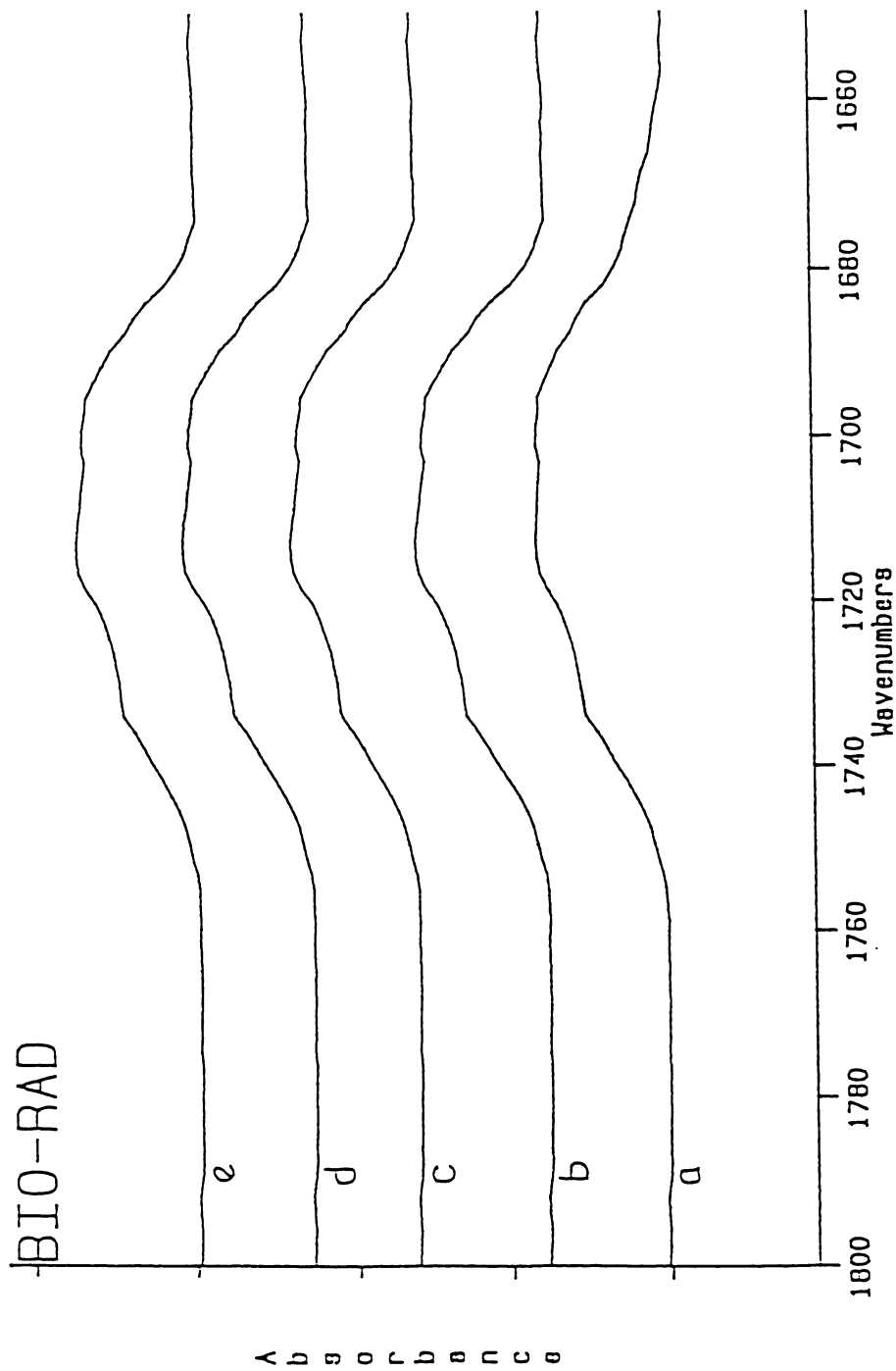


Figure 53. FT-IR spectra of C=O stretching region of “annealed” and “as-cast, heat-treated” blends of 80/20 (w/w) LCPU/PS-co-VPh(20). Curve (a) corresponds to sample at 30°C while the remaining curves are for samples heat-treated at b) 140°C (as-cast, heat-treated) c) 140°C (annealed) d) 180°C (as-cast, heat-treated) e) 180°C (annealed)

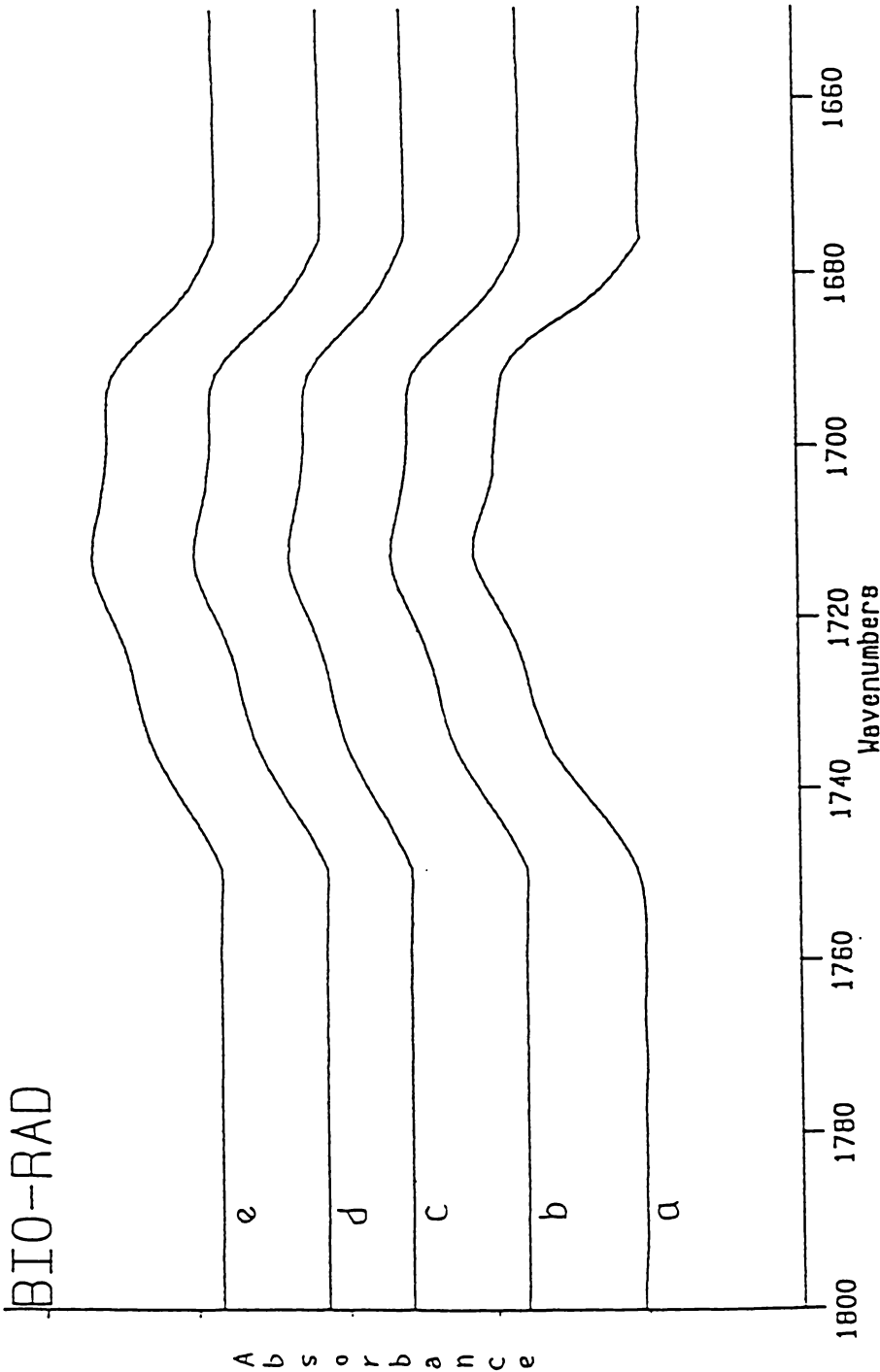


Figure 54. FT-IR spectra of C=O stretching region of "annealed" and "as-cast, heat-treated" blends of 40/60 (w/w) LCP/PS-co-VPh(20). Curve (a) corresponds to sample at 30°C while the remaining curves are for samples heat-treated at b) 140°C (as-cast, heat-treated) c) 140°C (annealed) d) 180°C (as-cast, heat-treated) e) 180°C (annealed)

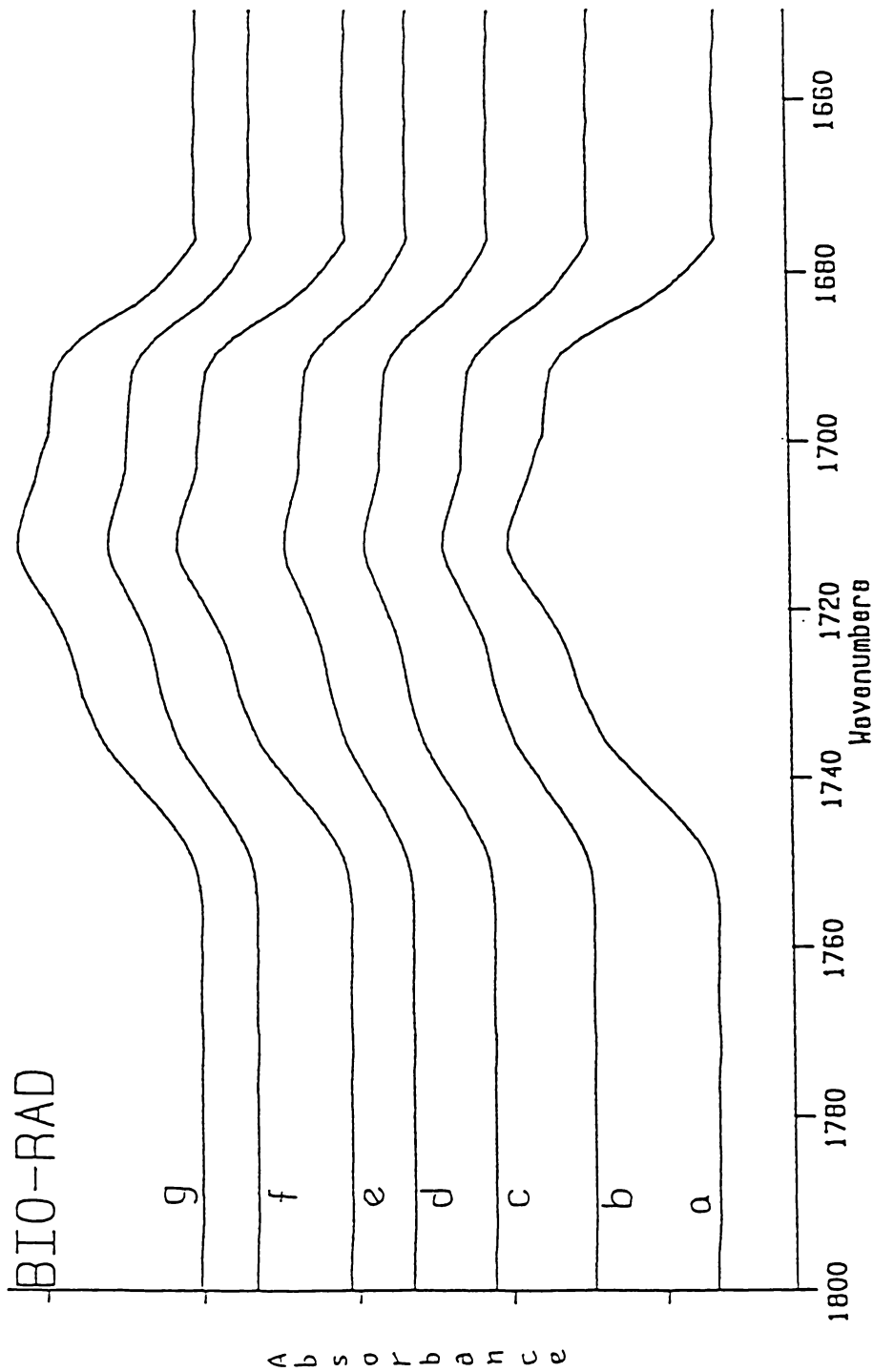


Figure 55. FT-IR spectra of C=O stretching region of "annealed" and "as-cast, heat-treated" blends of 30/70 (w/w) blend of LCP/PS-co-VPh(20). Curve (a) corresponds to sample at 30°C while the remaining curves are for samples heat-treated at b) 130°C (as-cast, heat-treated) c) 130°C (annealed) d) 160°C (as-cast, heat-treated) e) 160°C (annealed) f) 180°C (as-cast, heat-treated) g) 180°C (annealed)

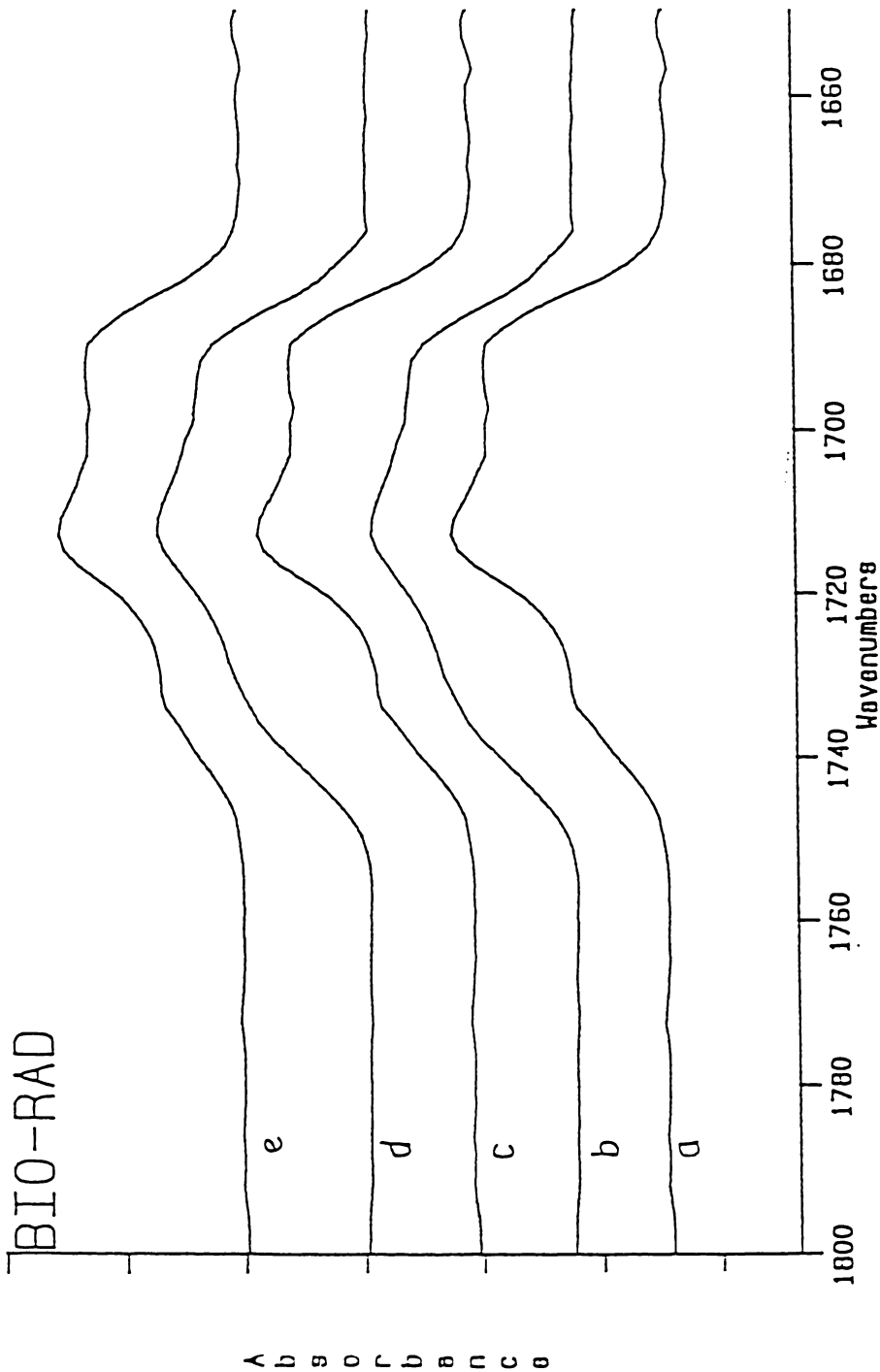
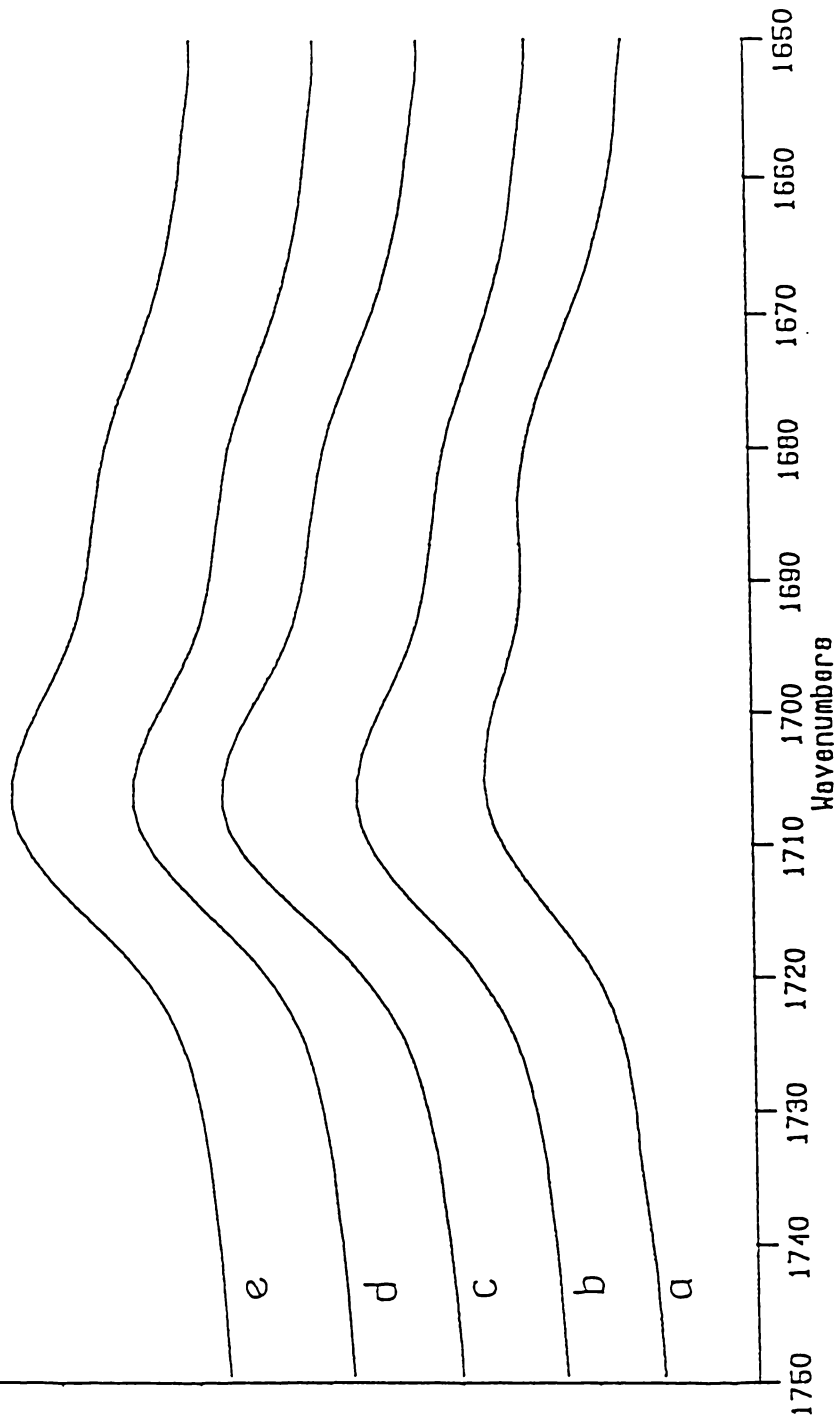


Figure 56. FT-IR spectra of C=O stretching region of "annealed" and "as-cast, heat-treated" blends of 20/80 (w/w) blend of LCP/PS-co-VPh(20). Curve (a) corresponds to sample at 30°C while the remaining curves are for samples heat-treated at b) 140°C (as-cast, heat-treated) c) 140°C (annealed) d) 180°C (as-cast, heat-treated) e) 180°C (annealed)

BIO-RAD



A
b
s
o
r
b
o
n
c
b

Figure 57. FT-IR spectra of C=O stretching region of “annealed” and “as-cast, heat-treated” blends of 80/20 (w/w) blend of LCPU-M/PS-co-VPh(40). Curve (a) corresponds to sample at 30°C while the remaining curves are for samples heat-treated at b) 140°C (as-cast, heat-treated) c) 140°C (annealed) d) 180°C (as-cast, heat-treated) e) 180°C (annealed)

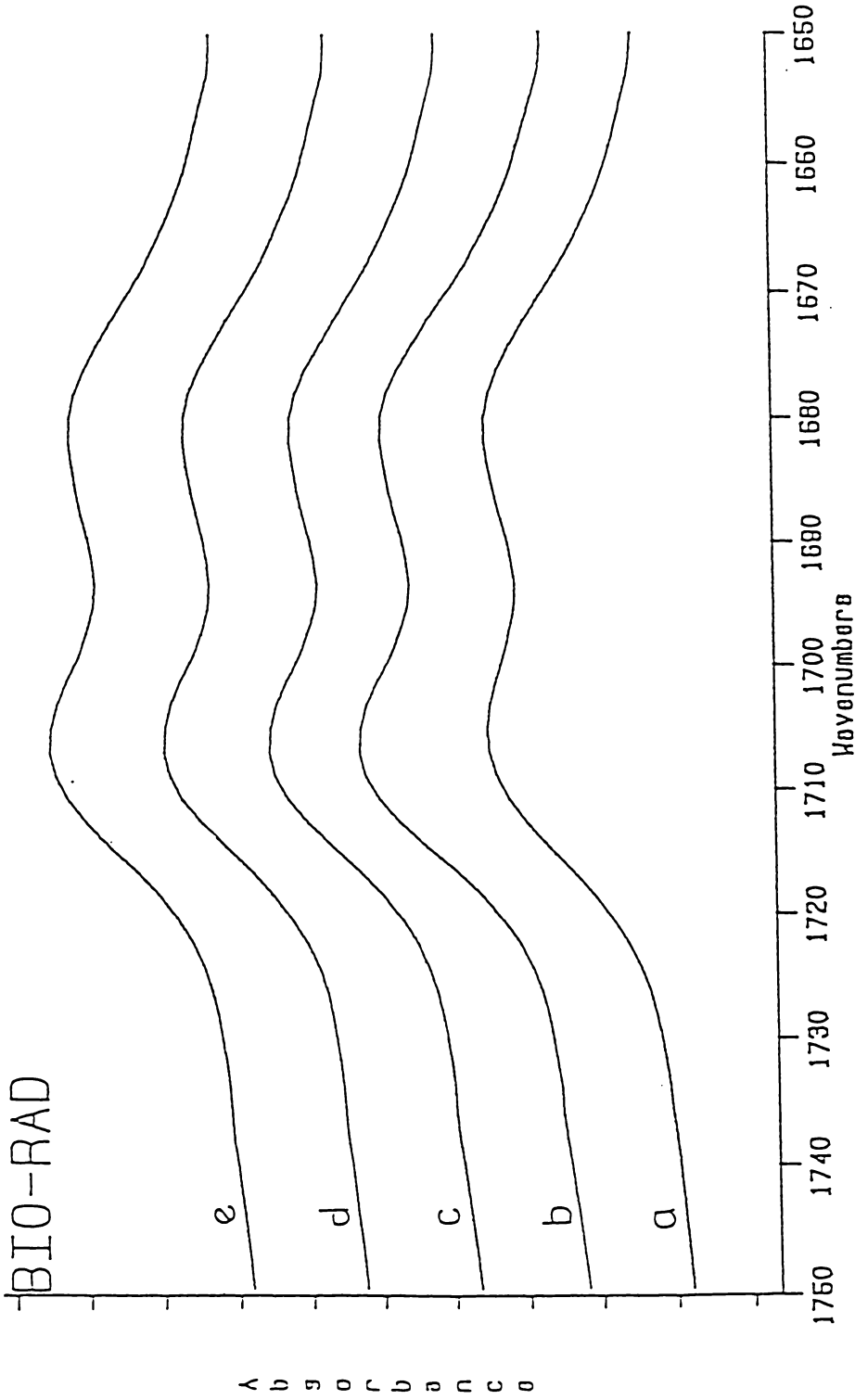


Figure 58. FT-IR spectra of C=O stretching region of "annealed" and "as-cast, heat-treated" blends of 50/50 (w/w) blend of LCPU-M/PS-co-VPh(40). Curve (a) corresponds to sample at 30°C while the remaining curves are for samples heat-treated at b) 140°C (as-cast, heat-treated) c) 140°C (annealed) d) 180°C (as-cast, heat-treated) e) 180°C (annealed)

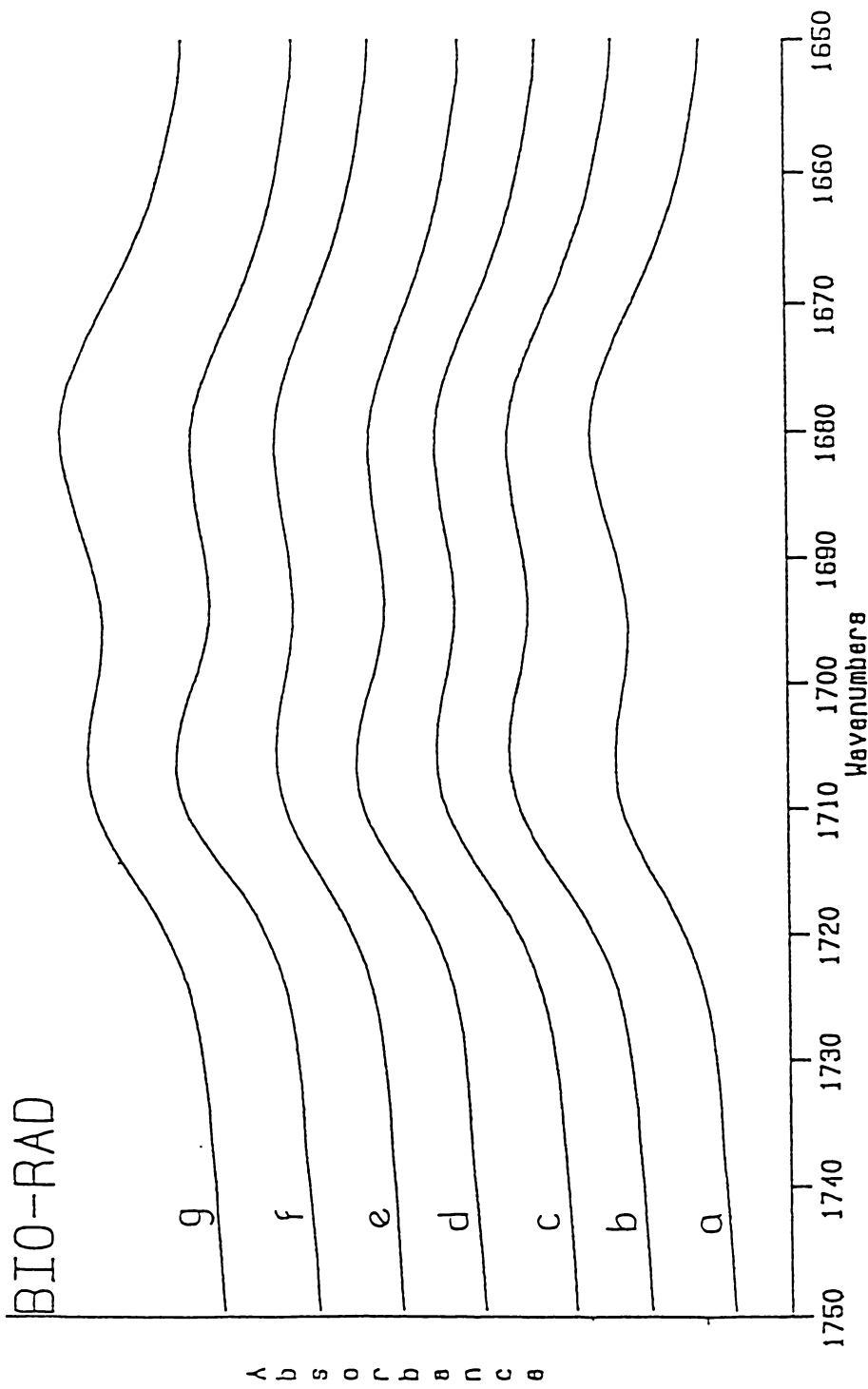


Figure 59. FT-IR spectra of C=O stretching region of “annealed” and “as-cast, heat-treated” blends of 45/55 (w/w) blend of LCPU-M/PS-co-VPh(40). Curve (a) corresponds to sample at 30°C while the remaining curves are for samples heat-treated at b) 130°C (as-cast, heat-treated) c) 130°C (annealed) d) 160°C (as-cast, heat-treated) e) 160°C (annealed) f) 180°C (as-cast, heat-treated) g) 180°C (annealed)

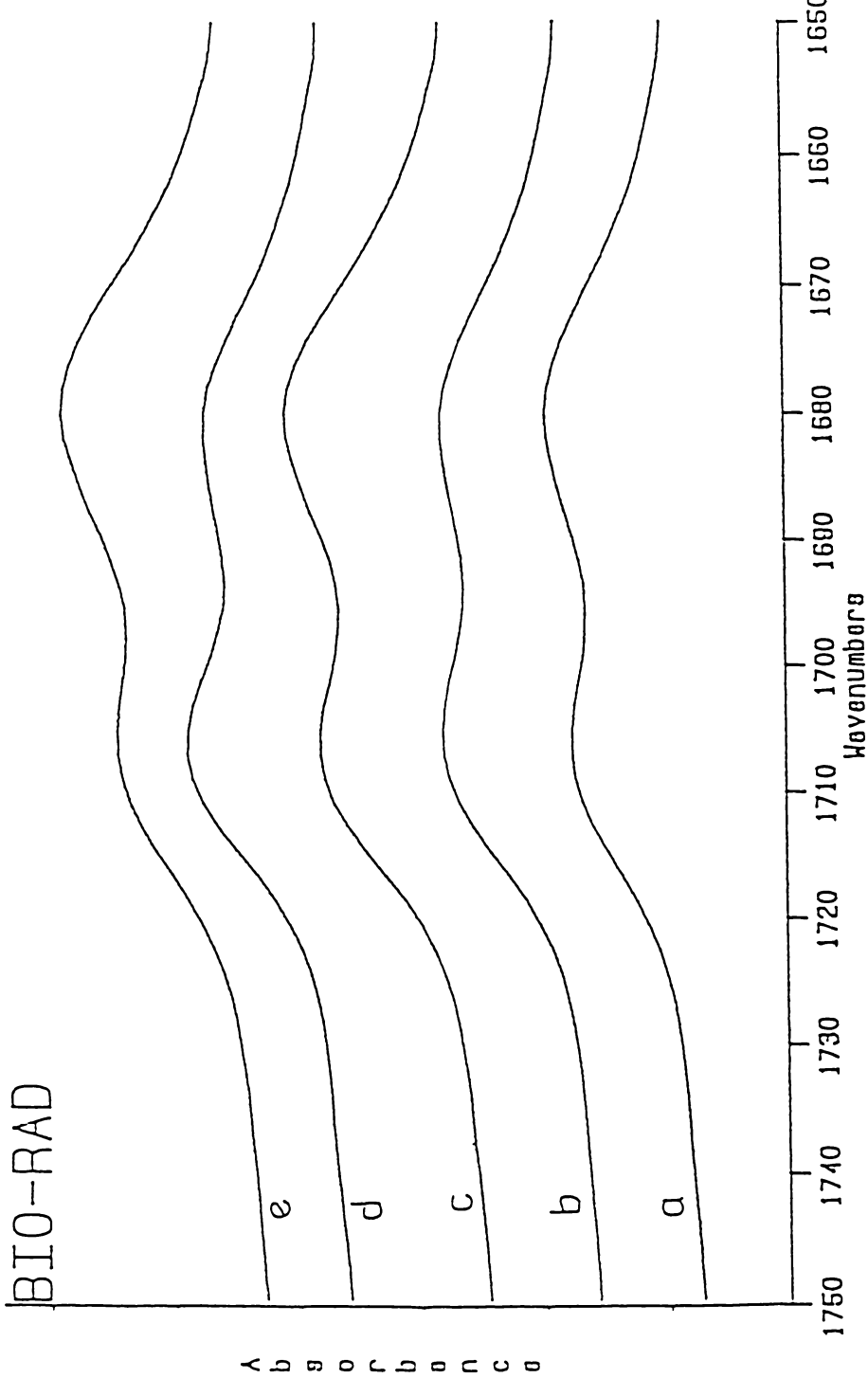


Figure 60. FT-IR spectra of C=O stretching region of "annealed" and "as-cast, heat-treated" blends of 40/60 (w/w) blend of LCPU-M/PS-co-VPh(40). Curve (a) corresponds to sample at 30°C while the remaining curves are for samples heat-treated at b) 140°C (as-cast, heat-treated) c) 140°C (annealed) d) 180°C (as-cast, heat-treated) e) 180°C (annealed)

Table 5. Deconvolution results of the C=O stretching region for 'as-cast', 'as-cast, heat-treated', and 'annealed' samples of LCPU-M blends containing 60 wt. % PS-co-VPh(40) copolymer.

| Temperature (°C) | Free C=O | | Intermolecularly H-bonded C=O | | | % C=O intermolecularly H-bonded | |
|------------------------------------|-----------------------------|-------------------------------|-------------------------------|---------------------------|-------------------------------|---------------------------------------|-------|
| | ν^* cm ⁻¹ | $W_{1/2}$ cm ⁻¹ | A_1 | ν cm ⁻¹ | $W_{1/2}$ cm ⁻¹ | | A_2 |
| 30 (as-cast) | 1707 | 18.0 | 3.172 | 1683.0 | 30.7 | 4.328 | 46.9 |
| 140 (as-cast, heat- treated) | 1707 | 18.2 | 3.859 | 1683.1 | 30.5 | 3.880 | 39.5 |
| 140 (annealed) | 1707 | 18.1 | 2.955 | 1682.8 | 30.6 | 4.795 | 51.3 |
| 180 (as-cast, heat- treated) | 1707 | 18.1 | 4.028 | 1683.3 | 30.8 | 3.786 | 37.9 |
| 180 (annealed) | 1707 | 18.3 | 2.502 | 1682.5 | 30.5 | 4.740 | 53.8 |

* Fixed during curve fitting Absorptivity Coefficient (K) = 1.54; $A_2' = A_2/K$; $A_T = A_1 + A_2'$
% C=O intermolecularly H-bonded = $(A_2'/A_T) * 100$

bonded bands by dividing the experimentally determined A_2 by the absorption coefficient ratio, K , which is 1.54 for this blend system and is represented by A_2' . The percent of C=O groups that participate in intermolecular H-bonding is then given by $A_2'/(A_2' + A_1)$. Detailed information on the deconvolution procedure and absorption coefficient ratio determination has already been provided in Chapter 2 of this dissertation.

The percent of C=O groups that are intermolecularly H-bonded is plotted against temperature for the 'as-cast', 'as-cast, heat-treated' and 'annealed' samples of the immiscible LCPU/PS-co-VPh and LCPU-M/PS-co-VPh blends and are shown in Figures 61-64. These plots for LCPU/PS-co-VPh(20) blends with compositions 80/20 (w/w) (Figure 61) and 40/60 (Figure 62) and LCPU-M/PS-co-VPh(40) blends 80/20 (Figure 63) and 50/50 (Figure 64) show data for blends predicted to be immiscible by optical microscopy. The plots for 80/20 (w/w) LCPU/PS-co-VPh(20) and 80/20 (w/w) LCPU-M/PS-co-VPh(40) show no significant change in intermolecular H-bonding on heat treatment. On the contrary, the plots for 40/60 (w/w) LCPU/PS-co-VPh(20) and 50/50 (w/w) LCPU-M/PS-co-VPh(40) indicate a decrease in intermolecular H-bonding in the 'as-cast, heat-treated' sample relative to the 'as-cast' sample. However, there appears to be very little change in the amount of intermolecular H-bonding in the annealed sample relative to the 'as-cast, heat-treated' sample.

Similar plots for 20/80 (w/w) of LCPU/PS-co-VPh(20) (Figure 65) and 40/60 (w/w) LCPU-M/PS-co-VPh(40) (Figure 66) show data for blends that are predicted to be miscible by optical microscopy. These plots indicate a decrease in intermolecular H-bonding in the 'as-cast, heat-treated' sample relative to the 'as-cast' sample. However, unlike immiscible blends, there appears to be an increase in intermolecular H-bonding with temperature in the

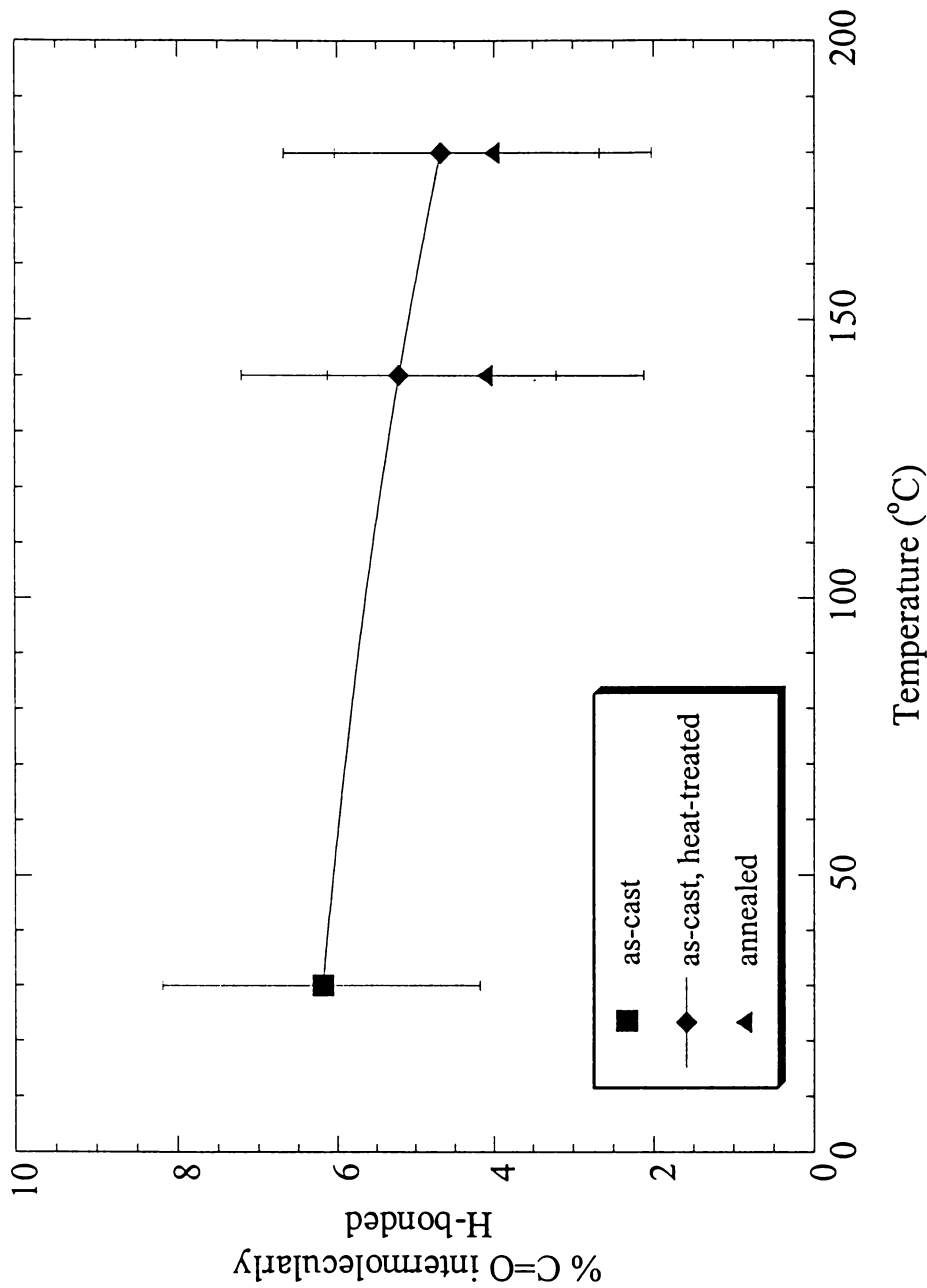


Figure 61. Percent of intermolecular hydrogen bonding as a function of temperature for annealed and as-cast, heat-treated blends of 80/20 (w/w) LCP/PS-co-VPh(20). Error Bar in the plot corresponds to ± 2.0 .

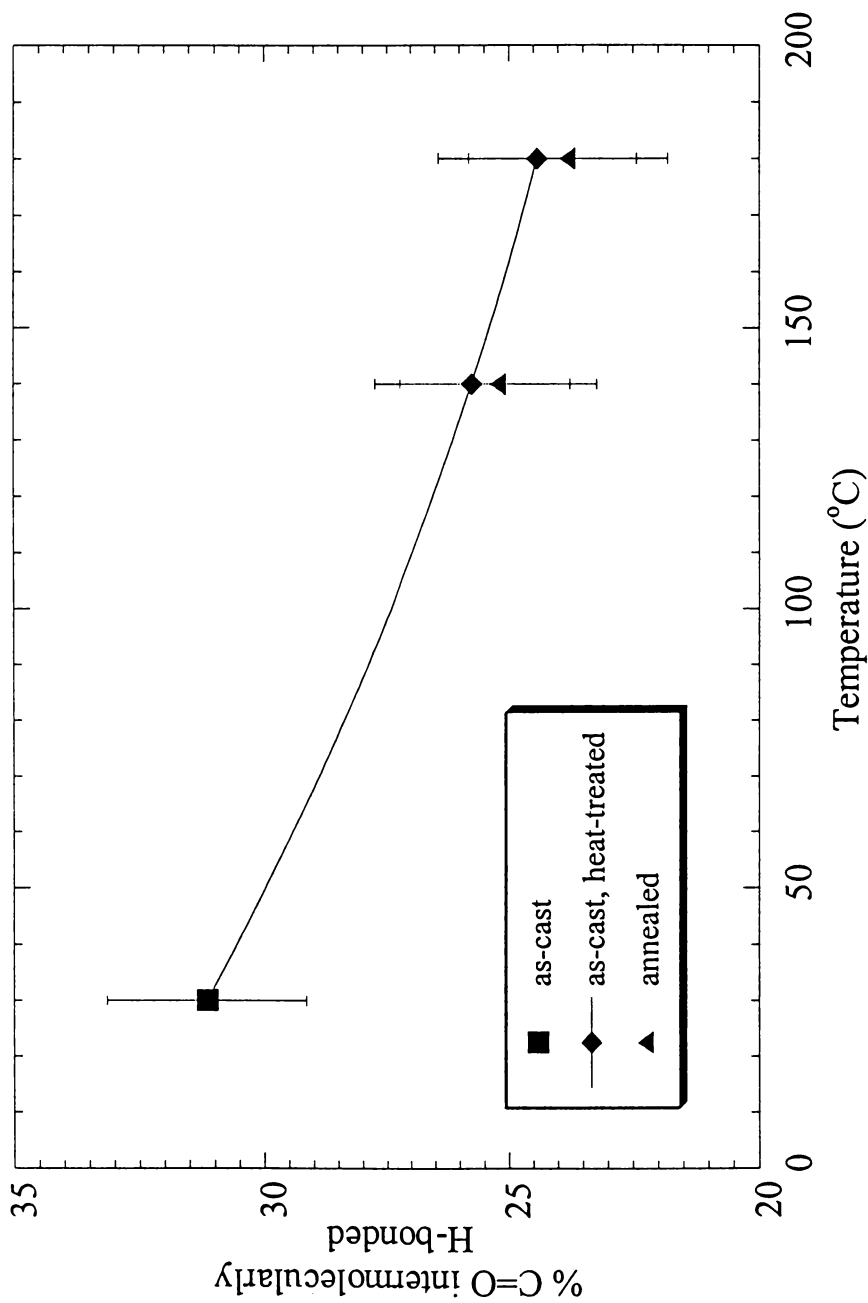


Figure 62. Percent of intermolecular hydrogen bonding as a function of temperature for annealed and as-cast, heat-treated blends of 40/60 (w/w) LCP/PS-co-VPh(20). Error Bar in the plot corresponds to ± 2.0 .

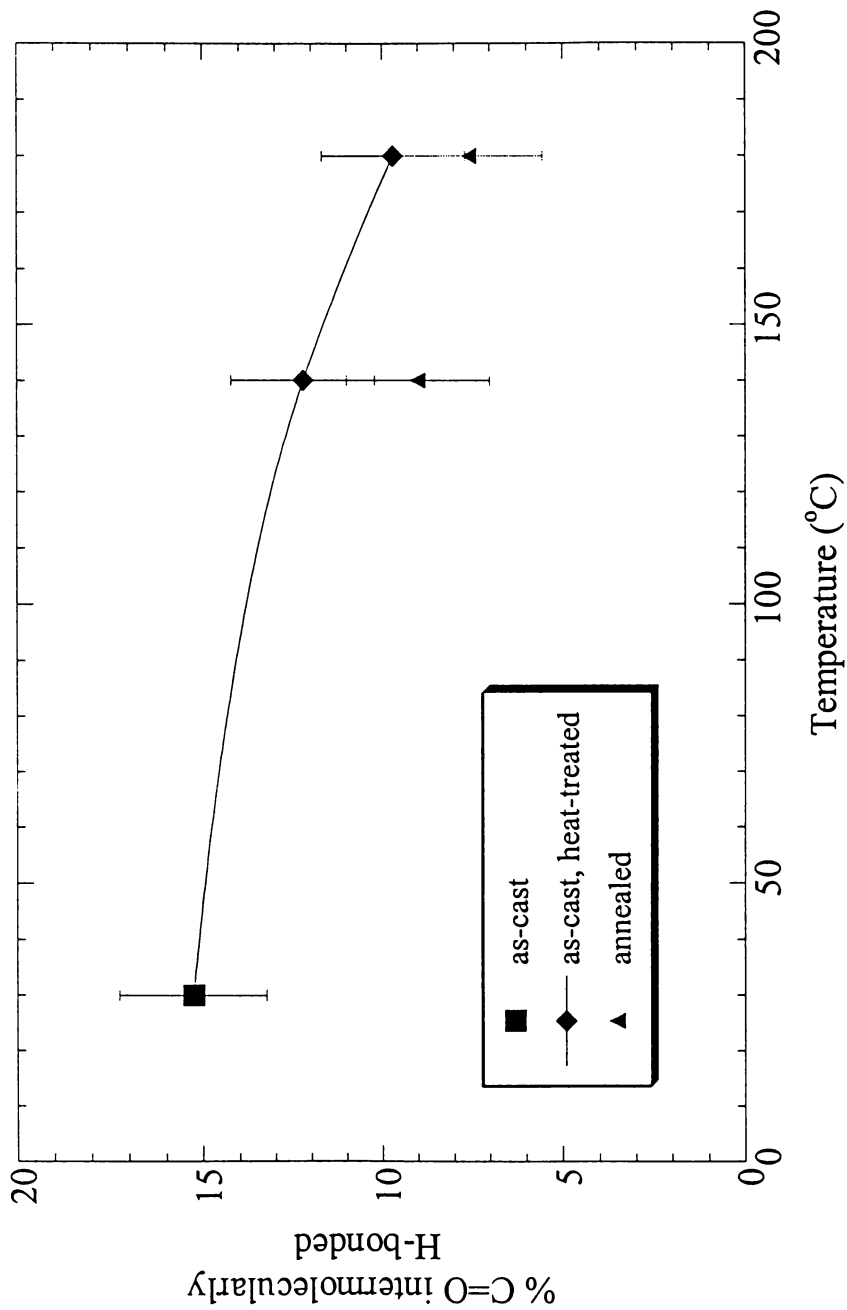


Figure 63. Percent of intermolecular hydrogen bonding as a function of temperature for annealed and as-cast, heat-treated blends of 80/20 (w/w) LCPU-M/PS-co-VPh(40). Error Bar in the plot corresponds to ± 2.0 .

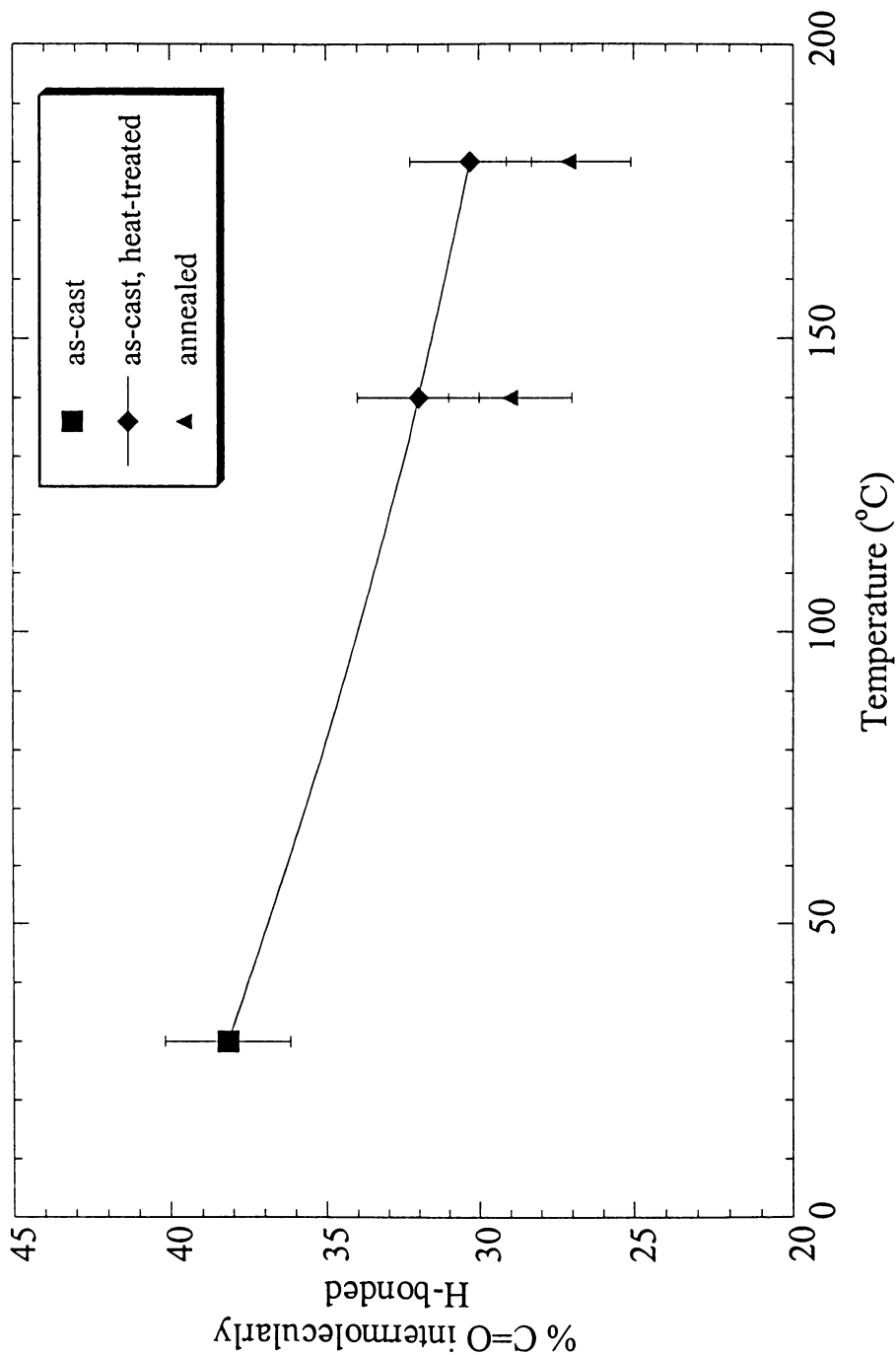


Figure 64. Percent of intermolecular hydrogen bonding as a function of temperature for annealed and as-cast, heat-treated blends of 50/50 (w/w) LCPU-M/PS-co-VPh(40). Error Bar in the plot corresponds to ± 2.0 .

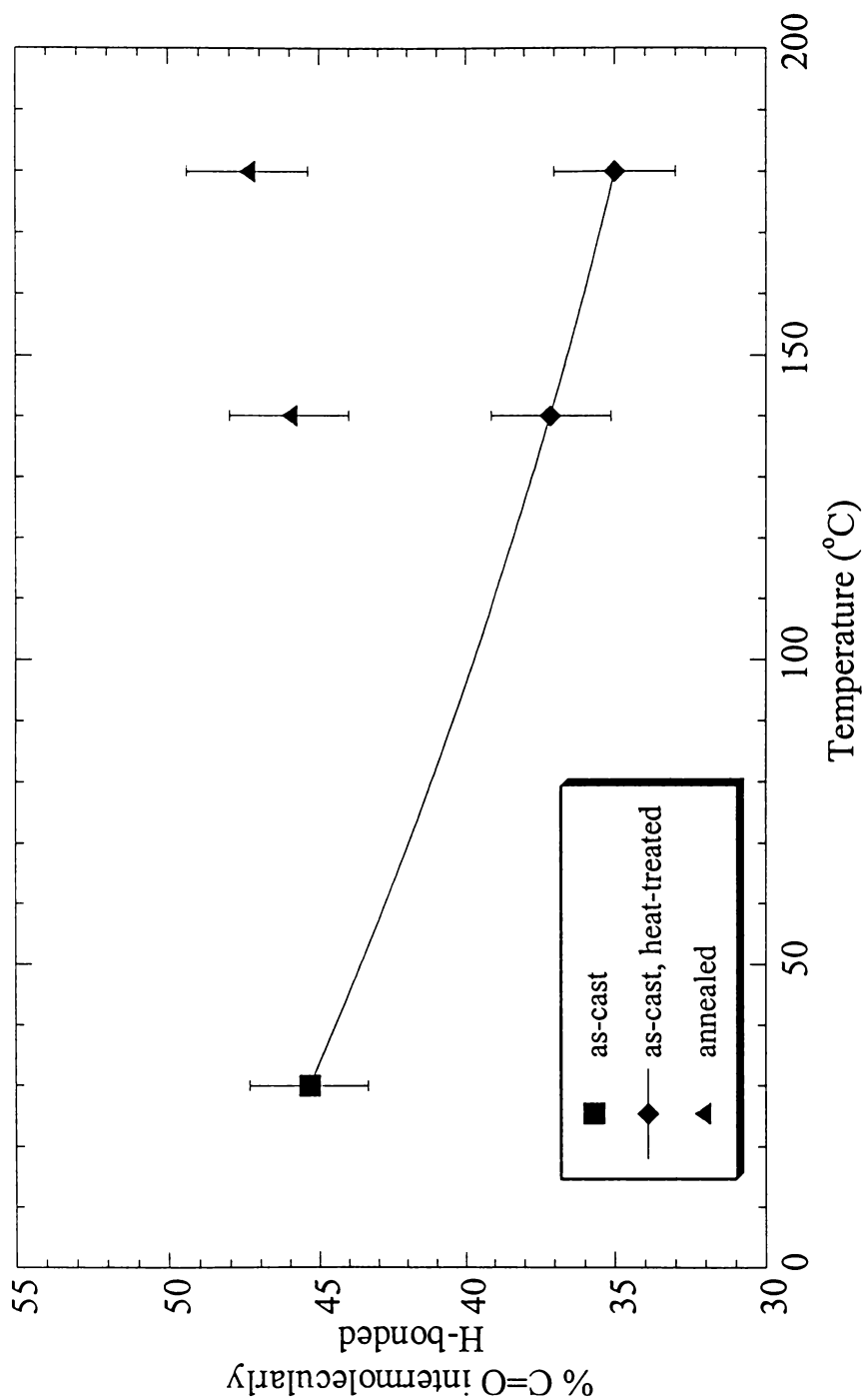


Figure 65. Percent of intermolecular hydrogen bonding as a function of temperature for annealed and as-cast, heat-treated blends of 20/80 (w/w) LCPU/PS-co-VPh(20). Error Bar in the plot corresponds to ± 2.0 .

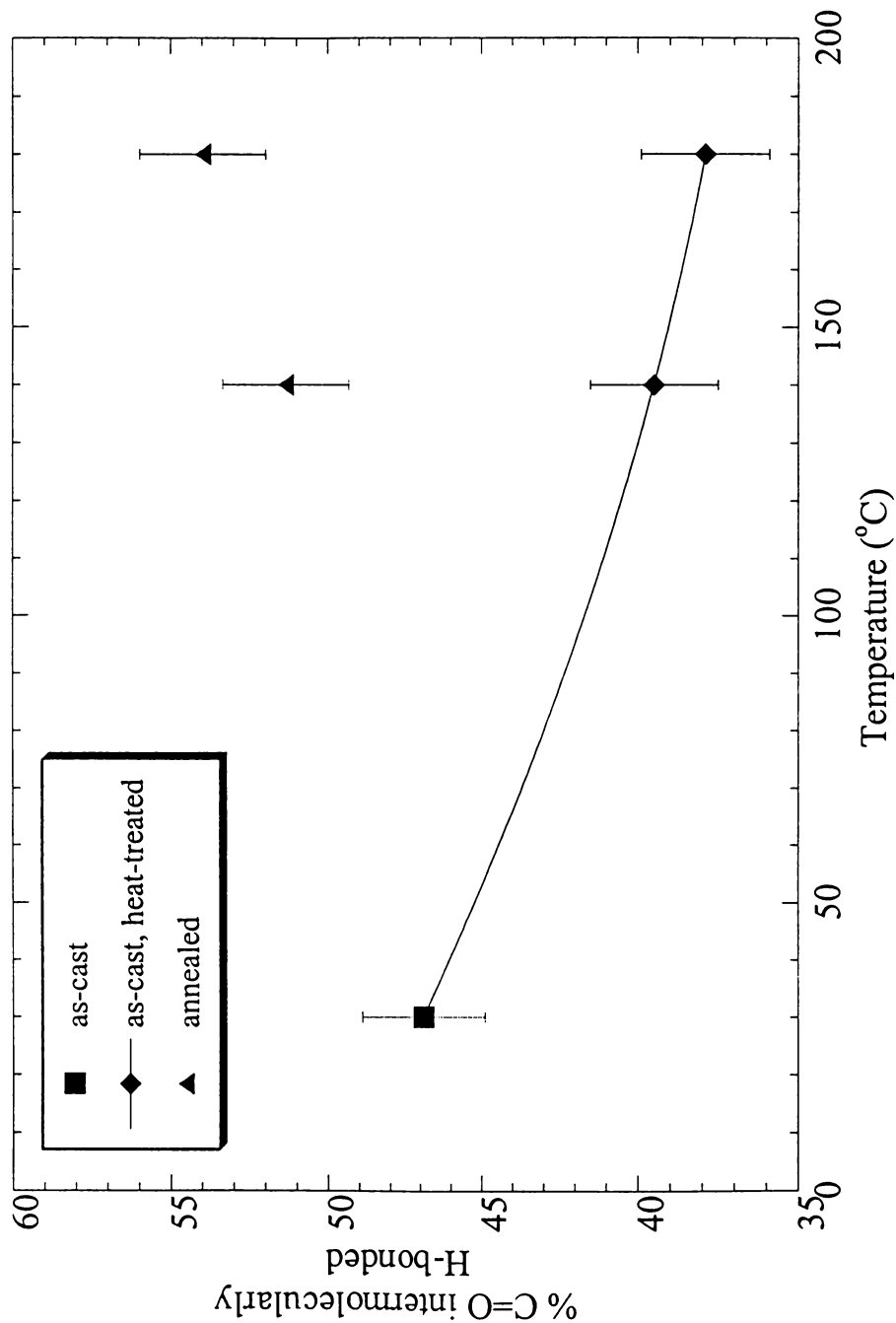


Figure 66. Percent of intermolecular hydrogen bonding as a function of temperature for annealed and as-cast, heat-treated blends of 40/60 (w/w) LCPU-M/PS-co-VPh(40). Error Bar in the plot corresponds to ± 2.0 .

annealed samples, relative to the 'as-cast, heat-treated' and the 'as-cast' samples.

The change in free energy that occurs upon mixing the polymer components of a blend governs the miscibility of the system. Hence, it is important to provide a general discussion of the thermodynamics of the 'as-cast' sample of any blend when it is heat-treated at a higher temperature. An 'as-cast' sample exists in a non-equilibrium condition owing to the polymer-solvent interaction effects in the system. When the 'as-cast' sample is heat-treated at a higher temperature, the system undergoes a change from a non-equilibrium condition to an equilibrium state. There must be a change in the free energy of the system that acts as the driving force for establishing equilibrium in the blend. This transition to an equilibrium condition could be associated with a change in phase dispersion in the blend resulting in a change in the phase behavior of the system. That is, for example, a blend that is miscible in its non-equilibrium state may remain miscible or become immiscible when equilibrium condition is established. This change in phase dispersion of the system could result in a change in the amount of intermolecular H-bonding in the blend.

In general, the annealing process gives the polymer chains more time to move about in the blend, (compared to the 'as-cast, heat-treated' samples) as the chains relax to their equilibrium state, and this gives rise to the possibility of a change in the phase dispersion of the blend. For immiscible blends, there clearly is no change in intermolecular H-bonding in 'as-cast, heat-treated' sample relative to the 'as-cast' sample. This decrease is due to breaking of H-bonds by an increase in thermal energy in the system. However, our annealing experiments show no significant change in the intermolecular H-bonding with thermal annealing relative to the 'as-cast, heat-treated' sample in these blends (Figures 61-64). These

results for immiscible blends demonstrate that annealing the sample at high temperatures does alter the amount of intermolecular H-bonding that occurs 'as-cast'. When annealed at a higher temperature, the sample reaches an equilibrium condition and this may be associated with a change in phase dispersion of the blend. Our interpretation is that a decrease in the number of intermolecular contacts between the two polymers of the blend is a result of the change in the phase dispersion of the blend. This decrease in the number of intermolecular contacts lowers the amount of intermolecular H-bonding in the blend. More importantly, these results show that the blends that are formed from solution casting do not represent the equilibrium structure.

We see that a sufficient thermal energy is produced even at 140°C (which is slightly above the T_g and T_m of the blend constituents) to mobilize the polymer chains that decreases the H-bonds in immiscible blends. However, as the annealing temperature is increased from 140°C to 180°C, the decrease in intermolecular H-bonding appears to be more pronounced relative to the 'as-cast' sample. This means that at 180°C, there is more thermal energy present in the system than at 140°C that works to break the H-bonds. As a result, the decrease in intermolecular H-bonding at 180°C is even greater.

For miscible blends, there is a decrease in intermolecular H-bonding in 'as-cast, heat-treated' samples relative to the 'as-cast' sample. This decrease is due to breaking of H-bonds by an increase in thermal energy in the system. However, our annealing experiments show an increase in intermolecular H-bonding with thermal annealing relative to the 'as-cast, heat-treated' and the 'as-cast' samples. These results for miscible blends demonstrate that annealing at higher temperatures does alter the amount of intermolecular H-bonding that

occurs relative to the 'as-cast' sample. The sample reaches an equilibrium condition when annealed at a higher temperature and this may be associated with a change in phase dispersion of the blend. We interpret that the increase in intermolecular H-bonding in the miscible blends is a result of the change in phase dispersion of the system. These results for miscible blends show that the blends that are formed from solution casting do not represent the equilibrium structure.

We see that sufficient thermal energy is available even at 140°C to mobilize the polymer chains causing an irreversible process that alters the H-bonds in immiscible blends. However, as we increase the annealing temperature from 140°C to 180°C, the increase in intermolecular H-bonding seems to be more pronounced relative to the 'as-cast' sample. This means that at 180°C, there is more thermal energy present in the system than at 140°C that allows the polymer chains to move about in the blend even more freely to form more H-bonds. As a result, the increase in intermolecular H-bonding at 180°C is even more.

Figures 67 and 68 show the FT-IR plots of 30/70 LCP/PS-co-VPh(20) and 45/55 LCP/M/PS-co-VPh(40), respectively. These partially miscible blends are of specific interest since the phase diagram determined by optical microscopy indicates that they are immiscible at 130°C and miscible at and above 140°C. Considering this, samples of these blends were annealed at 130°C, 160°C and 180°C to study the effects of thermal energy on intermolecular H-bonding. This decrease is due to breaking of H-bonds by an increase in thermal energy in the system. Annealing is found to cause a slight decrease in intermolecular H-bonding in the blend at 130°C relative to the 'as-cast' sample and this may be due to a change in phase dispersion of the system as it attains equilibrium and this lowers the number

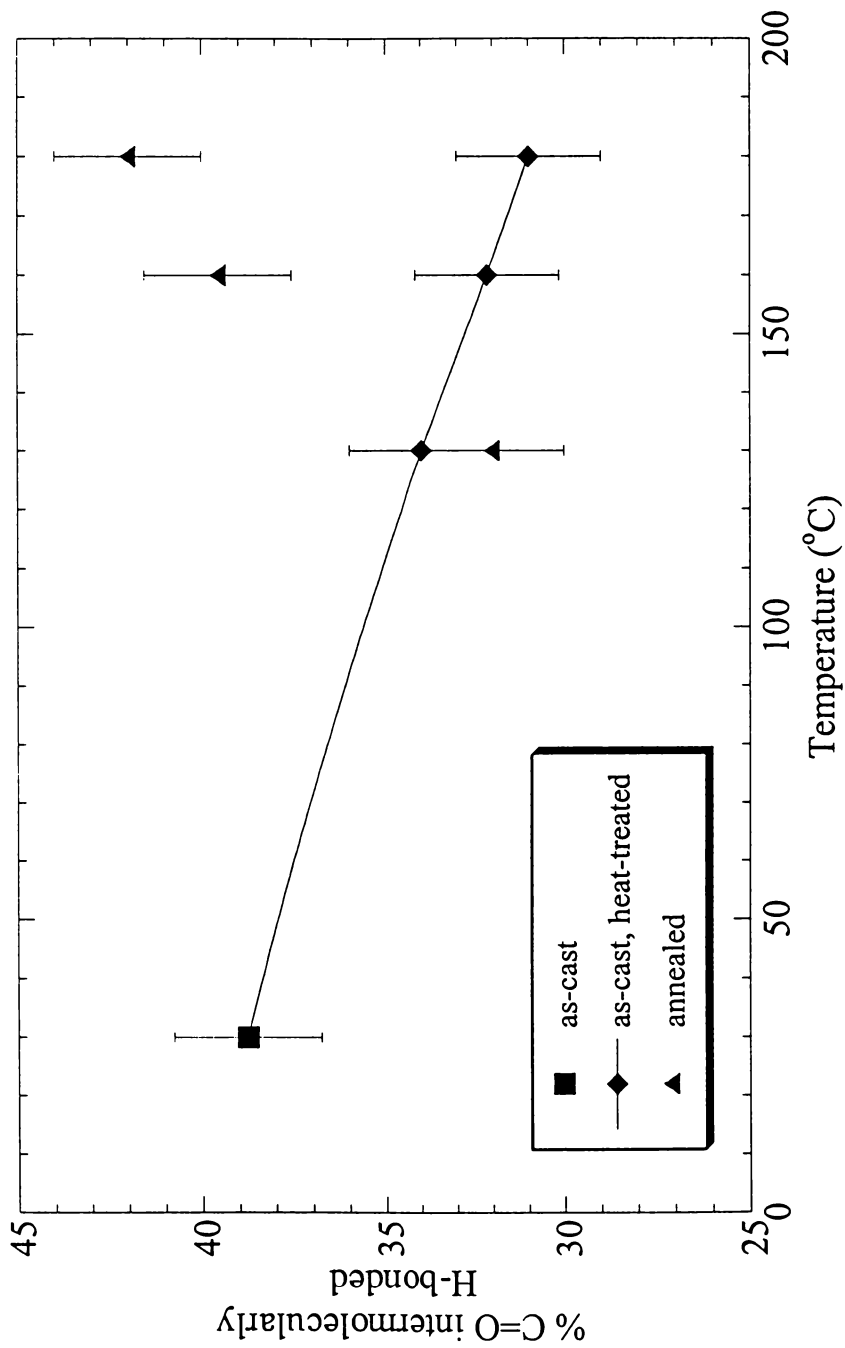


Figure 67. Percent of intermolecular hydrogen bonding as a function of temperature for annealed and as-cast, heat-treated blends of 30/70 (w/w) LCP/PS-co-VPh(20). Error Bar in the plot corresponds to ± 2.0 .

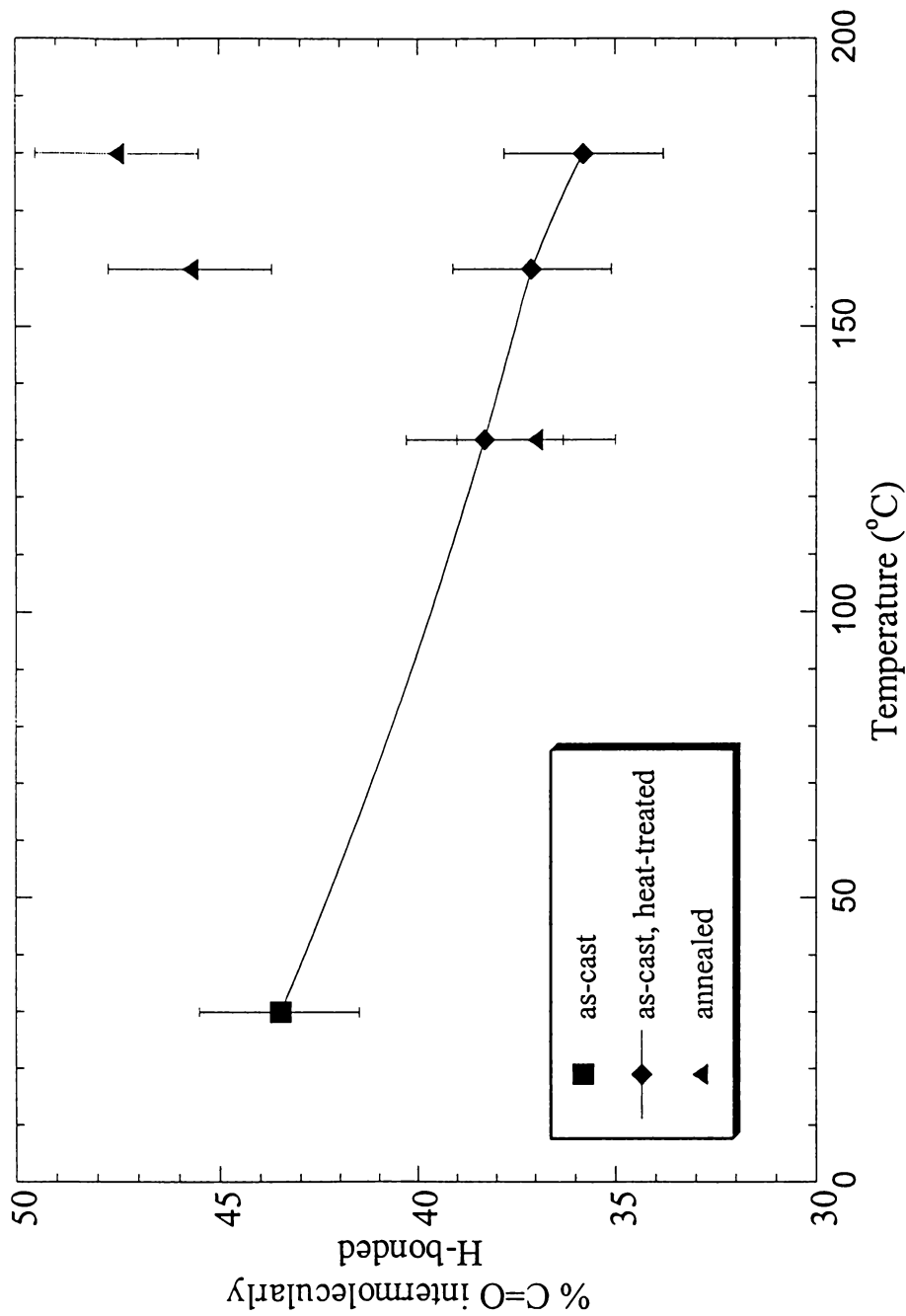


Figure 68. Percent of intermolecular hydrogen bonding as a function of temperature for annealed and as-cast, heat-treated blends of 45/55 (w/w) LCPU-M/PS-co-VPh(40). Error Bar in the plot corresponds to ± 2.0 .

of intermolecular contacts in the blend. These results indicate that the effect of thermal annealing on the partially miscible blends at 130°C is in agreement to that on the immiscible blends studied in this work. However, annealing is found to cause an increase at 160°C and 180°C relative to the 'as-cast' sample. As the system attains equilibrium, there may be a change in phase dispersion of the system that increases the intermolecular contacts. The effect of thermal annealing on the partially miscible blends at 160°C and 180°C agrees well to that on the miscible blends studied here.

Thermal annealing of LCP/PS-co-VPh system shows a change in intermolecular H-bonding that is intuitively obvious. This is evidenced by a correlation of the H-bonding data to the phase behavior of the blend. As the sample is annealed at higher temperatures, it reaches an equilibrium state associated with a change in the phase dispersion of the system that occurs as a result of phase mixing or phase separation. Consequently, we see a change in intermolecular H-bonding in the blend with heat treatment. The change in phase dispersion is found to decrease the intermolecular contacts in immiscible blends and increase the intermolecular contacts in miscible blends when equilibrium is reached. These annealing results correlate well to the phase behavior of the system as determined by optical microscopy.

Chapter 5

Correlation of Association Model to Hydrogen Bonding Liquid

Crystalline Polymer Blends

5.1 Introduction

In the previous chapters, the results of a study that seeks to correlate the extent of intermolecular hydrogen bonding between a LCP and an amorphous polymer in a blend to the phase behavior of the blend have been provided. The results show that by minor structural modification of the polymers, the amount of intermolecular hydrogen bonding in the system can be enhanced which in turn induces miscibility in otherwise immiscible polymer blends. It was found that the system that optimizes the extent of intermolecular hydrogen bonding corresponds to the broadest miscibility window in the blend studied. In this chapter, an association model⁴⁶ is applied to this blend system in order to map theoretical phase diagrams. Also, the problem of *functional group accessibility* that occurs due to insufficient spacing of functional groups along the polymer chain is also addressed as a separate section in this chapter.

Association Model

More than thirty years ago, Prigogine^{80,81} pointed out that there is no satisfactory theory of the strong orientation effects that occur in mixtures involving strong, specific interactions, principally because the rotational partition function is no longer independent of the translational partition function. Prigogine proposed that the formation of a complex be

treated by using the assumption of a chemical equilibrium between the monomers of the associated species. The great advantage of association models is the relatively simple way in which partition functions can be constructed. In contrast to the application of quasi-chemical models⁸³⁻⁸⁸ to the description of interactions, where a coordination number must be assumed in order to account for all contacts, in applying an association model to hydrogen bonds, the number of specific interaction contacts is usually known (e.g., an amide group can hydrogen bond up to two neighbors). Non-specific interactions can be handled using a χ parameter in the usual way. If we were to use a contact point approach to account for all interactions, however, we would end up with algebraically complex expressions and parameters that could not readily be determined from experimental measurements. It is necessary to account for the enthalpic component of specific interactions corresponding to both self- and inter-association, the entropic changes corresponding to loss of rotational freedom, interactions associated with non-specific contacts, and so on.

Association models start with the assumption of an equilibrium distribution of associated species present at a given temperature and composition. For molecules that interact through the formation of hydrogen bonds, we could describe this distribution through appropriately defined equilibrium constants that (in many mixtures) can be determined semi-empirically, that is, experimental input (infrared spectroscopy) applied to stoichiometric equations describing hydrogen bonding. Accordingly, if functional groups in a blend are able to form hydrogen bonds according to their intrinsic proclivities (as in completely miscible blends) and are not constrained into separate domains by phase separation, then equilibrium constants describing self-association and interassociation can be determined by the hydrogen

bonding data from FT-IR measurements. Once the equilibrium constants are available, the fraction of hydrogen bonded C=O groups can be theoretically calculated for any miscible and immiscible blends which in turn can be used to map theoretical phase diagram. The crucial point that must be grasped, however, is that it is not necessary to account for chain stiffness (or chain length) if equilibrium constants are obtained by direct spectroscopic measurements of the polymers being considered. This is because the experimentally determined fraction of hydrogen bonded species obviously includes the influence of such factors, as will the equilibrium constants then calculated from such measurements.

Let us, for example, consider the mixtures of simple (non-polymeric) amides and ethers. We have chains of reversibly associated molecules that have a known distribution of chain lengths. If we treat each of these species (amide “monomers”, amide “dimers”, etc., and equivalent amide-ether chains) as distinguishable (according to chain length), we can apply Flory’s treatment^{42,39} for the mixing of heterogeneous polymers. Essentially, these distinguishable species are initially considered as if they were separate and oriented. The free energy of disorienting and mixing the monomers, dimers, etc., with one another is then determined using Flory’s equations, thus obtaining a free energy relative to the separate and oriented reference state. The same procedure is applied to the distribution of species found in the initially pure amide and ether components, so that a free energy is again found relative to the same reference state. The difference in these two equations gives a free energy that includes the combinatorial entropy of mixing and the free energy changes that occur due to the change in the distribution of hydrogen-bonded species. Physical interactions can then be handled by defining a χ parameter, thus assuming random contacts between the associated

molecules (equivalent to the assumption of random mixing of covalent polymer molecules).

Moreover, the free energy term that describes changes due to hydrogen bonding accounts for both enthalpy and entropy changes by the equilibrium constants that define the distribution of species as a function of concentration and is a measure of the *enthalpic and entropic* contributions to the free energy per hydrogen bond. The various entropic contributions (combinatorial, rotational, etc.) to the free energy are accounted for simultaneously. In the amide/ether example discussed above, there will be fewer amide/amide hydrogen bonds as the mixture is diluted with ether molecules and thus an increase in entropy due to the gain in rotational freedom of the “liberated” amides. Similarly, there will be a contribution that decreases the entropy of mixing due to the formation of amide/ether hydrogen bonds. In an association model, these entropic contributions are accounted for simply in terms of the change in the number of species with concentration.

In this chapter, the association model⁴⁶ developed by Painter et al. has been applied to the N-methyl liquid crystalline polyurethane/poly (styrene-co-vinylphenol) [LCPU-M/PS-co-VPh] blends to compare theoretical phase diagrams determined by this model to experimental phase diagrams obtained by optical microscopy and DSC measurements. This system is much simpler to deal with than the liquid crystalline polyurethane/poly(styrene-co-4-vinylphenol) [LCPU/PS-co-VPh] system. This blend contains a self-associating component B (PS-co-VPh) and a second component A (LCPU-M) which does not self-associate but may associate with component B. However, in the LCPU/PS-co-VPh blends, there is a self-association present in both the polymer components [(C=O---H-N) in LCPU and (O-H---O-H) in PS-co-VPh] and two intermolecular H-bonding interactions present between them

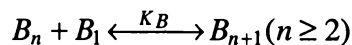
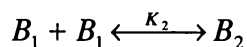
[(C=O---H-O) and (N-H---O-H)]. Each of these interactions must be defined by equilibrium constants in the Association model, which makes the stoichiometric equation derivation extremely complex and unmanageable.

The association model for the LCPU-M/PS-co-VPh system, therefore, involves self-associating equilibrium constants for polymer B (PS-co-VPh) describing the formation of hydrogen-bonded dimers and multimers of B units denoted by K_2 and K_B respectively, and an interassociating equilibrium constant describing the formation of B_nA complex, denoted by K_A , which represents intermolecular H-bonding between polymers A and B. For a better understanding, some relevant information on the stoichiometric relationships and the free energy of mixing expression describing these hydrogen bonding associations is provided below.

Stoichiometric Equations describing Hydrogen Bonding

In this section, the stoichiometric relationships describing hydrogen bonding associations in LCPU-M/PS-co-VPh system are derived.

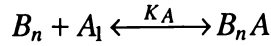
Self-association in Polymer B



$$K_2 = \frac{\Phi_{B_2}}{2\Phi_{B_1}^2} \quad (5.1)$$

$$K_B = \frac{\Phi_{B_{n+1}}}{\Phi_{B_n} \Phi_{B_1}} \left(\frac{n}{n+1} \right) \quad (5.2)$$

Interassociation between Polymer A and B



$$K_A = \frac{\Phi_{B_n A}}{\Phi_{B_n} \Phi_{A_1}} \left(\frac{nr}{n+r} \right) \quad (5.3)$$

where Φ_i represents the volume fractions of the i th polymer and r is the ratio of the molar volume of polymers A and B (V_A/V_B). In particular, Φ_A and Φ_B are the volume fractions of polymers A and B respectively and Φ_{A_1} and Φ_{B_1} are volume fractions of the respective repeat units that are not hydrogen bonded.

The stoichiometric relationships are simply obtained from materials balance considerations. The total volume fraction of all B units present in the mixture is given by:

$$\Phi_B = \Phi_{B_1} + \sum_{n=2}^{\infty} \Phi_{B_n} + \sum_{n=1}^{\infty} \Phi_{B_n A} \left(\frac{nr}{n+r} \right) \quad (5.4)$$

Note that for formation of dimer, trimer, ... n -mer, according to equations 1 and 2 we have:

$$\Phi_{B_2} = 2K_2 \Phi_{B_1}^2 \quad (5.4.1)$$

$$\Phi_{B_3} = \frac{3}{2} K_B \Phi_{B_2} \Phi_{B_1} \quad (5.4.2)$$

$$\text{and } \Phi_{B_n} = \frac{n}{n-1} K_B \Phi_{B_{n-1}} \Phi_{B_1} \quad (5.4.3)$$

By successive substitution of $\Phi_{B_{n-1}}$, $\Phi_{B_{n-2}}$, ..., Φ_{B_2} , one can obtain:

$$\Phi_{B_n} = n K_B^{n-2} \Phi_{B_1}^{n-2} K_2 \Phi_{B_1}^2 \quad (5.4.4)$$

hence:
$$\Phi_{B_n} = \frac{K_2}{K_B} n(K_B \Phi_{B_1})^n \quad (5.4.5)$$

and:
$$\sum_{n=2}^{\infty} \Phi_{B_n} = \frac{K_2}{K_B} \sum_{n=2}^{\infty} n(K_B \Phi_{B_1})^n \quad (5.4.6)$$

Applying equations 5.4.1 – 5.4.6 to equation 5.4, equation 5.5 can be formed as below:

$$\Phi_B = \Phi_{B_1} + \frac{K_2}{K_B} \sum_{n=2}^{\infty} n(K_B \Phi_{B_1})^n + \frac{K_2}{K_B} \sum_{n=1}^{\infty} \frac{K_A \Phi_{A_1}}{r} n(K_B \Phi_{B_1})^n \quad (5.5)$$

However, for $K_B \Phi_{B_1} < 1$,
$$\sum_{n=1}^{\infty} n(K_B \Phi_{B_1})^{n-1} = \frac{1}{(1 - K_B \Phi_{B_1})^2} \quad (5.6)$$

Applying equation 5.6 to equation 5.5, we get

$$\Phi_B = \Phi_{B_1} \Gamma_2 [1 + X] \quad (5.7)$$

and
$$\Phi_A = \Phi_{A_1} [1 + K_A \Phi_{B_1} \Gamma_1] \quad (5.8)$$

where
$$\Gamma_1 = \left(1 - \frac{K_2}{K_B}\right) + \frac{K_2}{K_B} \left[\frac{1}{(1 - K_B \Phi_{B_1})} \right] \quad (5.9)$$

$$\Gamma_2 = \left(1 - \frac{K_2}{K_B}\right) + \frac{K_2}{K_B} \left[\frac{1}{(1 - K_B \Phi_{B_1})^2} \right] \quad (5.10)$$

$$X = \frac{K_A \Phi_{A_1}}{r} \quad (5.11)$$

Finally, a useful relation will be
$$f_{HB}^{C=O} = 1 - \frac{\Phi_{A_1}}{\Phi_A} \quad (5.12)$$

where $f_{HB}^{C=O}$ is the fraction of hydrogen bonded C=O groups in the blend.

Free Energy of Mixing in Hydrogen Bonding Polymer Blends

Flory^{41,45} pointed out that for the treatment of chemical equilibria between polymeric species

(in this case the polymers formed by linking n groups to form a hydrogen-bonded chain), the proper standard state is where the individual species are separate and oriented. Therefore, first let us consider small molecules and treat the equilibrium distribution of hydrogen bonded chains as if they were covalently linked. Of course, the equilibrium distribution changes with composition, but as per Flory's suggestion, this can be handled with the appropriate choice of reference state, namely where the species are separate and oriented. In outline, the proper approach is to derive an expression for the ideal free energy of mixing such preformed associated species. This free energy term includes the combinatorial entropy of mixing the species in addition to the changes in the free energy due to the changes in distribution of hydrogen-bonded species present (ΔG_H). To obtain ΔG_H , we therefore must subtract the entropy of mixing just the units of the hydrogen-bonded chains. Physical interactions and the combinatorial entropy of mixing the covalently bonded polymer species can then be introduced to give the overall free energy of mixing. A detailed derivation of the free energy of mixing in hydrogen bonded systems has already been provided in studies by Coleman et al.⁸⁸⁻⁹⁰ Given below is a derivation of the free energy equation for the polymer blend system studied in this thesis, which comprises of a self-associating component B (PS-co-VPh) and a second component A (LCPU-M) which does not self-associate but may associate with component B. The procedure can be summarized as follows:

- 1) Consider the equilibrium distribution of self-associating component B in pure B. Put all monomers (i.e., B_1 units) into an ordered lattice, all dimers (B_2) into a second ordered lattice, and so on until we reach n-mers (B_n). Take the species out, athermally mix them and disorient them using Flory-Huggins equation, which is

$$\frac{\Delta G_{ch}^0}{RT} = \sum_{n=1} N_{B_n}^0 \ln \Phi_{B_n}^0 + \text{DisorientationTerms} \quad (5.13)$$

- 2) Put the equilibrium distribution of species found at a particular composition in the polymer mixture (consisting of units A and B) in a similar lattice. Athermally mix and disorient these species ($B_1, A, B_2, B_1A, B_2A, \dots B_n, B_nA$) in the same way

$$\frac{\Delta G_{ch}^{\wedge}}{RT} = \sum_{n=1} N_{B_n} \ln \Phi_{B_n} + \sum_{n=0} N_{B_nA} \ln \Phi_{B_nA} + \text{DisorientationTerms} \quad (5.14)$$

where N and Φ are the number of molecules and volume fraction of each species

- 3) The difference in these two equations (equation 5.14 minus equation 5.13) gives a free energy (ΔG_{ch}) that includes a combinatorial entropy of mixing and the free energy changes that occur due to the change in the distribution of hydrogen-bonded species.

The ‘disorientation terms’ in the equations above are the entropy of disorientation of the individual molecules and are omitted for clarity of presentation as they cancel in subsequent equations. The appropriate reference state for our purposes is therefore the entropy of mixing the pure liquids with no change in polymer species present ($\sum N_{B_n}^0 \ln \Phi_{B_n} + N_A \ln \Phi_A$).

The free energy of mixing, relative to Flory’s reference state, ΔG_{ch}^{\wedge} consists of two parts: a contribution from hydrogen bonding ΔG_H^* , an excess function that represents the change in free energy of a hydrogen bonded non-covalently linked system; a second part included in parentheses in equation 5.15, which is the entropy change that occurs if such non-hydrogen bonded units are randomly mixed. Taken together, we obtain:

$$\frac{\Delta G_{ch}^{\wedge}}{RT} = \frac{\Delta G_H^*}{RT} - (N_B \ln \Phi_B + N_A \ln \Phi_A) \quad (5.15)$$

By forming the hydrogen bonds found in pure B at the volume of the mixture we now obtain:

$$\frac{\Delta G_{ch}^0}{RT} = \frac{\Delta G_H^0}{RT} - (N_B \ln \Phi_B - \sum N_{B_n}^0 \ln \Phi_{B_n}) \quad (5.16)$$

where ΔG_H^0 is the result obtained for non-covalently linked B units, so that by subtracting equation 5.16 from 5.15, we obtain an expression for the free energy of mixing that is given by:

$$\frac{\Delta G_{ch}}{RT} = \left(\frac{\Delta G_H^*}{RT} - \frac{\Delta G_H^0}{RT} \right) - \left(\frac{N_B}{n_H^0} \ln \Phi_B + N_A \ln \Phi_A \right) \quad (5.17)$$

where n_H^0 is the number-average degree of association found in pure B and is equal to $N_B / \sum N_{B_n}^0$.

Now, it is essential to obtain the chemical potentials of the hydrogen-bonded n -mers B_n and the complexes B_nA by differentiating ΔG_{ch}^0 and ΔG_{ch}^{\wedge} with respect to the number of molecules of each chemical species to determine the phase behavior of these mixtures.

$$\frac{\mu_{B_n} - \mu_{B_n}^*}{RT} = \ln \Phi_{B_n} + 1 - \frac{V_{B_n}}{V} \quad (5.18)$$

$$\frac{\mu_{B_nA} - \mu_{B_nA}^*}{RT} = \ln \Phi_{B_nA} + 1 - \frac{V_{B_nA}}{V} \quad (5.19)$$

where μ stands for chemical potential and the asterisk refers to Flory's standard state and V , the total molar volume of the sample, is given by

$$\frac{1}{V} = \sum_{n=1} \frac{\Phi_{B_n}}{V_{B_n}} + \sum_{n=0} \frac{\Phi_{B_nA}}{V_{B_nA}} \quad (5.20)$$

The total differential of the Gibbs free energy of the mixture of these complexes can be written:

$$dG = \sum \mu_{B_n} dN_{B_n} + \sum \mu_{B_n A} dN_{B_n A} + \mu_{A_1} dN_{A_1} \quad (5.21)$$

$$= \mu_{B_1} \sum dN_{B_n} n + \mu_{B_1} \sum dN_{B_n A} n + \mu_{A_1} dN_{A_1} + \mu_{A_1} \sum dN_{B_n A} \quad (5.22)$$

If the total number of molecules (i.e., monomers) of A and B in the mixture are N_A and N_B , respectively, then:

$$N_B = \sum_{n=1}^{\infty} nN_{B_n} + \sum_{n=1}^{\infty} nN_{B_n A} \quad (5.23)$$

$$N_A = N_{A_1} + \sum_{n=1}^{\infty} nN_{B_n A} \quad (5.24)$$

We now use Prigogine's result that the hydrogen bonded chains are in chemical equilibrium with one another and the "monomers" (i.e., non-hydrogen bonded units, A_1 and B_1) which requires:

$$\mu_{B_n} = n\mu_{B_1} \quad (5.25)$$

$$\mu_{B_n A} = n\mu_{B_1} + \mu_{A_1} \quad (5.26)$$

Now, equation 5.22 becomes

$$dG = \mu_{B_1} dN_B + \mu_{A_1} dN_{A_1} \quad (5.27)$$

But for any binary system at constant T, P:

$$dG = \mu_B dN_B + \mu_A dN_A \quad (5.28)$$

and therefore:

$$\mu_B = \mu_{B_1} \quad (5.29)$$

$$\mu_A = \mu_{A_1} \quad (5.30)$$

so that the chemical potentials of the stoichiometric components are equal to the chemical potentials of the respective monomers. Equivalent equations are written for pure solutions of the individual

components μ_B^0 and μ_A^0 , which are then subtracted from equations 5.18 and 5.19 to transform to a standard state defined as these pure solutions. Hence,

$$\frac{\mu_B - \mu_B^*}{RT} = \ln \Phi_{B_1} + 1 - \frac{V_B}{V} \quad (5.31)$$

and

$$\frac{\mu_A - \mu_A^*}{RT} = \ln \Phi_{A_1} + 1 - \frac{V_A}{V} \quad (5.32)$$

At this point it should be recalled that we are using Flory's definition of the standard state, where individual species B_n are separate and oriented. We now wish to transform to a standard state defined as pure solutions of the individual components. Accordingly, we first write

$$\frac{\mu_B^0 - \mu_B^*}{RT} = \ln \Phi_{B_1}^0 + 1 - \frac{V_B}{V^0} \quad (5.33)$$

where the superscript (0) refers to solutions of pure B. Subtraction gives

$$\frac{\mu_B - \mu_B^0}{RT} = \ln \frac{\Phi_{B_1}}{\Phi_{B_1}^0} + \frac{V_B}{V^0} - \frac{V_B}{V} \quad (5.34)$$

Similarly

$$\frac{\mu_A - \mu_A^*}{RT} = \ln \Phi_{A_1} + 1 - \frac{V_A}{V} \quad (5.35)$$

These equations for the chemical potentials can be combined to give an expression for the free energy of mixing species A and B. However, this contains a combinatorial entropy of mixing component that needs to be subtracted to give the required "excess" function, ΔG_H , the change in free energy associated with just the change in the distribution of hydrogen-bonded polymer species. Thus, for a stoichiometric mixture of x_A and x_B moles we can then obtain a "chemical" free energy of mixing:

$$\frac{\Delta G_{ch}}{RT} = x_B \ln(\Phi_{B_1} / \Phi_{B_1}^0) + x_A \ln \Phi_{A_1} - \frac{V_M}{V} + x_A + x_B \frac{V_B}{V^0} \quad (5.36)$$

$$\text{where } V_M = x_A V_A + x_B V_B \quad (5.37)$$

Of course, the relationship of Φ_{B_1} and Φ_{A_1} to Φ_B and Φ_A follows the more complicated dependence on K_2 , K_B , and K_A and similarly, expressions for V and V^0 are also more complicated and it is these substitutions that we need to consider next.

With $V_{B_n} = nV_B$, the first term of equation 5.20 is given by

$$\begin{aligned} \sum_{n=1}^{\infty} \frac{\Phi_{B_n}}{V_{B_n}} &= \frac{1}{V_B} \left[\sum_{n=1}^{\infty} \frac{\Phi_{B_n}}{n} \right] = \frac{1}{V_B} \left[\Phi_{B_1} + \sum_{n=2}^{\infty} \frac{\Phi_{B_n}}{n} \right] = \\ & \frac{1}{V_B} \left[\Phi_{B_1} + \frac{K_2}{K_B^2} \sum_{n=1}^{\infty} (\Phi_{B_1} K_B)^n - \frac{K_2}{K_B^2} (\Phi_{B_1} K_B) \right] \end{aligned} \quad (5.38)$$

$$\text{For } K_B \Phi_{B_1} < 1 \quad \sum_{n=1}^{\infty} (\Phi_{B_1} K_B)^{n-1} = \frac{1}{1 - K_B \Phi_{B_1}} \quad (5.39)$$

$$\sum \frac{\Phi_{B_n}}{V_{B_n}} = \frac{\Phi_{B_1}}{V_B} \left[\left(1 - \frac{K_2}{K_B} \right) + \frac{K_2}{K_B} \left(\frac{1}{1 - K_B \Phi_{B_1}} \right) \right] \quad (5.40)$$

$$\text{Similarly } \sum_{n=0}^{\infty} \left(\frac{\Phi_{B_n A}}{V_{B_n A}} \right) = \frac{1}{V_B} \left[\frac{\Phi_{A_1}}{r} + \frac{K_A \Phi_{A_1}}{r} \left(\Phi_{B_1} \left(1 - \frac{K_2}{K_B} \right) + \frac{K_2}{K_B} \left(\frac{1}{1 - K_B \Phi_{B_1}} \right) \right) \right] \quad (5.41)$$

Using the already defined terms Γ_1 and Γ_2 , we can simplify the above equations to

$$-\frac{V_M}{V} = -V_M \left[\frac{\Phi_{B_1}}{V_B} (\Gamma_1) + \frac{\Phi_{A_1}}{r V_B} [1 + K_A \Phi_{B_1}] (\Gamma_1) \right] \quad (5.42)$$

$$\text{But } V_M = x_B V_B / \Phi_B = x_A V_A / \Phi_A \quad (5.43)$$

$$\text{Hence } -\frac{V_M}{V} = - \left[\frac{x_B \Phi_{B_1}}{\Phi_B} (\Gamma_1) + \frac{x_A \Phi_{A_1}}{\Phi_A} [1 + K_A \Phi_{B_1}] (\Gamma_1) \right] \quad (5.44)$$

Substituting for Φ_A and Φ_B from equation 5.7 and 5.8

$$-\frac{V_M}{V} = -\left[\frac{x_B}{1+X} \left(\frac{\Gamma_1}{\Gamma_2} \right) + x_A \right] \quad (5.45)$$

where X has already been defined before.

$$\text{Similarly for pure B, } x_B V_B / V^0 = x_B \Phi_{B_1}^0 \Gamma_1^0 \quad (5.46)$$

$$\text{Noting that } \Phi_B^0 = \Phi_{B_1}^0 \Gamma_2^0 = 1 \quad (5.47)$$

The last three terms in the free energy expression, equation 5.34, are given by

$$\begin{aligned} -\frac{V_M}{V} + x_A + x_B \frac{V_B}{V^0} &= -\frac{x_B}{1+X} \left(\frac{\Gamma_1}{\Gamma_2} \right) + x_B \left(\frac{\Gamma_1^0}{\Gamma_2^0} \right) = \\ x_B \left[\frac{\Gamma_1^0}{\Gamma_2^0} - \frac{\Gamma_1}{\Gamma_2} \right] + x_B \left(\frac{X}{1+X} \right) \left(\frac{\Gamma_1}{\Gamma_2} \right) &\quad (5.48) \end{aligned}$$

$$\text{a result obtained by using } \frac{1}{1+X} = 1 - \left(\frac{X}{1+X} \right) \quad (5.49)$$

This gives an equation in the same form as equation 5.45 upon conversion to a unit volume basis, multiplication by a reference volume V_r equal to the molar volume of species B, V_B , and subtraction of the combinatorial entropy term for mixing components A and B with no change in hydrogen bonding:

$$\frac{\Delta G_H}{RT} = \Phi_B \ln \left[\frac{\Phi_{B_1}}{\Phi_{B_1}^0} \right] + \frac{\Phi_A}{r} \ln \Phi_{A_1} - [\Phi_A V_B + \Phi_B V_B] \frac{1}{V} + \frac{\Phi_A}{r} + \frac{\Phi_B V_B}{V^0} - \left[\frac{\Phi_B}{n_H^0} \ln \Phi_B + \frac{\Phi_A}{r} \ln \Phi_A \right] \quad (5.50)$$

where the superscript (0) refers to solutions of pure polymers and $n_H^0 = \Gamma_2^0 / \Gamma_1^0$.

Using equation 5.20 and rearranging equation 5.50, we get the change in free energy on mixing due to hydrogen bonding interactions (ΔG_H) is shown below:

$$\frac{\Delta G_H}{RT} = \Phi_B \ln \left[\frac{\Phi_{B_1}}{\Phi_{B_1}^0 \Phi_B^{1/n_H}} \right] + \frac{\Phi_A}{r} \ln \left[\frac{\Phi_{A_1}}{\Phi_A} \right] + \Phi_B \left(\frac{\Gamma_1^0}{\Gamma_2^0} - \frac{\Gamma_1}{\Gamma_2} \right) + \Phi_B \left(\frac{\Gamma_1}{\Gamma_2} \right) \left[\frac{X}{1+X} \right] \quad (5.51)$$

Equation 5.51 can also be re-written as:

$$\frac{\Delta G_H}{RT} = \Phi_B \ln \left[\frac{\Phi_{B_1}}{\Phi_{B_1}^0} \right] + \frac{\Phi_A}{r} \ln \Phi_{A_1} + \Phi_B \left(\frac{\Gamma_1^0}{\Gamma_2^0} - \frac{\Gamma_1}{\Gamma_2} \right) + \Phi_B \left(\frac{\Gamma_1}{\Gamma_2} \right) \left[\frac{X}{1+X} \right] - \left[\frac{\Phi_B}{n_H^0} \ln \Phi_B + \frac{\Phi_A}{r} \ln \Phi_A \right] \quad (5.52)$$

In equation 5.51, the first two terms represent the entropy change corresponding to changes in the distribution of H-bonded species. Since the derivation initially assumes that B and A interacting units are not linked covalently into polymer chains, the free energy of mixing term includes a combinatorial entropy of mixing component (the last two terms of equation 5.52) that must be separated from the free energy changes associated solely with the change in hydrogen bonded species. Thus, the term equal to $(\Phi_B / n_H^0) \ln \Phi_B + (\Phi_A / r) \ln \Phi_A$ represents the free energy of athermally mixing A and B with no change in hydrogen bonding. Finally, the last two terms in equation 5.51 represent the enthalpy change, where the first of these two is related to the number of B-B hydrogen bonds broken and the second one to the number of A-B bonds formed.

5.2 Results and Discussion

Generally it is more likely that two (co)polymers will be miscible with one another if they contain polar substituents which are capable of forming specific interactions such as dipole-dipole forces, hydrogen bonds, and ionic interactions. The presence of such interactions contributes a favorable, negative enthalpic contribution to the free energy of mixing which can drive miscibility. The chemical forces term ($\Delta G_H/RT$) that the association

model includes in its overall free energy equation estimates the contribution to the free energy of mixing from hydrogen bonding. It is generally favorable to mixing and arises from the change in the distribution of hydrogen bonds found in the blend compared to the pure (co)polymers.⁹¹ Its magnitude is calculated from spectroscopically determined equilibrium constants, which describe the stoichiometry of hydrogen bonding in the blend, and enthalpies of hydrogen bond formation.⁹²⁻⁹⁴

Determination of self-association equilibrium constants

In the O-H group containing PS-co-VPh copolymer, two equilibrium constants are necessary to adequately describe the self-association of O-H groups: one that describes (OH--OH) dimer formation (K_2) and another that describes higher multimer formation (K_B). Usually, these equilibrium constants are determined from appropriate low molecular weight analogs.^{49,92-98} That is, molecules which have essentially identical chemical structures to the repeat unit of the polymer are examined. For example, K_2 and K_B for poly(4-vinyl phenol) (PVPh) can be determined from a low molecular weight compound such as phenol or 4-ethyl phenol. Self-association equilibrium constants are estimated from low molecular weight analogs because (co)polymers, such as PVPh or PS-co-VPh, are not soluble in non-hydrogen bonding solvents such as cyclohexane. Once an appropriate low molecular weight compound is chosen, a series of infrared spectra is obtained as a function of dilution in a non-hydrogen bonding solvent such as cyclohexane. From these spectra, the fraction of free phenolic monomers, f_m^{OH} , present is measured for each concentration. The values of the equilibrium constants can be determined from a least squares fit of the f_m^{OH} data to the previously derived stoichiometric equation which relates f_m^{OH} to the equilibrium constants.

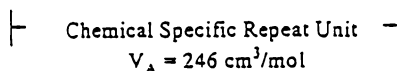
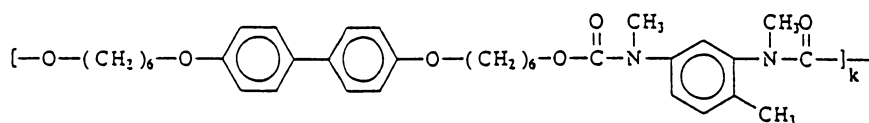
$$f_m^{OH} = \frac{\Phi_{B_1}}{\Phi_B} = \frac{1}{\Gamma_2} \quad (5.53)$$

Thus, the values of the equilibrium constants obtained for phenol in cyclohexane by Whetsel and Lady are $K_2 = 21.0$ and $K_B = 66.8$ at 25°C scaled up to a common reference volume of 100 cm³/mol.⁹⁷ These equilibrium constants can be transferred directly to (co)polymers on the basis of molar volume by the following equation:

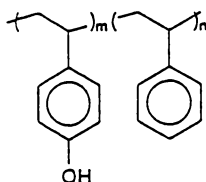
$$K_i^{Polymer} = \frac{V_B^{Model}}{V_B^{Polymer}} K_i^{Model} \quad (5.54)$$

where $K_i^{Polymer}$ and K_i^{Model} are equilibrium constants for the (co)polymer “chemical specific repeat” and the low molecular weight analog, respectively, and $V_B^{Polymer}$ and V_B^{Model} are the molar volumes for the (co)polymer “chemical specific repeat” (= 100 cm³/mol for PVPh) and the low molecular weight analog (VPh), respectively.^{46,49} An average chemical specific repeat of a (co)polymer is defined in such a manner that it contains one functional group that is capable of hydrogen bonding. For example, styrene in PS-co-VPh is viewed as an inert diluent and thus the chemical specific repeat unit of PS-co-VPh is defined in such a way that it has exactly one 4-vinyl phenol unit. As a result of this definition, the magnitude of the molar volume as well as equilibrium constants may be simply calculated as a function of copolymer composition. Figure 69 shows the chemical specific repeat units of the LCPU-M and the PS-co-VPh copolymers. The molar volume and molar volume ratios ($r = V_A / V_B$) calculated for different PS-co-VPh compositions are listed in Table 6. Table 7 and 8 give the self-association equilibrium constants for the different PS-co-VPh compositions at 25°C. To

Chemical Specific Repeat Units of Polymers



N-methyl Liquid Crystalline Polyurethane
(LCPU-M)



Poly(styrene-co-4-vinylphenol)
[PS-co-VPh] copolymer

In PS-co-VPh,
 $m = 1$, considering one hydrogen bonding functional group in a
 chemical specific repeat unit

Then, on an average,

| <u>mole% VPh in copolymer</u> | η |
|-----------------------------------|--------|
| 5 | 19.0 |
| 10 | 9.0 |
| 20 | 4.0 |
| 30 | 2.3 |
| 40 | 1.5 |
| 50 | 1.0 |
| 100 | 0.0 |

Figure 69. Chemical specific repeat units of N-methyl liquid crystalline polyurethane (LCPU-M) and poly (styrene-co-4-vinylphenol) [PS-co-VPh] copolymers

Table 6. Molar Volume Data for Different Copolymer Compositions of LCPU-M/PS-co-VPh Blends.

| Copolymer Composition (% VPh) | Molar Volume of Copolymer (V_B) | Molar Volume Ratio* ($r = V_A / V_B$) |
|-------------------------------|-------------------------------------|---|
| 5 | 1877 | 0.1310 |
| 10 | 942 | 0.2611 |
| 20 | 474 | 0.5189 |
| 30 | 318 | 0.7735 |
| 40 | 240 | 1.0250 |
| 50 | 194 | 1.2680 |
| 100 | 100 | 2.4600 |

* V_A = molar volume of LCPU-M = 246 cm³/mol

Table 7. Self-association Equilibrium Constant (K_2) of Hydroxyl-Hydroxyl Dimer Hydrogen Bonding for Different Copolymer Compositions and Temperatures of LCPU-M/PS-co-VPh blends.

| %VPh in copolymer | Temperature | | | | |
|-------------------|-------------|-------|-------|-------|-------|
| | 25°C | 150°C | 170°C | 190°C | 210°C |
| 5 | 1.10 | 0.067 | 0.050 | 0.038 | 0.029 |
| 10 | 2.20 | 0.135 | 0.100 | 0.076 | 0.059 |
| 20 | 4.40 | 0.270 | 0.200 | 0.152 | 0.118 |
| 30 | 6.60 | 0.405 | 0.300 | 0.228 | 0.177 |
| 40 | 8.80 | 0.541 | 0.401 | 0.304 | 0.236 |
| 50 | 10.8 | 0.663 | 0.492 | 0.373 | 0.290 |
| 100 | 21.0 | 1.290 | 0.957 | 0.726 | 0.564 |

Table 8. Self-association Equilibrium Constant (K_B) of Hydroxyl-Hydroxyl Multimer Hydrogen Bonding for Different Copolymer Compositions and Temperatures of LCPU-M/PS-co-VPh Blends.

| %VPh in copolymer | Temperature | | | | |
|-------------------|-------------|-------|-------|-------|-------|
| | 25°C | 150°C | 170°C | 190°C | 210°C |
| 5 | 3.60 | 0.271 | 0.206 | 0.159 | 0.125 |
| 10 | 7.10 | 0.534 | 0.405 | 0.313 | 0.248 |
| 20 | 14.1 | 1.061 | 0.804 | 0.623 | 0.493 |
| 30 | 21.0 | 1.581 | 1.198 | 0.928 | 0.734 |
| 40 | 27.8 | 2.093 | 1.587 | 1.228 | 0.972 |
| 50 | 34.4 | 2.590 | 1.963 | 1.520 | 1.203 |
| 100 | 66.8 | 5.030 | 3.813 | 2.952 | 2.337 |

determine the temperature dependence of the equilibrium constants, a Van't Hoff relationship^{46,49} is employed, in terms of the enthalpy of hydrogen bond formation ($h_2 = -5.63$ kcal/mol and $h_B = -5.22$ kcal/mol for pure PVPh) as shown below:

$$\ln\left(\frac{K_2}{K_1}\right) = -\frac{h}{R}\left(\frac{1}{T_2} - \frac{1}{T_1}\right) \quad (5.55)$$

where R is the gas constant with a value of 1.986 cal/K/mol.

Determination of Interassociation equilibrium constant

Interassociation refers to hydrogen bonding between the O-H groups of PS-co-VPh and the C=O group of the LCPU-M. Unlike self-association equilibrium constants which are determined from IR data of low molecular weight analogs, interassociation equilibrium constants are determined directly from experimental IR studies of polymer blend samples. However, a key requirement of the methodology used to determine the values of K_A is verification that the polymer blends studied are indeed miscible and above the glass transition temperature (T_g) and melting temperature (T_m) of the polymer components which facilitates attainment of equilibrium. To insure the blends chosen for determining K_A were single phase, optical microscopy and DSC measurements were completed. The experimental phase diagrams of LCPU-M/PS-co-VPh blends as determined by optical microscopy are shown in Figure 50 for different copolymer compositions. After verification that the polymer blends chosen for K_A determination are miscible, the fraction of hydrogen bonded C=O groups ($f_{HB}^{C=O}$) in the blends is quantitatively determined as a function of composition using IR spectroscopy. The number of hydrogen bonded C=O groups indicates the degree of intermolecular H-bonding that is present in a particular blend system and is used to

determine the interassociation equilibrium constant. In this work on the LCPU-M/PS-co-VPh blends, the extent of intermolecular H-bonding between the two polymers can be quantitatively estimated using FT-IR. In short, a least-squares deconvolution of the C=O stretching vibration at around 1700 cm^{-1} of FT-IR curve was completed to determine the fraction of C=O groups in the system participating in intermolecular H-bonding. The C=O stretching region splits into two distinct bands assigned to free (1707 cm^{-1}) and intermolecularly H-bonded (1680 cm^{-1}) C=O groups and $f_{HB}^{C=O}$ is calculated from the relative intensities of these two bands (taking into account the differences in their absorption coefficients). An explanation of the whole procedure has been provided in the earlier chapters and elsewhere.^{46,73-75} The $f_{HB}^{C=O}$ values obtained experimentally for different temperatures and copolymer compositions of miscible blends of 20/80 (w/w) LCPU-M/PS-co-VPh blends are shown in Table 9. In this work, the values of weight fraction and volume fraction (Φ) of blends have been used interchangeably since they work out to be almost the same for all blend compositions (within ± 0.01 units error). The derivation of the equations describing the stoichiometry of hydrogen bonding in LCPU-M/PS-co-VPh has already been discussed in the beginning of this chapter. The appropriate equations are

$$\Phi_B = \Phi_{B_1} \Gamma_2 [1 + X] \quad (5.56)$$

where

$$\Gamma_2 = \left(1 - \frac{K_2}{K_B} \right) + \frac{K_2}{K_B} \left[\frac{1}{(1 - K_B \Phi_{B_1})^2} \right] \quad (5.57)$$

$$X = \frac{K_A \Phi_{A_1}}{r} \quad (5.58)$$

where K_2 and K_B are the hydroxyl-hydroxyl dimer H-bonding and hydroxyl-hydroxyl

Table 9. Fraction of Hydrogen Bonded Carbonyl Groups (Determined Experimentally from IR Spectroscopy) of 20/80 (w/w) LCPU-M/PS-co-VPh Blends at Different Copolymer Compositions and Temperatures.

| Temperature (°C) | Copolymer Composition (mole% VPh) | | | | | |
|---------------------|-----------------------------------|-------|-------|-------|-------|-------|
| | 5 | 10 | 20 | 30 | 40 | 50 |
| 150 | 0.118 | 0.315 | 0.410 | 0.450 | 0.465 | 0.463 |
| 170 | 0.113 | 0.301 | 0.385 | 0.420 | 0.442 | 0.453 |
| 190 | 0.105 | 0.285 | 0.378 | 0.405 | 0.429 | 0.437 |
| 210 | 0.097 | 0.279 | 0.370 | 0.391 | 0.413 | 0.425 |

multimer self-association equilibrium constants, K_A is the interassociation equilibrium constant, Φ_A and Φ_B are the volume fractions of non-self-associating species A and self-associating species B, respectively, Φ_{A_1} and Φ_{B_1} are the volume fractions of the respective totally “free monomers”, and r is the ratio of the molar volumes of the repeat units V_A/V_B .

$$\text{Finally, an obvious, useful relation will be } f_{HB}^{C=O} = 1 - \frac{\Phi_{A_1}}{\Phi_A} \quad (5.59)$$

where $f_{HB}^{C=O}$ is the fraction of hydrogen bonded C=O groups in the blend.

The values of all the parameters describing the above equations are known for a particular blend composition and temperature except Φ_{A_1} , Φ_{B_1} , and K_A . Using the value of experimentally determined $f_{HB}^{C=O}$ (see Table 9), Φ_{A_1} can be determined easily using equation 5.59. Selecting an initial value of with an appropriate value of [$0 < \Phi_{B_1} < 0.999 / K_A$, since it was previously established that $K_B \Phi_{B_1} < 1$ (see equation 5.6)], the K_A and Φ_{B_1} values were systematically varied in equation 5.56 to determine the best fit of the calculated Φ_B (referred to as Φ_B^*) to the actual Φ_B of the blend. As an example, K_A and Φ_{B_1} values for 20/80 (w/w) LCPU-M/PS-co-VPh(30) blend at 150°C are varied in equation 5.56 to calculate Φ_B^* and a best fit of Φ_B^* to the actual Φ_B value (0.8) [i.e., $|\Phi_B - \Phi_B^*| \cong 0$] is shown as a Table in the Appendix. This table indicates a K_A of 2.732 and a Φ_{B_1} of 0.320 at which a minimum of 1.17×10^{-5} for $|\Phi_B - \Phi_B^*|$ is obtained. The K_A values found for different miscible copolymer compositions and temperatures of 20/80 (w/w) LCPU-M/PS-co-VPh blends are reported as K_A^{HT} in Table 10. Considering the fact that $f_{HB}^{C=O}$ is most sensitive to the magnitude of K_A for miscible

Table 10. Interassociation Equilibrium Constant (K_A) for Different Copolymer Compositions and Temperatures of Miscible 20/80 (w/w) LCPU/PS-co-VPh Blends

| Copolymer composition (%VPh) | Temperature (°C) | K_A^{HT} | K_A^{25degC} | Molar Volume (cm ³ /mol) | K_A^{STD} |
|------------------------------|------------------|------------|----------------|-------------------------------------|-------------|
| 5 | 150 | 0.629 | 3.31 | 1877 | 62.2 |
| | 170 | 0.486 | | | |
| | 190 | 0.448 | | | |
| | 210 | 0.360 | | | |
| 10 | 150 | 1.072 | 6.65 | 942 | 62.6 |
| | 170 | 0.832 | | | |
| | 190 | 0.733 | | | |
| | 210 | 0.600 | | | |
| 20 | 150 | 1.877 | 13.08 | 474 | 62.0 |
| | 170 | 1.366 | | | |
| | 190 | 1.294 | | | |
| | 210 | 1.020 | | | |
| 30 | 150 | 2.732 | 19.37 | 318 | 61.6 |
| | 170 | 2.200 | | | |
| | 190 | 1.930 | | | |
| | 210 | 1.620 | | | |
| 40 | 150 | 3.762 | 25.66 | 240 | 61.6 |
| | 170 | 2.940 | | | |
| | 190 | 2.500 | | | |
| | 210 | 2.130 | | | |
| 50 | 150 | 4.318 | 28.8 | 194 | 56.0 |
| | 170 | 3.390 | | | |
| | 190 | 2.895 | | | |
| | 210 | 2.380 | | | |

blends and that the variation of $f_{HB}^{C=O}$ with K_A is quite insensitive for immiscible blend compositions, it is reasonable to use the same K_A values determined for miscible blends of a particular copolymer composition to determine the theoretical values for all blend compositions of that copolymer composition.^{46,55,56} Having obtained the values of the equilibrium constants for this system, the theoretical $f_{HB}^{C=O}$ was calculated as a function of blend composition for different copolymer compositions using the stoichiometric equations (see equations 5.56-5.59). Since the value of K_A is known for a particular copolymer composition and temperature, Φ_{A_1} and Φ_{B_1} values were systematically varied in equation 5.56 to determine the best fit of the calculated Φ_B (referred to as Φ_B^*) to the actual Φ_B of the blend. The value of Φ_{A_1} thus obtained can be used in equation 5.59 to give the theoretical fraction of intermolecular H-bonding ($f_{HB}^{C=O}$). As an example, a $f_{HB}^{C=O}$ comparison of theory and experiment has been made for different copolymer compositions as determined at 150°C in Figures 70-75. These figures compare the experimental data points to the theoretical curve (represented by a thick continuous line) for both one- and two-phase blend compositions where an excellent agreement is present for one-phase and a marked deviation for two-phase systems.

Mapping theoretical phase diagrams

For a particular blend composition, the fraction of H-bonded C=O groups in a two-phase system must necessarily be less than that present in the single-phase (miscible) counterpart. Although Painter et al.^{46,98,99} have discussed this subject in detail elsewhere, it is worthwhile to briefly review some of the important features of mapping theoretical phase

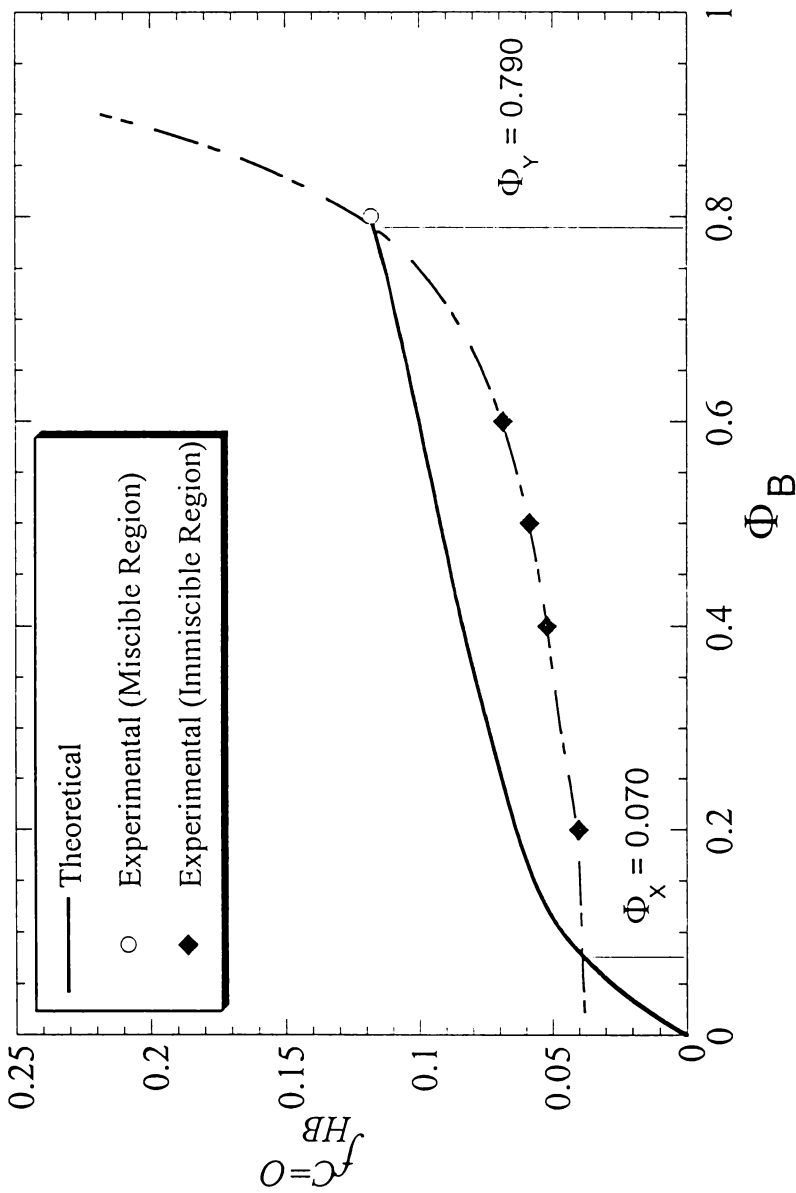


Figure 70. Comparison of experimental data (IR spectroscopy) with theoretical curves for the one- and two-phase systems for plots of fraction of hydrogen bonded C=O ($f_{HB}^{C=O}$) versus blend composition of LCPU-M/PS-co-VPh(5) blends at 150°C: thick, continuous line (theory, single phase) and dashed line (lever rule, two phase)

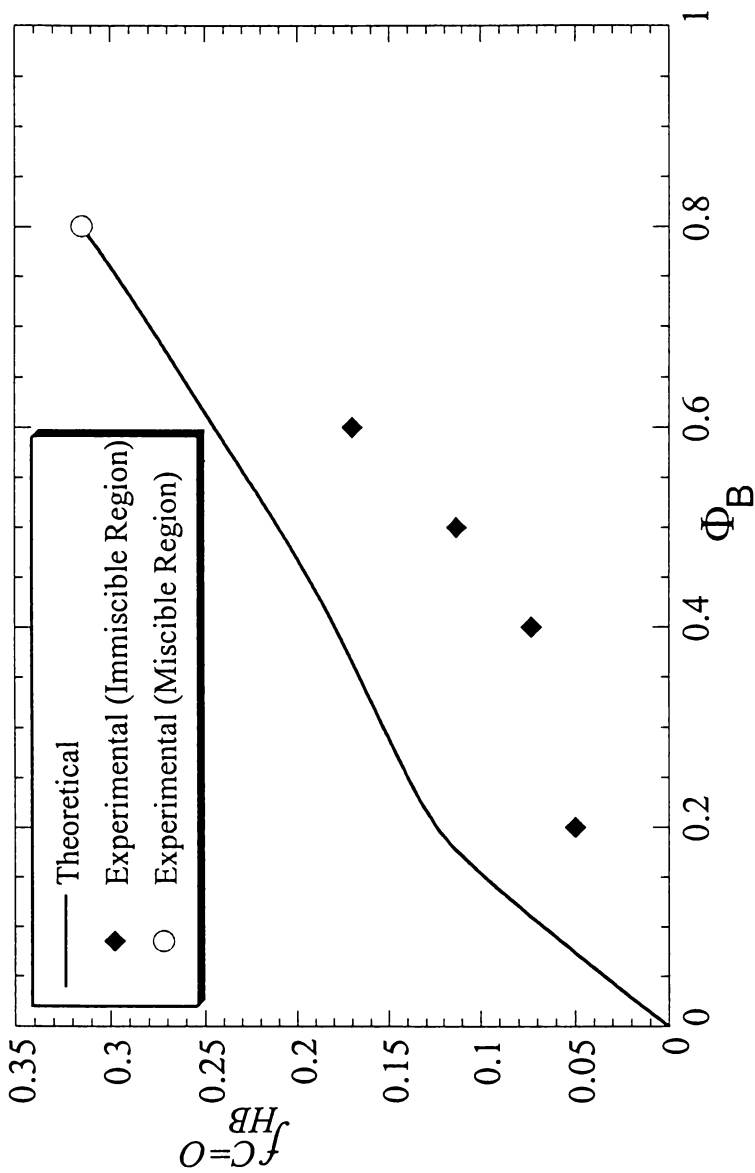


Figure 71. Comparison of experimental data (IR spectroscopy) with theoretical curves for the one- and two-phase systems for plots of fraction of hydrogen bonded C=O ($f_{HB}^{C=O}$) versus blend composition of LCPU-M/PS-co-VPh(10) blends at 150°C

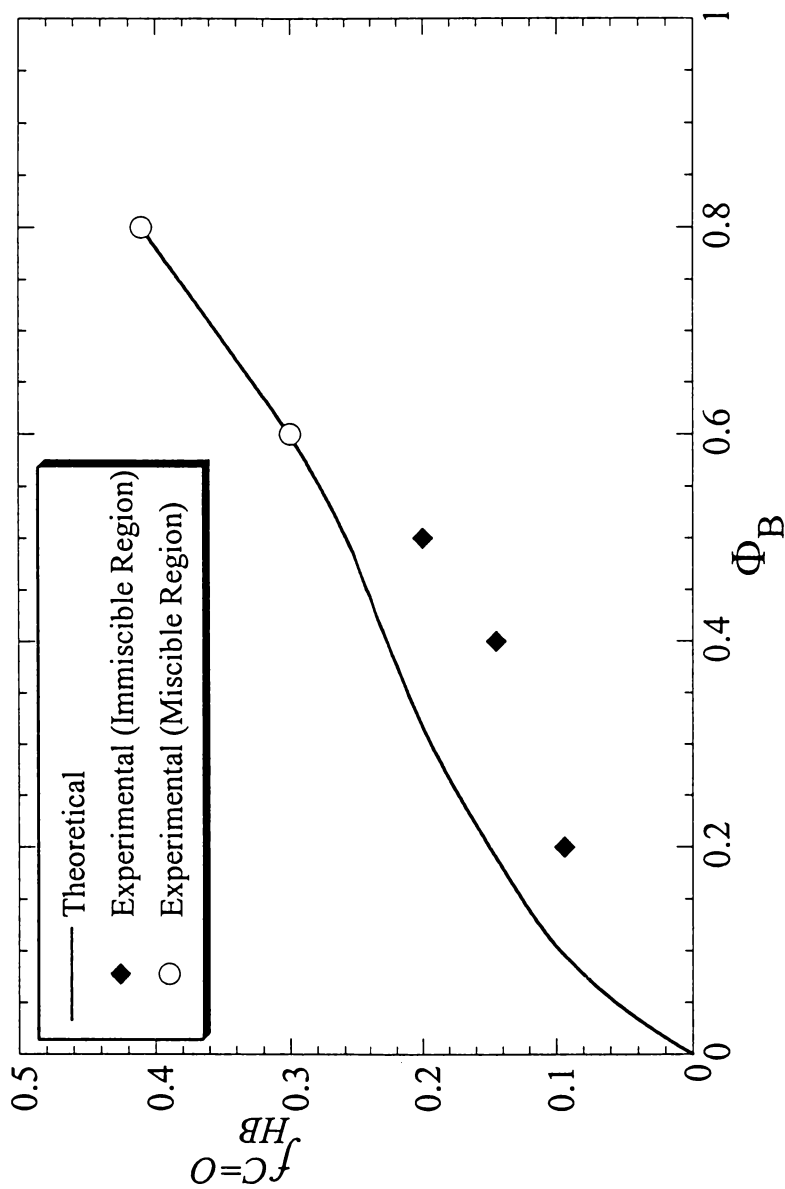


Figure 72. Comparison of experimental data (IR spectroscopy) with theoretical curves for the one- and two-phase systems for plots of fraction of hydrogen bonded C=O ($f_{HB}^{C=O}$) versus blend composition of LCPU-M/PS-co-VPh(20) blends at 150°C

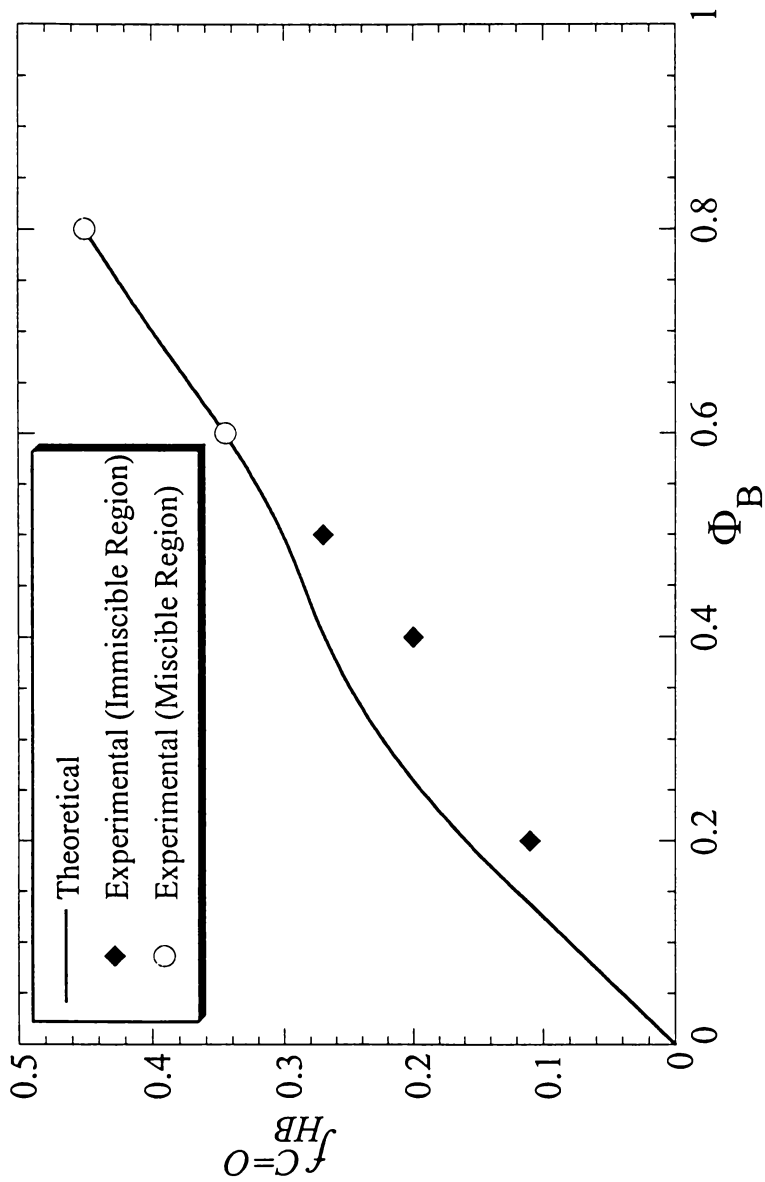


Figure 73. Comparison of experimental data (IR spectroscopy) with theoretical curves for the one- and two-phase systems for plots of fraction of hydrogen bonded C=O ($f_{HB}^{C=O}$) versus blend composition of LCPU-M/PS-co-VPh(30) blends at 150°C

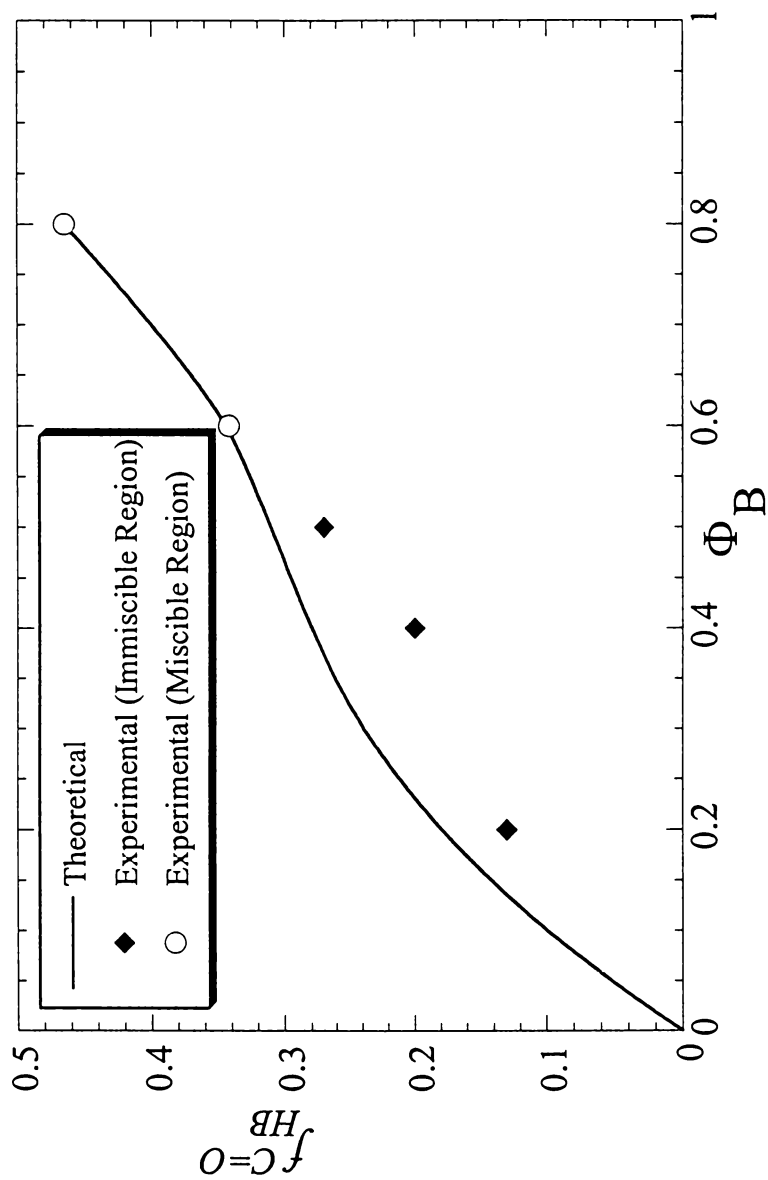


Figure 74. Comparison of experimental data (IR spectroscopy) with theoretical curves for the one- and two-phase systems for plots of fraction of hydrogen bonded C=O ($f_{HB}^{C=O}$) versus blend composition of LCPU-M/PS-co-VPh(40) blends at 150°C

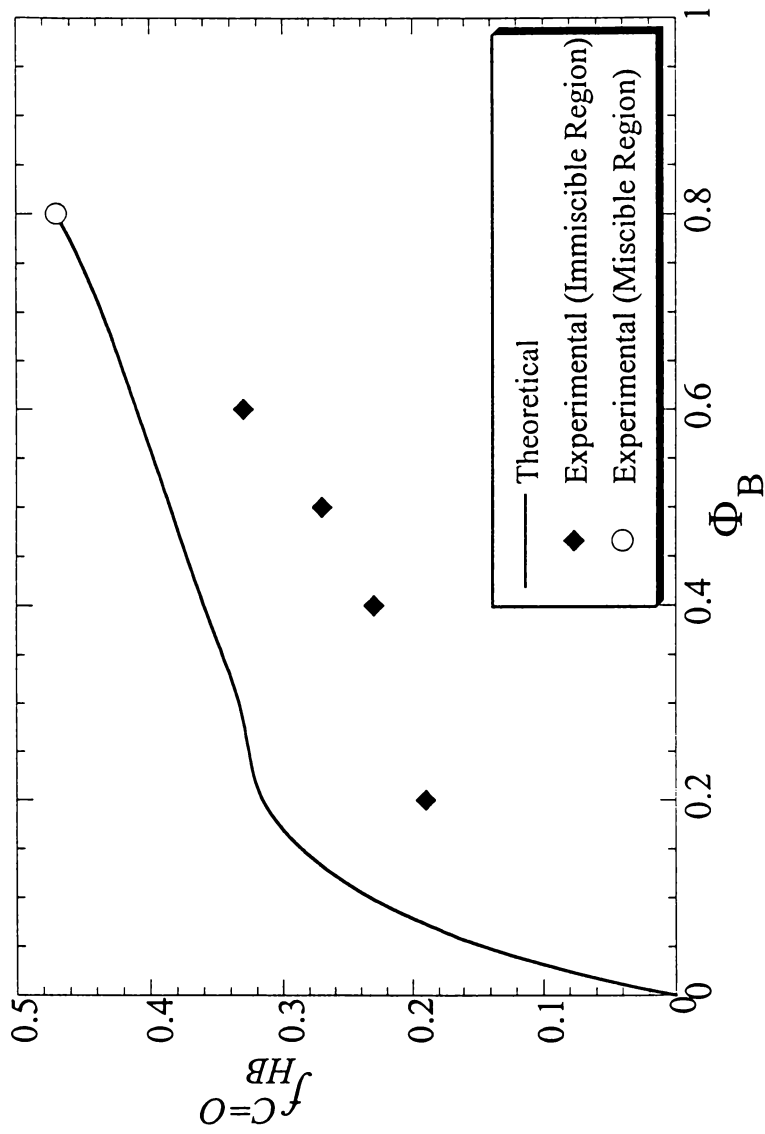


Figure 75. Comparison of experimental data (IR spectroscopy) with theoretical curves for the one- and two-phase systems for plots of fraction of hydrogen bonded C=O ($f_{HB}^{C=O}$) versus blend composition of LCPU-M/PS-co-VPh(50) blends at 150°C

diagrams by “two-phase lever rule” method. Consider the phase diagram shown in Figure 76.

If, at blend composition Φ_A and temperature T, the system is in a two-phase region, then separation will occur into phases Φ_A^X and Φ_A^Y . The $f_{HB}^{C=O}$ present in the two phases, by the lever rule, is then given by

$$f_{HB}^X = \frac{\Phi_A^Y - \Phi_A}{\Phi_A^Y - \Phi_A^X} \left[\frac{\Phi_A^X}{\Phi_A} \right] \quad \text{and} \quad f_{HB}^Y = \frac{\Phi_A - \Phi_A^X}{\Phi_A^Y - \Phi_A^X} \left[\frac{\Phi_A^Y}{\Phi_A} \right] \quad (5.60)$$

where f_{HB}^X and f_{HB}^Y are defined as the fraction of hydrogen bonded C=O groups at compositions Φ_A^X and Φ_A^Y , respectively. Then, $f_{HB}^{C=O}$ (or simply f_{HB}) can be obtained at Φ_A from the equation below.

$$\Phi_A f_{HB} = \frac{\Phi_A^X \Phi_A^Y (f_{HB}^X - f_{HB}^Y)}{\Phi_A^Y - \Phi_A^X} + \Phi_A \frac{(\Phi_A^Y f_{HB}^Y - \Phi_A^X f_{HB}^X)}{\Phi_A^Y - \Phi_A^X} \quad (5.61)$$

Thus for a blend system at a given temperature within a two-phase region at equilibrium, a plot of $\Phi_A f_{HB}$ versus Φ_A should yield a straight line with an intercept ξ_1 and a slope ξ_2 .

$$\text{where } \xi_1 = \frac{\Phi_A^X \Phi_A^Y (f_{HB}^X - f_{HB}^Y)}{\Phi_A^Y - \Phi_A^X} \quad \text{and} \quad \xi_2 = \frac{(\Phi_A^Y f_{HB}^Y - \Phi_A^X f_{HB}^X)}{\Phi_A^Y - \Phi_A^X}$$

As an example, Table 11 gives the values of $\Phi_A f_{HB}$ for different Φ_A (and Φ_B) for LCPU-M/PS-co-VPh(5) blends at 150°C and a plot of $\Phi_A f_{HB}$ versus Φ_A is shown in Figure 77.

Blend compositions $\Phi_B \geq 0.4$ and above, satisfactorily fit a straight line suggesting a two-phase system in this region and blend composition $\Phi_A = 0.8$ ($\Phi_B = 0.2$) deviates significantly from the straight line that satisfactorily fits the remaining data. Assuming equilibrium has been attained, it implies that at $\Phi_A = 0.8$ ($\Phi_B = 0.2$), the blend exists in a single phase. The

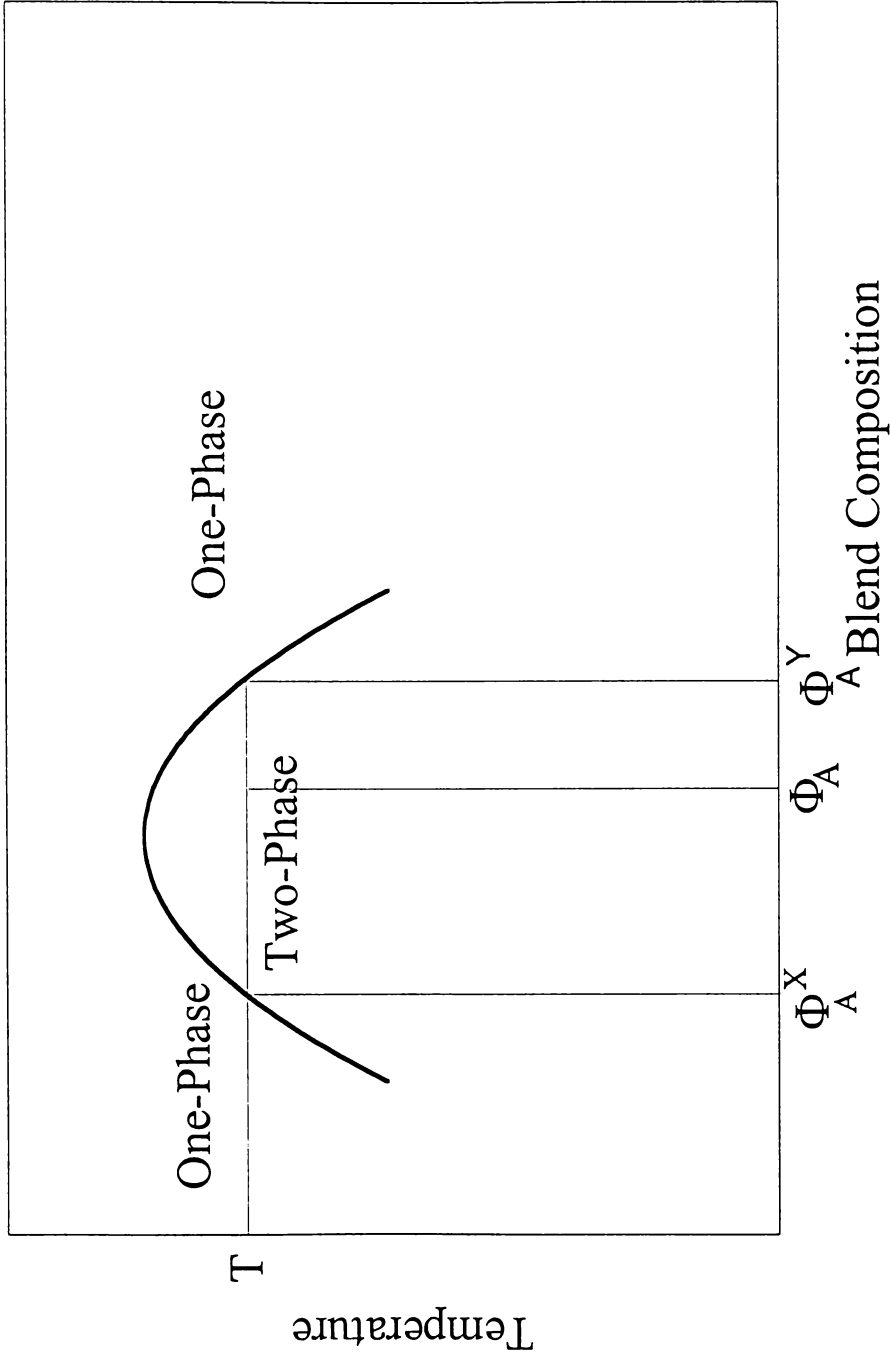


Figure 76. Schematic representation of a typical phase diagram

Table 11. Useful Parameters for $\Phi_A f_{HB}^{C=O}$ versus Φ_A plot (Figure 77) Obtained for Different Blend Compositions of LCPU-MPS-co-VPh(5). $f_{HB}^{C=O}$ is Obtained Experimentally at 150°C from IR Spectroscopy.

| Φ_B | Φ_A | $f_{HB}^{C=O}$ | $\Phi_A f_{HB}^{C=O}$ |
|----------|----------|----------------|-----------------------|
| 0.8 | 0.2 | 0.1186 | 0.0237 |
| 0.6 | 0.4 | 0.0686 | 0.0274 |
| 0.5 | 0.5 | 0.0586 | 0.0293 |
| 0.4 | 0.6 | 0.0519 | 0.0312 |
| 0.2 | 0.8 | 0.0400 | 0.0320 |

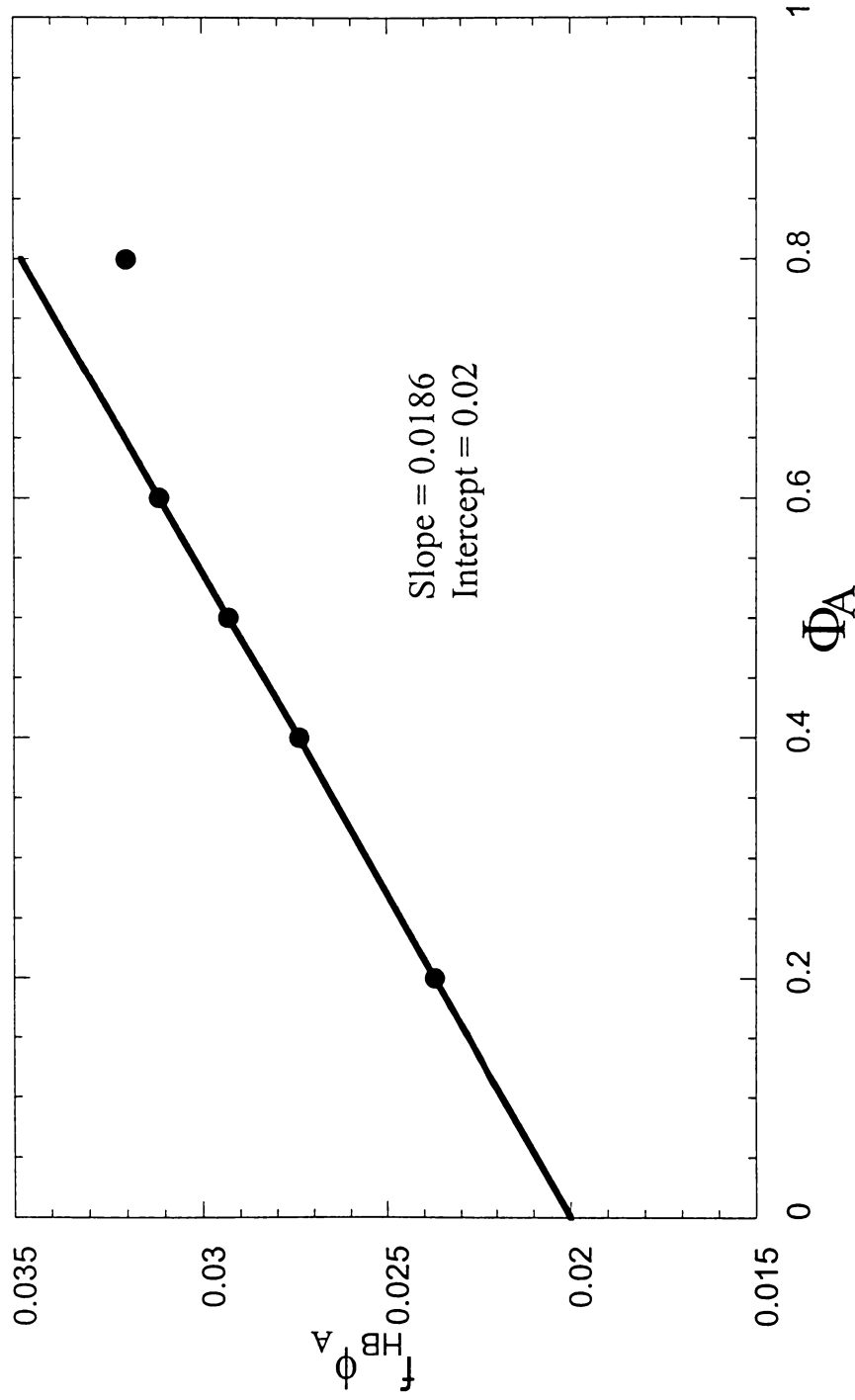


Figure 77. A plot of $\Phi_A f_{HB}^{C=O}$ versus Φ_A obtained for LCPU-M/PS-co-VPh(5) blends. $f_{HB}^{C=O}$ is obtained experimentally at 150°C from IR spectroscopy

values of intercept (ξ_1) and slope (ξ_2) of the straight line are shown in Figure 77. The above equation can be simplified to

$$f_{HB} = \frac{\xi_1}{\Phi_A} + \xi_2 \quad (5.62)$$

Table 12 gives the values of $f_{HB}^{C=0}$ for all blend compositions (in terms of both Φ_A and Φ_B) calculated at an interval of 0.1 using the previously estimated ξ_1 and ξ_2 and a plot of $f_{HB}^{C=0}$ versus Φ_B gives a parabolic deconvolution of all the experimental data points that exist in two-phase in the blend and is represented by the dashed line in Figure 70. At a given temperature, the intercept of the two theoretical curves in Figure 70, yields the composition limits (Φ_x and Φ_y) of the two-phase region of the phase diagram. Accordingly, we can now map a phase diagram that has been derived using the two-phase lever rule method, and Table 13 shows the Φ_x and Φ_y values for different copolymer compositions and temperatures which will be used as data points for mapping theoretical phase diagrams. Figures 78-83 compare the theoretical phase diagrams to those obtained by experiment and demonstrate an excellent agreement of theory and experiment. This re-establishes the fact that the theoretical phase diagrams based on an association model developed by Painter et al.⁴⁶ that utilizes experimental IR data works with great precision.

Effect of functional group accessibility on blend miscibility

The methodology used to calculate the interassociation equilibrium constant (K_A^{HT}) at different copolymer compositions and temperatures has already been discussed in this paper and the results have been shown in Table 10. Using K_A^{HT} in a Van't Hoff equation, a Van't

Table 12. Useful Parameters for $f_{HB}^{C=O}$ versus Φ_B plot (dashed line in Figure 70) Obtained for Different Blend Composition of LCPU-M/PS-co-VPh(5). $f_{HB}^{C=O}$ is Obtained Experimentally at 150°C from IR Spectroscopy.

| Φ_B | Φ_A | $f_{HB}^{C=O}$ |
|----------|----------|----------------|
| 0.9 | 0.1 | 0.2180 |
| 0.8 | 0.2 | 0.1186 |
| 0.7 | 0.3 | 0.0852 |
| 0.6 | 0.4 | 0.0686 |
| 0.5 | 0.5 | 0.0586 |
| 0.4 | 0.6 | 0.0519 |
| 0.3 | 0.7 | 0.0471 |
| 0.2 | 0.8 | 0.0400 |
| 0.1 | 0.9 | 0.0390 |

Table 13. Useful Parameters Obtained Using “Two-Phase Lever Rule” Method for Different Copolymer Compositions and Temperatures of LCPU-M/PS-co-VPh Blends. Φ_X and Φ_Y Denote the Composition Limits of the Two-Phase Region of the Phase Diagram.

| Copolymer Composition (% VPh) | Φ_X | | | Φ_Y | | | | |
|-------------------------------------|----------|-------|-------|----------|-------|-------|-------|-------|
| | 150°C | 170°C | 190°C | 150°C | 170°C | 190°C | 210°C | |
| 5 | 0.070 | 0.075 | 0.083 | 0.095 | 0.790 | 0.782 | 0.775 | 0.770 |
| 10 | 0.075 | 0.083 | 0.091 | 0.102 | 0.700 | 0.690 | 0.679 | 0.670 |
| 20 | 0.085 | 0.100 | 0.115 | 0.130 | 0.590 | 0.575 | 0.560 | 0.540 |
| 30 | 0.105 | 0.113 | 0.130 | 0.155 | 0.565 | 0.557 | 0.540 | 0.520 |
| 40 | 0.125 | 0.138 | 0.170 | 0.185 | 0.525 | 0.510 | 0.480 | 0.450 |
| 50 | 0.080 | 0.082 | 0.084 | 0.096 | 0.740 | 0.730 | 0.721 | 0.714 |

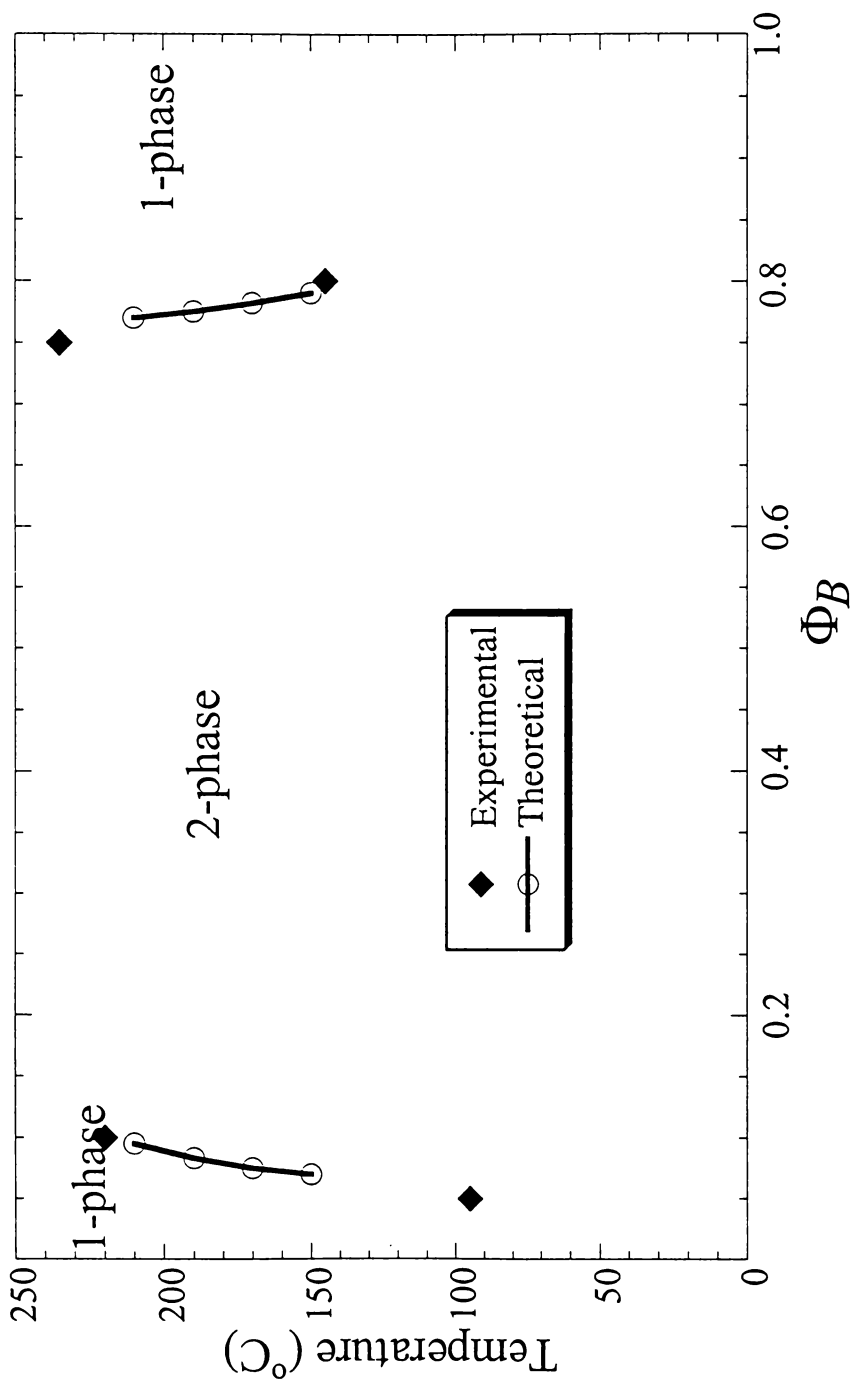


Figure 78. Comparison of theoretical (from association model) and experimental (from optical microscopy) phase diagrams of LCPU-M/PS-co-VPh(5)

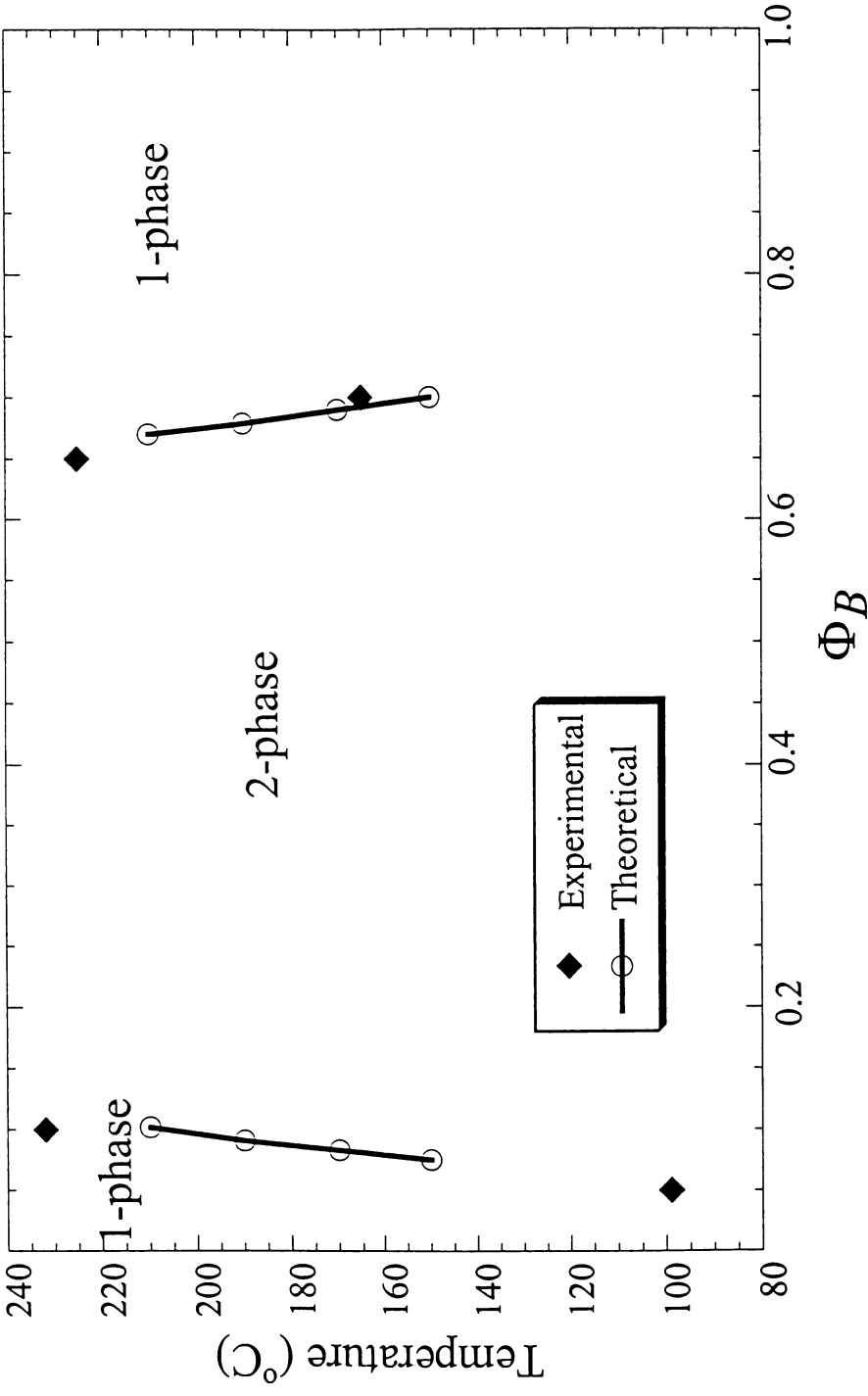


Figure 79. Comparison of theoretical (from association model) and experimental (from optical microscopy) phase diagrams of LCPU-M/PS-co-VPh(10)

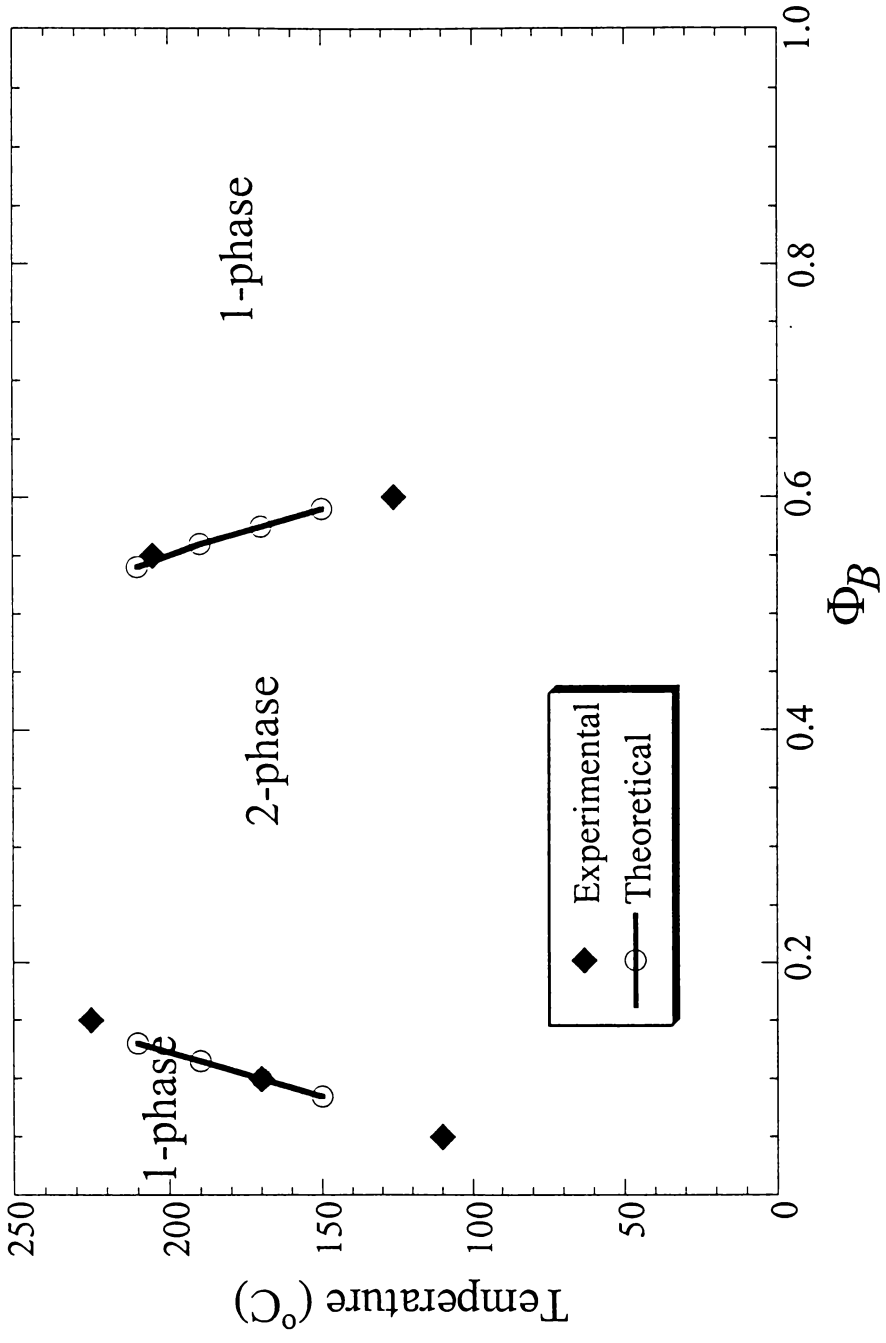


Figure 80. Comparison of theoretical (from association model) and experimental (from optical microscopy) phase diagrams of LCPU-M/PS-co-VPh(20)

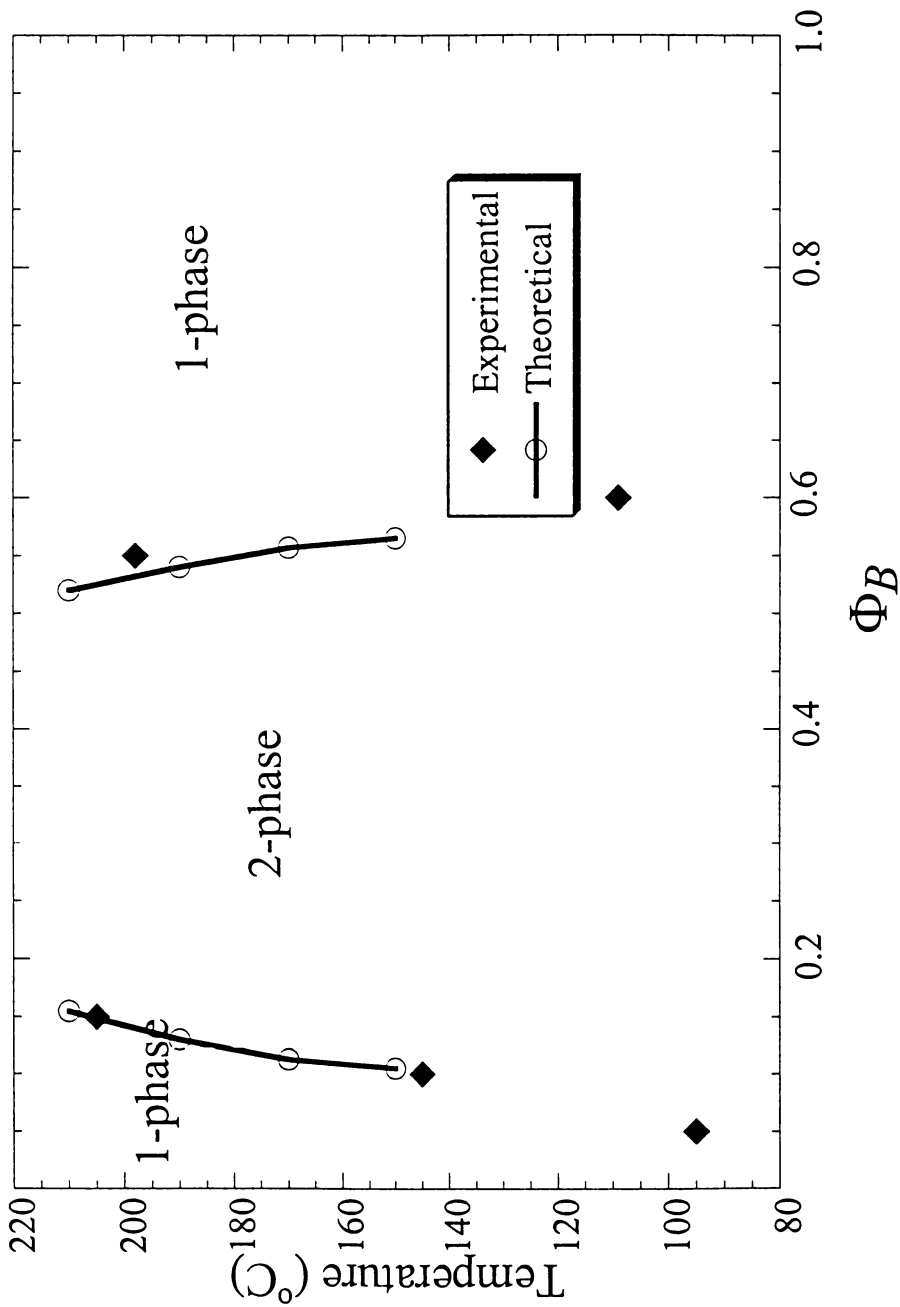


Figure 81. Comparison of theoretical (from association model) and experimental (from optical microscopy) phase diagrams of LCPU-M/PS-co-VPh(30)

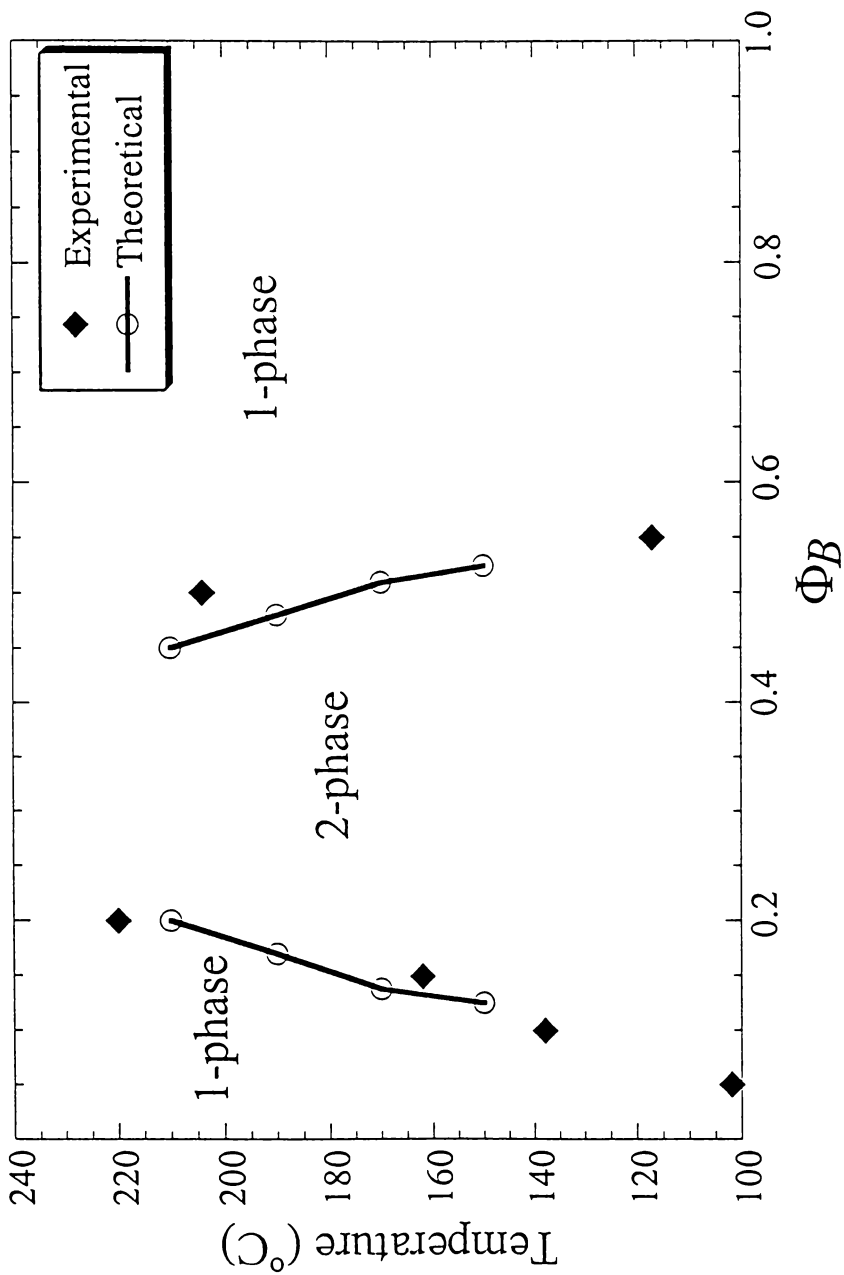


Figure 82. Comparison of theoretical (from association model) and experimental (from optical microscopy) phase diagrams of LCPU-M/PS-co-VPh(40)

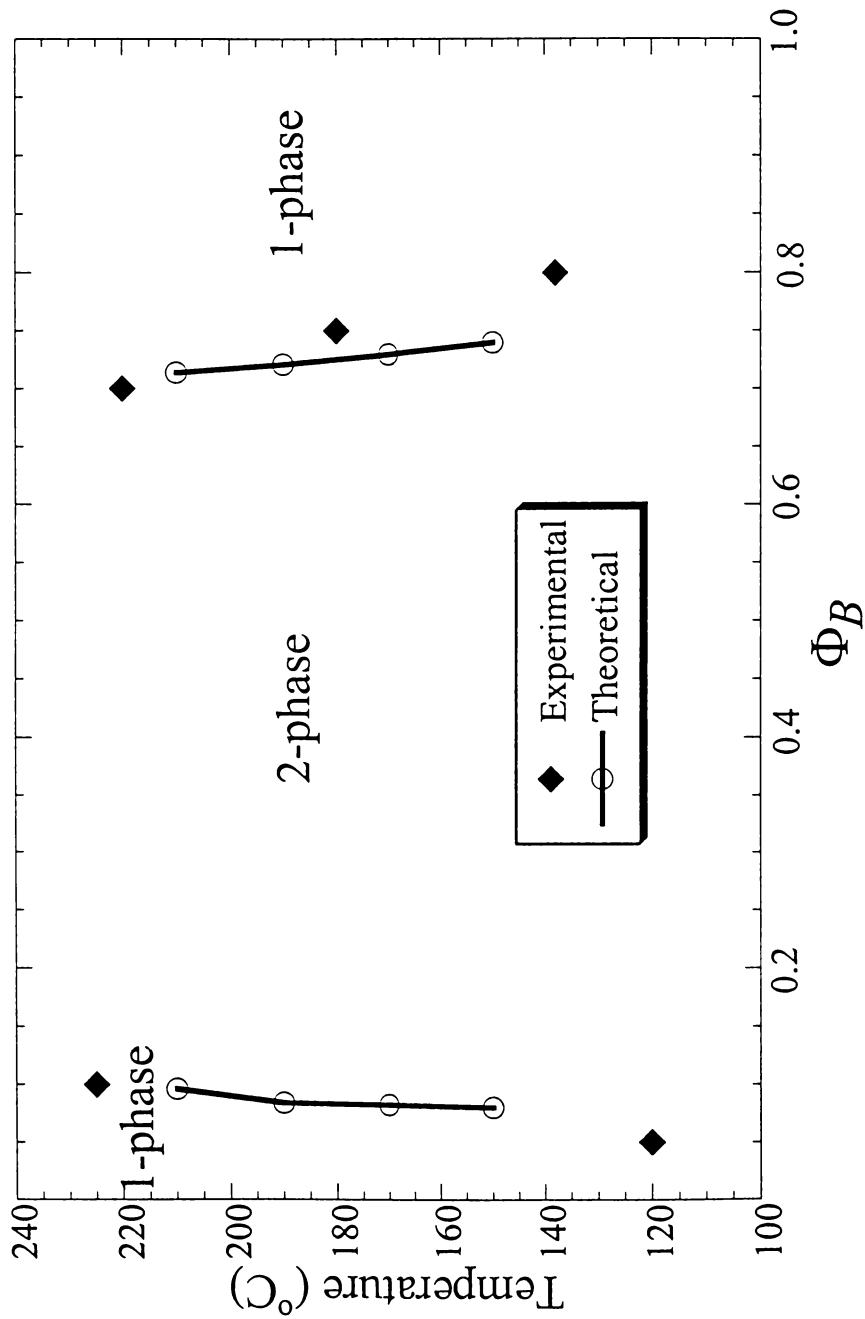


Figure 83. Comparison of theoretical (from association model) and experimental (from optical microscopy) phase diagrams of LCPU-M/PS-co-VPh(50)

Hoff plot of $\ln K_A$ versus inverse temperature can be obtained (see Table 14 and Figure 84). The enthalpy of intermolecular H-bond formation, h_A may be readily obtained from the slope which equals h_A/R , where R is the gas constant with a value of 1.986 cal/K/mol. K_A was then calculated at 25°C using the Van't Hoff equation with $h_A = -3.6$ kcal/mol and summarized in Table 10 as $K_A^{25^\circ C}$. The $K_A^{25^\circ C}$ values for the different copolymer compositions can be compared with each other only if they are based on a common reference volume (100 cm³/mol). The scaled $K_A^{25^\circ C}$ values (referred to as K_A^{STD} in Table 10) represent K_A determined at 25°C and 100 cm³/mol. K_A^{STD} , in effect, describes the fraction of H-bonded C=O groups found in a miscible polymer blend of a particular composition that is composed of a (co)polymer containing phenolic hydroxyl groups [e.g., PS-co-VPh(40)] and another containing a C=O group [e.g., LCPU-M], with the premise that the comonomers under consideration (i.e., styrene in this case) are 'inert' diluents (i.e., non-hydrogen bonding). The variation of K_A^{STD} with copolymer composition is useful in determining functional group accessibility for a particular blend system.⁵⁷⁻⁶⁴ The problem of functional group accessibility occurs when the hydrogen bonding hydroxyl functional groups are not well-separated along the PS-co-VPh copolymer chain, a parameter that can be controlled by varying the copolymer composition (% VPh in PS-co-VPh). If there were no problems of functional group accessibility, K_A^{STD} for miscible blends of LCPU-M/PS-co-VPh should be identical for all copolymer compositions. Studies by Painter et al.⁵²⁻⁵⁸ show that K_A^{STD} increases with increasing space between the O-H groups along the PS-co-VPh copolymer chain (expressed

Table 14. Van't Hoff Plot Parameters for Different Copolymer Compositions and Temperatures of Miscible LCPU-M/PS-co-VPh Blends.

| T (°C) | 1/T (K ⁻¹) | Mole% VPh in PS-co-VPh | | | | | | | | | | | |
|-----------|---------------------------|------------------------|-------------------|----------------|-------------------|----------------|-------------------|----------------|-------------------|----------------|-------------------|----------------|-------------------|
| | | 5 | | 10 | | 20 | | 30 | | 40 | | 50 | |
| | | K _A | ln K _A | K _A | ln K _A | K _A | ln K _A | K _A | ln K _A | K _A | ln K _A | K _A | ln K _A |
| 25 | 0.00335 | 3.31 | 1.196 | 6.65 | 1.894 | 13.08 | 2.564 | 19.37 | 2.963 | 25.66 | 3.251 | 28.80 | 3.360 |
| 150 | 0.00236 | 0.629 | -0.463 | 1.072 | 0.070 | 1.877 | 0.630 | 2.732 | 1.010 | 3.762 | 1.325 | 4.318 | 1.463 |
| 170 | 0.00225 | 0.486 | -0.720 | 0.832 | -0.183 | 1.366 | 0.312 | 2.200 | 0.789 | 2.940 | 1.077 | 3.390 | 1.221 |
| 190 | 0.00215 | 0.448 | -0.802 | 0.733 | -0.310 | 1.294 | 0.258 | 1.930 | 0.657 | 2.500 | 0.915 | 2.895 | 1.063 |
| 210 | 0.00207 | 0.360 | -1.020 | 0.600 | -0.510 | 1.020 | 0.020 | 1.620 | 0.482 | 2.130 | 0.758 | 2.380 | 0.868 |

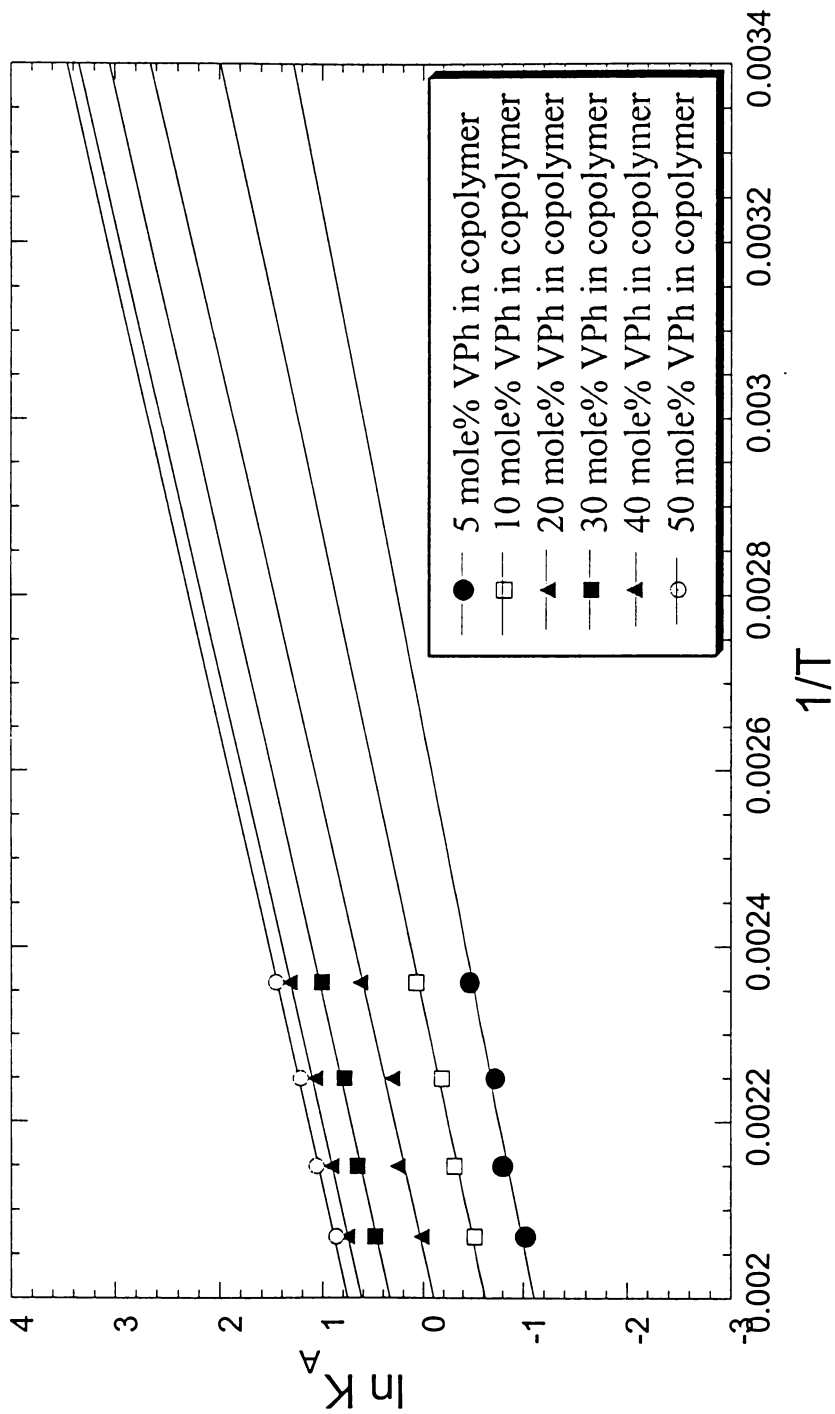


Figure 84. Van't Hoff plot for determining interassociation equilibrium constant at 25°C using data obtained at higher temperatures (see Table 10) for different copolymer compositions of 20/80 (w/w) LCPU-M/PS-co-VPh blends

in terms of R_B , the average molar volume *between* VPh groups in the chemical specific repeat of PS-co-VPh). In other words, R_B is the molar volume of the chemical specific repeat unit of the copolymer (V_B) minus the molar volume of the H-bonding VPh segment (R_B°). Table 15 lists the values of K_A^{STD} and R_B for the different miscible copolymer compositions of the 20/80 (w/w) LCPU-M/PS-co-VPh blends. A plot of K_A^{STD} versus R_B (Figure 85) indicates that as the copolymer composition decreases from 50% VPh to 40%, there is a sharp increase in K_A^{STD} . However, a further decrease in the % VPh in the copolymer doesn't show further significant improvement in the value of K_A^{STD} (saturation limit) since the number of O-H groups in the copolymer becomes so low as to limit the number of possible intermolecular H-bonds that can be formed. These results correlate well with our experimental findings which indicate that LCPU-M/PS-co-VPh(40) [i.e., 40% VPh in PS-co-VPh] shows the optimum amount of intermolecular H-bonding of all the copolymer compositions and manifests itself as the broadest miscibility window in the phase diagram. Thus K_A^{STD} proves to be a very good indicator for determining the copolymer composition that offers the optimum accessibility to O-H groups in the copolymer chain.

Table 15. Useful Parameters for K_A^{STD} versus R_B plot (Figure 85) for Different Copolymer Compositions of 20/80 (w/w) LCPU-M/PS-co-VPh Blends.

| Copolymer Composition (% VPh) | K_A^{STD} | V_B | R_B (cm ³ /mol) |
|-------------------------------|-------------|-------|------------------------------|
| 5 | 62.2 | 1877 | 1777 |
| 10 | 62.6 | 942 | 842 |
| 20 | 62.0 | 474 | 374 |
| 30 | 61.6 | 318 | 218 |
| 40 | 61.6 | 240 | 140 |
| 50 | 56.0 | 194 | 94 |

* $R_B^{\circ} = 100$ cm³/mol; and $R_B = V_B - R_B^{\circ}$

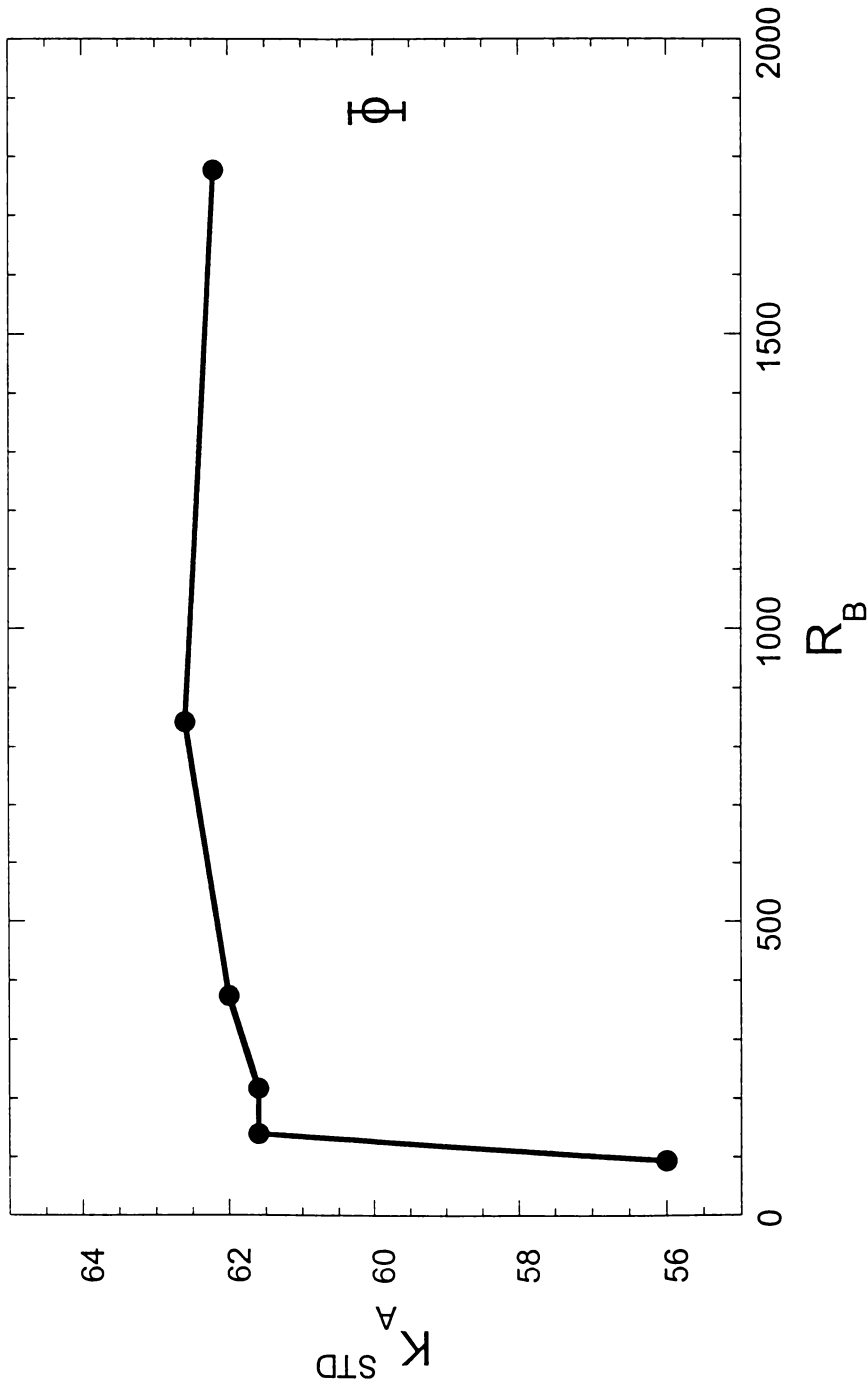


Figure 85. A plot of interassociation equilibrium constant based on a common reference volume of $100 \text{ cm}^3/\text{mol}$ at 25°C (K_A^{STD}) versus molar volume between vinyl phenol units of PS-co-VPh copolymer (R_B) for miscible LCPU-M/PS-co-VPh blends. Error Bar in the plot corresponds to ± 0.3 .

Chapter 6

Conclusions and Future Work

The results of this study on blends containing a rod-like liquid crystalline polymer and a coil-like amorphous polymer demonstrate that it is possible to create a true molecular composite by inducing miscibility by slightly modifying the amorphous polymer to promote hydrogen bonding between the two polymers. The results show that by optimizing the extent of hydrogen bonding between the two blend components, the broadest miscibility window in the phase diagram is found. Furthermore, this optimization occurs when the hydrogen bonding functional groups are separated along the polymer chain, a parameter that can be controlled by varying the composition of the amorphous copolymer (i.e., by spacing the vinyl phenol units apart along the copolymer chain) [*functional group accessibility*]. This is in marked agreement with similar work by other authors.⁵⁵⁻⁶² Improvement of the rotational freedom of the functional groups with increased spacing contributes to this trend. Also important is the decrease in the probability of intra-molecular H-bonding with an increase in the distance between O-H groups, which improves the probability that a given O-H group can participate in intermolecular H-bonding.

Furthermore, by modifying the structure of the LCP in addition to modifying that of the copolymer, the amount of intermolecular hydrogen bonding was improved even further in the LCP/PS-co-VPh blends, thereby expanding the miscibility window of the blends. To be specific, the N-H groups in the LCPU were converted to N-CH₃, and by this step, intramolecular hydrogen bonding among the LCP chains was eliminated. This resulted in an

increase of the C=O groups availability for intermolecular hydrogen bonding in the LCPU-M. The results of this study reveal a higher amount of intermolecular hydrogen bonding and broader miscibility windows in LCPU-M/PS-co-VPh blends than in LCPU/PS-co-VPh blends, for all copolymer compositions studied.

Annealing of blends gives a true representation of the equilibrium blend condition. Annealing of the LCP/PS-co-VPh blends provides additional insight into the structure and thermodynamics of these blends. Thermal annealing of this system shows a change in intermolecular H-bonding that is intuitively obvious. This is evidenced by a correlation of the H-bonding data to the phase behavior of the blend. As the sample is annealed at higher temperatures, it reaches an equilibrium state associated with a change in the phase dispersion of the system that occurs as a result of phase mixing or phase separation. Consequently, we see a change in intermolecular H-bonding in the blend with heat treatment. The change in phase dispersion is found to decrease the intermolecular contacts in immiscible blend and increase in the intermolecular contacts miscible blends when equilibrium is reached. These annealing results correlate well to the phase behavior of the system as determined by optical microscopy.

Finally, theoretically mapped phase diagrams (based on an association model) for these blends are compared to their experimentally determined phase diagrams. The results of the study indicate an excellent agreement between theory and experiment. In addition, our study of the effect of functional group accessibility on blend miscibility indicates that more spacing of the H-bonding O-H groups along the copolymer chain improves the value of interassociation equilibrium constant (K_A^{STD}) which means an increase in the extent of

intermolecular H-bonding and therefore miscibility. This is well supported by our experimental results which explicitly indicate strong intermolecular H-bonding when H-bonding moieties are sufficiently spaced along the polymer chain.

Future work will be focused on the following:

- a) Determining the macroscopic properties (such as viscoelasticity and tensile strength) of the polymer blends and correlating the results to the microscopic properties determined in this thesis.
- b) Obtaining information on the molecular motion of polymer chains and the miscibility scale of the LCP/PS-co-VPh blends by measuring the spin-spin relaxation times using solid-state NMR spectroscopy experiments.

LIST OF REFERENCES

- 1 Bruins, P. F., ed. *Polyblends and Composites*, *Appl. Polym. Symp.*, Vol. 15, New York, Wiley Interscience, **1970**.
- 2 Platzer, N. A., ed. *Copolymers, Polyblends, and Composites*, *Adv. Chem. Ser.*, Vol. 142, Washington D. C. Am. Chem. Soc., **1975**.
- 3 Manson, J. A.; Sperling, L. H. *Polymer Blends and Composites*, New York, Plenum, **1976**.
- 4 Paul, D. R.; Newman, S., eds. *Polymer Blends*, Vols. 1, 2, New York, Academic, **1978**.
- 5 Olabisi, O.; Robeson, L. M.; Show, M. T. *Polymer-Polymer Miscibility*, New York, Academic, **1979**.
- 6 Sanchez, I. C. *Ann. Rev. Mater. Sci.*, **1983**, *13*, 387.
- 7 Walsh, D. J., Huggins, J. S.; Maconnachie, A., eds. *Polymer Blends and Mixtures*, Vol. 1, Hingham, Kluwer Academic, **1985**.
- 8 Rudolph, H. *Polymer Journal*, **1987**, *17*, 13.
- 9 Kaempf, G. *Polymer Journal*, **1987**, *19*, 257.
- 10 Patterson, D., *Polym. Eng. Sci.*, **1982**, *22*, 64.
- 11 Rudolph, H. *Makromol. Chem., Macromol. Symp.*, **1988**, *16*, 57.
- 12 Moro, A.; Chiolle, L.; Foschini, G. *Makromol. Chem., Macromol. Symp.*, **1988**, *16*, 137.
- 13 Paul, D. R.; Barlow, J. W. *Macromol. Sci. Rev., Macromol. Chem.*, **1980**, *C18*, 109.
- 14 Solc, K., ed., *Polymer Compatibility and Incompatibility: Principle and Practice*, MMI Symp. Ser., Vol. 3, Cooper Station, New York, Harwood, **1981**.
- 15 Capaccio, G.; Gardner, A. J.; Hope, P. S.; Wilkinson, K. *Makromol. Chem., Macromol. Symp.*, **1990**, *38*, 267.
- 16 Folkes, M. J.; Hope, P. S., In “*Polymer Blends and Alloys*”, Blackie Academic and Professional; London, **1993**.
- 17 Sweeney, F. M., In “*Polymer Blends and Alloys Guide Book to Commercial*

- Products*"; Technomic Publishing, Inc., Lancaster, PA, **1988**.
- 18 Utracki, L. A., In "*Polymer Alloys and Blends, Thermodynamic and Rheology*", Oxford University Press, Hanser, NY, **1990**.
- 19 Xanthos, M., *Polym. J.*, **1988**, 28, 1392.
- 20 Sperling, L. H. ed., In "*Recent Advances in Polymer Blends, Grafts and Blocks*", Plenum Press, New York, **1974**.
- 21 Platzer, N. A. J. ed., In "*Multi-component Polymer systems*", Adv. Chem. Ser., No. 99, Am. Chem. Soc., Washington, D. C., **1971**.
- 22 Ottenbrite, R. M.; Utracki, L. A.; Inoue, T. eds. In "*Current Topics in Polymer Science, Vol. II, Rheology and Polymer Processing/Multiphase Systems*", Hansen Publishers, New York, **1987**.
- 23 Paul, D. R.; Sperling, L. H., eds. "*Multicomponent Polymer Materials*", Adv. Chem. Ser., No. 211, Am. Chem. Soc., Washington, D. C., **1986**.
- 24 Wissburn, K.F. *J. Rheol. (N.Y.)* **1981**, 25(6), 619.
- 25 Wissburn, K.F.; Griffin, A.C. *J. Polym. Sci., Polym. Phys. Ed.* **1982**, 20, 1835.
- 26 Wissburn, K.F. *Br. Polym. J.* **1980**, 12, 163.
- 27 Cogswell, F.N. *Br. Polym. J.* **1980**, 12, 170.
- 28 Prasadarao, M.; Pearce, E.M.; Han, C.N. *J. Appl. Polym. Sci.* **1982**, 27, 1343.
- 29 Takayanagi, M.; Ogata, T.; Morikawa, M.; Kai, T. *J. Macromol. Sci. Phys.* **1980**, B17, 591.
- 30 Hwang, W.F.; Wiff, D.R.; Verschoore, C.; Price, G.E.; Helminiak, T.E.; Adams, W.W. *Polym. Eng. And Sci.* **1983**, 23, 784.
- 31 Hwang, W.F.; Wiff, D.F.; Benner, C.; Helminiak, T.E. *J. Macromol. Sci. Phys.* **1983**, B22(2), 231.
- 32 Pawlikowski, G.T.; Dutta, D.; Weiss, R.A. *Ann. Rev. Mat. Sci.* **1991**, 21, 159.
- 33 Painter, P.C.; Tang, W.L.; Graf, J.F.; Thomson, B.; Coleman, M.M. *Macromolecules* **1991**, 24, 3929.

- 34 Stein, R.S.; Sethumadhavan, M.; Gaudhania, R.A.; Adams, T.; Guarrera, D.; Roy, S.K. *Pure Appl. Chem.* **1992**, *29*, 517;
- 35 Cowie, J.M.G.; Nakata, S.; Adams, G.W. *Macromol. Symp.* **1996**, *112*, 207.
- 36 Dadmun, M.D.; Han, C.C. *Mat. Res. Soc. Symp. Proc.* **1993**, *305*, 171.
- 37 Tsou, L.; Sauer, J.A.; Hara, M. *Polymer*, **2000**, *41*, 8103.
- 38 Weiss, R.A.; Ghebremeskel, Y.; Charbonneau, L. *Polymer*, **2000**, *41*, 3471.
- 39 Flory, P.J. "*Principles of Polymer Chemistry*", Cornell University press, Ithaca, New York, **1953**.
- 40 Flory, P. J.; Orwoll, R. A.; Vrij, A. *J. Am. Chem. Soc.*, **1964**, *86*, 3507.
- 41 Flory, P. J.; Orwoll, R. A.; Vrij, A. *J. Am. Chem. Soc.*, **1964**, *86*, 3515.
- 42 Flory, P.J. *J. Chem. Phys.* **1942**, *10*, 51.
- 43 Huggins, M.L. *J. Am. Chem. Soc.* **1942**, *64*, 1712.
- 44 Flory, P.J. *Macromolecules* **1978**, *11*, 1138.
- 45 Flory, P.J. *J. Am. Chem. Soc.* **1965**, *87*, 1833.
- 46 Coleman, M.M.; Graf, J.F.; Painter, P.C. "*Specific Interactions and the Miscibility of Polymer Blends*", Technomic Publishing Co., Lancaster, PA, **1991**.
- 47 Painter, P.C.; Graf, J.F.; Coleman, M.M. *J. Chem. Phys.* **1990**, *10*, 6166.
- 48 Vetsmann, B.A.; Painter, P.C. *J. Chem. Phys.* **1993**, *99*, 9272.
- 49 Coleman, M.M.; Painter, P.C. *Prog. Polym. Sci.*, **1995**, *20*, 1-59.
- 50 Helminiak, F. E.; Arnold, F. E.; Bener, C. L. *Am. Chem. Soc. Polym. Preprints*, **1975**, *16*, 659.
- 51 Ballauf, M. *Mol. Cryst. Liq. Cryst.*, **1986**, *136*, 175.
- 52 Tang, W. L.; Coleman, M. C.; Painter, P. C. *Makromol. Chem., Macromol. Symp.*, **1994**, *54*, 315.
- 53 Painter, P. C.; Tang, W. L.; Graf, J. F.; Thomas, B.; Coleman, M. M.

Macromolecules, **1991**, *24*, 3929.

- 54 Khatri, C.A.; Vaidya, M.M.; Levon, K.; Jha, S.K.; Green, M.M. *Macromolecules* **1995**, *28*, 4719.
- 55 Coleman, M.M.; Pehlert, G.J.; Painter, P.C. *Macromolecules* **1996**, *29*, 6820.
- 56 Pehlert, G.H.; Painter, P.C.; Veytsman, B.; Coleman, M.M. *Macromolecules* **1997**, *30*, 3671.
- 57 Hu, Y.; Painter, P.C.; Coleman, M.M. *Macromolecules* **1998**, *31*, 3394.
- 58 Pehlert, G.H.; Painter, P.C.; Coleman, M.M. *Macromolecules* **1998**, *31*, 8423.
- 59 Radmard, B.; Dadmun, M.D. *Polymer* **2001**, *42(4)*, 1591-1600.
- 60 Painter, P.C.; Veytsman, B.; Kumar, S.; Shenoy, S.; Graf, J.F.; Xu, Y.; Coleman, M.M. *Macromolecules* **1997**, *30*, 932.
- 61 Painter, P.C.; Berg, L.P.; Veytsman, B.; Coleman, M.M. *Macromolecules* **1997**, *30*, 7529.
- 62 Pruthikul, R.; Painter, P.C.; Coleman, M.M.; Tan, N.R. *Macromolecules* **2001**, *34(12)*, 4145; Pruthikul, R.; Painter, P.C.; Coleman, M.M.; Tan, N.R. *J. Polym. Sci., Part B: Polym. Phys.* **2001**, *39(14)*, 1651-58.
- 63 Tang, W.L.; Coleman, M.M.; Painter, P.C. *Macromol. Symp.* **1994**, *84*, 315-324.
- 64 Viswanathan, S.; Dadmun, M.D. *Macromol. Rapid Comm.*, **2001**, *22(10)*, 779-82.
- 65 Viswanathan, S.; Dadmun, M.D. "Guidelines to creating a true molecular composite: Inducing miscibility in blends by optimizing intermolecular hydrogen bonding" *Macromolecules*, submitted.
- 66 Viswanathan, S.; Dadmun, M.D. "Guidelines to creating a true molecular composite: 2. Enhancing miscibility in blends by improving intermolecular hydrogen bonding" *Macromolecules*, submitted.
- 67 Stenhouse, P.J.; Valles, E.M.; Kantor, S.W.; MacKnight, W.J. *Macromolecules* **1989**, *22*, 1467-1473.
- 68 Ledwith, A.; Rahnema, M.; Sengupta, P. K. *J. Polym. Sci., Polym. Chem. Ed.*, **1980**, *8*, 2239.

- 69 Coleman, M.M.; Painter, P.C. “*Fundamentals of Polymer Science*”, 2nd Edn., Technomic Publishing Co., Lancaster, PA., 1997.
- 70 Radmard, B. *Thesis*, The University of Tennessee, Knoxville, Dec. 1999.
- 71 Coleman, M.M.; Lee, K.H.; Skrovanek, D.J.; Painter, P.C. *Macromolecules* **1986**, *19*, 2149-2157.
- 72 Dean, L.; Brisson, J. *Polymer*, **1998**, *39*(4), 793-800.
- 73 Moskala, E. J.; Howe, S. E.; Painter, P. C.; Coleman, M. M., *Macromolecules*, **1984**, *17*, 1671.
- 74 Moskala, E. J.; Varnell, D. F.; Coleman, M. M. *Polymer*, **1985**, *26*, 228.
- 75 Lee, J.Y.; Painter, P.C.; Coleman, M.M. *Macromolecules* **1988**, *21*, 346-354.
- 76 Coleman, M. M.; Moskala, E. J. *Polymer*, **1983**, *24*, 253.
- 77 Coleman, M. M.; Moskala, E. J. *Polym. Commun.*, **1983**, *24*, 207.
- 78 Fox, T.G. Bull. Am. Phys. Soc., **1956**, *1*, 123.
- 79 Mihara, T.; Naoyuki, K. *Polymer J.*, **1997**, *29*(2), 138-141.
- 80 Prigogine, I., with Bellemans, A. and Mathot, V. “*The Molecular Theory of Solutions*”, North Holland Publishing Co., **1957**.
- 81 Prigogine, I. And Defay, R. “*Chemical Thermodynamics*”, translated by Everett, D., Longmans, **1954**.
- 82 Guggenheim, E. A. “*Mixtures*”, Clarendon Press, Oxford, **1952**.
- 83 Barker, J. A. *J. Chem. Phys.*, **1952**, *20*, 794.
- 84 Barker, J. A. *J. Chem. Phys.*, **1952**, *20*, 1526.
- 85 Tompa, H. *J. Chem. Phys.*, **1953**, *21*, 1526.
- 86 Ten Brinke, G. and Karasz, F. E. *Macromolecules*, **1984**, *17*, 815.
- 87 Sanchez, I. C; Balaz, A. C. *Macromolecules*, **1989**, *22*, 2325.
- 88 Painter, P.C.; Park, Y.; Coleman, M.M. *Macromolecules* **1988**, *21*, 66.

- 89 Painter, P.C.; Park, Y.; Coleman, M.M. *Macromolecules* **1989**, 22, 570.
- 90 Painter, P.C.; Park, Y.; Coleman, M.M. *Macromolecules* **1989**, 22, 580.
- 91 Yang, X.; Painter, P. C.; Coleman, M. M.; Pearce, E. M.; Kwei, T. K. *Macromolecules*, **1992**, 25, 2156.
- 92 Coleman, M. M.; Xu, Y.; Painter, P. C. *Macromolecules*, **1994**, 27, 127.
- 93 Xu, Y.; Painter, P. C.; Coleman, M. M. *Polymer*, **1993**, 34, 3010.
- 94 Xu, Y., *Ph.D. Thesis*, The Pennsylvania State University, University Park, PA, **1991**;
Lichkus, A. M., *Ph.D. Thesis*, The Pennsylvania State University, University Park, PA, **1988**.
- 95 Coleman, M. M.; Pehlert, G. J.; Yang, X.; Stallman, J. B.; Painter, P. C. *Polymer*, **1996**, 37, 4753.
- 96 Pehlert, G. J.; Yang, Y.; Coleman, M. M.; Painter, P. C. *Polymer*, **1996**, 37, 4763.
- 97 Whetsel, K.B., Lady, J.H. *Spectrometry of Fuels*; Friedel, H., Ed.; Plenum: London, **1970**; p.259.
- 98 Bhagwagar, D. E.; Painter, P. C.; Coleman, M. M.; Krizan, T. D. *J. Polym. Sci., Polym. Phys. Ed.*, **1991**, 29, 1547.
- 99 Bhagwagar, D. E.; Painter, P. C.; Coleman, M. M.; Krizan, T. D. *Macromolecules*, **1992**, 25, 1361-65.

APPENDIX

GPC curve for LCPU

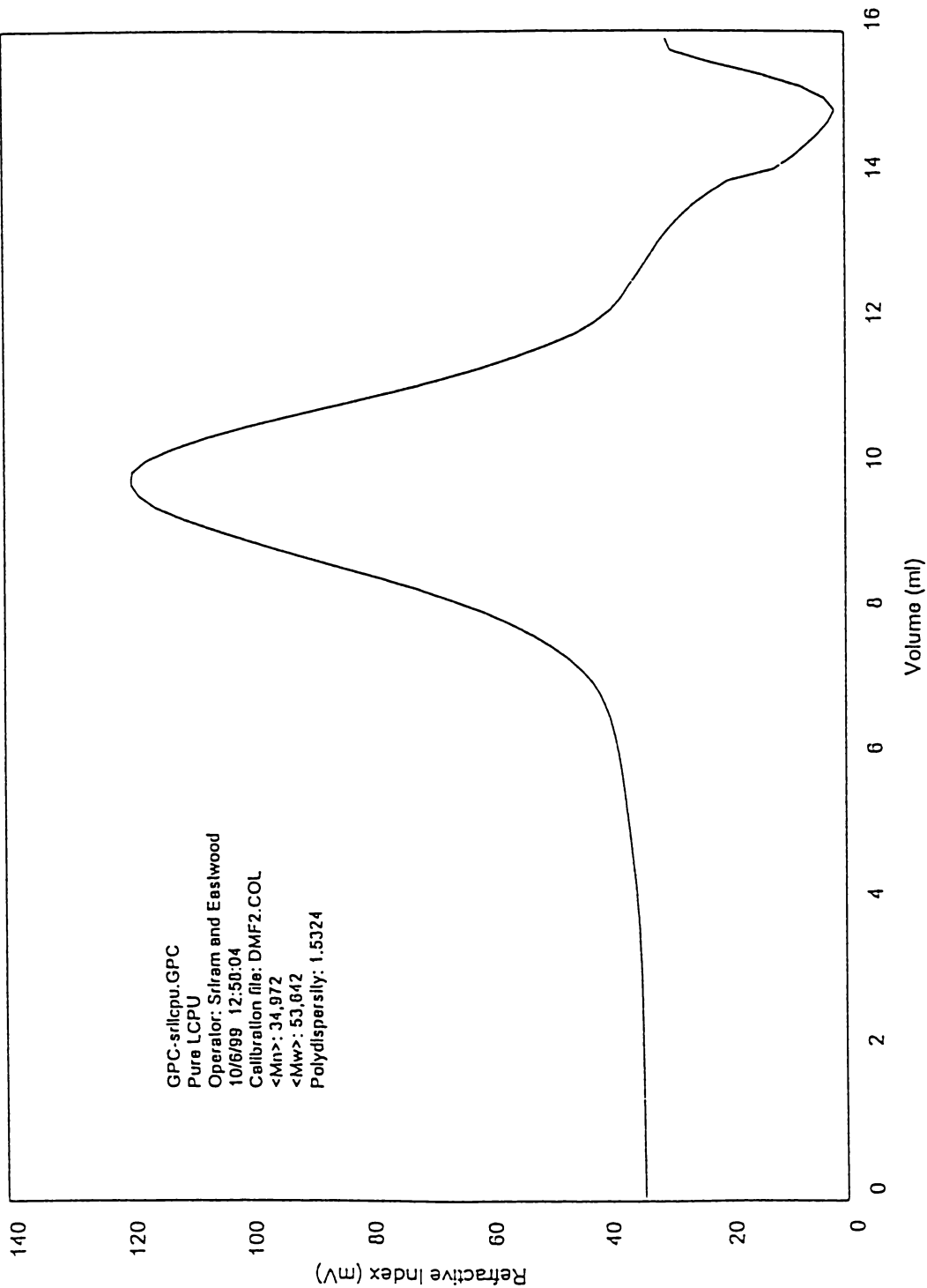
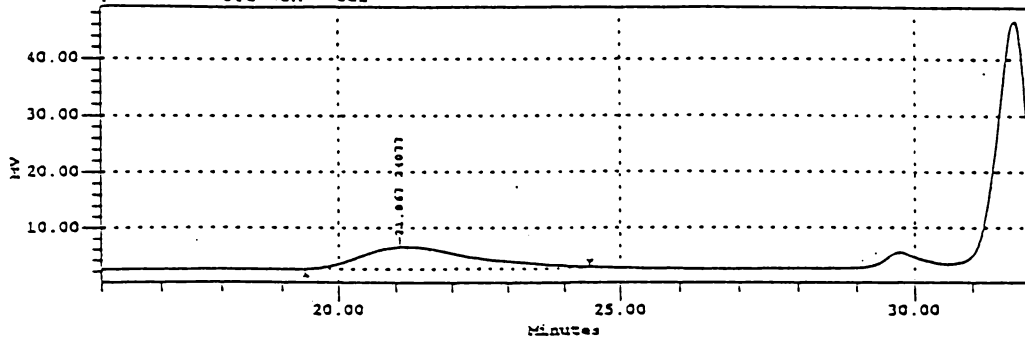


Figure 86. GPC data of pure LCPU.

Millennium Sample Information

Project Name: WSM
 Sample Name: SRI-2
 Vial: 4
 Injection: 1
 Channel: 410
 Acq Meth Set: GPC_DAD
 Processing Method: gpc_dad3
 Result Report: GPC WSM w cal

Sample Type: Broad Unknown
 Volume: 250.00
 Run Time: 45.0 min
 Date Acquired: 08/03/99 09:35:54 PM
 Date Processed: 08/04/99 01:22:20 PM



Millennium GPC Data

SampleName: SRI-2
 MW: 21287
 Mx: 11694
 Polydispersity: 1.5545
 Polydispersity: GPC_WSM_w_cal

Date Acquired: 08/03/99 09:35:54 PM
 Mn: 30347
 Mw+1: 40042
 Mz+1: 24077
 MP:

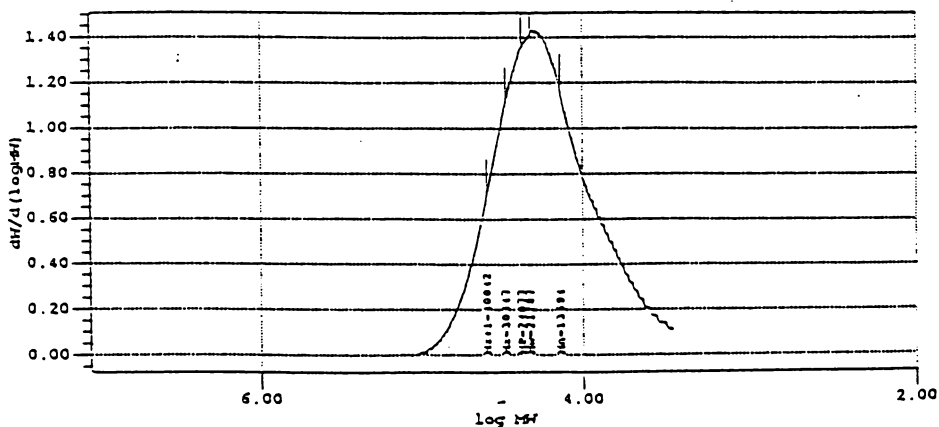
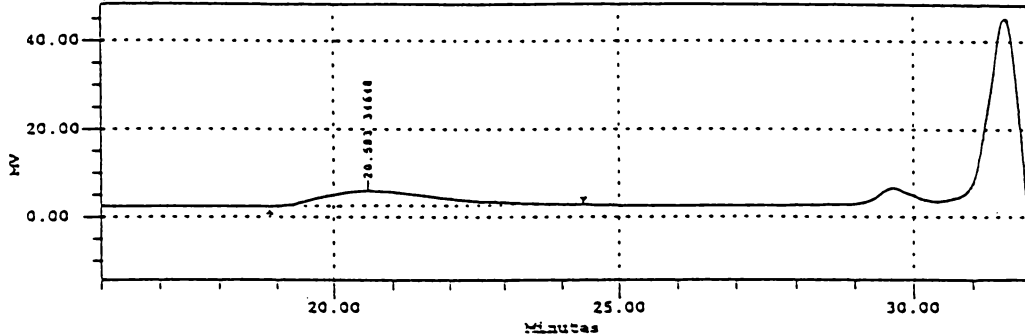


Figure 87. GPC data of PS-co-VPh (5 mol% VPh).

Millennium Sample Information

Project Name: WSM
 Sample Name: SRI-1
 Vial: 5
 Injection: 1
 Channel: 410
 Acq Meth Set: GPC_DAD
 Processing Method: gpc_dad1
 Result Report: GPC_WSM_w_cal

Sample Type: Broad Unknown
 Volume: 250.00
 Run Time: 45.0 min
 Date Acquired: 08/03/99 10:24:22 PM
 Date Processed: 08/04/99 01:22:45 PM



Millennium GPC Data

SampleName: SRI-1
 MW: 34463
 Mx: 20704
 Polydispersity: 1.6646
 Polydispersity: GPC_WSM_w_cal

Date Acquired: 08/03/99 10:24:22 PM
 Mr: 52543
 Mw+1: 72507
 Mz+1: 14648
 Mz:

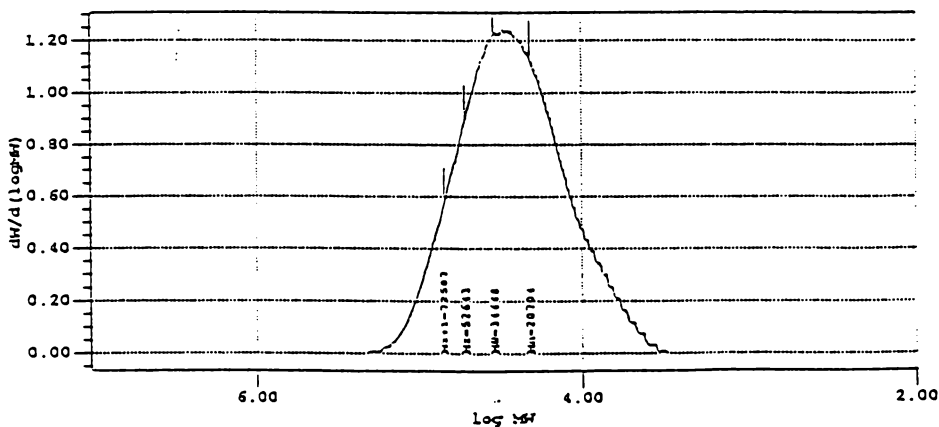
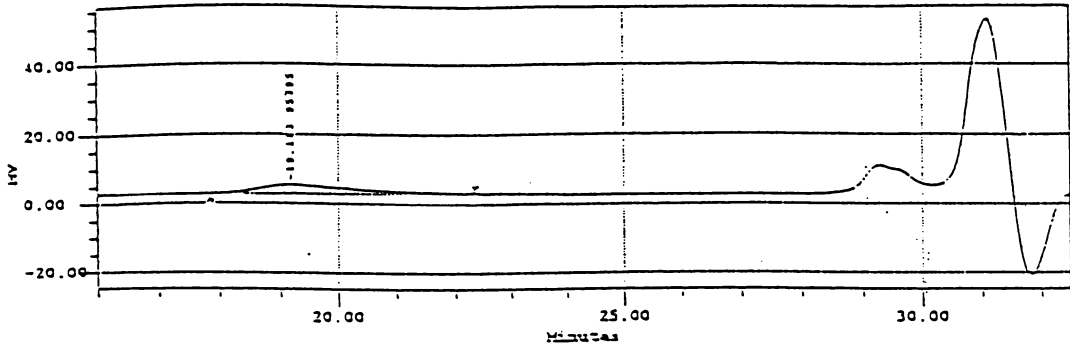


Figure 88. GPC data of PS-co-VPh (10 mol% VPh).

Millennium sample information

Project Name: WSM
 Sample Name: sri-4
 Vial: 5
 Injection: 1
 Channel: 410
 Acq Meth Sec: GPC_DAD
 Processing Method: gpc_dad1
 Result Report: GPC_WSM_vo_Cal

Sample Type: Broad Unknown
 Volume: 250.00
 Run Time: 45.0 min
 Date Acquired: 09/10/99 03:13:29 PM
 Date Processed: 09/11/99 11:58:09 AM



Millennium GPC Data

SampleName: sri-4
 Y: 30069
 X: 47122
 Polydispersity: 1.9114
 SampleDispersion: GPC_WSM_vo_Cal

Date Acquired: 09/10/99 03:13:29 PM
 M: 143719
 M+1: 256461
 M+2: 93795
 M0:

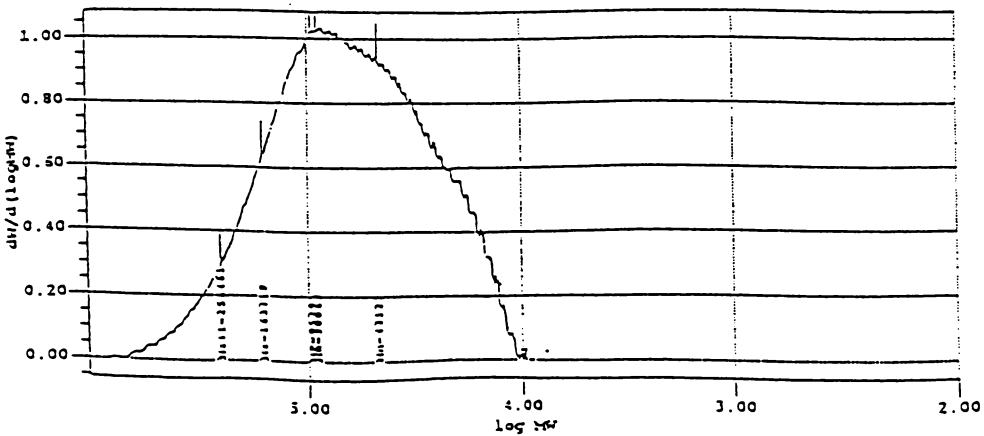
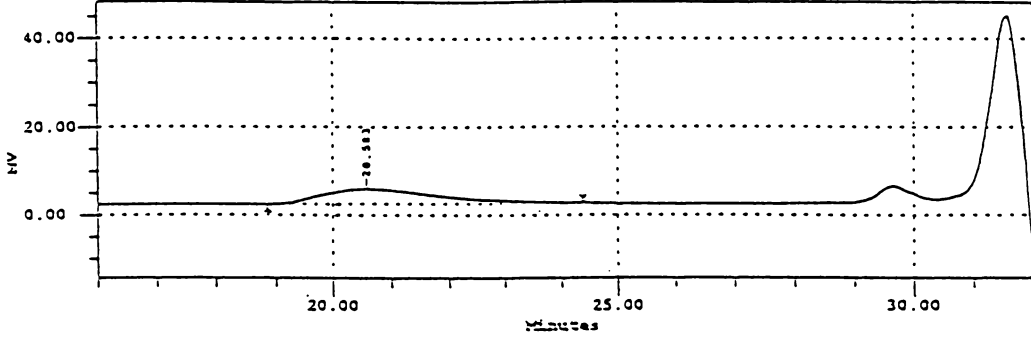


Figure 89. GPC data of PS-co-VPh (20 mol% VPh).

Millennium Sample Information

Project Name: WSM
 Sample Name: sri-3
 Vial: 5
 Injection: 1
 Channel: 410
 Acq Meth Set: GPC_DAD
 Processing Method: gpc_dad3
 Result Report: GPC_WSM_u_cal

Sample Type: Broad Unknown
 Volume: 250.00
 Run Time: 45.0 min
 Date Acquired: 08/03/99
 Date Processed: 08/04/99



Millennium GPC Data

SampleName: sri-3
 MW: 32423
 MX: 22125
 Polydispersity: 1.4650
 RelDispersion: GPC_WSM_u_cal

Date Acquired: 08/03/99
 Mz:
 Mz+1:
 Mz-1:
 Mz:

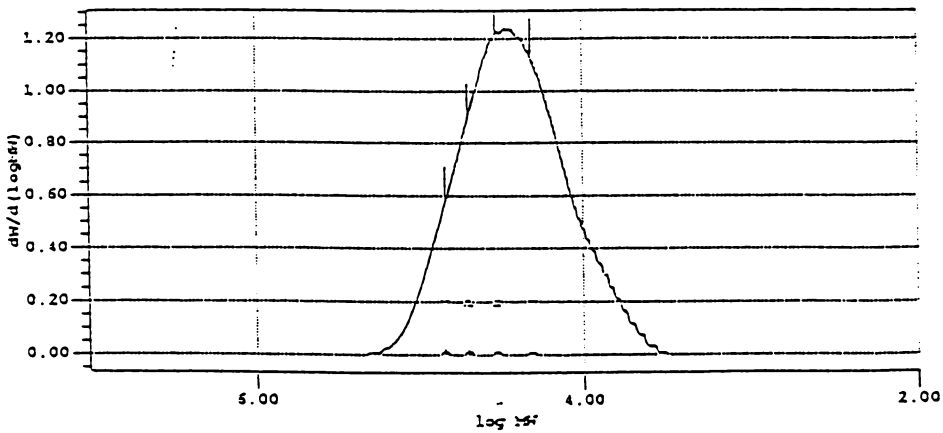
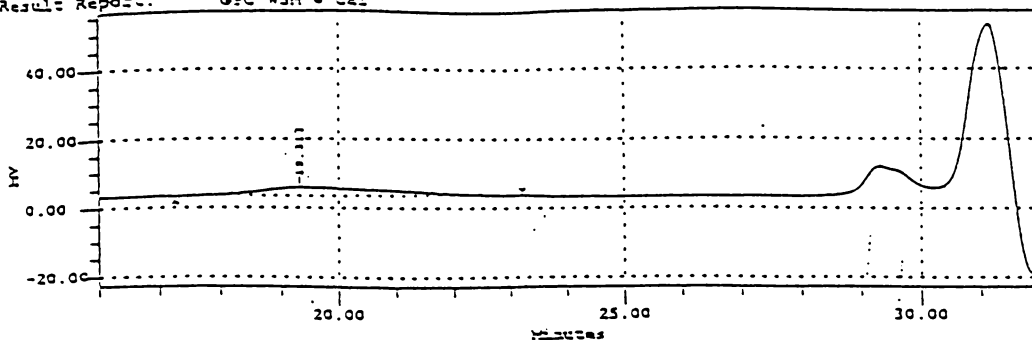


Figure 90. GPC data of PS-co-VPh (30 mol% VPh).

Millennium sample information

Project Name: WSM
 Sample Name: sri-6
 Vial: 6
 Injection: 1
 Channel: 410
 Acq Meth Set: GPC_DAD
 Processing Method: gpc_dad1
 Result Report: GPC WSM u cal

Sample Type: Broad Unknown
 Volume: 250.00
 Run Time: 45.0 min
 Date Acquired: 09/10/99
 Date Processed: 09/11/99



Millennium GPC Data

SampleName: sri-6
 Mv: 61125
 Mx: 11250
 Polydispersity: 1.9560
 Reference: GPC_WSM_u_cal

Date Acquired: 09/10/99
 Mv: 61125
 Mx+1: 11250
 Polydispersity: 1.9560
 Reference: GPC_WSM_u_cal

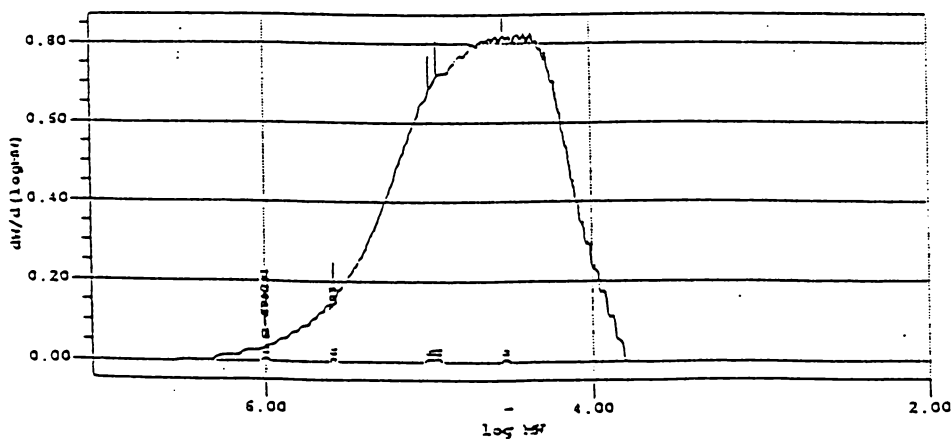
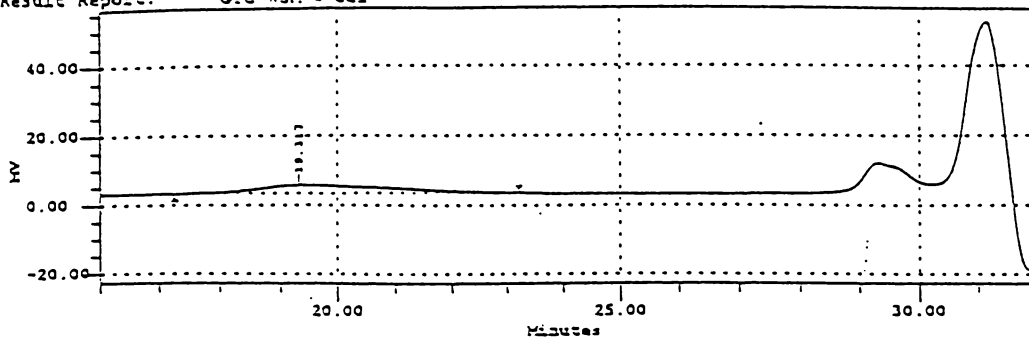


Figure 91. GPC data of PS-co-VPh (40 mol% VPh).

Millennium Sample Information

| | | | |
|--------------------|---------------|-----------------|----------------------|
| Project Name: | WSM | Sample Type: | Broad Unknown |
| Sample Name: | sri-5 | Volume: | 250.00 |
| Vial: | 6 | Run Time: | 45.0 min |
| Injection: | 1 | Date Acquired: | 09/10/99 04:06:56 PM |
| Channel: | 410 | Date Processed: | 09/11/99 12:06:54 PM |
| Acq Meth Sec: | GPC_DAD | | |
| Processing Method: | gpc_dad1 | | |
| Result Report: | GPC WSM 4 cal | | |



Millennium GPC Data

| | | | |
|--------------------|---------------|----------------|----------------------|
| SampleName: | sri-5 | Date Acquired: | 09/10/99 04:06:56 PM |
| MW: | 65174 | Mn: | |
| MX: | 34144 | M+1: | |
| Molydispersity: | 1.9088 | M+1: | |
| RelMolydispersity: | GPC_WSM_4_cal | M2: | |

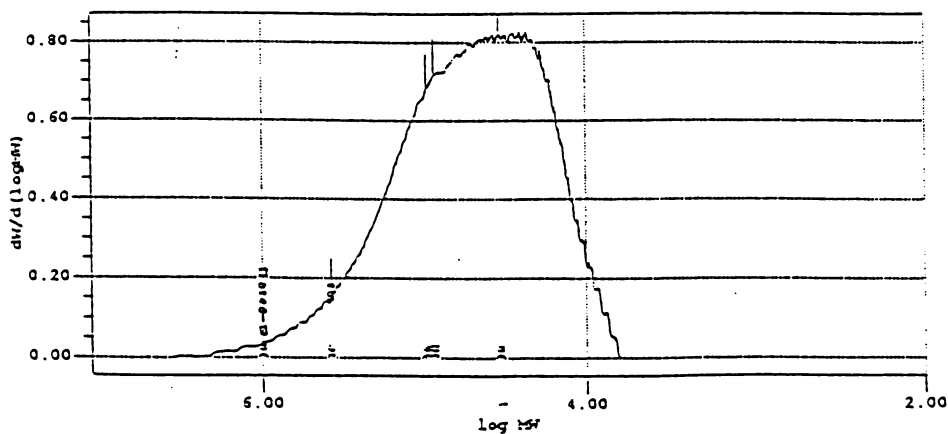


Figure 92. GPC data of PS-co-VPh (50 mol% VPh).

GPC curve for LCPU-M

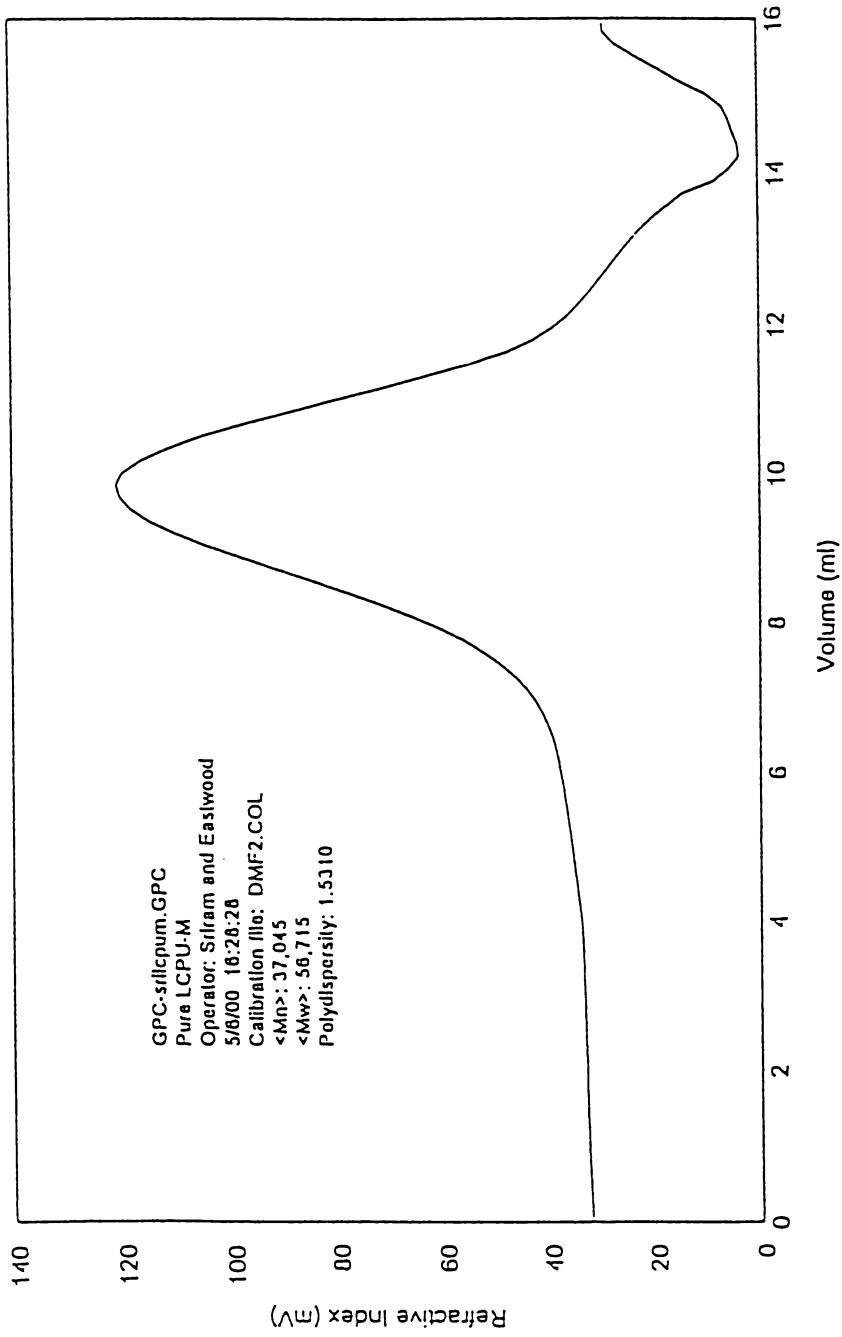


Figure 93. GPC data of the N-methyl Liquid Crystalline Polyurethane (LCPU-M).

Table 16. Results of the Best-fit Method for Determining the Interassociation Equilibrium Constant (K_A) of 20/80 (w/w) LCPU-M/PS-co-VPh(30) blend measured at 150°C.

| Φ_{B1} | $ \Phi_B - \Phi_B^* $ | | | | | | | | | |
|-------------|-----------------------|----------------------|----------------------|----------------------|----------------------|----------------------|----------------------|-------|--|--|
| | 2.730 | 2.731 | 2.732 | 2.733 | 2.734 | 2.735 | 2.736 | 2.737 | | |
| | K_A | | | | | | | | | |
| 0.319 | $5.76 \cdot 10^{-3}$ | $5.64 \cdot 10^{-3}$ | $5.59 \cdot 10^{-3}$ | $5.51 \cdot 10^{-3}$ | $5.43 \cdot 10^{-3}$ | $5.34 \cdot 10^{-3}$ | $5.26 \cdot 10^{-3}$ | | | |
| 0.320 | $1.77 \cdot 10^{-4}$ | $9.00 \cdot 10^{-5}$ | $1.17 \cdot 10^{-5}$ | $7.13 \cdot 10^{-5}$ | $1.54 \cdot 10^{-4}$ | $2.37 \cdot 10^{-4}$ | $3.20 \cdot 10^{-4}$ | | | |
| 0.321 | $5.40 \cdot 10^{-3}$ | $5.48 \cdot 10^{-3}$ | $5.57 \cdot 10^{-3}$ | $5.65 \cdot 10^{-3}$ | $5.74 \cdot 10^{-3}$ | $5.82 \cdot 10^{-3}$ | $5.90 \cdot 10^{-3}$ | | | |
| 0.322 | $1.12 \cdot 10^{-2}$ | $1.13 \cdot 10^{-2}$ | $1.14 \cdot 10^{-2}$ | $1.15 \cdot 10^{-2}$ | $1.16 \cdot 10^{-2}$ | $1.17 \cdot 10^{-2}$ | $1.18 \cdot 10^{-2}$ | | | |
| 0.323 | $1.69 \cdot 10^{-2}$ | $1.70 \cdot 10^{-2}$ | $1.71 \cdot 10^{-2}$ | $1.72 \cdot 10^{-2}$ | $1.73 \cdot 10^{-2}$ | $1.74 \cdot 10^{-2}$ | $1.75 \cdot 10^{-2}$ | | | |
| 0.324 | $2.25 \cdot 10^{-2}$ | $2.26 \cdot 10^{-2}$ | $2.27 \cdot 10^{-2}$ | $2.28 \cdot 10^{-2}$ | $2.29 \cdot 10^{-2}$ | $2.30 \cdot 10^{-2}$ | $2.31 \cdot 10^{-2}$ | | | |
| 0.325 | $2.83 \cdot 10^{-2}$ | $2.84 \cdot 10^{-2}$ | $2.85 \cdot 10^{-2}$ | $2.86 \cdot 10^{-2}$ | $2.87 \cdot 10^{-2}$ | $2.87 \cdot 10^{-2}$ | $2.88 \cdot 10^{-2}$ | | | |

VITA

Sriram Viswanathan was born in Madras, India on July 22, 1973. He graduated with a Bachelor of Technology degree in Chemical and Electrochemical Engineering and Technology from Central Electrochemical Research Institute, Karaikudi, India in 1994. After graduation, he worked as a research associate on various projects involving Electrochemical, Environmental and Polymer Technologies in Madras, India. He then decided to pursue an advanced degree in the United States and was admitted to the graduate school at the University of Tennessee, Knoxville in 1997. Since that time, he has been a doctoral candidate in the Polymer Chemistry program of the Chemistry Department of the same university.

